Processes Controlling Stratospheric Dynamic Variability, the Implications for Ozone Levels, and the Coupling to the Troposphere and Mesosphere

Dissertation

in fulfillment of the requirements for the Degree of
Doctor of Natural Sciences
(Dr. rer. nat)
to the **Faculty of Mathematics and Natural Sciences**
of the **Christian-Albrechts-Universität zu Kiel**

by

Sandro W. Lubis

Kiel, 2016

First Referee: Prof. Dr. Katja Matthes

Second Referee: Prof. Dr. Nili Harnik

Date of the oral examination: 27.06.2016

Approved for publication: 27.06.2016

Signed: Prof. Dr. Wolfgang J. Duschl, Dean

"The fear of the LORD is the beginning of knowledge,

but fools despise wisdom and instruction."

(Proverbs 1:7)

Abstract

Stratospheric variability plays an important role in driving the weather and climate of the Earth system. The extent to which various forcing factors explain this variability and the involved mechanisms are not fully understood. This thesis investigates processes controlling the variability of the stratosphere and the implication of this variability on ozone and on circulations in the troposphere and mesosphere. A series of sensitivity simulations with NCAR's CESM1(WACCM) model was performed to understand how these coupling processes are influenced by different natural and anthropogenic factors. The focus of this thesis is mainly on new aspects of the stratosphere-troposphere coupling mechanism via downward wave coupling (DWC), which is the most direct way by which the stratospheric background wind can affect tropospheric circulation.

Based on a series of sensitivity simulations, it is shown that although DWC is suppressed in the absence of the Quasi-Biennial Oscillation (QBO) variability, the tropospheric signal to DWC is enhanced, and vice versa when the sea surface temperature (SST) variability is excluded. This apparent mismatch is explained by the differences in the strength of the synoptic-scale eddy-mean flow feedback and the possible contribution of SST anomalies during DWC events. In particular, a weaker eddy-mean flow feedback in the absence of SST variability is consistent with modest Eady growth rate and synoptic wave source anomalies, which results in decreased synoptic-scale wave divergence. For the first time, the downward influence of DWC on the surface weather is suggested to be related to enhanced baroclinic instability in the troposphere.

This thesis also provides the first evidence for an effect of DWC on Arctic stratospheric ozone. A statistically significant decrease in Arctic column ozone is observed towards late winter during years with enhanced DWC. This is attributed to an increased net amount of wave reflection that leads to a cold polar vortex and less ozone transport to the pole. The results establish a new perspective on dynamical processes controlling Arctic ozone variability.

Under extreme climate change conditions, a significant reduction in DWC events is detected in the future, with a shift of their timing from early to midwinter. This variation is related to changes of the vertical reflecting surfaces and an increased wave absorption in early winter. The result also indicates that future changes in midwinter surface weather during DWC event are related to changes in baroclinic eddy feedback in the troposphere.

In the last part of this thesis, the impact of the Antarctic ozone hole on the vertical coupling of the stratosphere and mesosphere-lower thermosphere (MLT) system is investigated in detail. The results highlight that a proper accounting of both, dynamical and radiative effects, is required in order to correctly attribute the causes of the polar MLT response to the Antarctic ozone hole.

This thesis provides an advanced understanding of the mechanisms responsible for the coupling between the troposphere, stratosphere, and beyond in both the upward and downward directions. This knowledge has the potential to improve the representation of middle atmosphere circulation in climate models, and thus to improve predictions of ozone, climate, and even tropospheric weather.

Zusammenfassung

Die Variabilität in der Stratosphäre spielt eine wichtige Rolle für das Wetter und Klima des Erdsystems. Welche unterschiedlichen Faktoren diese Variabilität beeinflussen und wie diese zu den physikalischen Mechanismen beitragen, ist bisher nicht vollständig verstanden und Gegenstand dieser Arbeit. Außerdem werden die Auswirkungen der stratosphärischen Variabilität auf die Ozonkonzentration und auf die Zirkulation in der Tropo- und Mesosphäre untersucht. Um den Einfluss verschiedener natürlicher und anthropogener Faktoren auf diese Kopplung besser zu verstehen, wurden verschiedene Sensitivitätsexperimente mit NCAR's Erdsystemmodell, CESM1 (WACCM), durchgeführt. Der Fokus dieser Arbeit liegt hauptsächlich auf neuen Aspekten der Stratosphären-Troposphären Kopplung durch abwärts gerichtete Wellenkopplung (DWC, von engl.: downward wave coupling). Abwärts gerichtete Wellenkopplung ist der direkteste Weg, über den stratosphärische Winde die Zirkulation in der Troposphäre beeinflussen können.

Mit Hilfe dieser Sensitivitätsexperimente wird gezeigt, dass das troposphärische Signal, welches auf DWC-Ereignisse folgt, ohne das Vorhandensein einer quasi zweijährigen Schwingung der tropischen Winde in der Stratosphäre verstärkt wird, obwohl die abwärts gerichtete Wellenkopplung schwächer ist. Bei fehlender Variabilität der Meeresoberflächentemperaturen hingegen verhält es sich genau umgekehrt. Dieser scheinbare Widerspruch wird auf die unterschiedlich starke Wechselwirkung von synoptischen Wellen mit dem Grundstrom sowie auf einen möglichen Einfluss der Variabilität der Meeresoberflächentemperatur während eines DWC-Ereignisses zurückgeführt. Eine schwächere Wechselwirkung zwischen synoptischen Wellen und dem Grundstrom bei fehlender Variabilität der Meeresoberflächentemperatur steht im Zusammenhang mit einer geringeren Eady-Wachstumsrate und mit Anomalien im Auftreten von Quellen synoptischer Wellen. Dies resultiert in verringerter Divergenz synoptischer Wellen. Zum ersten Mal wird der abwärts gerichtete Einfluss von Wellenkopplung auf das Wetter mit verstärkter barokliner Instabilität in der Troposphäre in Zusammenhang gebracht.

Erstmals wird in dieser Arbeit der Einfluss von abwärts gerichteter Wellenkopplung auf die Ozonkonzentration in der arktischen Stratosphäre untersucht. In Jahren mit erhöhter Anzahl von DWC-Ereignissen wird eine statistisch signifikante Abnahme in der Ozonkonzentration zum Ende des Winters beobachtet. Dies wird auf eine erhöhte Gesamtanzahl von Wellenreflektionen in der Stratosphäre zurückgeführt, welche zu einem kalten Polarwirbel und zu einem verringerten Transport von Ozon in Richtung Pol führen. Diese Ergebnisse ermöglichen eine neue Perspektive in Hinblick auf die dynamischen Prozesse, die die Variabilität von arktischem Ozon bestimmen.

Unter Verwendung eines extremen Klimawandelszenarios wird eine Abnahme der DWC-Ereignisse in der Zukunft bei gleichzeitiger zeitlicher Verschiebung des Auftretens dieser Ereignisse zur Mitte des Winters festgestellt. Dies wird auf Veränderungen der vertikalen Reflektionsflächen und erhöhte Wellenabsorption zurückgeführt. Die Ergebnisse lassen außerdem darauf schließen, dass zukünftige Änderungen des Winterwetters während DWC-Ereignissen mit Änderungen der baroklinen Wellenwechselwirkungen in der Troposphäre in Zusammenhang stehen.

Im letzten Teil dieser Arbeit wird der Einfluss des antarktischen Ozonlochs auf die vertikale Kopplung von der Stratosphäre in die Meso- und untere Thermosphäre (MLT, von engl.: mesosphere and lower thermosphere) im Detail untersucht. Die Ergebnisse machen deutlich, dass eine Berücksichtigung von Strahlungs- und dynamischen Effekten für die Auswirkungen des antarktischen Ozonlochs auf die MLT notwendig ist.

Diese Arbeit liefert ein vertieftes Verständnis der dynamischen Prozesse, welche für die abwärts und aufwärts gerichtete Kopplung zwischen Troposphäre, Stratosphäre und höheren Atmosphärenschichten von Bedeutung sind. Dieses Wissen hat das Potential, die Repräsentation der mittleren Atmosphäre in Klimamodellen zu verbessern und damit bessere Klima-, Ozon- und Wetterprognosen zu ermöglichen.

Contents

1 General Introduction **1**
1.1 Theory of Vertically Propagating Rossby Waves . . . 2
1.2 Stratosphere-Troposphere Coupling . . . 5
1.3 Downward Wave Coupling (DWC) . . . 8
1.3.1 Fundamental Properties of DWC . . . 8
1.3.2 Tropospheric Impact of DWC . . . 11
1.4 Impact of Stratospheric Variability on Polar Stratospheric Ozone . . . 12
1.5 External Forcing Factors Influencing Stratospheric Variability . . . 13
1.5.1 The Quasi-Biennial Oscillation . . . 14
1.5.2 Sea Surface Temperatures . . . 16
1.5.3 Greenhouse Gases and Ozone Depleting Substances . . . 17
1.6 Dynamical Coupling of the Stratosphere and Mesosphere . . . 19
1.7 The Advantages of Climate Models . . . 21
1.8 Scientific Questions of This Thesis . . . 24

2 Influence of the Quasi-Biennial Oscillation and Sea Surface Temperature Variability on Downward Wave Coupling in the Northern Hemisphere **27**

3 How Does Downward Planetary Wave Coupling Affect Polar Stratospheric Ozone in the Arctic Winter Stratosphere? **53**
3.1 Introduction . . . 54
3.2 Data and Methods . . . 56
3.2.1 MERRA Ozone . . . 56
3.2.2 Model and Simulation . . . 56
3.2.3 Dynamical Diagnostics . . . 57
3.2.4 Identification of DWC Event . . . 57
3.3 Observed Effects of DWC on Ozone . . . 58
3.3.1 Connection between DWC, Stratospheric Residual Circulation, and Arctic Temperatures . . . 58
3.3.2 Observed Ozone Changes Induced by DWC . . . 59
3.4 Modeled Effects of DWC on Ozone . . . 62
3.4.1 Connection between DWC, Residual Circulation, and Arctic Temperatures in CESM1(WACCM) . . . 63

3.4.2 Simulated Ozone Changes Induced by DWC . . . 64
3.5 Seasonal Impact of DWC on Ozone . . . 65
3.5.1 Reflective versus Absorptive Winters . . . 66
3.5.2 Seasonal Impact on Arctic Column Ozone . . . 67
3.6 Conclusions and Discussion . . . 69

4 Climate Change Effects on the Variability of Downward Wave Coupling in the Northern Hemisphere 73
4.1 Introduction . . . 74
4.2 Data and Methods . . . 75
4.2.1 Model Simulations . . . 75
4.2.2 Statistical-Dynamic Approach . . . 76
4.3 Seasonality of DWC Events . . . 76
4.4 Mechanisms for Changes in Seasonality of DWC Events . . . 78
4.5 Tropospheric Impact of DWC in the Future . . . 80
4.6 Concluding Remarks . . . 81
4.7 Appendix : Supplementary Figures . . . 84

5 Impact of the Antarctic Ozone Hole on the Vertical Coupling of the Stratosphere- Mesosphere-Lower Thermosphere System 87

6 Conclusions and Outlook 109
6.1 Conclusions . . . 109
6.2 Outlook . . . 112

Acknowledgements 115

Bibliography 117

Declaration of Authorship 135

Chapter 1

General Introduction

Atmospheric layers are coupled vertically by radiative, dynamical, and chemical processes acting on different timescales. These couplings do not only comprise atmospheric processes, but also include interactions with other components of the Earth's systems, such as ocean, sea-ice, and land surface. For example, changes in the chemical composition of radiatively active gases, such as ozone (O_3) in the stratosphere cause significant changes in stratospheric temperatures as well as surface radiative forcing (e.g., Ramaswamy et al. 2001). On the other hand, variations in the stratospheric polar vortex induced by the variation in solar ultraviolet radiation could influence the tropospheric circulation by modifying vertically propagating planetary waves (e.g., Geller and Alpert 1980). Although these three coupling processes are equally important for the climate system, this thesis focuses mostly on the dynamical coupling mechanisms between the troposphere, stratosphere, and higher layers in both the upward and downward directions.

The dynamical coupling between the troposphere and stratosphere is primarily driven by a two-way interaction between atmospheric waves and the mean flow. Planetary waves originating from the troposphere propagate upward into the stratosphere, where they interact with the polar vortex. In extreme cases, the breaking or dissipating waves exert a systematic mean force that leads to a destruction of the polar vortex, causing a sudden stratospheric warming (SSW) event. SSWs evolve downwards into the troposphere where they can affect surface weather and climate (e.g., Baldwin and Dunkerton 2001; Limpasuvan et al. 2004). During periods following a sudden warming, studies have shown that a knowledge of the winds in the stratosphere increases predictability of the troposphere (e.g., Baldwin et al. 2003; Kuroda 2008). On the other hand, upward propagating planetary waves into the stratosphere can also be reflected back down to the troposphere, resulting in downward planetary wave coupling (DWC, Perlwitz and Harnik 2003). DWC has been found to significantly affect the tropospheric weather and surface climate over the North Atlantic sector (e.g., Shaw and Perlwitz, 2013; Dunn-Sigouin and Shaw, 2015; Lubis et al., 2016b). However, the underlying physical mechanisms that affect the variability of DWC and the associated impact on the troposphere are far from being fully understood. Thus, a better understanding of dynamical stratosphere-troposphere coupling via planetary wave coupling processes is required to improve predictions of tropospheric weather and climate.

Several studies have linked variations in stratospheric weather phenomena to the temperature and circulation changes in the mesosphere through gravity wave modulation (Smith et al., 2010; Lossow et al., 2012). Smith et al. (2010) showed that the ozone-hole-induced changes in

the stratospheric wind field leads to a warming of the polar summer mesopause, as a result of enhanced westerly gravity wave drag filtering. Other studies showed that enhanced easterly gravity wave drag filtering in the stratosphere during SSW events leads to a polar mesospheric cooling (analogous to the ozone hole's impact but with an opposite sign) [e.g., Walterscheid et al. 2000; Liu and Roble 2002; Hernandez 2003; Cho et al. 2004]. However, there are still gaps in our knowledge about the importance of planetary wave forcing for the stratosphere-mesosphere coupling. Thus, a better knowledge of dynamical stratosphere-mesosphere coupling and the involved mechanisms will help to improve the representation of mesospheric circulation in climate models.

The goal of this thesis is to investigate various aspects of the variability of the stratospheric polar vortex and the effect of this variability on ozone and circulations in the troposphere and mesosphere. The first part of this thesis investigates the stratospheric-troposphere coupling mechanism via downward planetary wave reflection. This includes investigation of the effects of different natural and anthropogenic factors on the variability of DWC, the impact of DWC on polar stratospheric ozone, and the underlying mechanism responsible for the tropospheric responses to DWC. In the last part of the thesis, a complete mechanism of the stratosphere-mesosphere-lower thermosphere (MLT) coupling during the Antarctic ozone hole period is proposed. This is the first study that investigates the combined effects of dynamical (resolved and non-resolved wave driving) and radiative forcings on the MLT response to the ozone hole. All underlying physical mechanisms for these couplings will be investigated in this thesis.

1.1 Theory of Vertically Propagating Rossby Waves

Fundamental properties of vertically propagating planetary waves, which is the basis of studies of the dynamical coupling between the stratosphere and the troposphere, are reviewed briefly. On a β plane, the linearized quasi-geostrophic potential vorticity q in the logarithmic pressure coordinate (z=-H log p), under assumption of conservative flow, can be expressed as follows (Charney and Drazin, 1961):

$$(\frac{\partial}{\partial t} + \bar{u}\frac{\partial}{\partial x})q' + \bar{q}_y\frac{\partial \psi'}{\partial y} = 0 \tag{1.1}$$

where $\psi = \Phi/f$ is the geostrophic streamfunction, q is quasigeostrophic potential vorticity, Φ is geopotential, and f is the Coriolis parameter. The overbar and prime denote zonal mean and eddies (deviations from zonal mean), respectively. Equation (1.1) has solutions in the form of harmonic waves with zonal and meridional wavenumbers (k and l), respectively, and angular frequency ω:

$$\psi'(x, y, z, t) = \Psi(z)exp\left[i(kx + ly - \omega t) + \frac{z}{2H}\right] \tag{1.2}$$

where Ψ is a function only of z. Note that the altitude factor $\exp(z/2H)$ takes into account the fact that a propagating non-dissipating wave will conserve energy, which is proportional to $|\psi'|^2$. Substituting (1.12) to the equation (1.1), yields

$$\frac{d^2\Psi}{dz^2} + m^2\Psi = 0 \tag{1.3}$$

where

$$m^2 = \frac{N^2}{f^2}\left[\frac{\bar{q}_y}{\bar{u} - C_{px}} - (k^2 + l^2)\right] - \frac{1}{4H^2}. \tag{1.4}$$

and zonal phase speed $C_p = \omega/k$. We recall that m^2 must be positive for the vertical propagation, and thus vertically propagating modes can exist only for zonal mean flows that satisfy the following condition:

$$C_{px} < \bar{u} < C_{px} + \frac{\bar{q}_y}{k^2 + l^2 + \frac{f^2}{4N^2H^2}} \equiv U_c. \tag{1.5}$$

where U_c is called as the Rossby critical velocity and H is the density scale height. This condition suggests that stationary ($C_{px} > 0$) Rossby waves cannot propagate vertically in the easterlies (Charney and Drazin, 1961). In the westerlies, only the Rossby waves with longer zonal wavelength can propagate vertically in the strong wind speed. If the westerly speed increases with height under condition of constant $\bar{q}_y$, upward propagating waves reaching at some level where $\bar{u} = U_c$ for each k cannot propagate farther above that level. This can be seen in Fig. 1.1, that long waves are able to propagate upward in contrast to high wavenumbers ($K > 5$). Such waves are already filtered by a moderate zonal wind ($U > 20$ m/s). This property has a consequence in the seasonal pattern of vertical propagating Rossby waves.

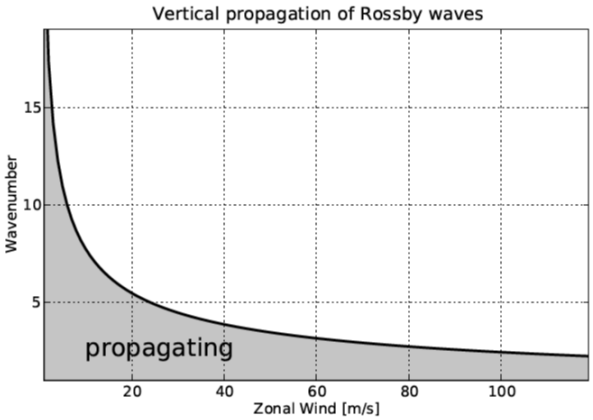

FIGURE 1.1: Vertically propagating Rossby waves as a function of background flow (U) and the total wavenumber K at 50°N and a buoyancy frequency of $N = 2 \cdot 10^{-2}$ s^{-1} (see Eq. 1.5).

Furthermore, if $\bar{u}$ satisfies the above condition (1.5), thus Ψ may be written as: $\Psi(z) = \psi_0 \exp(imz)$, where ψ_0 is a constant and i represents imaginary part. The equation (1.12) becomes

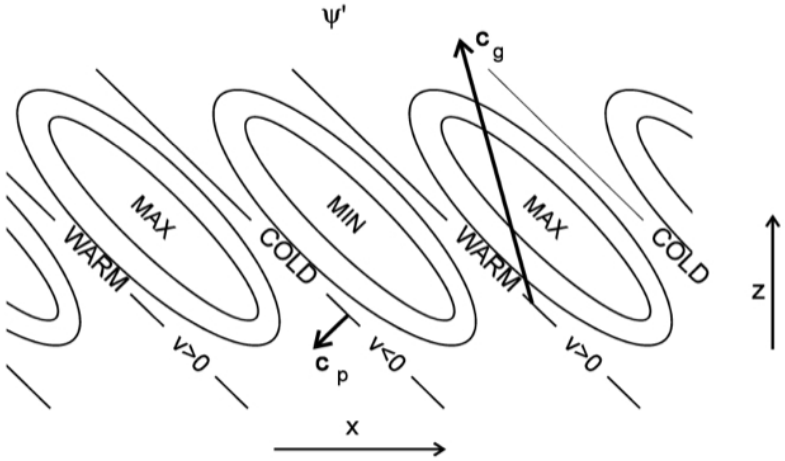

FIGURE 1.2: A vertically propagating Rossby wave in the NH (warm/cold are reversed in the Southern Hemisphere). Note that this should be multiplied by $\exp(z/2H)$ to give the actual result for ψ'. Figure adapted from Charney and Drazin, 1961.

$\psi'(x,y,z,t) = \psi_0 \exp(i(kx+ly+mz) + z/(2H))$, for which we obtain a dispersion relation as:

$$\omega = \bar{u}k - \frac{k\,\bar{q}_y}{K^2 + \frac{f^2}{4N^2H}}, \tag{1.6}$$

where

$$K^2 = k^2 + l^2 + \frac{f_0^2}{N^2}m^2 = \frac{\bar{q}_y}{\bar{u} - C_{px}} - \frac{f^2}{4N^2H^2}. \tag{1.7}$$

Therefore, the group velocity, $C_g = (C_{gx}, C_{gy}, C_{gz})^T$, can be expressed as:

$$C_{gx} = C_{px} + \frac{2\,\bar{q}_y k^2}{K^2 + (\frac{f^2}{4HN^2})^2}; \tag{1.8}$$

$$C_{gy} = \frac{2\,\bar{q}_y kl}{K^2 + (\frac{f^2}{4HN^2})^2}; \tag{1.9}$$

$$C_{gz} = \frac{2\,\frac{f^2}{N^2}\bar{q}_y km}{K^2 + (\frac{f^2}{4HN^2})^2}; \tag{1.10}$$

For stationary waves (C_{px}=0), the group velocity may be simplified as:

$$C_g = (k, l, \frac{f^2}{N^2}m) \times \frac{2\bar{u}k}{K^2 + \frac{f}{4HN^2}}, \tag{1.11}$$

Thus, the group velocity of a stationary Rossby wave is tangent to phase lines in a horizontal plane, phase lines associated with the upward- (downward-) propagating Rossby wave group velocity are tilted westward (eastward) with height (see schematic diagram in Fig 1.2). On the other hand a west-and eastward tilt of the waves with increasing latitude characterizes pole- and

equatorward propagation, respectively. It is also shown that the magnitude of the group velocity is almost twice as large as $\bar{u}$ (i.e., $|C_g = 2\bar{u}\cos\alpha|$), where α is the angle between lines of constant phase and the y axis .

1.2 Stratosphere-Troposphere Coupling

Recently, the dynamical influence of the stratosphere on the troposphere has been extensively studied due to its implication for extended-range forecasts and climate variability (e.g., Baldwin and Dunkerton 2001; Limpasuvan et al. 2004; Kuroda 2008). As a pioneer work for this study, Quiroz (1977) showed that a large increase of temperature anomalies in the troposphere was linked to extreme stratospheric phenomena, SSWs. Through numerical experiments, Geller and Alpert (1980) argued that changes in the tropospheric circulation were attributed to variations in the stratospheric polar night jet (PNJ) through modulation of planetary wave propagation. Likewise, Boville (1984) showed that changes in the stratospheric PNJ could alter the tropospheric circulation by modifying the transmission-refraction properties of vertically propagating waves.

The downward propagation of the stratospheric zonal-mean zonal wind anomalies to troposphere in the NH was firstly shown by Kodera et al. (1990). In that process, the observed westerly anomalies first appear in the upper stratosphere and then propagate downward into the troposphere within a month, accompanied by anomalous meridional propagation of planetary waves (Kodera et al. 1990; Kodera et al. 1991). Much of the evidence for a stratospheric impact on the troposphere has been widely described using the so-called annular modes: the Northern Annular Mode (NAM) and Southern Annular Mode (SAM) (e.g., Baldwin and Dunkerton 1999; Thompson and Wallace 2000). These modes are the dominant patterns of variability in the extra tropical troposphere and stratosphere, characterized by a zonally-symmetric, barotropic dipole pattern between the polar region and mid-latitude in the stratosphere and troposphere winter. Baldwin and Dunkerton (1999) showed that the NAM anomalies first appear in the stratosphere and subsequently progress downward into the troposphere over periods of a few weeks. Figure 1.3 shows composites of weak vortex events from the NCEP-NCAR Reanalysis taken from Baldwin and Dunkerton (2001). It is evident that anomalous values of the NAM are evident in the troposphere and at the surface for up to two months after they first appear in the stratosphere. In the stratosphere the annular mode values are a measure of the strength of the polar vortex, while the near surface is recognized as the "Arctic Oscillation (AO)" or the North Atlantic Oscillation (NAO). Moreover, subsequent studies showed that the best extended-range forecasts of the AO in the winter can be achieved by using the lower stratospheric NAM as a predictor (e.g., Baldwin et al. 2003).

While the influence of the troposphere on the stratosphere is well established, the influence in the opposite direction is more difficult to determine. A simple schematic diagram to illustrate the stratospheric downward influence on the troposphere during strong polar vortex conditions is given in Fig 1.4 (Kidston et al., 2015). First, weaker planetary wave forcing in the stratosphere

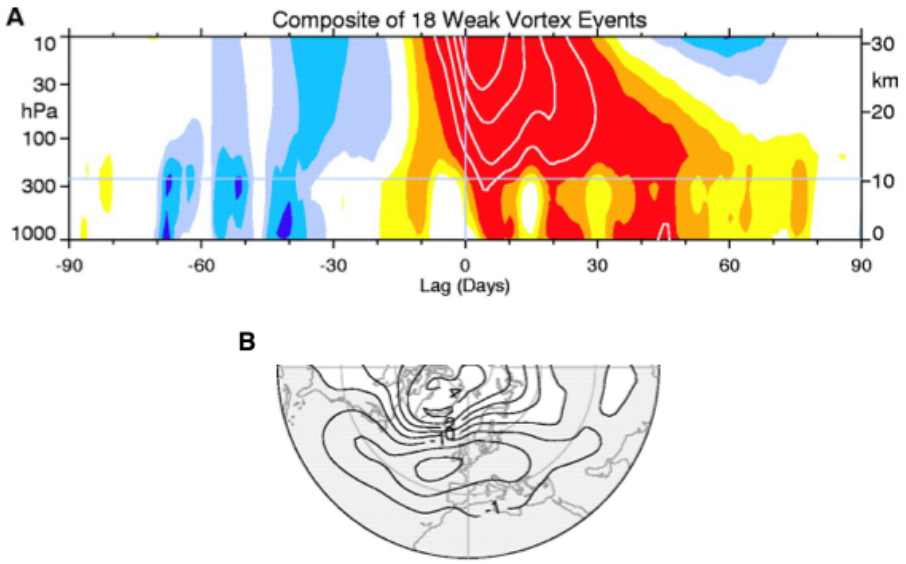

FIGURE 1.3: (a) composite of time-height development of the NAM for 18 weak vortex events (top). The contour interval for the colour shading is 0.25 and 0.5 for the white contours. (b) Average sea-level pressure anomalies (hPa) for the 1080 days during weak vortex regimes. Figure from Baldwin and Dunkerton (2001).

leads to strengthening of the polar vortex (1). The reduced stratospheric wave forcing is in turn balanced by the Coriolis force, resulting in upward (downward) residual circulation at high latitudes (mid-to-low latitudes) and subsequent adiabatic cooling (warming) in this region (2). The mass redistribution – through upwelling/downwelling – increases the tropopause heights and reduced mean sea level pressure in polar latitudes and vice versa in mid-latitudes (3). The tropospheric eddy feedbacks (4), in turn, induce and maintain a poleward shift of both the tropospheric jet and the storm tracks (5). Although it is generally recognized that the tropospheric eddy feedbacks are linked to a poleward shift of tropospheric jet, the involved mechanism is not completely clear.

According to the timescales of the process, the stratosphere-troposphere coupling can be distinguished into: (1) **short term coupling** that includes planetary wave activity: wave absorption (e.g., Matsuno 1970; McIntyre and Palmer 1983), wave reflection (e.g., Harnik and Lindzen 2001; Perlwitz and Harnik 2003), and wave resonance (e.g., Tung and Lindzen 1979; Esler and Scott 2005), (2) **intraseasonal coupling** including downward influence of sudden and final stratospheric warmings (e.g., Baldwin and Dunkerton 2001; Limpasuvan et al. 2004; Sun and Robinson 2009), and (3) **interannual coupling** that includes modification of eddy-mean flow interactions by El Niño-Southern Oscillation (ENSO, e.g., Loon and Labitzke 1987; Manzini et al. 2006), Quasi-Biennial Oscillation (QBO, e.g., Holton and Tan 1980; Coughlin and Tung 2001), solar cycle (e.g., Kodera and Kuroda 2002; Matthes et al. 2006), volcanoes (e.g., Robock and Mao 1992; Fischer et al. 2007), sea-ice changes (e.g., Jaiser et al. 2013), Atlantic meridional overturning circulation (e.g., Reichler et al. 2012) etc.

The exact dynamical mechanism by which the stratospheric signals can be transmitted to the

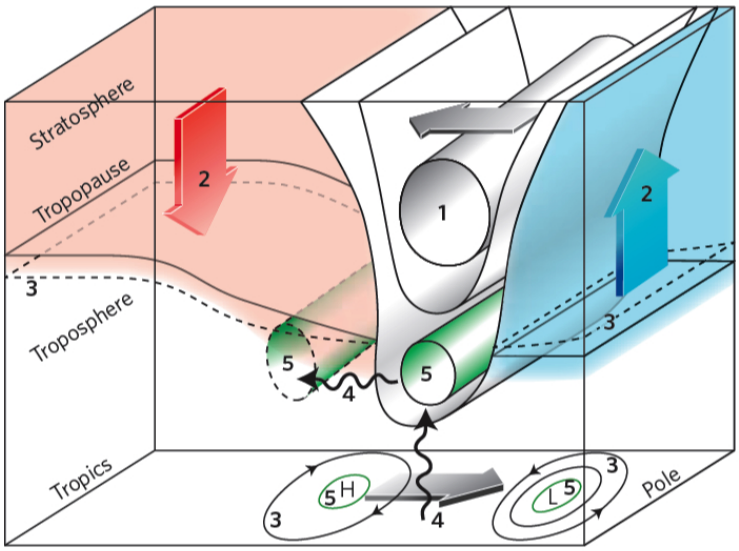

FIGURE 1.4: A sketch of stratospheric downward influence during a strong vortex event. Figure from Kidston et al. (2015).

troposphere and surface, however, is unknown, but a number of theories have been proposed. The first theory is a direct adjustment of the tropospheric flow to stratospheric potential vorticity (PV) anomalies (diagnosed by PV inversions; Hartley et al. 1998; Ambaum and Hoskins 2002; Black 2002). This theory explains how tropospheric wind anomalies can be influenced by stratospheric potential vorticity. In particular, enhanced positive stratospheric PV anomalies associated with a strong stratospheric polar vortex cause both a rise of the tropopause height and stretching of the tropospheric column. This results in lower pressure levels in polar latitudes and increase of the tropospheric westerlies (Ambaum and Hoskins 2002). An equivalent mechanism to the non-local effect of the PV inversion is the "downward control" principle (Haynes et al. 1991; Holton et al. 1995). This mechanism shows that the meridional circulation is non-locally controlled by wave induced forcing. In other words, the meridional circulation at each level is controlled only by the forces acting above it. Another idea includes changes in refractive properties and Rossby wave propagation (Hartmann et al. 2000; Limpasuvan and Hartmann 2000). In this mechanism, changes in the vertical structure of stratospheric winds (shear and curvature) cause changes in transmission and refraction properties of vertically propagating waves. The last mechanism is associated with the downward reflection of wave activity by the stratosphere back into the troposphere (e.g., Perlwitz and Harnik 2003).

Recent model and observational studies also reported the importance of synoptic eddies in shaping and maintaining the downward influence of stratospheric anomalies in the troposphere (e.g., Limpasuvan et al. 2004; Song and Robinson 2004; Simpson et al. 2009; Kunz and Greatbatch 2013; Domeisen et al. 2013). In particular, Simpson et al. (2009) performed spin-up experiments with an idealized general circulation model (GCM) by looking at the response to many different stratospheric forcings and reported that changes to eddies are related to changes in the refractive

index near the tropopause. Other studies also reported that changes in the mean flow conditions in the vicinity of the tropopause, can affect synoptic eddies in the troposphere via changes in lower stratospheric shear (Wittman et al., 2007), isentropic slope (Thompson and Birner, 2012), eddy length scale (Kidston et al., 2010), and eddy phase speed (Chen and Held, 2007). However, the direct impact of planetary wave coupling on synoptic scale eddies in the troposphere is still not fully understood.

In this thesis, the mechanism of stratosphere-troposphere dynamical coupling via downward planetary wave reflection is investigated in detail. Planetary waves are generated in the troposphere by orographic and non-orographic forcing (diabatic heating and/or interaction with transient eddies) (e.g., Kuroda and Kodera 1999; Kodera and Kuroda 2000; Baldwin and Dunkerton 2001; Christiansen 2001; Plumb and Semeniuk 2003; Polvani and Waugh 2004). These waves propagate upward into the stratosphere where they either dissipate or are reflected downward toward the troposphere, resulting in downward wave coupling.

1.3 Downward Wave Coupling (DWC)

Although a mechanism of a downward dynamic influence – reflection of wave activity by the stratosphere back into the troposphere – has been suggested by several authors in the past (Hines 1974; Geller and Alpert 1980; Schmitz and Grieger 1980; Bates 1981), Perlwitz and Harnik (2003) was the first to clearly show the impact of reflected wave-packets on tropospheric planetary waves. In this section, the fundamental properties of DWCs and their effects on the tropospheric circulation are reviewed.

1.3.1 Fundamental Properties of DWC

DWC occurs when the upward propagating waves decelerate the polar vortex in the upper stratosphere, causing the formation of a reflecting surface that redirects waves back to the troposphere (Harnik and Lindzen 2001; Lubis et al. 2016b, see also Fig 1.5). The reflecting surface forms as a result of the negative vertical westerly shear that leads to negative meridional PV gradient (see Eq. 1.12). When the zonal mean winds decrease with height in the upper stratosphere, the index of refraction squared for these waves becomes negative, blocking the waves from propagating further up. As a result, the waves are reflected back down to the troposphere, instead of being absorbed in the stratosphere (Harnik and Lindzen, 2001; Perlwitz and Harnik, 2003; Lubis et al., 2016b), leaving the vortex strong and the pole cold. Harnik (2009) showed that a lower stratospheric acceleration also contributes to this negative vertical shear, and that this acceleration occurs at the trailing edge of the upward pulse of wave activity. Thus, reflection is associated with short wave forcing, while SSWs are associated with long wave pulses (e.g., Harnik 2009; Sjoberg and Birner 2012), which are often manifested as blocking events (e.g., Quiroz 1986; Naujokat et al. 2002; Woollings et al. 2010). The meridional PV gradient, which is an important ingredient for the formation of vertical

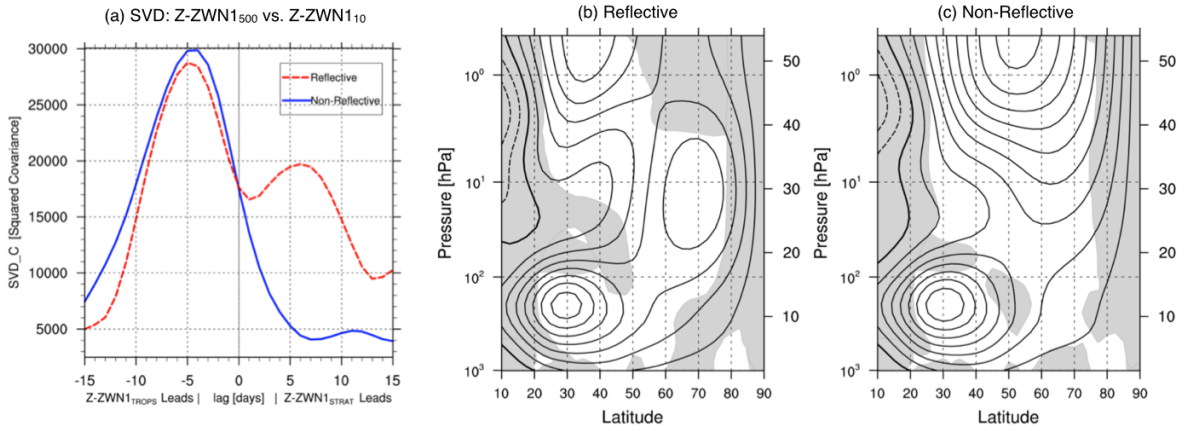

FIGURE 1.5: (a) The squared covariance between Z-ZWN1$_{500}$ and Z-ZWN1$_{10}$ calculated from the time-lagged SVD analyses for negative (reflective) or positive (non-reflective) U$_{2-10}$ index in JFM. A positive (negative) time lag indicates that the stratospheric (tropospheric) wave field is leading. (b-c) The composites of vertical and meridional wavenumbers, calculated for each of the reflective and non-reflective years. Gray shading indicates regions of wave evanescence in the meridional ($l < 0$) and vertical ($m < 0$) directions. Data was obtained from ERA reanalysis. See Chapter 2 for a detailed methodology description.

reflecting surface, can be approximately written as:

$$\overline{q}_y \equiv \beta - \frac{1}{a^2}\frac{\partial}{\partial\phi}\left[\frac{1}{\cos\phi}\frac{\partial\left(\overline{u}\cos\phi\right)}{\partial\phi}\right] - \left(\frac{f^2}{HN^2} + \frac{f^2}{N^4}\frac{\partial N^2}{\partial z}\right)\frac{\partial\overline{u}}{\partial z} + \frac{f^2}{N^2}\frac{\partial^2\overline{u}}{\partial z^2}. \tag{1.12}$$

where N^2 is the buoyancy frequency, and β is the variation of the Coriolis parameter with latitude. The third term of the right hand side can be negative associated with a decreasing zonal-mean zonal wind speed with height. Hence, this quantity contributes to decreasing total wavenumber K (see Eq. 1.7) to yield m=0 (reflecting surface).

Perlwitz and Harnik (2003, 2004) showed that NH winters tend to be either reflective (very cold and undisturbed), or non-reflective (absorptive, with a SSW), with the two occurring approximately equally in the observational record. In the non-reflective state, most of the waves gets deposited in the stratosphere, resulting in strong wave-mean-flow interaction, while in the other state, wave activity is reflected back down to the troposphere resulting in more DWC events and affecting the structure of tropospheric planetary waves (Fig 1.5). The reflective state is characterized by a well-defined high-latitude meridional waveguide in the lower stratosphere that is bounded above by a vertical reflecting surface (Fig 1.5). This configuration is favourable for the occurrence of DWCs and known as bounded wave geometry. The bounded wave geometry can be diagnosed by determining the existence and location of turning surfaces for meridional and vertical propagation. For a non-isothermal atmosphere, a general refractive index (n_r^2) decomposition for waves with a zonal wavenumber k and a phase speed c, is written as (for details, see Harnik and Lindzen 2001 and Chapter 2):

$$n_r^2 \equiv \frac{N^2}{f^2}\left\{\frac{\bar{q}_y}{\overline{u}-c} - k^2 + f^2\frac{e^{z/2H}}{N}\frac{\partial}{\partial z}\left[\frac{e^{-z/H}}{N}\frac{\partial}{\partial z}\left(e^{z/2H}N\right)\right]\right\} \equiv m^2 + \frac{N^2}{f^2}l^2. \tag{1.13}$$

From (1.13), the waves propagate in the vertical (meridional) direction when $m^2 > 0$ ($l^2 > 0$), are evanescent when $m^2 < 0$ ($l^2 < 0$), and are reflected when $m^2 = 0$ ($l^2 = 0$).

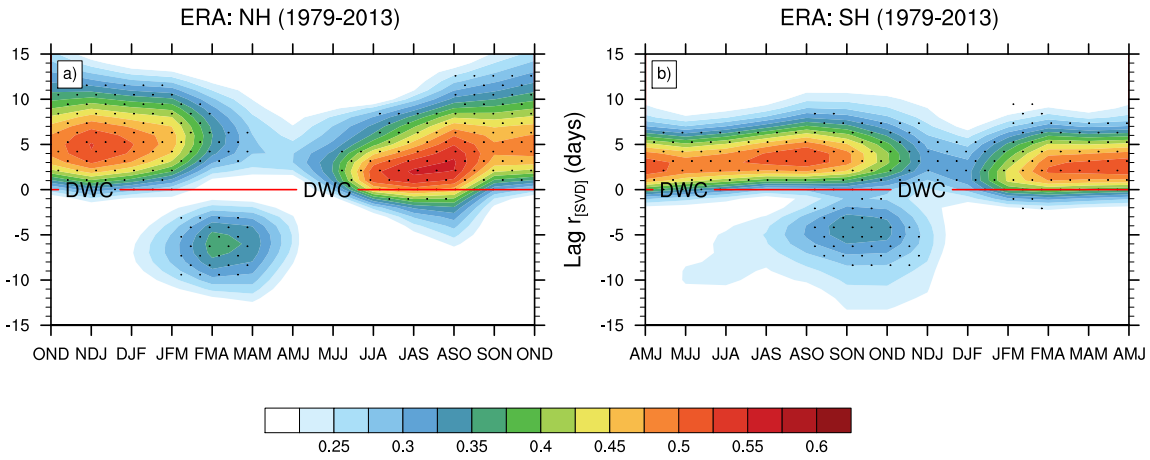

FIGURE 1.6: Three-month overlapping periods of lagged SVD correlations between Z-ZWN1 at 500 hPa and 10 hPa calculated from ERA reanalysis for (a) NH and (b) SH. Black dots represent statistically significant values at the 99% level calculated using a Monte Carlo approach (see Chapter 2 for a detailed methodology description).

In the NH, the formation of bounded wave geometry happens intermittently, when waves decelerate the vortex only in the upper stratosphere. However, in the SH this happens every year towards the end of winter, as part of the seasonal cycle (Shaw et al., 2010). In Figure 1.6, the seasonal cycles of DWC in the Northern and Southern Hemispheres are presented by time-lagged singular value decomposition (SVD) correlations between geopotential height wave number 1 (Z-ZWN1) at 500 hPa and 10 hPa from ERA reanalysis. A negative (positive) time lag indicates that the stratospheric (tropospheric) wave field is leading. Therefore, the most favourable season for DWCs in the NH is during midwinter from January to March, while in the SH it occurs from September to December (Fig 1.6).

Although the mechanism by which tropospherically forced waves are reflected downwards in the stratosphere is already well established, what factors determine the variability and the source of DWCs remains a difficult question, and is one of subjects of this thesis. In this thesis, the influence of different natural and anthropogenic forcing factors on the DWC variability was investigated using a unique set of model simulations, which include both an interactive ocean and an interactive chemistry module, extending up to the thermosphere.

1.3.2 Tropospheric Impact of DWC

DWC is the most direct way by which the stratospheric background wind can affect tropospheric circulation. Recent studies have revealed that the wintertime distribution of high-latitude planetary wave-1 heat flux exhibits extreme values that are linked to the tropospheric circulation in the North Atlantic (Shaw and Perlwitz, 2013; Shaw et al., 2014; Dunn-Sigouin and Shaw, 2015; Lubis et al., 2016b). Shaw and Perlwitz (2013) investigated the dynamics of DWC in the NH using total (anomaly plus climatology) negative wave-1 heat flux values. They showed that the life cycle of DWC in the stratosphere occurred over a few weeks and involved vertical coupling via a clear high-latitude wave-1 pattern in the troposphere that results in a poleward jet shift in the Atlantic sector. The growth of wave-1 amplitude began around the time of minimum heat flux and was followed by the development of a reflecting surface. The associated near-surface temperature and mean sea level pressure anomalies are very reminiscent of the positive phase of the North Atlantic Oscillation (NAO). Subsequent studies by Shaw and Perlwitz (2014) and Dunn-Sigouin and Shaw (2015) showed that extreme positive and negative stratospheric wave-1 heat flux values are instantaneously linked to poleward and equatorward shifts of the tropospheric jet. However, the mechanism by which the DWC affects the tropospheric jet shifts and what factors control the strength of tropospheric response to DWC remain unclear.

The basic principle of the dynamical coupling between stratosphere and troposphere via DWC, as well as the unclear mechanisms related to this coupling process are illustrated in Fig 1.7.

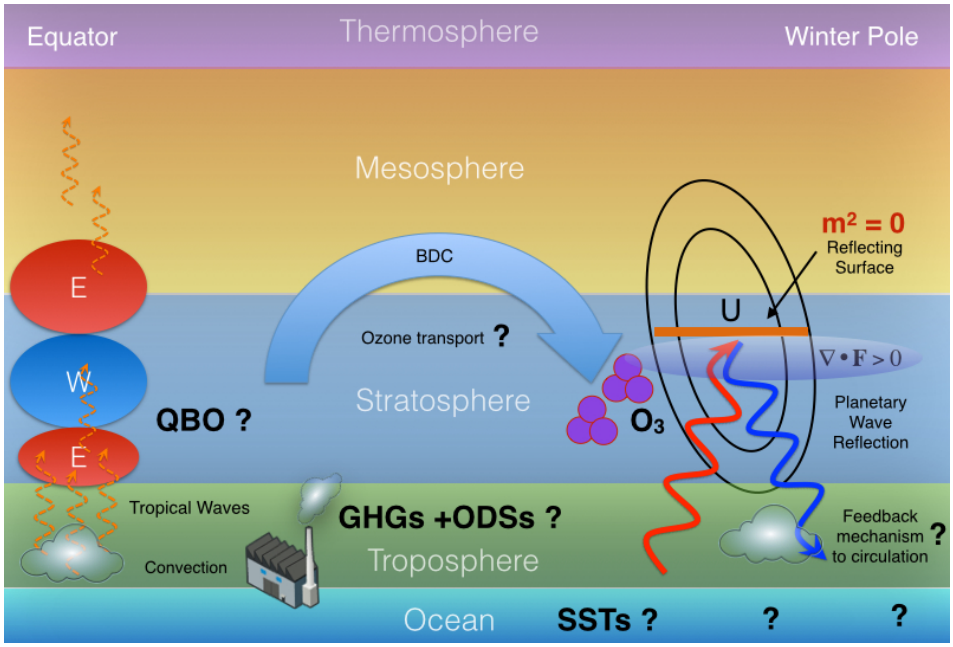

FIGURE 1.7: A stratosphere-troposphere coupling mechanism via DWC. The red (blue) arrow indicates the direction of the planetary wave propagation. The shaded oval indicates Eliassen-Palm (EP) flux divergence. The horizontal orange solid line indicates vertical reflecting surface ($m^2 = 0$). The effects of the QBO, SST and anthropogenic (GHG and ODSs) forcings on this coupling mechanism are unclear and marked with "?". Likewise, the mechanisms responsible for downward influence on the troposphere and the implication for ozone levels are not understood. **These questions will be answered in this thesis**.

1.4 Impact of Stratospheric Variability on Polar Stratospheric Ozone

Much of the interannual variability in the stratosphere is caused by variations in planetary wave activity, with the amount of ozone depletion strongly correlating with the total amount of wave activity entering the stratosphere from the troposphere during winter (Fusco and Salby, 1999; Randel et al., 2002; Weber et al., 2003). Randel et al., 2002 show that variations in planetary wave forcing in the lower stratosphere during winter-spring exhibit a strong correlation with column ozone. The mechanism for this is that increased (decreased) wave dissipation in the stratosphere leads to strengthening (weakening) of residual circulation, which in turn increases (decreases) the transport of ozone-rich air to the polar lower stratosphere. On the other hand, strong (weak) midwinter planetary wave forcing causes a warmer (cooler) Arctic lower stratosphere in early spring (Newman et al., 2001), resulting in smaller (larger) chemical ozone losses in spring. A recent study by Manney et al. (2011) revealed that the unprecedented Arctic ozone loss in 2011 is highly correlated with extremely cold lower-stratospheric temperatures in early spring. These extremely low temperatures are attributed to the unusually weak midwinter planetary wave forcing in the stratosphere (Hurwitz et al., 2011), as expected from a close relationship between polar spring temperatures and eddy heat flux in mid to late winter (Newman et al., 2001).

The NH winter stratosphere is characterized by large interannual variability, which either results in very disturbed winters with SSWs, or very cold undisturbed winters. SSWs are dramatic events that cause the stratospheric pole to heat up by tens of degrees within a period of days, and cause the strong winds circulating the pole to reverse direction (e.g., Baldwin et al. 2003; Kuroda 2008). Enhanced stratospheric wave dissipation during SSW events causes strengthening of the residual circulation and a warmer polar vortex. This in turn leads to more dynamical ozone transport to the pole and less springtime ozone destruction (e.g., Rose and Brasseur 1985; Randel 1993; Hocke et al. 2015). On the other hand, cold and undisturbed stratospheric winters provide opportunity for temperatures to drop below the threshold for the formation of Polar Stratospheric Clouds (PSCs), on which ozone destruction processes take place. In the SH, this results in an ozone hole in the polar stratosphere every spring, the pole being dynamically isolated from lower latitudes by the strong winds that circulate it. The NH pole is not as dynamically isolated as the SH, and winter temperatures do not regularly drop as low, so the degree of ozone destruction is much smaller and more variable from year to year.

Though very different in their type of influence, both of the aforementioned dynamical influences – SSWs and cold winters with low ozone levels – involve the interaction of the polar vortex with planetary waves' large-scale undulations of the vortex which propagate up from the troposphere, then break and are absorbed in the vortex, slowing it down and heating the pole in the process (e.g., Solomon 1999; Fusco and Salby 1999; Randel et al. 2002). When wave absorption is very strong, a SSW occurs, and when it is very weak, polar temperatures become cold enough for ozone to be destroyed. Since the amount of wave-induced heating in the NH is highly variable, the occurrences of cold winters with ozone depletion, or winters with SSWs, are also highly variable. One process that is associated with reduced wave absorption is DWC (Harnik, 2009).

The vortex remains strong and cold when the waves are reflected back down to the troposphere, instead of being absorbed in the stratosphere (Harnik and Lindzen, 2001; Perlwitz and Harnik, 2003). Therefore, winters with increased DWC activity are expected to be related with strong ozone destruction.

In this thesis, the impact of the DWC on stratospheric circulation, polar temperatures, and ozone is investigated in Chapter 3. Determining the connection between DWC, residual circulation, and polar temperatures is one of the keys to improving our understanding of the link between stratospheric dynamics and ozone variability both in the real atmosphere and in stratosphere-resolving chemistry-climate models (CCMs). The schematic diagram showing a possible influence of DWC on polar stratospheric ozone is also illustrated in Fig 1.7.

1.5 External Forcing Factors Influencing Stratospheric Variability

Variability in the stratosphere is the result of complex and nonlinear relationships between various forcings affecting the evolution of the stratosphere (e.g., Calvo et al. 2009; Richter et al. 2011). Recent studies have shown that understanding the factors influencing the polar vortex can improve tropospheric weather forecasts and seasonal predictions for different latitudes and regions (e.g., Baldwin and Dunkerton 2001; Thompson and Solomon 2002; Domeisen et al. 2015). In addition, it is well established that the two-way vertical (upward and downward) planetary wave propagation, which influence the strength of the polar vortex, can be modified by changes in the vertical and meridional structures of the zonal mean wind (Charney and Drazin 1961; Limpasuvan and Hartmann 2000; Perlwitz and Harnik 2003). Therefore, examining which factors affect the variability of the polar vortex can help us understand what processes control the variability of DWC and its associated impact on tropospheric circulation.

The forcing factors influencing stratospheric variability can be distinguished into "natural" and "anthropogenic" forcings. The natural forcing factors are responsible for natural or internal climate variability (IPCC, 2013). These forcings include the QBO of equatorial stratospheric winds, variations in sea surface temperatures (SSTs), volcanic eruptions, and variations in solar radiation. Many studies have shown that these natural forcing factors have significant impact on the variability of the polar vortex (e.g., Holton and Tan 1982; Loon and Labitzke 1987; Labitzke and Loon 1996; Matthes et al. 2006). Recent studies with CCMs have also shown the QBO and SSTs play important roles for representation of mutually dynamical relations between the stratosphere and troposphere in climate models (e.g, Calvo et al. 2009; Richter et al. 2011; Hansen et al. 2014; Lubis et al. 2016b). On the other hand, anthropogenic forcings are human-induced factors that include greenhouse gases (GHG, prominent examples are carbon dioxide (CO_2) and methane (CH_4)) and ozone-depleting substances (ODS, e.g, chlorofluorocarbons). Changes in GHG and ODS concentrations in the atmosphere have been reported to significantly influence the climate system. Under increased GHG emissions, a globally averaged tropospheric warming and stratospheric cooling are expected (e.g., Bell et al., 2010a; IPCC, 2013; Marsh et al., 2013). Increased ODSs that lead to the

ozone hole, on the other hand, has caused a significant climate change in the SH during the last three decades (e.g., Gillett and Thompson 2003; Marsh et al. 2013).

In this thesis, special attention is paid to the effects of the QBO, SST, and anthropogenic (GHG and ODSs) forcings on the DWC variability in the NH. The importance of these natural and anthropogenic forcing factors for tropospheric and stratospheric variability are briefly introduced in the following sections. More detailed descriptions about the QBO and SST variability patterns can also be found in the next chapters.

1.5.1 The Quasi-Biennial Oscillation

The quasi-biennial oscillation (QBO) is the primary mode of variability of the equatorial mean wind in the stratosphere ($\sim$ 16-50 km), which is characterized by downward propagating easterly and westerly wind regimes, with a variable period averaging approximately 28 months (Baldwin et al., 2001). The maximum amplitude is observed in the middle and lower tropical stratosphere, with the easterly phase having larger amplitudes compared to the westerly phase. Figure 1.8a shows the equatorial zonal wind anomalies from 1965 to 1991, from control simulation performed with CESM1(WACCM) (see Chapter 2 for detailed simulation description). QBO first appears in the upper stratosphere and then propagates downward to the lower stratosphere. In the upper stratosphere, the more chaotic zonal wind regime are observed with a period of approximately 6 months, which is mainly attributed to the Semi-Annual Oscillation (SAO). QBO is forced by the interaction of long-period, vertically propagating tropical atmospheric waves (e.g., gravity, inertia-gravity, Kelvin and mixed Rossby-gravity waves) with the zonal mean flow, including (Lindzen and Holton, 1968). These waves transfer momentum in the stratosphere and initiate the downward migration of easterly and westerly wind regimes (Lindzen and Holton 1968; Andrews et al. 1987; Baldwin et al. 2001).

The dependence of the strength of stratospheric polar vortex on the phase of the tropical QBO was first proposed by Holton and Tan (1980). In the so-called Holton-Tan (HT) mechanism, the vortex remains in an undisturbed, colder state when the QBO is in its westerly phase, and favors a disturbed, warmer state during the east phase of the QBO (Holton and Tan 1980, 1982). This is shown exemplarily in Fig 1.8b for QBO west (WQBO) minus QBO east (EQBO) years in a 145-year control simulation performed with the CESM1(WACCM)[1]. The mechanism for this is related to the shifting of the critical line toward the NH subtropics, followed by a poleward displacement of the planetary waveguide during the QBO east phase, which directs more waves to polar regions and decelerates the vortex through enhanced wave-mean flow interactions. In addition, the warmer and more disturbed polar vortex during the QBO east phase are often reflected with a higher frequency of sudden stratospheric warming (SSW) events (Labitzke, 1982).

Lu et al. (2014) further elucidate the H-T mechanism by showing that a formation of a mid-latitude waveguide during the QBO east phase provides a favorable pathway for more upward

[1]Here the QBO is defined as the time series of the zonal wind, averaged between 2.8°S and 2.8°N and between 43 and 51 hPa. Values above 5 m/s represent the WQBO phase, values below -2.5 m/s the EQBO phase.

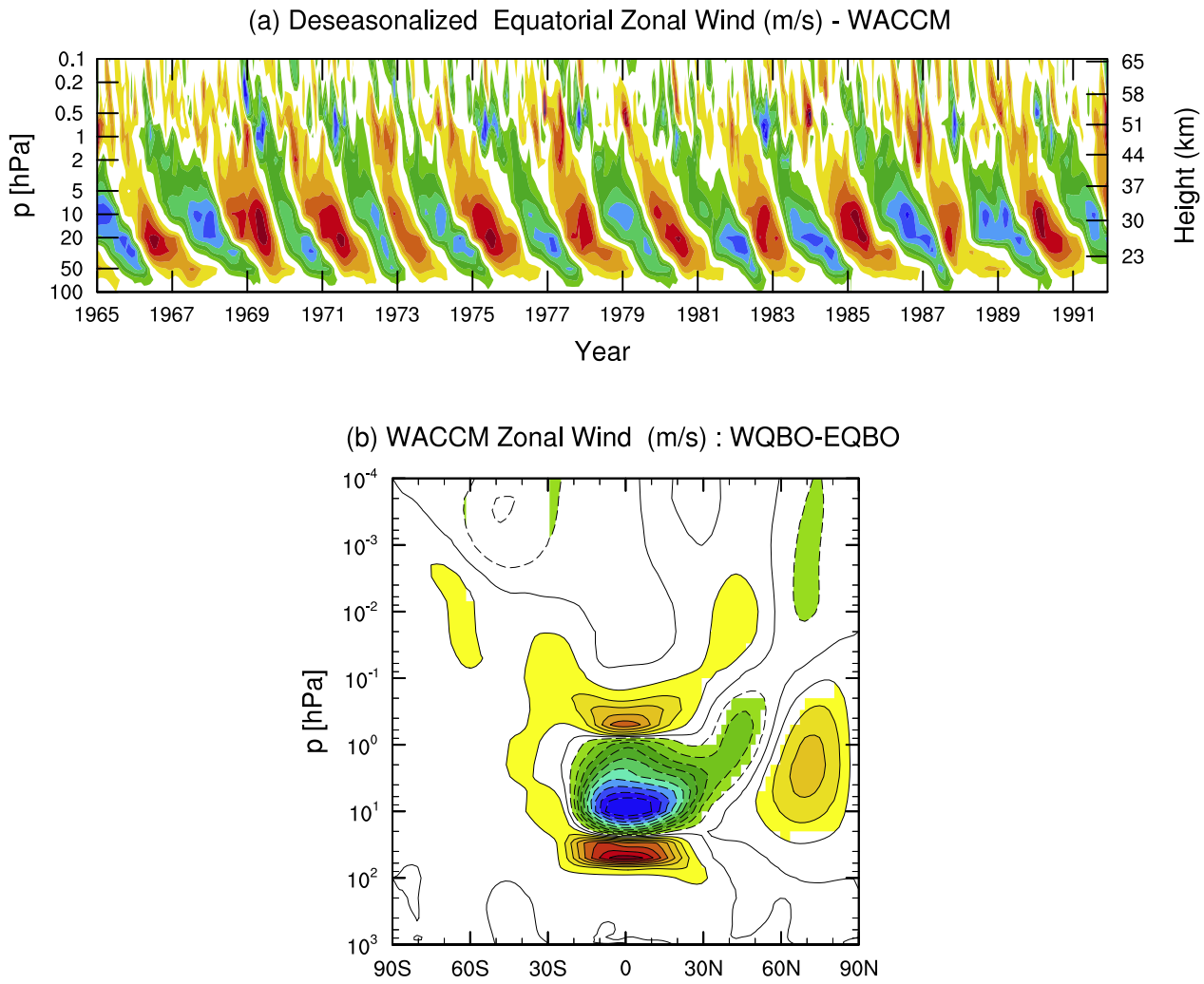

FIGURE 1.8: (a) The time evolution of equatorial winds averaged between 2.8°S to 2.8°N from CESM1(WACCM) 1965 -1991. The seasonal cycle was removed from the data. Contour Interval is 5 m/s. (b) Differences in zonal mean wind (m/s) between westerly and easterly QBO phase in DJF, from control simulation performed with CESM1(WACCM), 1955-2099. Colours indicate statistical significance ($> 95\%$) based on a two-tailed t test. Contour interval is 2 m/s.

(35-50°N, 30-200 hPa) and northward (35-60°N, 20-5 hPa) propagating planetary waves, which eventually dissipate and break in the high-latitude upper to middle stratosphere. However, some studies (e.g., Naoe and Shibata 2010; Garfinkel et al. 2012) argued that the QBO-induced secondary meridional circulation is more important than the subtropical critical line for the polar QBO signals during the east phase of the QBO. The secondary QBO circulation acts as a barrier for planetary wave propagation in the middle to upper stratosphere during the easterly phase, resulting in enhanced wave convergence in the polar stratosphere and therefore, a more disturbed polar vortex. Even though the evidence is inconclusive as to which mechanism dominates the QBO-vortex interaction, both the aforementioned mechanisms contribute to the breakdown of the polar vortex.

The direct impact of the QBO on the tropical and subtropical troposphere involve a modification of temperature and vertical wind shear along the tropopause (e.g., Gray et al. 1992; Ho

et al. 2009; Yoo and Son 2016). In the high latitudes, the QBO impact on the polar stratosphere is mostly indirect, which involves a modulation of the mid latitude planetary wave activity and the subsequent wave-mean flow interaction in the polar stratosphere (e.g., Holton and Tan 1982; Garfinkel et al. 2012). The QBO signal in the NH high latitudes can propagate downward to the surface through the NAM, with a lag of approximately a few weeks (e.g., Baldwin and Dunkerton, 1999; Coughlin and Tung, 2001). Connections have also been found between QBO and regional winter surface climate (e.g., Marshall and Scaife 2009).

In this thesis, the importance of the QBO signal for the stratosphere-troposphere coupling mechanism via DWC will be discussed in Chapter 2. A detailed description of more aspects of the QBO can also be found in Chapter 2.

1.5.2 Sea Surface Temperatures

Sea surface temperature (SST) is the interference between the ocean and the overlying atmosphere. As such, it controls the exchange of heat and gases between the atmosphere and ocean. SST anomalies can affect the atmosphere through altering the flux of latent and sensible heat from the ocean, and thus providing anomalous heating patterns. Like the QBO, SSTs play a significant role in driving stratospheric variability at high latitudes. For example, Figure 1.9 shows the observed upper tropospheric height anomalies during the Northern Hemisphere winter during an El Niño-Southern Oscillation (ENSO) event in the tropical Pacific. The patterns resemble the Pacific North American (PNA) pattern of middle and upper tropospheric height anomalies. The anomaly pattern strongly suggests a train of stationary Rossby waves that emanates from the equatorial source region and follows a great circular path, as predicted by barotropic Rossby wave theory (Horel and Wallace, 1981). In this manner, tropical SST anomalies may generate low-frequency variability in the extratropics.

Several mechanisms have been proposed to explain the impact of SSTs on the variability of the polar stratosphere (e.g., Loon and Labitzke 1987; Manzini et al. 2006; Calvo et al. 2009; Hurwitz et al. 2012; Li and Lau 2013; Omrani et al. 2014). For example, Loon and Labitzke (1987) firstly presented how tropical SSTs can influence the stratospheric polar vortex during the warm phase of ENSO (i.e., El Niño). They showed that warm ENSO events are associated with increased frequency of SSWs, and therefore a warmer and more disturbed polar vortex. This was further confirmed by some general circulation model (GCM) studies (e.g., Hamilton 1993; Manzini et al. 2006) showing that the warmings observed during El Niño years are associated with the amplification of upward planetary wave convergence. More recently, using the global coupled climate model GFDL-CM3, Li and Lau (2013) showed that enhancement or attenuation of the amplitudes of zonal wavenumbers 1 and 2 during ENSO events modulates the frequency of occurrence of stratospheric polar vortex anomalies. By combining ENSO-QBO effects on the vortex state, Calvo et al. (2009) showed that weak and warm polar vortex occur during warm ENSO in the late winter during both QBO phases. In addition to ENSO, other mechanisms including large scale North Atlantic temperature (Omrani et al., 2014; Keenlyside and Omrani, 2014; Omrani et al., 2015),

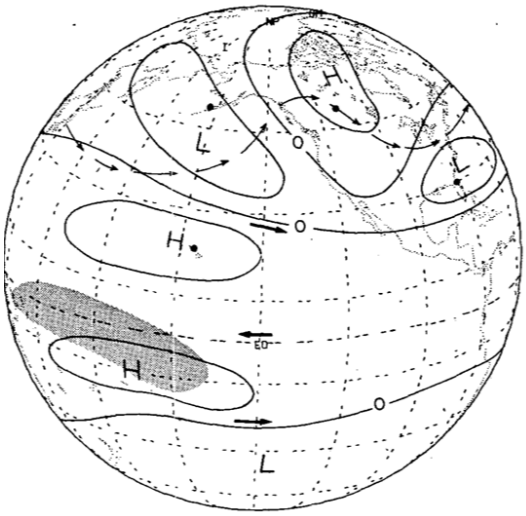

FIGURE 1.9: Global pattern of middle and upper tropospheric geopotential height anomalies (solid) for NH winter during an ENSO event in the tropical Pacific. The anomaly pattern propagates along a great circle path with an eastward component of group velocity as predicted by stationary Rossby wave theory (Horel and Wallace, 1981). Arrows depict a 500-hPa streamline for the anomaly conditions. H and L designate anomalous highs and lows, respectively. Region of enhanced tropical precipitation is shown by shading. Figure from Horel and Wallace (1981).

extra-tropical SST in the Pacific basin (Hurwitz et al., 2012) and sea-ice (Jaiser et al., 2013) are also important for stratospheric variability through ocean-atmosphere coupling mechanisms.

There is a growing body of literature, much of it very recent, showing the importance of SSTs in modifying storm track dynamics and enhancing the tropospheric response to stratospheric forcing. This includes the response to the solar cycle (e.g., Thieblemont et al. 2015; Scaife et al. 2013, and ozone (Ogawa et al., 2015). While the exact dynamical mechanism by which SSTs enhance the tropospheric response needs further study, a possible relevant mechanism is the enhancement of storm tracks and their associated internal variability (the annular modes) in the presence of SST gradients or fronts (e.g., Nakamura et al. 2008; Sampe et al. 2013).

Since SST variability influences the tropospheric wave source and the polar vortex, the coupling to the ocean can therefore influence the strength of DWC between the stratosphere and troposphere. In this thesis, the impact of SST variability on DWC in the NH is investigated in detail in Chapter 2.

1.5.3 Greenhouse Gases and Ozone Depleting Substances

Significant changes in concentrations of key radiative gases in the stratosphere are expected over the 21st century (ozone is expected to increase as the concentrations of ODS decrease back to 1960 levels, and GHGs are expected to continue to increase e.g., IPCC 2013; WMO 2014). Figure 1.10 shows the simulated global column ozone from 1960-2100, carried out using CCM simulations during Validation Activity for the second round (CCMVal-2). The projection represents a mean across the different CCM simulations. It is shown that the continuing slow decline of ODSs, and

the expected further increase of CO_2, will contribute to a recovery of stratospheric ozone (Fig 1.10). In the second half of the century, ozone columns may even exceed historical levels.

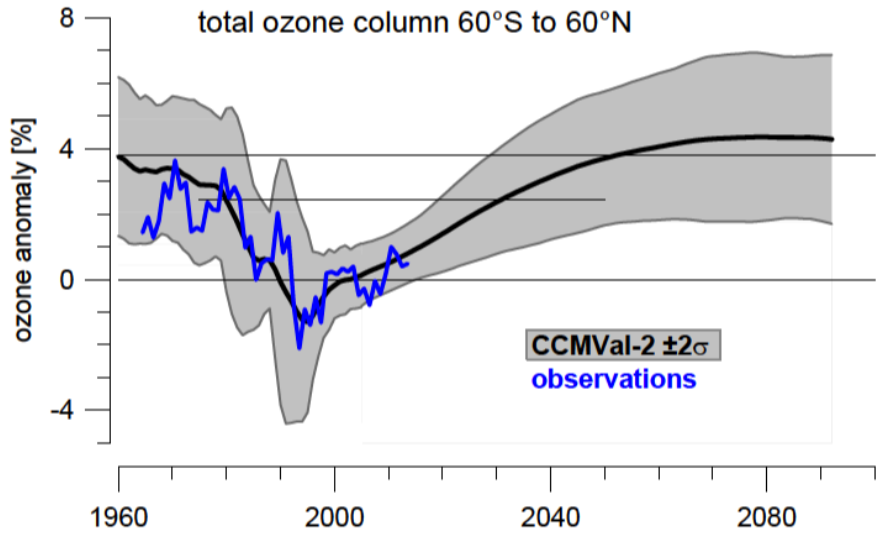

FIGURE 1.10: Simulated and observed evolution of the near global total ozone column. Observations are annual mean anomalies averaged over all available ground- and satellite-based measurements (blue line). Black line and gray range give multi-model mean and ±2 standard deviations of simulated individual model annual mean anomalies for the CCMVal-2 simulations. Figure from WMO (2014).

The role of stratospheric ozone in driving recently observed SH circulation and climate changes over last three decades has been shown by a number of observation and model studies (e.g., Arblaster and Meehl 2006; Karpechko et al. 2008; Butler et al. 2010; McLandress et al. 2010; Polvani et al. 2011; Thompson et al. 2011). By comparing simulations with both ozone and GHG forcings to simulations with GHG forcing alone, Polvani et al. (2011) showed that ozone depletion has been the dominant driver of recently observed atmospheric circulation changes in the SH during summer, with the GHG increases only playing a secondary role. This conclusion is not based solely on this model result, but is substantiated by the large number of observational and modelling studies mentioned above.

Most studies on the impact of GHG and ODS on the polar stratosphere in the NH are mainly addressed in model studies using 21st century GHG and ODS emission scenarios. An early study by Shindell et al. (1998) showed a significant cooling (and strengthening) of the Arctic vortex in the future as GHGs increased, which leads to significant ozone depletion and formation of an Arctic ozone hole. However, more recent simulations with more sophisticated CCMs, which have a better representation of the dynamics and chemistry (and couplings between them), do not show a significant strengthening or formation of Arctic ozone holes during the 21st century (e.g., Austin and Butchart 2003; Eyring et al. 2007). The CCMs also predict a limited impact of increased GHGs on the Antarctic vortex during the 21st century. However, the same simulations all predict an increase in the tropical upwelling as GHGs increase, which has been attributed to changes in subtropical wave forcing (e.g., Garcia and Randel 2008; Oman et al. 2009).

In terms of SSWs, a consensus regarding future changes in the frequency of SSWs could not be achieved due to the wide range of results, ranging from an increase in the frequency of MSWs in the future to a decrease (e.g., Charlton-Perez et al. 2008; Bell et al. 2010a; Mitchell et al. 2012; Ayarzaguena et al. 2013). These discrepancies have also been found in different CCM simulations under the same future scenario (SPARC CCMVal, 2010). A possible reason for these discrepancies might be related to the weak amplitude of future changes in the Arctic polar vortex due to the competition of different contributors (e.g., GHG and ODS), or the biases in reproducing the related processes (SPARC CCMVal, 2010; Mitchell et al., 2012). More recently, Manzini et al. (2014) showed that the majority of the Coupled Model Intercomparison Project Phase 5 (CMIP5) models tends to predict future weakening of the winter stratospheric polar vortex under the extreme emission Representative Concentration Pathways (RCP8.5) scenario. Previous studies have proposed that there are at least two possible mechanisms that elucidate future weakening of the polar vortex associated with increased GHG emissions: (1) it is related to changes in the stratospheric meridional overturning circulation due to changes in the tropospheric wave source (e.g., Butchart and Scaife 2001; Garcia and Randel 2008; Wang and Kushner 2011); (2) changes in the location of critical layers within the subtropical lower stratosphere (e.g., Eichelberger and Hartmann 2005; McLandress and Shepherd 2009; Shepherd and McLandress 2011).

This thesis examines how DWC variability between the stratosphere and troposphere, particularly their seasonality, will change in the future, and how different anthropogenic forcing factors individually impact the occurrence of these events (Chapter 4). In addition, the relative roles of GHG and ODS in controlling the vertical coupling of the stratosphere-MLT system in the SH during the Antarctic ozone hole period will be also investigated in this thesis (Chapter 5).

1.6 Dynamical Coupling of the Stratosphere and Mesosphere

The dynamical linkage between the stratosphere and mesosphere has been discussed with respect to the upward influence of small-scale gravity waves, in recognition of the fact that the source of upward-propagating gravity waves is in the lower atmosphere (e.g., Holton 1983; Andrews et al. 1987; Fritts and Vadas 2008). Gravity waves can be generated by mountain barriers, deep convection, and shear instability of the mean flow. Vertically propagating gravity waves from the troposphere into the mesosphere are strongly dependent on the variation of background stratospheric winds (e.g., Holton 1983; Plumb 2002). Figure 1.11 shows an approximate total non-resolved (gravity) wave drag in the middle atmosphere calculated as a residual of the transformed Eulerian mean (TEM) zonal momentum equation (see for details in Chapter 5). It is shown that the underlying stratospheric winds selectively filter upward propagating gravity waves, leaving only a net westerly drag in the summer mesosphere and a net easterly drag in the winter hemisphere (Holton 1983, Fig 1.11). The breaking of gravity waves in the mesosphere deposits angular momentum and energy on the mean flow, which therefore affect the residual-mean circulation and temperatures there (e.g., Manzini et al. 2003; Yamashita et al. 2010; Li and Lau 2013).

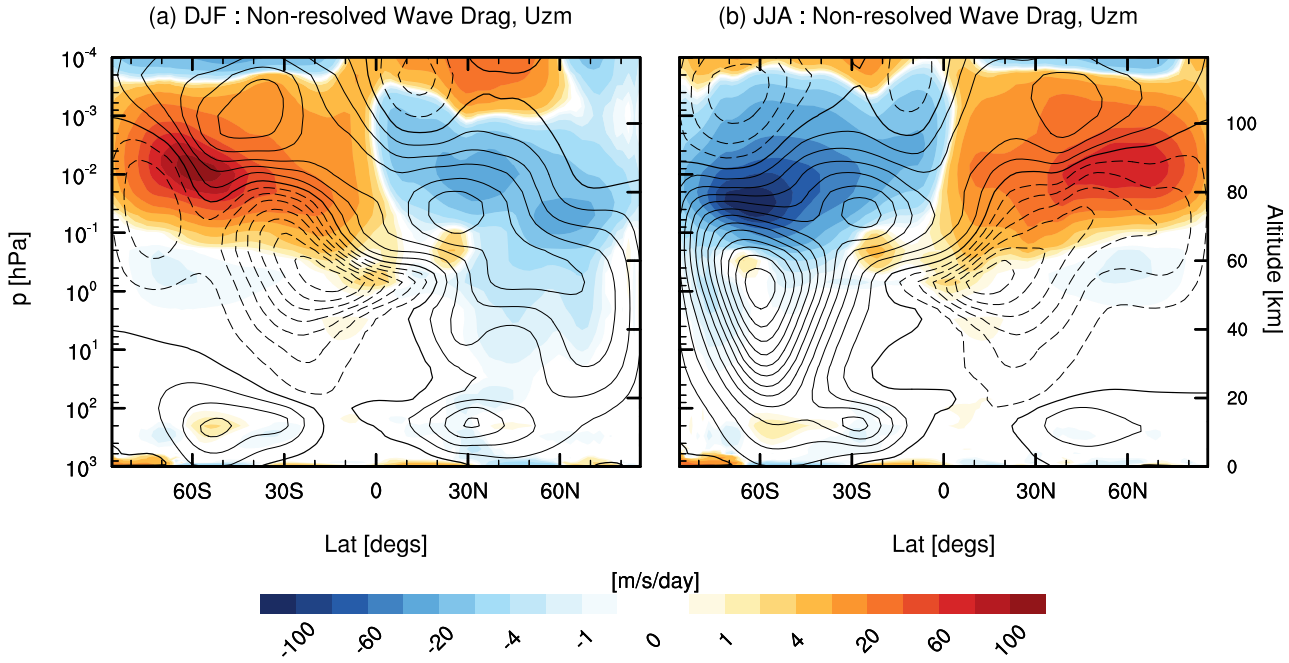

FIGURE 1.11: Total non-resolved wave drag computed as a residual of the TEM zonal momentum equation averaged over (a) December to February (DJF) and (b) June to August (JJA), from the 145-yr control simulation performed with CESM1(WACCM). Contour lines indicate the zonal mean wind climatology. Contour interval is 10 m/s. See detailed formulation in Chapter 5.

The dynamical coupling of the stratosphere and mesosphere can be examined during SSW events (e.g., Walterscheid et al. 2000; Liu and Roble 2002; Cho et al. 2004; Limpasuvan et al. 2012). Previous studies showed that the polar mesospheric temperature and wind during NH winter can change significantly during SSW events (e.g., Walterscheid et al. 2000; Liu and Roble 2002), characterized by mesospheric cooling, deceleration or reversal of the mesospheric zonal wind, and change of the residual circulation. In the SH, the mesospheric cooling and mesospheric jet reversal (Dowdy et al., 2004) were observed above Antarctica prior to the unprecedented major SSW in 2002 (Baldwin et al., 2003). These changes in the mesosphere are likely caused by changes in gravity wave forcing (e.g., Liu and Roble 2002). In addition, the associated changes in the polar mesospheric zonal wind can also affect the wave growth and propagation in the lower atmosphere (e.g., Tung and Lindzen 1979; Liu and Roble 2002; Coughlin and Tung 2005), which in turn affect the course of the SSW event.

Another evidence of the stratosphere-mesospheric coupling can be examined during the Antarctic ozone hole period (e.g., Smith et al. 2010; Lossow et al. 2012; Lubis et al. 2016a). The primary mechanism for this is changes in the propagation of gravity waves due to the strengthening of the stratospheric winds induced by the ozone hole (Smith et al., 2010; Lossow et al., 2012; Lubis et al., 2016a). The ozone hole leads to trends in the lower stratosphere temperature and winds during late spring to early summer. The trend in the stratospheric wind, as simulated in the Whole Atmosphere Chemistry Climate Model (WACCM), affected the propagation of gravity waves into

the mesosphere (Smith et al., 2010). As a result, the model simulations showed a weakening of polar summer mesosphere and a warming summer mesopause due to change in gravity wave interaction. This proposed mechanism by Smith et al. (2010) was later confirmed by other CCM studies (e.g., Lossow et al. 2012; Lubis et al. 2016a) and was verified by observation (Venkateswara Rao et al., 2015). However, until now an explicit interplay between planetary and gravity waves in explaining the enhanced anomalous polar descent from the mesosphere during the Antarctic ozone hole period remains unclear. In addition, it is still not well understood how large the radiative effects from increased GHGs affect the polar MLT response to the ozone hole. The results in this thesis reveal that a proper accounting of both dynamical and radiative effects is required in order to correctly attribute the causes of the polar stratosphere-MLT responses to the Antarctic ozone hole. These results are given in Chapter 5.

1.7 The Advantages of Climate Models

Climate models are sophisticated numerical tools designed to simulate the interactions of the important drivers of climate, and to project the future state of the global climate system (IPCC, 2013). While progress in computer science in the past decades has been rapid, the capability of state-of-the-art climate models to realistically simulate the complex interactions of processes in the Earth's climate system has increased (Reichler and Kim, 2008). State-of-the-art GCMs are not only run in a stand-alone version with many prescribed input datasets, but are also used as a part of Earth System Models, which includes the interactive simulation of the ocean, land surface, and also recently, chemical processes. Figure 1.12 shows the development of climate models over the last 35 years, and shows how the different components were coupled into comprehensive climate models over time. The first climate model was initiated in the mid 1970s (Fig 1.12), when scientists began to measure and interpret increasing atmospheric CO_2. As satellite technology developed, the representations of Earth system processes in climate models are much more extensive and improved, particularly for the radiation and the aerosol cloud interactions and for the treatment of the cryosphere. The representation of the carbon cycle was added to a larger number of models and has been improved since the fourth assessment report (AR4) of the IPCC. A high-resolution stratosphere with interactive chemistry and an enhanced representation of nitrogen effects on the carbon cycle have now been included in many climate models in AR5 (IPCC, 2013).

The Coupled Model Intercomparison Project 5 (CMIP5) [e.g., Taylor et al. 2011], an important input to the AR5, has produced a multi-model data set that is designed to advance our understanding of climate variability and climate change. Building on previous CMIP efforts, CMIP5 includes long-term simulations of 20th century climate and projections for the 21st century and beyond. Previous studies have shown CMIP5 models with a comparably higher lid height or boundary ("high top") have a better representation of the stratosphere and its coupling to the troposphere (e.g., Manzini et al. 2014), while CMIP5 models with a lower lid height ("low top") tend to

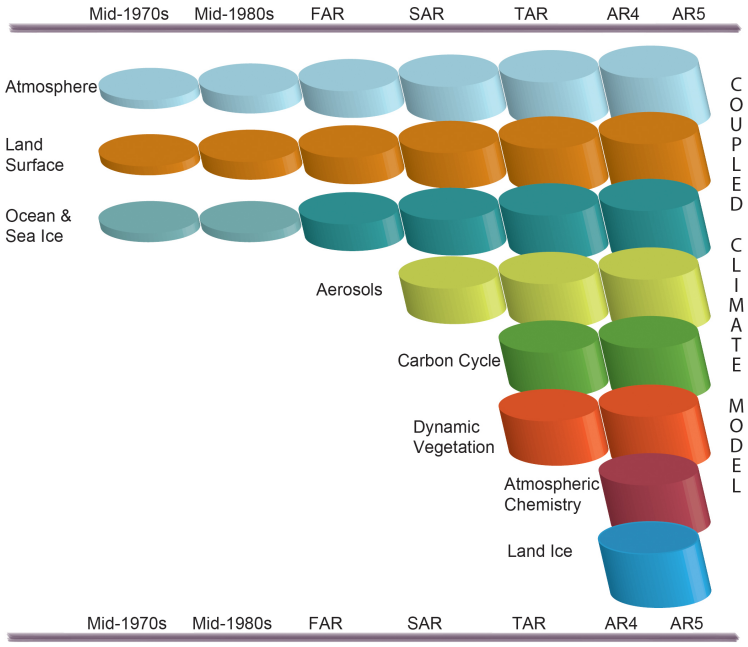

FIGURE 1.12: The development of climate models over the last 35 years showing how the different components were coupled into comprehensive climate models over time. In each aspect (e.g., the atmosphere, which comprises a wide range of atmospheric processes) the complexity and range of processes has increased over time (illustrated by growing cylinders). Note that during the same time the horizontal and vertical resolution has increased considerably. Figure from (IPCC, 2013).

underestimate stratospheric variability on daily and interannual time scales (e.g., Charlton-Perez et al. 2013).

More recently, sophisticated climate models with interactive atmospheric chemistry (CCMs) have been developed to improve representation of the middle atmosphere and ozone evolution. CCMs are a new generation of climate models that include a fully resolved stratosphere with interactive radiative, chemical and dynamical processes (e.g., Eyring et al. 2006; SPARC CCMVal 2010). One of advantages of CCMs is their ability to simulate the impact of aerosols and chemical processes on atmospheric dynamics and radiation, which are important for producing a realistic middle atmosphere mean state and variability. Up to now, simulations with coupled ocean-atmosphere CCMs are very limited. One of the most powerful models, such as the NCAR's Community Earth System Model (CESM), now have the capability of simulating a broad range of atmospheric processes, including their interaction with other Earth's system components (land, ocean, and sea-ice). In this model, the interactive chemistry modules are integrated within the Whole Atmosphere Community Climate Model (WACCM). Previous studies have shown that CESM1(WACCM) are able to simulate a realistic middle atmosphere mean state and variability (Marsh et al. 2013; Richter et al. 2008, respectively). In this thesis, the CESM1(WACCM) was employed for all simulations.

One of the advantages of climate models is their ability to perform multiple simulation experiments (i.e., ensemble members) using different forcing scenarios (e.g., different initial and

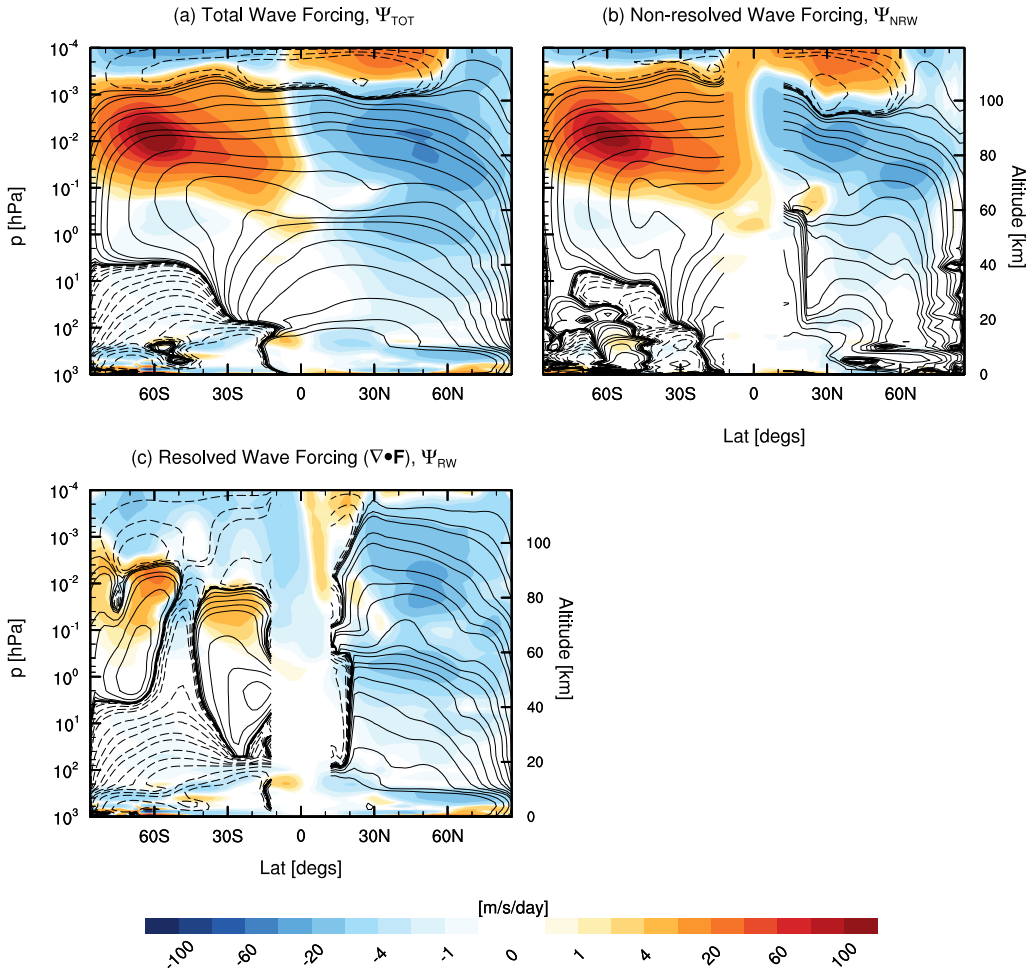

FIGURE 1.13: (a) DJF-mean directly calculated mass streamfunction and (b-c) the downward-control streamfunction from the contribution of different wave drags via downward control principle, calculated from CESM1(WACCM) control simulation (1955-2099). Colour shadings indicate the corresponding wave forcing. Tropical latitudes are masked as the downward-control principle is not applicable here. Solid lines indicate clockwise movement, while dashed lines indicate counterclockwise movement of air parcels. See detailed formulations in Chapter 5.

boundary conditions) and hence increase the robustness of the results. The use of a climate model also makes it possible to study the influence of natural and anthropogenic forcing factors on the climate system, and the coupling between different layers in the atmosphere. This can be done by performing multiple sensitivity experiments, where single processes or factors are switched on or off, so that the importance of specific phenomenon or processes that may interact in a complex or non-linear way in the system can be elucidated. In this thesis, a set of CESM1(WACCM) simulations with different forcing set-ups has been designed and analyzed to isolate the effects of different forcing factors.

Another advantage of climate models is the ability to simulate the atmospheric circulation and variability at the higher altitudes (e..g, the middle and upper atmosphere), which cannot be analyzed using the available observational records. For example, Fig 1.13 shows the DJF-mean

mass streamfunction Ψ (ϕ, z) of the residual circulation, for (a) total wave drag and (b-c) the contribution of different wave drags via the downward control principle (see in details in Lubis et al. 2016a). Using climate model simulation, the mesospheric transport from pole to pole can be quantified as a result of the equatorward pumping in the summer mesosphere induced by westerly wave drag, and the poleward pumping in the winter hemisphere induced by easterly wave drag. Since a significant impact of the middle and upper atmosphere on the lower atmosphere has been identified in the previous studies (e.g., Baldwin and Dunkerton 2001; Becker 2012; Limpasuvan et al. 2012; Lubis et al. 2016a), the interactive simulation of processes taking place in the middle and upper atmosphere should be considered. Therefore, for this thesis all experiments have been performed with the CESM1(WACCM) model, which has a vertical model domain extending upward to 5 x 10^{-6} hPa ($\sim$140 km).

1.8 Scientific Questions of This Thesis

This thesis investigates processes controlling variability of the stratospheric polar vortex and the effects of this variability on ozone and circulations in the troposphere and mesosphere. In the first part, new aspects of the stratospheric-troposphere coupling mechanism via downward planetary wave reflection is investigated in detail. This includes investigation of the effects of different natural and anthropogenic forcing factors, like the QBO, SSTs, GHGs, and ODSs, on the variability DWC between the stratosphere and troposphere, and the associated impacts for the ozone levels and downward coupling to the troposphere. In the last part of the thesis, detailed mechanisms of the vertical coupling between the stratosphere and the MLT in the SH during the Antarctic ozone hole condition is investigated. The following questions are addressed in the coming chapters, which are all reprints of publications accepted in or to be submitted to scientific journals:

- How do various natural forcing factors, like the QBO and SST variability, contribute to the variability of DWC between the stratosphere and troposphere? How do these factors affect the downward influence of DWC in the troposphere? What is a dominant feedback mechanism responsible for the poleward shift of the tropospheric jet during DWC events? (Chapter 2)
- What is the impact of DWC on the residual circulation and stratospheric temperatures in the Arctic? How is this related to ozone levels? (Chapter 3)
- What is the effect of climate change on the variability of DWC in the future? Do future changes in DWC influence the troposphere-surface system? (Chapter 4)
- What are the responses of the polar mesosphere and lower thermosphere (MLT) coupled system to the Antarctic ozone hole? What are the roles of resolved and non-resolved wave drag, as well as radiative forcing on the MLT temperature responses? What are the dynamical mechanisms responsible for maintaining the downward propagation of zonal wind anomalies in the MLT? (Chapter 5)

This thesis will answer these questions using both reanalysis datasets – which are considered to provide a good approximation to the real world – and a series of climate simulations using the CESM1(WACCM) model. All model simulations used in this work were run with an interactive ocean/sea ice and an interactive chemistry module, and integrated over longer time periods (about 145 years). To study the relative importance of natural and anthropogenic forcings on the stratospheric variability and climate system, each forcing factor, like the QBO, SST, GHG and ODS, are separately simulated by switching on/off the corresponding factor in the model configurations. Currently, only one ensemble per CESM1(WACCM) experiment was performed, as performing separate simulations for each type of forcings with interactive ocean and interactive atmospheric chemistry up to the lower thermosphere is computationally very expensive. In addition, several 40-year timeslice simulations with different combinations of ODS and GHG forcings were also performed.

All simulations have been performed in the working group of Prof. Matthes, using the German Climate Computing Centre [Deutsches Klimarechenzentrum (DKRZ)], Hamburg and the NEC-HPC Linux Cluster at Kiel University, Kiel. The timeslice simulations with different combinations of ODS and GHG forcings, have been performed by the author as part of the project in collaboration with Tel Aviv University, Israel. Details of the model and the setups of the simulations can be found in the respective chapters of this thesis.

Chapter 2

Influence of the Quasi-Biennial Oscillation and Sea Surface Temperature Variability on Downward Wave Coupling in the Northern Hemisphere

This chapter examines the influence of natural forcing factors, like the QBO and SST variability, on the DWC between the stratosphere and troposphere, and its subsequent influences on surface climate patterns. In this chapter, a key mechanism for the stratosphere- troposphere response to the DWC is highlighted.

A suite of sensitivity experiments with the fully-coupled CESM1(WACCM) model were performed and analyzed by systematically switching the corresponding factors on and off. The impact of the QBO and SSTs variability on DWC is presented by first discussing their influences on the background winds, the seasonal planetary wave-coupling correlation and the seasonal variation of wave geometries. In addition, the influence of these forcing factors on the tropospheric impact of DWC is examined by using a metric based on stratospheric heat flux extremes.

This chapter is a reprint of **Lubis, S., K. Matthes, N. Omrani, N. Harnik, and S. Wahl, 2016: Influence of the Quasi-Biennial Oscillation and Sea Surface Temperature Variability on Downward Wave Coupling in the Northern Hemisphere. J. Atmos. Sci. 73, 1943-1965, doi: 10.1175/JAS-D-15-0072.1**.

The authors' contributions to this publication are as follows:

- S. Lubis contributed to ideas, performed all the analyses, produced all figures and wrote the manuscript.
- K. Matthes initiated the study and model experiments, contributed to ideas and discussions on the analysis.
- N-E. Omrani and N. Harnik contributed with ideas and discussion on the analysis and with comments on the manuscript.

- S. Wahl contributed with comments on the manuscript and extended the three model simulations.

Influence of the Quasi-Biennial Oscillation and Sea Surface Temperature Variability on Downward Wave Coupling in the Northern Hemisphere

SANDRO W. LUBIS

GEOMAR Helmholtz Centre for Ocean Research Kiel, Kiel, Germany

KATJA MATTHES

GEOMAR Helmholtz Centre for Ocean Research Kiel, and Christian-Albrechts Universität zu Kiel, Kiel, Germany

NOUR-EDDINE OMRANI

Geophysical Institute, University of Bergen, and Bjerknes Centre for Climate Research, Bergen, Norway, and GEOMAR Helmholtz Centre for Ocean Research Kiel, Kiel, Germany

NILI HARNIK

Department of Geophysical, Atmospheric and Planetary Sciences, Tel Aviv University, Tel Aviv, Israel, and Department of Meteorology, Stockholm University, Stockholm, Sweden

SEBASTIAN WAHL

GEOMAR Helmholtz Centre for Ocean Research Kiel, Kiel, Germany

(Manuscript received 6 March 2015, in final form 24 January 2016)

ABSTRACT

Downward wave coupling occurs when an upward-propagating planetary wave from the troposphere decelerates the flow in the upper stratosphere and forms a downward reflecting surface that redirects waves back to the troposphere. To test this mechanism and potential factors influencing the downward wave coupling, three 145-yr sensitivity simulations with NCAR's Community Earth System Model [CESM1(WACCM)], a state-of-the-art high-top chemistry–climate model, are analyzed. The results show that the quasi-biennial oscillation (QBO) and SST variability significantly impact downward wave coupling. Without the QBO, the occurrence of downward wave coupling is significantly suppressed. In contrast, stronger and more persistent downward wave coupling occurs when SST variability is excluded.

The above influence on the occurrence of downward wave coupling is mostly due to a direct influence of the QBO and SST variability on stratospheric planetary wave source and propagation. The strengths of the tropospheric circulation and surface responses to a given downward wave coupling event, however, behave differently. The surface anomaly is significantly weaker (stronger) in the experiment with fixed SSTs (without QBO), even though the statistical signal of downward wave coupling is strongest (weakest) in this experiment. This apparent mismatch is explained by the differences in the strength of the synoptic-scale eddy–mean flow feedback and the possible contribution of SST anomalies in the North Atlantic during the downward wave coupling event. The weaker synoptic-scale eddy–mean flow feedback and the absence of the positive NAO-related SST-tripole pattern in the fixed SST experiment are consistent with a weaker tropospheric response to downward wave coupling. The results highlight the importance of synoptic-scale eddies in setting the tropospheric response to downward wave coupling.

Supplemental information related to this paper is available at the Journals Online website: http://dx.doi.org/10.1175/JAS-D-15-0072.s1.

Corresponding author address: Sandro W. Lubis, GEOMAR Helmholtz Centre for Ocean Research Kiel, Düsternbrooker Weg. 20, 24105 Kiel, Germany.
E-mail: slubis@geomar.de

DOI: 10.1175/JAS-D-15-0072.1

1. Introduction

The vertical transport of energy via planetary-scale waves, forced by orography and land–ocean heating asymmetries, represents an important source of mutual dynamic coupling between the stratosphere and troposphere. The waves transport total eddy momentum and heat fluxes and therefore lead to a deviation of the stratospheric mean state from radiative equilibrium. An intensification of these planetary-scale waves occurs in winter, in the presence of westerly winds weaker than a critical value that depends on the horizontal scale of the waves (Charney and Drazin 1961; Eliassen and Palm 1961; Matsuno 1970). The variability of the stratospheric polar vortex during winter is primarily driven by the interaction between tropospheric forced planetary waves and the stratospheric mean flow. The strength of the polar vortex is further determined by a combination of natural and anthropogenic forcings, such as the quasi-biennial oscillation (QBO) of equatorial stratospheric winds, variations in sea surface temperatures (SSTs), volcanic eruptions, the 11-yr solar cycle, and anthropogenic emissions (e.g., Holton and Tan 1980; van Loon and Labitzke 1987; Robock 2000; Gray et al. 2010; Schimanke et al. 2013).

The dependence of the strength of stratospheric polar vortex on the phase of the tropical QBO was first proposed by Holton and Tan (1980). In the so-called Holton–Tan (HT) mechanism, the vortex remains in an undisturbed, colder state when the QBO is in its westerly phase and favors a disturbed, warmer state during the east phase of the QBO. This is related to the shifting of the critical line toward the Northern Hemisphere (NH) subtropics, followed by a poleward displacement of the planetary waveguide during the QBO east phase, which directs more waves to polar regions and decelerates the vortex through enhanced wave–mean flow interactions. The warmer and more disturbed polar vortex during the QBO east phase is often reflected with a higher frequency of sudden stratospheric warming (SSW) events (Labitzke 1982). Lu et al. (2014) recently illustrated this process by showing that a formation of a midlatitude waveguide during the QBO east phase provides a favorable pathway for more upward- (35°–50°N, 30–200 hPa) and northward- (35°–60°N, 20–5 hPa) propagating planetary waves, which eventually dissipate and break in the high-latitude upper to middle stratosphere. However, Garfinkel et al. (2012) argue that the QBO-induced secondary meridional circulation is more important than the subtropical critical line for the polar QBO signals during the east phase of the QBO. The secondary QBO circulation acts as a barrier for planetary wave propagation in the middle to upper stratosphere during the easterly phase, resulting in enhanced wave convergence in the polar stratosphere and therefore a more disturbed polar vortex. Even though the evidence is inconclusive as to which mechanism dominates the QBO–vortex interaction, both above-mentioned mechanisms contribute to the probability of the breakdown of the vortex.

The SST variations can impact the stratospheric polar vortex through different mechanisms. For example, van Loon and Labitzke (1987) first presented how tropical SSTs can influence the stratospheric polar vortex during the warm phase of ENSO (i.e., El Niño). They showed that warm ENSO events are associated with increased frequency of SSWs and therefore a warmer and more disturbed polar vortex. This was further confirmed by some general circulation model (GCM) studies (e.g., Hamilton 1993; Manzini et al. 2006) showing that the warmings observed during El Niño years are associated with the amplification of upward planetary wave convergence. More recently, using the global coupled climate model GFDL CM3, Li and Lau (2013) showed that enhancement or attenuation of the amplitudes of zonal wavenumbers 1 and 2 during ENSO events modulates the frequency of occurrence of stratospheric polar vortex anomalies. By combining ENSO–QBO effects on the vortex state, Calvo et al. (2009) showed that weak and warm polar vortices occur during warm ENSO in the late winter during both QBO phases. In addition to ENSO, other mechanisms including large-scale North Atlantic temperature (Omrani et al. 2014; Keenlyside and Omrani 2014; Omrani et al. 2016), extratropical SST in the Pacific basin (Hurwitz et al. 2012), and sea ice (Jaiser et al. 2013) are also important for stratospheric variability through ocean–atmosphere coupling mechanisms.

Over the past two decades, the role of downward-propagating planetary waves, in particular the wave reflection, has been continuously investigated to elucidate mechanisms for stratosphere–troposphere coupling (e.g., Harnik and Lindzen 2001; Perlwitz and Harnik 2003; Harnik 2009; Shaw and Perlwitz 2013). The so-called downward wave coupling (DWC) describes the stratospheric downward wave reflection that impacts the troposphere. DWC occurs when upward-propagating planetary waves from the troposphere decelerate the flow in the upper stratosphere and form a negative meridional potential vorticity (PV) gradient and a vertical reflecting surface as well as a vertically bounded high-latitude meridional waveguide. During NH winter, reflecting surfaces typically develop above 10 hPa on a weekly time scale. They act as a stratospheric barrier for upward-propagating waves. In the high-latitude stratosphere, a meridional waveguide forms at around 50°–80°N and further directs downward-propagating stratospheric waves toward the troposphere (Harnik

and Lindzen 2001; Shaw et al. 2010). Recently, Shaw and Perlwitz (2013) defined a wave coupling index based on stratospheric eddy meridional wave-1 heat flux to examine the impact of DWC on the NH winter troposphere (see also Dunn-Sigouin and Shaw 2015). They show that multiple stratospheric wave reflection events are associated with a strong polar vortex and a positive phase of a North Atlantic–like oscillation in the troposphere. However, the factors which influence DWC and its subsequent impacts on the tropospheric circulation are still unclear. We try to address this question within this study.

The goal of the present study is to examine to what extent natural forcing factors, such as the QBO and SST variability, influence the occurrence and variability of DWC. For that purpose, we perform a set of sensitivity experiments with the fully coupled Community Earth System Model, version 1.0.2, with the Whole Atmosphere Community Climate Model [CESM1(WACCM)], where we systematically switch on and off the influence of the QBO or the interactively calculated SSTs and sea ice. We also examine how these natural forcing factors affect the impact of DWC on the tropospheric circulation. The paper is organized as follows. A description of the model, experiments, reanalysis data, and our statistical–dynamical approach are provided in section 2. In section 3, we discuss the general assessment of DWC variability in CESM1(WACCM) and compare it to reanalysis data, while section 4 deals with the response of the mean climate behavior and DWC characteristics with respect to the QBO and variable SSTs and sea ice. In section 5, the implication of DWC for the troposphere–surface system is examined based on extreme negative stratospheric wave-1 heat flux (DWC) events. We also discuss the differences of tropospheric changes associated with DWC in the absence of the QBO and SST variability. We close in section 6 with a summary of our results.

2. Data, model experiments, and analysis

a. Model, experiments, and reanalysis data

NCAR's Community Earth System Model, version 1.0.2, is a fully coupled climate model consisting of atmosphere [optionally NCAR's Community Atmosphere Model (CAM) or WACCM], ocean (POP), land (CLM), and sea ice (CICE) components, based on the Community Climate System Model (CCSM4; Gent et al. 2011). The atmospheric component of CESM used in this study is the Whole Atmosphere Community Climate Model, version 4 (Marsh et al. 2013), a high-top chemistry–climate model, which is an extension of NCAR's Community Atmosphere Model. WACCM has a horizontal resolution of 1.9° latitude × 2.5° longitude and 66 vertical levels from the surface to the lower thermosphere (~140 km and ~5.1×10^{-6} hPa). Interactive chemistry is calculated with the 3D chemical transport Model of Ozone and Related Chemical Tracers, version 3 (MOZART-3; Kinnison et al. 2007). It includes the O_x, NO_x, HO_x, ClO_x, and BrO_x chemical families, along with CH_4 species within the chemical and physical processes in the troposphere through the lower thermosphere (i.e., fully interactive and fully coupled chemistry and physics). Additional processes important for the mesosphere and lower thermosphere, such as ion chemistry, auroral processes, extreme ultraviolet, and non–local thermodynamic equilibrium radiation are also implemented (Marsh et al. 2007).

To investigate the influence of the QBO and the SST variability on DWC, three CESM1(WACCM) simulations were performed by systematically switching on and off particular forcing factors (Table 1). The control simulation (CTL) covers the period 1955–2099 (i.e., a 145-yr control run). This experiment is run with an interactive ocean and a QBO nudging in the tropical stratosphere between 22°S and 22°N following Matthes et al. (2010). The effects of QBO nudging in CESM1 (WACCM) on extratropical and high-latitude dynamics resemble observations. In particular, the planetary wave propagation and residual circulation responses to the forcing from the equatorial QBO agree well with ERA-40 (Hansen et al. 2013). The QBO is projected into the future by developing Fourier coefficients for the QBO time series based on climatological values of Giorgetta[1] from the past records (1954–2004). To exclude external anthropogenic influences, all anthropogenic forcings, such as greenhouse gases (GHGs), ozone depleting substances (ODS), or airplane emissions were kept constant at the 1960s level (i.e., annual cycle values were repeated for the whole modeling time).

The second simulation is the fixed (noninteractive) SST–sea ice experiment (FSST), which spans the period from 1955 to 2099 (145-yr simulated period). The FSST is the same as the CTL, except the underlying SSTs and sea ice are held constant for each year based on climatological monthly varying SSTs and sea ice of the CTL experiment. This simulation therefore neglects any effects of interannual and intraseasonal varying SSTs–sea ice and excludes any atmosphere–ocean–sea ice feedbacks. While SST variability influences the stratospheric planetary wave source, and thus the strength of DWC, the coupling to the ocean and sea ice can influence the response of the troposphere to a given DWC event. The

[1] http://www.pa.op.dlr.de/CCMVal/Forcings/qbo_data_ccmval/u_profile_195301-200412.html.

TABLE 1. Summary of CESM experiments and ERA data.

Experiment	Period	QBO	GHGs + ODSs	SSTs–sea ice
CTL	1955–2099 (145 yr)	Nudged	Fixed at 1960s level	Interactively
FSST	1955–2099 (145 yr)	Nudged	Fixed at 1960s level	Fixed[a]
NOQBO	1955–2099 (145 yr)	No	Fixed at 1960s level	Interactively
All forcing	1958–2005 (48 yr)	Nudged	Obs	Interactively
ERA	1958–2005 (48 yr)[b]	Obs	Obs	Obs

[a] SSTs follow the climatological cycle of the CTL.
[b] Includes 1958–1978 from the ERA-40 and 1979 onward from the ERA-Interim.

third simulation uses the same settings as CTL but without the QBO nudging for the 145-yr simulated period (1955–2099) (NOQBO). The NOQBO experiment exhibits constant easterly winds in the equatorial stratosphere with an amplitude of about $-10\,\mathrm{m\,s^{-1}}$. Finally, the comparison of the CTL with the NOQBO and the FSST experiments allows us to investigate the relative role of the QBO and the SST variability on DWC and its subsequent impacts on the troposphere.

To evaluate how realistic the DWC is in CESM1 (WACCM), daily 3D geopotential, wind, and temperature fields from the combined European Centre for Medium-Range Weather Forecast (ECMWF) ERA-40 (Uppala et al. 2005) and the ERA-Interim (Dee et al. 2011) (hereinafter referred to as ERA) from January 1958 to December 2005 (48 yr) and altitudes from the surface to 1 hPa (23 vertical pressure levels) were used (see Table 1). The CESM simulation for this comparison employs the most realistic setting [i.e., natural and anthropogenic forcings (for details see Table 1)]. The time-varying anthropogenic forcings (GHG and ODS) were obtained from the observational records until 2005. This simulation is referred to as "all forcings" in the following. Currently, only one ensemble per CESM experiment was performed, as performing separate simulations for each type of forcing with interactive ocean and interactive atmospheric chemistry up to the lower thermosphere is computationally very expensive.

b. Statistical–dynamic diagnosis

In this study, the impact of the QBO and SST variability on DWC are examined by using both statistical and dynamical approaches, which include the wave geometry diagnostic, the time-lagged singular value decomposition (SVD), and the transformed Eulerian mean (TEM) diagnostics.

1) WAVE GEOMETRY

To diagnose the wave propagation characteristics of a two-dimensional zonal-mean basic state, the wave geometry diagnostic of Harnik and Lindzen (2001) was employed in this study. Principally, this diagnostic partitions the widely used refractive index (n_r^2; e.g., Charney and Drazin 1961; Matsuno 1970) into vertical (m) and meridional (l) wavenumber components by solving the conservation of the quasigeostrophic potential vorticity (QGPV) equation in spherical coordinates. This separation provides the barriers of wave propagation in the vertical and meridional directions. For a nonisothermal atmosphere, a general n_r^2 decomposition for waves with a zonal wavenumber k and a phase speed c is written as follows (for details, see Harnik and Lindzen 2001):

$$n_r^2 \equiv \frac{N^2}{f^2}\left\{\frac{\overline{q}_y}{\overline{u}-c} - k^2 + f^2\frac{e^{z/2H}}{N}\frac{\partial}{\partial z}\left[\frac{e^{-z/H}}{N}\frac{\partial}{\partial z}(e^{z/2H}N)\right]\right\} \equiv m^2 + \frac{N^2}{f^2}l^2, \tag{1}$$

where $\overline{q}_y$ is the meridional gradient of zonal-mean PV, calculated following Matsuno (1970) as

$$\overline{q}_y \equiv \beta - \frac{1}{a^2}\frac{\partial}{\partial\phi}\left[\frac{1}{\cos\phi}\frac{\partial(\overline{u}\cos\phi)}{\partial\phi}\right] - \frac{f^2}{\rho_0}\frac{\partial}{\partial z}\left(\frac{\rho_0}{N^2}\frac{\partial\overline{u}}{\partial z}\right). \tag{2}$$

Expansion of the last term on the left-hand side of Eq. (2) gives:

$$-\frac{f^2}{\rho_0}\frac{\partial}{\partial z}\left(\frac{\rho_0}{N^2}\frac{\partial\overline{u}}{\partial z}\right) \equiv \left(\frac{f^2}{HN^2} + \frac{f^2}{N^4}\frac{\partial N^2}{\partial z}\right)\frac{\partial\overline{u}}{\partial z} - \frac{f^2}{N^2}\frac{\partial^2\overline{u}}{\partial z^2}, \tag{3}$$

where N^2 is the buoyancy frequency, and β is the variation of the Coriolis parameter with latitude. The results of an n_r^2 decomposition are interpreted similarly as discussed by Charney and Drazin (1961) and Matsuno (1970). The waves propagate in the vertical (meridional) direction where $m^2 > 0$ ($l^2 > 0$), are evanescent where $m^2 < 0$ ($l^2 < 0$), and are reflected where $m^2 = 0$ ($l^2 = 0$). It is worth noting that if the waves propagate with the background flow ($\overline{u} = c$), then there exist critical

surfaces (l^2, $m^2 \to \infty$) that tend to absorb or over-reflect the propagating waves[2] (e.g., McIntyre and Palmer 1983). To retain pure real–imaginary wavenumber quantities, all averages in time and space were calculated by squaring the wavenumber and then taking a square root of the respective values [e.g., $\langle l \rangle = \text{sign}(\langle l^2 \rangle) \times (|\langle l^2 \rangle|)^{1/2}$].

2) TIME-LAGGED SINGULAR VALUE DECOMPOSITION

To study the linear statistical relationship between tropospheric and stratospheric geopotential height associated with a single zonal wavenumber, a time-lagged SVD of the coupled fields was used as in Perlwitz and Harnik (2003). This technique identifies pairs of leading EOFs and PCs, which account for a fraction of the covariance between two single zonal waves jointly (for details see Perlwitz and Harnik 2003). The daily temporal expansion coefficients were calculated as the weighted linear projection of data at each grid point onto their corresponding EOFs, as follows (Bretherton et al. 1992):

$$A^k(t) = \sum_{i=1}^{M_p} V_i^k P_i(t) = \mathbf{V}_k^{\mathrm{T}} P(t) \quad \text{and} \tag{4}$$

$$B^k(t+\tau) = \sum_{j=1}^{M_s} U_j^k S_j(t+\tau) = \mathbf{U}_k^{\mathrm{T}} S(t+\tau). \tag{5}$$

Here, P and S denote tropospheric and stratospheric zonal wavenumber-1 geopotential heights (Z-ZWN1), M is number of grid points, and $\mathbf{V}_k$ and $\mathbf{U}_k$ are the left and right singular vectors at mode k, respectively. The time-lagged SVD analysis is repeated for entire seasons with 3-month overlapping periods only for zonal wave 1, as it represents the dominant source of DWC (Perlwitz and Harnik 2003; Shaw et al. 2010). The tropospheric field is held fixed at 500 hPa, and the respective stratospheric levels are shifted in such a way that a negative (positive) time lag indicates that the stratospheric (tropospheric) wave fields are leading.

3) PLANETARY WAVE FORCING OF THE MEAN FLOW

To quantify the drag exerted by planetary-scale waves on the mean flow, the Eliassen–Palm flux (Andrews et al. 1987) and the Plumb 3D wave activity flux (Plumb 1985) in spherical log-pressure coordinates are used also in this study. The detailed formulation is described in the appendix.

[2] In the nonlinear limit, waves undergo cycles of absorption, reflection, or over-reflection near the critical surface when $K^2 \equiv k^2 + l^2 + (f_o^2/N^2)m^2$ increases toward infinity.

3. Evaluation of DWC in CESM1(WACCM)

a. DWC behavior during midwinter

We begin our evaluation with an analysis of DWC in the all-forcings experiment of CESM1(WACCM) from 1958 to 2005 and a comparison to reanalysis data. We first focus on the northern midwinter January–March (JFM) mean, as it represents the most dynamically active season. The background wind is westerly; planetary wave activity is large; thus, its vertical propagation is enhanced (e.g., Charney and Drazin 1961; Lorenz and Hartmann 2003); and therefore dynamical coupling between the stratosphere and the troposphere is largest (e.g., Baldwin and Dunkerton 2001; Perlwitz and Harnik 2003, Shaw et al. 2010).

Figure 1 compares the JFM climatological zonal-mean zonal wind and zonal-mean temperature between the CESM1(WACCM) simulation and ERA. The stratospheric polar night jet in the model is significantly stronger and broader throughout the stratosphere. The midlatitude jet at 1 hPa is about 5 m s^{-1} stronger in the model, and the 20 m s^{-1} isoline reaches further down to 20 km (Fig. 1c). The subtropical tropospheric jet is also about 5 m s^{-1} stronger in the model as compared to reanalysis. Consistent with the positive wind bias in the stratosphere is the cold bias in the polar stratosphere (Figs. 1b,d), which is a common bias in chemistry–climate models (SPARC CCMVal 2010). In addition to the zonal wind, Figs. 1a and 1c also shows the wave geometry; that is, the configurations of meridional waveguide and vertical reflecting surfaces. The shaded areas (unshaded) indicate regions where waves cannot (can) propagate in meridional [l^2(blue)] and vertical [m^2(red)] directions. In general, the wave geometry structure in CESM1(WACCM) is in fairly good agreement with ERA, except that the meridional waveguide in the model is slightly narrower between 45° and 60°N in the troposphere, which may be related to biases in the meridional structure of modeled zonal-mean winds in this region. In the upper stratosphere (above 5 hPa), a vertical reflecting surface appears at around 65°–80°N in the model, which suggest that the configuration of the modeled stratospheric polar night jet during JFM allows downward reflection of planetary waves.

To characterize up- and downward propagation of wave-1 anomalies, correlations from the time-lagged leading SVD mode between wave-1 height fluctuations at a tropospheric pressure level (500 hPa) and four different stratospheric pressure levels (50, 20, 30, and 10 hPa) in both CESM1(WACCM) and ERA data are shown in Fig. 2. This investigation is an example for wave 1, which contributes most to the DWC. Positive lags denote upward wave coupling from the troposphere

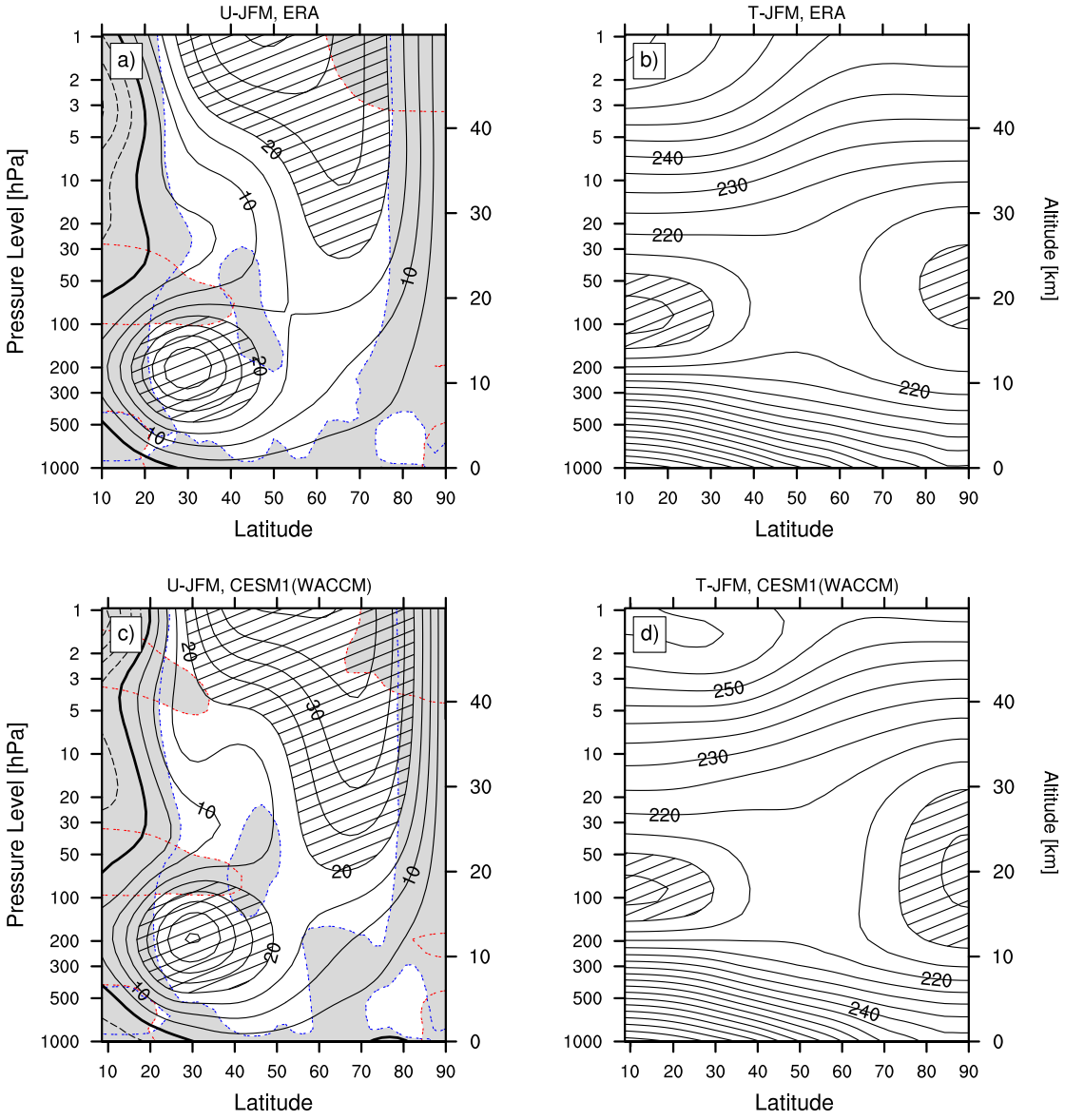

FIG. 1. JFM average of the zonal-mean zonal wind and zonal-mean temperature between 10° and 90°N and 1000 and 1 hPa for the (a),(b) ERA and (c),(d) CESM1(WACCM) from 1958 to 2005. Shading in (a) and (c) indicates regions of wave evanescence in the meridional ($l < 0$) and vertical ($m < 0$) directions. Contour intervals are 5 m s^{-1} and 5 K for wind and temperature, respectively. The regions where the wind (temperature) exceeds 20 m s^{-1} (210 K) are hatched. The red (blue) dashed contours indicate the vertical reflecting surface (meridional waveguide) when $m = 0$ ($l = 0$). The zero contour lines are plotted in thick solid black.

to the stratosphere, whereas negative lags denote downward wave coupling from the stratosphere to the troposphere. The time-lagged SVD correlations in CESM1(WACCM) exhibit a fairly similar twofold-peaked structure as those observed in ERA (Figs. 2a,d). In particular, the maximum positive correlations (i.e., the troposphere leads the stratosphere) occur one day early and are higher than the observed peaks in ERA. This suggests that the simulated upward wave coupling between the troposphere and the stratosphere has a faster vertical group velocity than in ERA. Consistent with the upward wave-energy flux propagation, there is a westward phase tilt with height (Figs. 2c,f; Table 2). Note that the group velocity of a quasi-stationary Rossby wave is tangent to phase lines in a horizontal plane, where phase lines associated with the upward- (downward-) propagating Rossby wave group velocity are tilted westward (eastward) with height (Charney and Drazin 1961). In addition, the associated wave-1 amplitudes at 10 and 500 hPa in the model are larger compared to ERA and therefore are consistent with higher SVD correlation peaks at positive time lags.

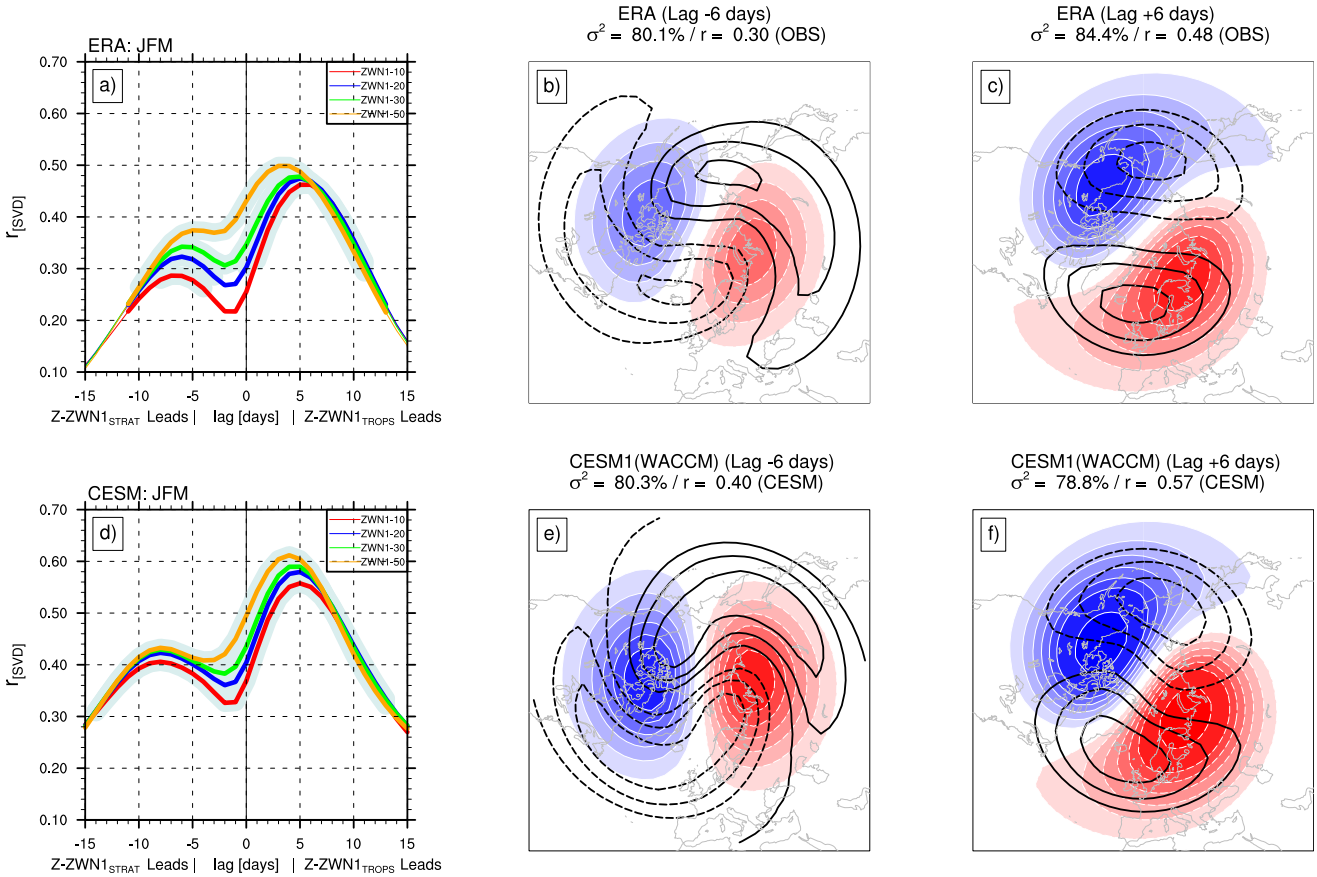

FIG. 2. (left) Lagged correlations of temporal expansion coefficients (a_k, b_k) between the leading wave-1 SVD mode (Z-ZWN1) at 500 hPa (fixed level) and four stratospheric levels [50 (yellow), 30 (green), 20 (blue), and 10 hPa (red)] for (a) ERA and (d) CESM1 (WACCM) during mid–late winter (JFM). The 99% and 95% significance levels are denoted with light gray shading and thicker lines, respectively. (center) Heterogeneous regression patterns at 10 hPa (color shaded) and 500 hPa (contours) associated with downward wave coupling (Z-ZWN1$_{10}$ leads Z-ZWN1$_{500}$ by 6 days) for (b) ERA and (e) CESM1(WACCM) . The contour interval is 30 m (color shading) for Z-ZWN1 at 10 hPa, and 5 m for Z-ZWN1 at 500 hPa. (right) As in (b),(e), but for upward wave coupling (Z-ZWN1$_{500}$ leads Z-ZWN1$_{10}$ by 6 days). The 0-m contour is omitted.

In the period when the stratosphere is leading (negative lags), the correlation peak in CESM1(WACCM) is again higher and the time lag is slightly longer compared to ERA (Fig. 2d). Although there is virtually no separation in correlation peaks at negative time lags for stratospheric levels below 10 hPa in the model, the eastward phase tilt with height consistent with downward flux of wave energy associated with DWC can still be seen in CESM1(WACCM) (Table 2; Fig. 2e). A similar characteristic of DWC signals has also been found in Shaw et al. (2010, their Fig. 7) using the high-top CMAM version. Shaw et al. (2010) argue that no separation in peaks of DWC signals may be caused by the internal dynamical damping processes in the model. In CESM1(WACCM), the amplitudes of the wave-1 pattern associated with DWC in the stratosphere and troposphere are larger compared to ERA, which is again consistent with higher correlations found in the model when the stratosphere is leading (Fig. 2d). In addition, we also applied the statistical and wave geometry diagnostics for wave-2 coupling in ERA and CESM (not shown). While the formation of reflecting surfaces for wave-2 is found during midwinter, we do not find evidence for a second peak in SVD correlations associated with DWC. Perlwitz and Harnik (2003) previously found a similar behavior and argued that this is because of a short propagating period of wave 2 into the midstratosphere (of about 2 days), which makes it hard to separate statistically the downward from the upward wave-2 propagating signals.

In summary, CESM1(WACCM) is able to capture DWC during NH midwinter (JFM). However, there are still small discrepancies in the time lags, phase shifts, and strength of DWC. This could be due to the common model biases in the background circulation which feeds back on the wave dynamics and wave–mean flow interaction (e.g., Charney and Drazin 1961; Lorenz and Hartmann 2003). In particular, the stronger background wind in CESM1(WACCM) (Fig. 1) can be associated

TABLE 2. The phase differences $d\lambda$ at 65°N between the associated SVD wave-1 patterns at 500 hPa (fixed) and various stratospheric levels (50, 30, and 10 hPa) in the ERA and all-forcing experiment from CESM1(WACCM) from 1958 to 2005. Negative (positive) time lag indicates that the stratospheric (tropospheric) wave fields are leading.

		$d\lambda$ (°E)	
Height range (hPa)	Lag (days)	ERA	All forcings
500–10	−6	108.4	114.2
500–30	−5	81.6	90.3
500–50	−4	60.3	53.2
500–10	6	−133.5	−122.7
500–30	5	−102.3	−94.9
500–50	4	−78.1	−75.1

with stronger downward wave activity between the stratosphere and troposphere, as highlighted by Perlwitz and Harnik (2003) and Shaw et al. (2010).

b. Seasonal evolution of DWC

To completely assess the representation of DWC in CESM1(WACCM), we also examine its seasonal evolution by calculating SVD correlations (r_{SVD}) of Z-ZWN1 for corresponding PCs at each time lag for 3-month overlapping periods (Fig. 3). DWC events occur if the r_{SVD} at a negative time lag is highly statistically significant at the 99% level. Compared to ERA, DWC in CESM1 (WACCM) persists throughout the winter (November–March, Fig. 3b) whereas it only occurs between January and March in ERA (Fig. 3a). In addition, the time scales of downward wave propagation in the model are relatively longer, which indicate a slower downward group velocity of Z-ZWN1 from the stratosphere to the troposphere.

To further understand the seasonal evolution of DWC in CESM1(WACCM) in comparison with ERA, we also consider the seasonal evolution of the wave geometry. Figure 4 highlights the climatological seasonal evolution of the meridional wavenumber (l^2) averaged between 16 and 24 km and the vertical wavenumber (m^2) averaged from 60° to 80°N for ERA (Figs. 4a,b) and CESM1 (WACCM) (Figs. 4c,d). In ERA data, a meridional waveguide occurs only from January through March, with a meridional extent from 45° to 75°N (Fig. 4a), whereas in CESM1(WACCM) the meridional waveguide occurs earlier from November through March (Fig. 4c) and is slightly narrower with a meridional extent from 51° to 75°N. This narrower meridional waveguide potentially increases the occurrence of DWC in CESM1(WACCM), as it limits the meridional wave propagation into a subtropical critical surface. In addition, a narrower waveguide also implies the l^2 is larger, and the larger l^2 for a given index of refraction implies a smaller m^2, thus leading to more downward reflection.

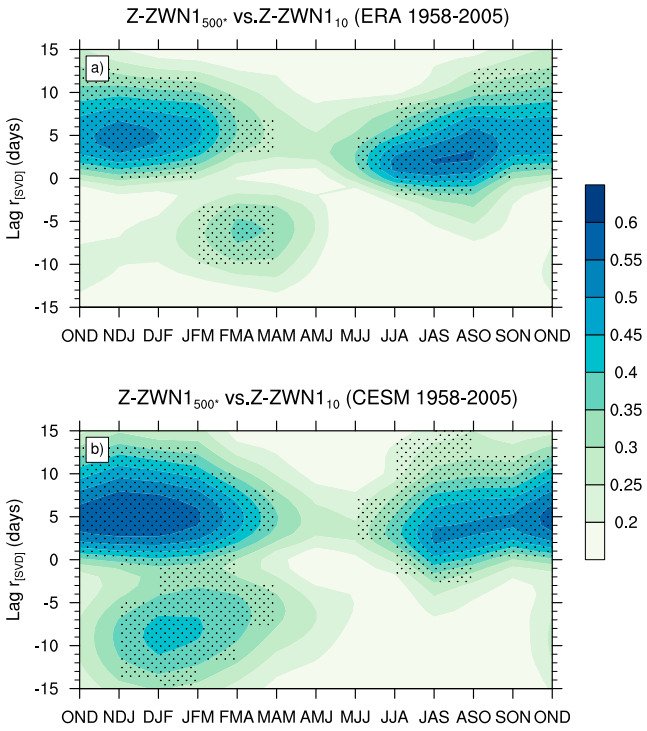

FIG. 3. Three-month overlapping periods of lagged SVD correlations between Z-ZWN1 at 500 and 10 hPa for (a) ERA and (b) CESM1(WACCM) from 1958 to 2005. Black dots represent statistically significant values at the 99% level. A negative (positive) time lag indicates that the stratospheric (tropospheric) wave field is leading.

Stratospheric vertical reflecting surfaces in ERA form in early winter (November–December) and during midwinter (February–March) (Fig. 4b). The vertical reflecting surface is very high in the stratosphere (between 1–3 hPa) in November–December and very low from March onward. This wave geometry evolution is in qualitative agreement with previous finding by Shaw et al. (2010) using a 27-yr ERA dataset (note that about 21 more years of the combined ERA dataset have been included in our study). In contrast to ERA, the stratospheric reflecting surface in CESM1(WACCM) persists from early to late winter (October–November to March–April). The extended meridional waveguide and the longer persistence of vertical reflecting surfaces in CESM1 (WACCM) as compared to ERA are consistent with the extended significant downward wave correlations in Fig. 3b from November through March. However, in October the stratospheric reflecting surface does not coincide with the meridional waveguide. The waves therefore disperse in the meridional direction and get absorbed in the subtropical critical surface, thus causing an absence of DWC signals during OND (Fig. 3b).

To summarize, our results show that the seasonal evolution of DWC in CESM1(WACCM) persists longer compared to ERA. This extension coincides with a

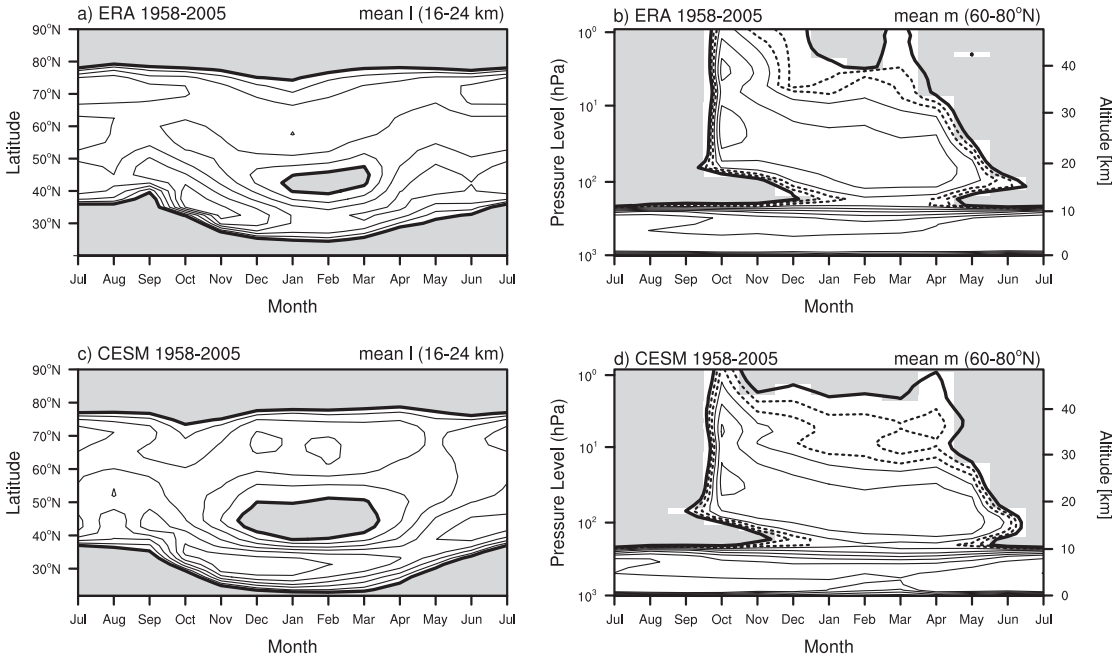

FIG. 4. The climatological seasonal cycle of the meridional and vertical wavenumbers averaged (a),(c) between 16 and 24 km and (b),(d) between 60° and 80°N for ERA and CESM1(WACCM), respectively. The meridional wavenumbers are contoured with 1 (solid) and 0.01 rad^{-1} (thick solid line). For the vertical wavenumber, the contours are shown at 0.01×10^{-5} (thick line), 0.02×10^{-5} and 0.04×10^{-5} (dashed lines), and $0.06–0.3 \times 10^{-5}\,\text{m}^{-1}$ in jumps of $3 \times 10^{-5}\,\text{m}^{-1}$ (thin lines). Finally, the gray shading indicates the regions of wave evanescence in meridional ($l < 0$) and vertical directions ($m < 0$).

persistent formation of a mid- to high-latitude meridional waveguide and a vertical reflecting surface at the same time, which allow more DWC to occur. The early onset of the wave geometry is consistent with a stronger background zonal-mean zonal wind in the model. These results emphasize that an accurate representation of the stratospheric mean states and wave geometries (l^2 and m^2) are necessary to properly represent the evolution of DWC in a climate model. This evaluation also suggests that the wave geometries and the DWC can be employed to examine the discrepancies of winter states between models and observations.

4. The influence of QBO and SST variability on DWC

In this section, the impact of removing QBO or specifying climatological seasonally varying SSTs on DWC is presented by first discussing their influences on the background winds, the wave coupling correlation and the seasonal variation of wave geometries.

a. Polar night jet strength

The two-way vertical (upward and downward) planetary wave propagation, which modifies the strength of the polar vortex, can be changed by the vertical and meridional structure of the zonally averaged zonal wind (Charney and Drazin 1961; Limpasuvan and Hartmann 2000; Perlwitz and Harnik 2003). Therefore, it is important to first examine how the strength and structure of the background winds have changed in each of the experiments.

Figure 5 shows the zonal-mean zonal wind differences between the NOQBO and the CTL experiments for 3-month overlapping periods from November through April. Without the QBO nudging, the tropical stratospheric winds resemble a weak but persistent east QBO state throughout the year, with easterly winds of about $-10\,\text{m}\,\text{s}^{-1}$. At high latitudes, the effect of removing the QBO and thus weak easterlies in the tropical lower stratosphere notably weakens the polar vortex. In particular, the zonal-mean zonal wind speed is significantly weaker by up to $-2\,\text{m}\,\text{s}^{-1}$ from November through February and shifts downward to 100 hPa in JFM. The QBO effect on the polar vortex weakens and loses significance from February to April (FMA) onward. The weakening of the stratospheric polar vortex in NOQBO experiment resembles the impact of the easterly phase of the QBO on the polar stratospheric vortex (e.g., Richter et al. 2011; Lu et al. 2014; Garfinkel et al. 2012). This is associated with a significantly increased upward wave propagation (which results in strong wave convergence) and redistribution the region of wave absorption (see Fig. S1).

In the fixed SSTs experiments, in contrast, the vortex is stronger and less disturbed (Figs. 5e–h). The zonal-mean

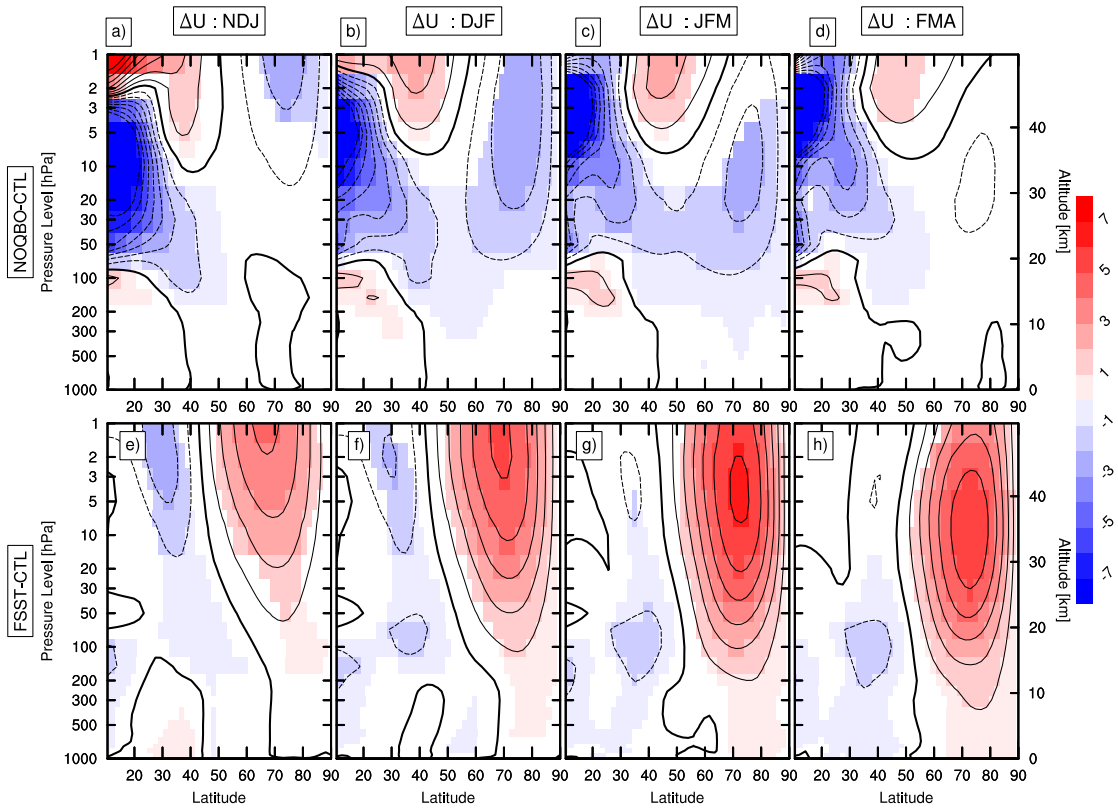

FIG. 5. The climatological zonal-mean wind differences between 10° and 90°N and 1000 and 1 hPa for (a)–(d) NOQBO − CTL and (e)–(f) FSST − CTL during (left to right) NDJ, DJF, JFM, and FMA. The contour interval is 1 m s^{-1}, and shaded areas represent regions with Student's *t* test values at the 95% significance level. The 0 m s^{-1} contour is plotted in thick solid black lines.

zonal wind exhibits a statistically significant increase of about 1–4 m s^{-1} in the mid- to upper stratosphere in November–January (NDJ) and stays stronger up to 5 m s^{-1} in December–February (DJF). The positive zonal wind anomalies are strongest in JFM, with differences up to 6 m s^{-1}, and get weaker during FMA with a downward shift of the peak toward the surface. The strengthening of the stratospheric vortex in the FSST experiment is accompanied by a significant anomalous downward wave propagation and decreased wave dissipation/breaking in the stratosphere (Fig. S1).

In summary, the NOQBO and FSST experiments represent opposite responses on the polar vortex. The lack of the QBO (SST variability) in CESM1(WACCM) significantly weakens (strengthens) the stratospheric polar night jet. These changes in the mean state will interact with upward and downward planetary wave propagation. A strong (weak) background zonal-mean zonal wind in the model can be associated with a more (less) downward wave reflection in the stratosphere toward the troposphere.

b. *Wave coupling correlations*

To measure seasonal variations of DWC, 3-month overlapping correlation coefficients of the time-lagged SVD between Z-ZWN1 at 500 hPa and at 10 hPa are computed throughout the seasons for the three different CESM1(WACCM) experiments (Figs. 6a–c), similar to Fig. 3. The DWC events occur if the correlation peaks at a negative time lag (when the stratospheric field is leading) and is statistically significant at the 99% level. The seasonal evolution of DWC in the CTL experiment is in reasonable agreement with the all-forcing CESM1(WACCM) experiment (including both natural and anthropogenic forcings), where DWC activity maximizes at about 6–7 days from DJF to FMA (cf. Fig. 3). Therefore, the focus in the subsequent analysis will be on the comparison between the CTL, NOQBO, and FSST experiments.

In the NOQBO experiment (Fig. 6b), DWC occurs over a shorter time period from January to March with a weaker correlation compared to that in the CTL experiment (Fig. 6a). On the other hand, DWC is significantly stronger and more persistent over a longer period of time (from November through April) in the FSST (Fig. 6c) as compared to the CTL and NOQBO experiments. In particular, the maximum correlation of DWC in the FSST experiment in JFM–FMA, when the polar night jet is strengthened and extends into the

troposphere (Figs. 5g–h). The statistically significant correlations in April–June to May–July (AMJ–MJJ) (Fig. 6c) are not related to downward wave reflection in the upper stratosphere, as the wave evanescence (region with negative refractive index) covers almost the whole NH stratosphere because of a reversal of the background winds during this period (not shown). The DWC can thus not explain the high correlation when the stratosphere leads in AMJ–MJJ, which might require other dynamical processes [e.g., nonlinear wave dynamics during final vortex breakdown (Shaw et al. 2010)]. Furthermore, to better understand the DWC changes between the CTL and NOQBO experiments, we also analyze the CTL experiment separately for east and west QBO seasons. Indeed, we find that the DWC signal is weaker in the CTL during east QBO and is much strengthened during west QBO (Fig. S3). This is consistent with weaker DWC signals in the NOQBO, since the tropical winds in this experiment resemble a weak persistent east-QBO state.

Based on the stratosphere–troposphere wave coupling correlations, we showed that in the absence of the QBO, the occurrence of DWC between stratosphere and troposphere is suppressed, and only weak DWC appears in JFM. Without SST variability, in contrast, the DWC is stronger and seasonally persistent from November to April. These results are consistent with differences in the climatological strength of the stratospheric polar night jet together with differences in planetary wave propagation and wave–mean flow interaction, which are all influenced by the QBO and SST variability (Figs. 5, S1, and S2).

c. *Evolution of the wave geometry*

To better understand the influence of the QBO and atmosphere–ocean coupling on the nature of DWC throughout the seasonal cycle, we consider the evolution of the wave geometry. Similar to Fig. 4, Fig. 7 shows the seasonal evolution of the zonal wave-1 meridional wavenumbers (l) averaged between 25 and 30 km (left) and the vertical wavenumbers (m) averaged between 60° and 80°N (right) for the three CESM1(WACCM) experiments. The vertical averaging of l from 25 to 30 km quantifies the equatorward boundary of the mid-stratospheric meridional waveguide, which limits equatorward propagation of extratropical waves. On the other hand, the meridional averaging of m between 60° and 80°N quantifies the vertical extent of the reflecting surfaces in the stratosphere.

The climatological seasonal evolution of the meridional wavenumber shows that, in the absence of QBO, the meridional waveguide exhibits a shorter seasonal persistence than in CTL (January–February to February–March in NOQBO vs November–December to February–March in CTL; Figs. 7a,b). Without SST variability, in contrast, the meridional waveguide undergoes a longer seasonal persistence as compared to the CTL (November–December to March–April in FSST vs November–December to February–March in CTL; Figs. 7a,c). This suggests that the wave reflection in the absence of SST variability may persist longer as a result of less meridional wave dispersion in the stratosphere.

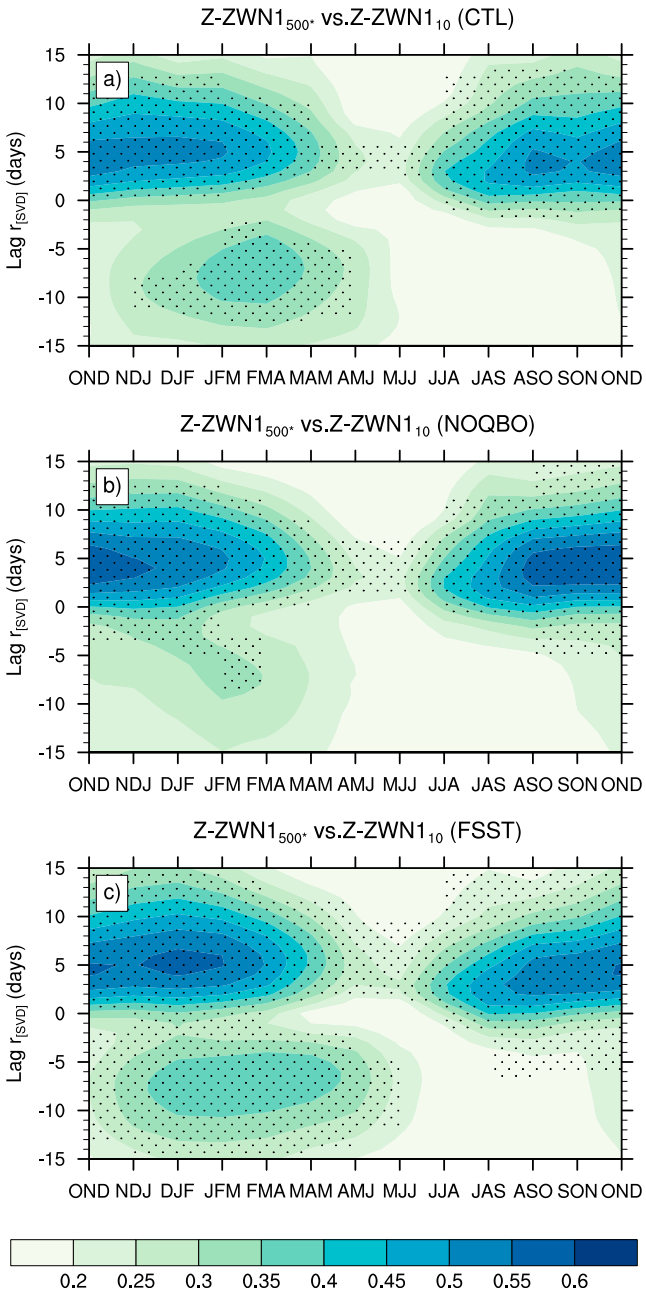

FIG. 6. Three-month overlapping periods of lagged SVD correlations between Z-ZWN1 at 500 and 10 hPa for (a) CTL, (b) NOQBO, and (c) FSST. Black dots represent values significant at the 99% level. A negative (positive) time lag indicates that the stratospheric (tropospheric) wave field is leading.

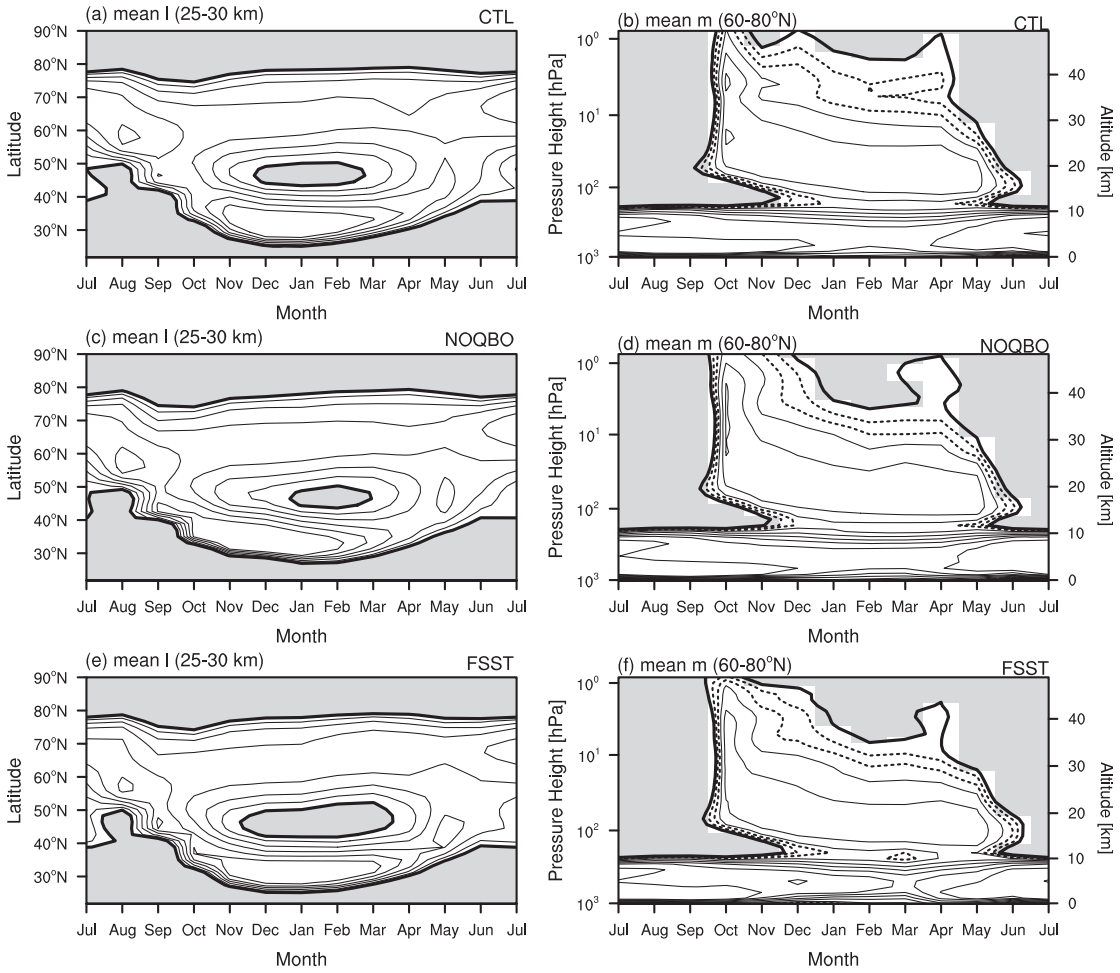

FIG. 7. As in Fig. 4, but the meridional wavenumbers are averaged between 25 and 30 km.

On the other hand, the climatological seasonal cycle of vertical wavenumbers shows that, without the QBO, vertical reflecting surfaces occur only from January to March (Fig. 7d). From May onward, the reflecting surface builds at very low altitudes because of a gradual descent of the zero wind line toward high latitudes after the polar vortex breakup. In contrast, without SST variability, the reflecting surface persists longer over an extended wintertime from October to April, as compared to CTL and NOQBO (Fig. 7f). The reflecting surfaces in November and December in the FSST are located at higher altitudes near 1 hPa compared to that in January–April. We note here that the higher reflecting surface in October occurs as a result of the strong background wind in the model, which exceeds the critical value and leads to negative refractive index (wave evanescence).

By combining the seasonal cycles of meridional and vertical wavenumbers in Fig. 7, the high-latitude meridional waveguide l in the absence of QBO is completely bounded above by a vertical reflecting surface m from January to March [which is shorter, compared to CTL from November to March (Figs. 7a,b and 7c,d)]. This configuration coincides with the maximum DWC in Fig. 6b during JFM. In contrast, the wave geometry during November–December and April in NOQBO is not bounded (Figs. 7c,d). In particular, there is no meridional waveguide during these periods, and therefore, instead of propagating vertically, the waves can propagate meridionally into the subtropics where they encounter subtropical critical surfaces. These dynamical features are in fairly good agreement with the anomalous upward and equatorward direction of Eliassen–Palm (EP) flux vectors in the absence of the QBO (Figs. S1a–d).

On the other hand, without SST variability, the high-latitude meridional waveguide l is completely bounded above by a vertical reflecting surface m over an extended wintertime from November to April (Figs. 7e,f). This configuration supports a longer seasonal activity of DWC and is thus consistent with the persistent DWC signals in

Fig. 6c. An increased DWC activity is also in good agreement with an amplification of anomalous downward wave flux, which strengthens the downward wave propagation (Figs. S1e–h). As we noted previously, the high correlation in AMJ–MJJ for negative time lags (when the stratosphere is leading) is not related to DWC, as the wave geometry configuration during this period is not bounded by the meridional waveguide (Fig. 7e).

5. Impact of DWC on the troposphere–surface system

Our previous results showed that the absence of the QBO or SST variability significantly influence the strength of DWC during NH winter. Therefore, it is worthwhile to examine whether the absence of the QBO and SST variability affect the impact of DWC on the tropospheric circulation. We focus on the most active winter season JFM, as it is a favorable period for planetary wave coupling and a period where the CESM1 (WACCM) experiments exhibit significant DWC signals in the troposphere (see Figs. 6a–c).

a. Statistics of stratospheric wave-1 heat flux extremes

Previous studies have shown that a dynamical metric based on negative stratospheric wave-1 heat flux extremes, can be used to isolate the tropospheric impacts of DWC (Shaw et al. 2014; Dunn-Sigouin and Shaw 2015). The extreme negative (positive) high-latitude stratospheric heat flux events are defined as the days with a total (climatology plus anomaly) wave-1 meridional heat flux value (i.e., $\overline{v'T'}_{k=1}$)[3] at 50 hPa averaged between 60° and 90°N below (above) the 10th (90th) percentile of the JFM distribution. In this section, we first examine the statistical distribution of total stratospheric wave-1 heat flux extremes and then quantify the relative occurrence of downward versus upward wave events among the model experiments.

The statistics of high-latitude wave-1 heat flux distribution for three CESM1(WACCM) experiments are listed in Table 3. The 10th (90th) percentile values in Table 3 indicate the heat flux value below which 10% (90%) of each model's total heat flux distribution can be found. Consistent with our previous findings, the highest downward (upward) wave activity is seen in the FSST (NOQBO) experiment. In particular, without SST variability, the wave-1 heat flux value at the 10th percentile is lower by about 24.4% (33.8%) compared to the CTL (NOQBO) experiment (Table 3), while without the QBO, the wave-1 heat flux at the 90th percentile is higher by 7.2% (22.5%) compared to the CTL (FSST, Table 3). Correspondingly, the mean value of the wave-1 heat flux of the NOQBO (FSST) experiment is higher (lower) than in the CTL experiment, which indicates an increased (decreased) climatological-mean upward wave activity in the stratosphere during wintertime. According to the random sampling of a Kolmogorov–Smirnov test, the distribution of the wave-1 heat flux in FSST (NOQBO) is significantly different from the CTL distribution at the 95% (93%) level (see p values in Table 3).

TABLE 3. Kolmogorov–Smirnov (KS) two-sample test of $\overline{v'T'}_{k=1}$ (m s^{-1} K) averaged from 60° to 90°N at 50 hPa during JFM. The 10th (90th) percentile is the heat flux value below which 10% (90%) of the total distribution can be found. The p values shown are relative to the CTL.

Experiment	Mean	Std dev	10th percentile	90th percentile	p value
CTL	15.40	25.26	−10.22	49.15	1.00
FSST	12.71	22.60	−12.71	43.02	<0.05
NOQBO	16.70	27.11	−9.50	52.69	<0.07

Figure 8 shows percentage (frequency) of extreme negative wave-1 heat flux events (y axis) versus extreme positive wave-1 heat flux events (x axis) between the NOQBO (triangles) and the FSST (asterisks) with respect to the CTL experiment at different stratospheric levels, that is, 70, 50, 30, and 10 hPa. Extreme negative (positive) heat flux days are defined as the days below (above) the 10th (90th) percentile values of the CTL experiment. It is clearly seen that the NOQBO (FSST) experiment shows clustering of higher frequency of days with extreme positive (negative) wave-1 heat fluxes at different stratospheric levels compared to the CTL. Extreme positive (negative) wave-1 heat flux events indicate strong net upward (downward) wave-1 activity in the NOQBO (FSST) experiment. This frequency of wave-1 heat flux events is in good agreement with statistically increased (decreased) occurrence of DWC in the FSST (NOQBO) experiment. The changes in frequency of extreme heat flux events are also consistent with the climatological differences in planetary wave propagation and wave–mean flow interaction among model experiments (Fig. S1). Further examination of the coupled structures (the SVD patterns at the times of maximum upward and downward coupling) shows that the amplitude of the waves varies between the different runs (largest for FSST and weakest for NOQBO); the phase differences between the stratospheric and tropospheric waves are similar for both time lags (Table 4; see

[3] For pure plane waves, $\overline{v'T'}_{k=1}$ is proportional to the vertical group velocity of planetary waves by assuming wave activity density (Λ) is positive definite [e.g., in Charney and Drazin (1961), $F_z \equiv c_{gz}\Lambda$, where $\Lambda \cong (\rho_o/4)[(\partial Q/\partial y)/(\overline{u}-c)^2]|\Psi_o|^2]$; that is, if ($\overline{v'T'}_{k=1} \propto c_{gz}$) and $\Lambda > 0$, thus $F_z < 0$ (downward-propagating wave).

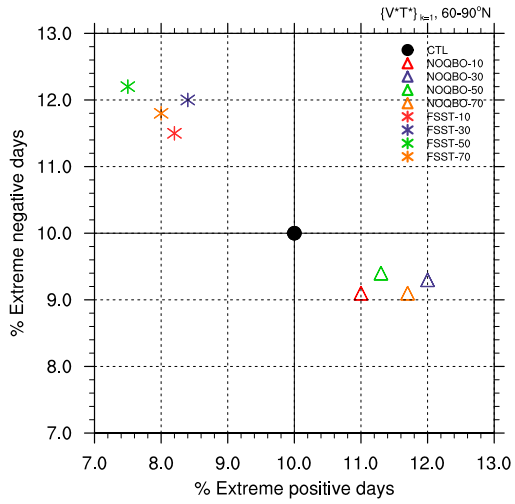

FIG. 8. Percentage (frequency) of extreme negative high-latitude averaged wave-1 heat flux events at 10-, 30-, 50-, and 70-hPa levels vs extreme positive events at the same levels during JFM for CTL, NOQBO, and FSST. See text for definition of negative and positive extremes.

also Figs. S4 and S5). Thus, the changes in the DWC correlations (e.g., Fig. 6) come both from a change in the frequency of occurrence of wave events and a change in the amplitude of the waves, but not from a difference in the phase tilt of the waves.

b. *Impact on the tropospheric circulation*

We now examine the impact of individual DWC events on the tropospheric circulation by looking at composites of various fields. An individual DWC event is identified as the day of minimum extreme negative heat flux value, where each central event must be separated by at least 15 days according to the time scale of planetary wave coupling[4] (Perlwitz and Harnik 2003). The composite anomalies are calculated as the deviations from the climatological seasonal cycle. The statistical significance of the composites is estimated using a Monte Carlo approach (Schreck et al. 2013) by randomly choosing 1000 combinations of N days, N being the number of composite members. Note that we focus on the tropospheric impacts in the North Atlantic region since there is a clear connection between that region and negative extreme stratospheric wave-1 heat flux values (Shaw and Perlwitz 2013; Shaw et al. 2014; Dunn-Sigouin and Shaw 2015).

[4] By using this definition, the composites of the total geopotential wave-1 structure for ERA and the three CESM1(WACCM) experiments exhibit a clear eastward phase tilt with height, which thus is consistent with downward propagation of wave activity from the stratosphere to the troposphere (Fig. S5).

TABLE 4. The phase differences $d\lambda$ at 65°N between the associated SVD wave-1 patterns at 500 hPa (fixed) and various stratospheric levels (50, 30, and 10 hPa) in CTL, NOQBO, and FSST from 1955 to 2099. Negative (positive) time lag indicates that the stratospheric (tropospheric) wave fields are leading.

Height range (hPa)	Lag (days)	$d\lambda$ (°E)		
		CTL	NOQBO	FSST
500–10	−6	106.4	104.8	109.3
500–30	−5	89.2	90.9	88.7
500–50	−4	66.0	68.7	66.7
500–10	6	−125.4	−129.6	−126.4
500–30	5	−101.7	−99.7	−100.4
500–50	4	−82.5	−81.4	−80.9

Figure 9 shows the composites of 500-hPa geopotential height (Figs. 9a–d), 700-hPa zonal-mean wind (Figs. 9e–h), and mean sea level pressure (Figs. 9i–l) anomalies north of 20°N during the time when DWC impact on the troposphere maximizes (i.e., 5-days average around the central date), for the ERA, CTL, NOQBO, and FSST experiments. On average, the impact of downward stratospheric wave activity in both ERA and CESM1(WACCM) experiments resembles the patterns projecting onto the positive phase of the North Atlantic Oscillation (NAO) (Hurrell et al. 2013). This is similar to the result shown by Shaw and Perlwitz (2013), which has been related to DWC impact. In particular, the geopotential height anomalies exhibit a seesaw shape between mid- and high latitudes (Figs. 9a–d), while the tropospheric zonal wind anomalies reflect the strengthening and poleward shift of the tropospheric jet over the North Atlantic basin (Figs. 9e–h). The sea level pressure anomalies show a similar pattern as the 500-hPa geopotential height anomalies, indicating a quasi-barotropic tropospheric NAO-like structure in association with downward wave activity (Figs. 9i–l). The discrepancies between ERA and CESM1(WACCM) are mainly discernible over the North Atlantic basin, especially in its western half, where all associated surface responses in CESM1(WACCM) are relatively modest. Nevertheless, the main features associated with the positive NAO-like responses are relatively well captured in CESM1(WACCM) experiments.

Comparing all CESM1(WACCM) sensitivity experiments, it can be seen that without QBO nudging (Figs. 9c,g,k), the DWC's impact on the tropospheric circulation enhances significantly compared to that in the CTL experiment (Figs. 9b,f,j). In particular, the geopotential height anomalies exhibit a stronger amplitude over the Atlantic basin and correspondingly a strengthening and poleward shift of the tropospheric jet (Figs. 9b,c and Figs. 9f,g). The mean sea level pressure anomalies are stronger in the Atlantic basin

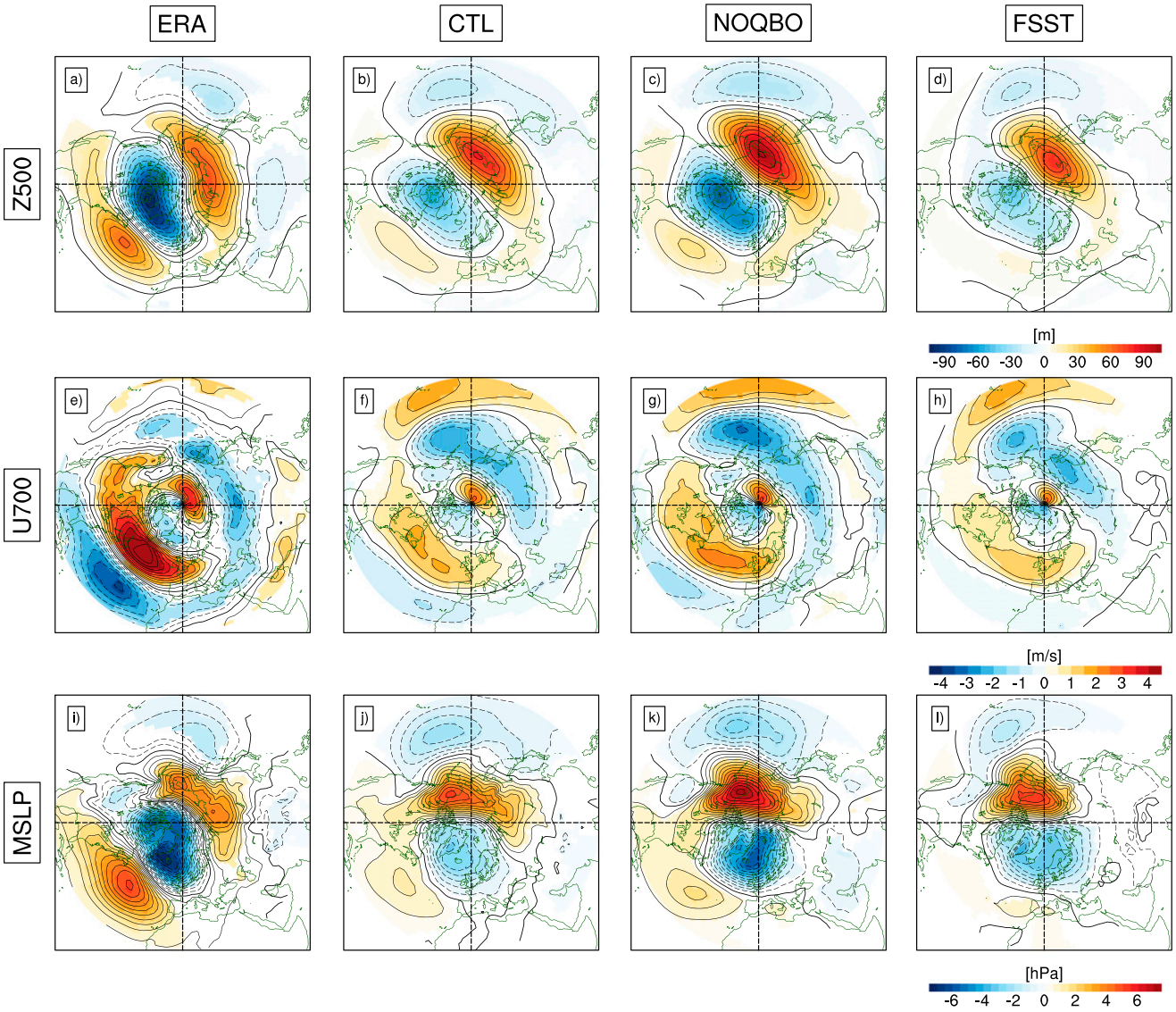

FIG. 9. The composites of (a)–(d) 500-hPa geopotential height, (e)–(h) 700-hPa zonal wind, and (i)–(l) mean sea level pressure anomalies during the period of maximum DWC impact on the troposphere (5-day average around the central date) in JFM for (left to right) ERA, CTL, NOQBO, and FSST. Contours (black) indicate the variances of (a)–(d) 500-hPa geopotential height (interval 500 m), (e)–(h) 700-hPa zonal wind (interval 2 m s^{-1}), and (i)–(l) mean sea level pressures (interval 0.5 hPa). The color shadings are only drawn for anomalies that are statistically significant at the 95% confidence level using a Monte Carlo approach.

compared to the CTL experiment, which is consistent with the strengthening of geopotential height anomalies aloft (Figs. 9k,c). In contrast, without SST variability, the surface influence of DWC in the North Atlantic basin is significantly weaker and prevails only over limited regions compared to those found in the CTL experiment (Figs. 9j,l). The poleward jet shift in the Atlantic basin (Fig. 9h) is weaker than in the CTL and NOQBO experiments (Figs. 9f,g), which is consistent with a weakening of geopotential height and mean sea level pressure anomalies over this region (Figs. 9d,l). These results have been verified to be robust to details of the composite calculation, event definition,[5] and the number of DWC events. In particular, by randomly choosing the same number of composite members N as in the CTL experiment, we find that weaker (stronger) surface signals associated with DWC in the FSST (NOQBO) experiments are robust and independent from the number of DWC events used in our composite (not shown).

[5] The results are not sensitive to the choice of stratospheric pressure level of $\overline{v'T'}_{k=1}$ (e.g., 30 or 70 hPa), to the thresholds of extreme negative stratospheric $\overline{v'T'}_{k=1}$ (e.g., at 1st, 3rd, 5th, and 7th percentiles), and to the choice of significance levels (e.g., 99%).

A priori, one might expect the tropospheric and surface response to DWC to be stronger in the model runs for which the statistical signal of DWC is stronger and more persistent and for which the amplitude of the downward-propagating waves is stronger. However, we see that the opposite is true: a stronger tropospheric response is observed in the NOQBO experiment, for which the DWC signal is weakest, and vice versa for the FSST experiment. Indeed, the differences in acceleration of the flow because of planetary-scale waves during DWC events (Figs. 10a–d) are not able to explain the differences in the tropospheric responses between FSST and NOQBO experiments. The planetary-scale wave drag anomalies (color shading) in the North Atlantic basin are strongest in the FSST experiment and weakest in the NOQBO experiment. These differences would suggest a stronger response for FSST, but we get the opposite for tropospheric responses. Furthermore, these planetary-scale wave drag anomalies are located more poleward from the position of the westerly wind anomalies (Figs. 9e–h) and coincide partially with upward-propagating planetary-scale wave sources (see solid contour lines in the North Atlantic basin). This suggests that other factors besides the frequency and strength of the downward wave propagation from the stratosphere influence the strength of the tropospheric response. Other studies have shown that internal tropospheric dynamics involving feedbacks from synoptic-scale eddy activity are important for stratosphere–troposphere coupling (e.g., Song and Robinson 2004; Garfinkel et al. 2013; Kunz and Greatbatch 2013). We thus proceed to examine those feedbacks here.

Figure 11 shows the composites of the anomalous synoptic-scale horizontal component of the **E** vectors,[6] alongside its divergence at 250 hPa (representing the influence of the synoptic-scale eddies on the horizontal large scale flow; Figs. 11a–d), anomalous vertical component of the **E** vectors at 700 hPa (representing the source of synoptic-scale eddies; Figs. 11e–h), anomalous Eady growth rate at 700-hPa (representing the baroclinicity of the mean flow; Figs. 11i–l), and anomalous synoptic geopotential height variance at 250 hPa (representing the storm-track strength; Figs. 11m–p). We see that the synoptic eddy-induced accelerations are much larger than the accelerations due to planetary-scale waves (cf. to Figs. 10a–d). Moreover, as found for the mean flow composites (Figs. 9f–h), we see that the synoptic eddy growth and induced accelerations in the North Atlantic basin are strongest in the NOQBO and weakest in the FSST experiment. In particular, the anomalous acceleration pattern induced by synoptic-scale eddy anomalies (Figs. 11b–d) enhances the mean flow anomaly pattern (Figs. 9f–h), with this enhancement being stronger for the NOQBO experiment and weakest for the FSST experiment. This strengthened tropospheric mean flow anomaly is accompanied by strengthening and poleward shift of the tropospheric synoptic wave source (Figs. 11f–h) and Eady growth rate (Figs. 11j–l) anomalies. At the same time, these mean flow baroclinicity anomalies are reinforcing the storm-track anomalies (Figs. 11n–p). This overall suggests that the eddy–mean flow feedback is strongest in the NOQBO experiment and weakest in the FSST experiment, being consistent with their respective tropospheric responses (Fig. 9).

Another obvious explanation for the weaker response in the FSST experiment is the lack of atmosphere–ocean feedbacks in this experiment. This may be because of the adjustment of SSTs to the atmospheric temperatures above reducing the thermal damping on atmospheric anomalies (Barsugli and Battisti 1998). In addition, previous studies have also shown that the wintertime SST tripole in the Atlantic basin can feed back positively to the large-scale atmospheric circulation changes associated with the NAO (Kushnir et al. 2002; Czaja and Frankignoul 2002; Peng et al. 2003; Deser et al. 2007) as well as with other external forcings (Chen et al. 2013; Chen and Schneider 2014). Other studies have also shown that enhanced extratropical SST gradients can lead to a substantial strengthening in eddy activity, storm tracks, and the annular mode in winter (Nakamura et al. 2008; Sampe et al. 2013).

To further examine the possible role of the ocean, we composite the global SST anomalies (Figs. 12a,c,e) and the Atlantic basin meridional SST gradient anomalies (Figs. 12b,d,f). We see a typical positive NAO-related SST-tripole anomaly pattern, with enhanced negative SST gradients in midlatitudes all across the Atlantic ocean, with a slight northeast tilt. Moreover, the southern more positive–negative dipole of the SST gradient pattern coincides with a similar dipole in the anomalous Eady growth rate field (as in Figs. 11i–k plotted on Figs. 12d,f as contour lines). This may suggest that the positive NAO SST-tripole pattern could enhance the anomalies in lower level baroclinicity that further generate synoptic wave activity (Figs. 11b–d) and strengthen the eddy–mean flow feedback during DWC event. We note these SST-tripole-like anomalies, which are shown for the 5 days centered around the DWC events, are already established in the month leading to the DWC peak (see Fig. S6). This apparent ocean preconditioning may be playing an enhancing role, similar to

[6] The synoptic-scale eddy activity is described by **E** vectors [$\mathbf{E} = (\overline{v'^2 - u'^2}, -\overline{u'v'}$; Hoskins et al. 1983)] of the 250-hPa 2–6-day bandpass-filtered winds u' and v'. The overbar signifies a time average and the prime a deviation from this average.

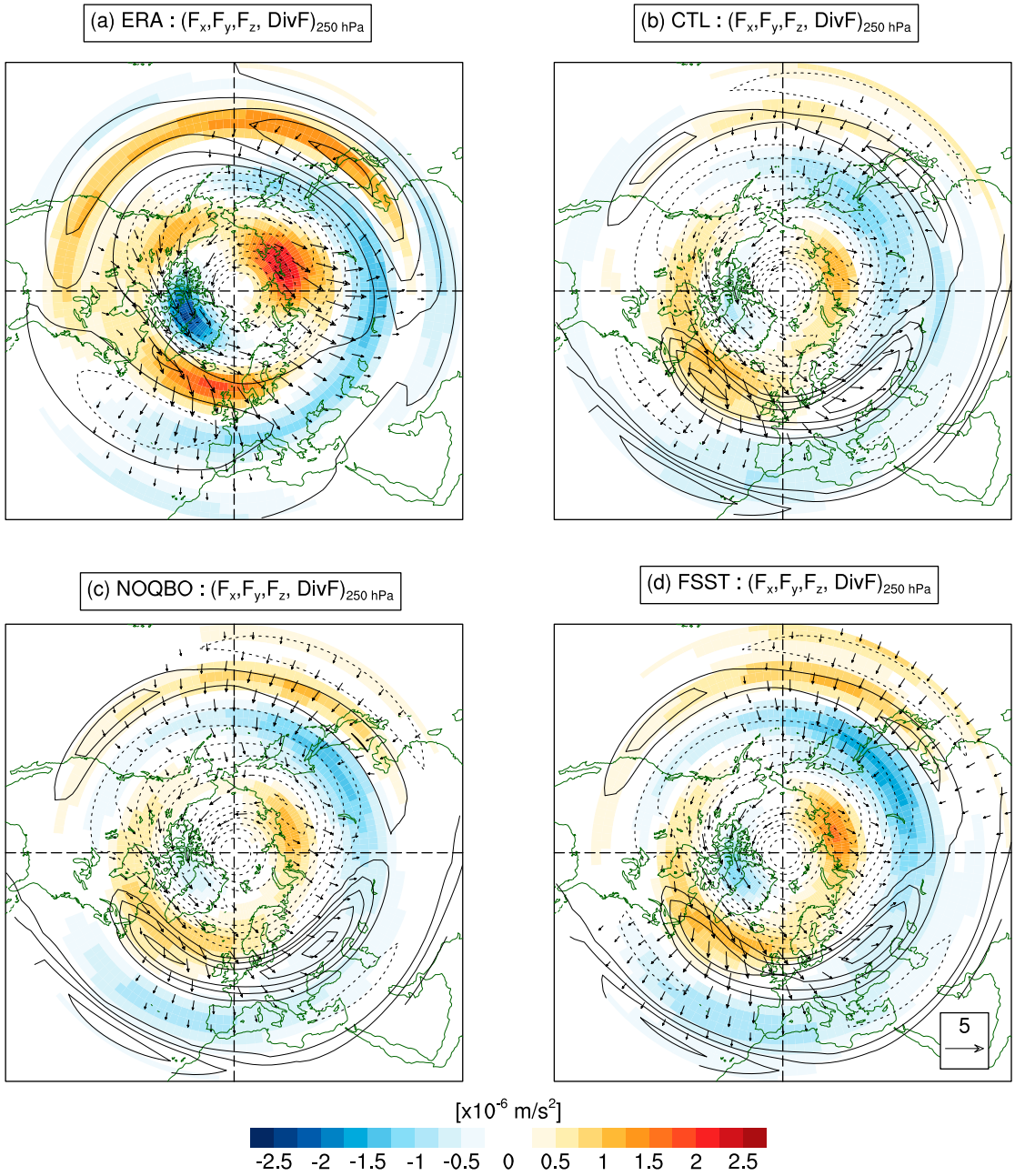

FIG. 10. The composites of planetary-scale wave divergence anomalies (colored shading, $\times 10^{-6}$ m s^{-2}) at 250 hPa during the period of maximum DWC impact on the troposphere (5-day average around the central date) in JFM for (a) ERA, (b) CTL, (c) NOQBO, and (d) FSST. The $\mathbf{F}_s$ vectors (horizontal components: F_x and F_y) are shown as arrows (m s^{-1}); the vertical vector component (F_z) is given by contours [solid (dashed) upward (downward) planetary-scale wave source]. The shadings are drawn only for anomalies that are statistically significant at the 95% confidence level using a Monte Carlo approach. The $\mathbf{F}_s$ vector is approximately parallel to the wave-energy propagation direction, and its zonal mean is equivalent to the Eliassen–Palm flux. (See the appendix for a detailed formulation.)

that of SST fronts in a number of idealized model studies (e.g., Nakamura et al. 2008; Brayshaw et al. 2008). However, more detailed studies are needed to understand this effect. The lack of this positive NAO SST-tripole pattern and the weaker synoptic-scale eddy feedback in the fixed SST experiment thus altogether may explain a weaker tropospheric response to DWC in this experiment.

Examining the SST fields in the NOQBO experiment suggests they may also explain part of the differences in this run as well, since the SST anomalies are stronger in this run than in the CTL experiment. Another striking difference between the NOQBO and CTL experiments is the much stronger tropical Pacific cold anomaly in the former (green boxes in the Pacific in Figs. 12c,e). Several

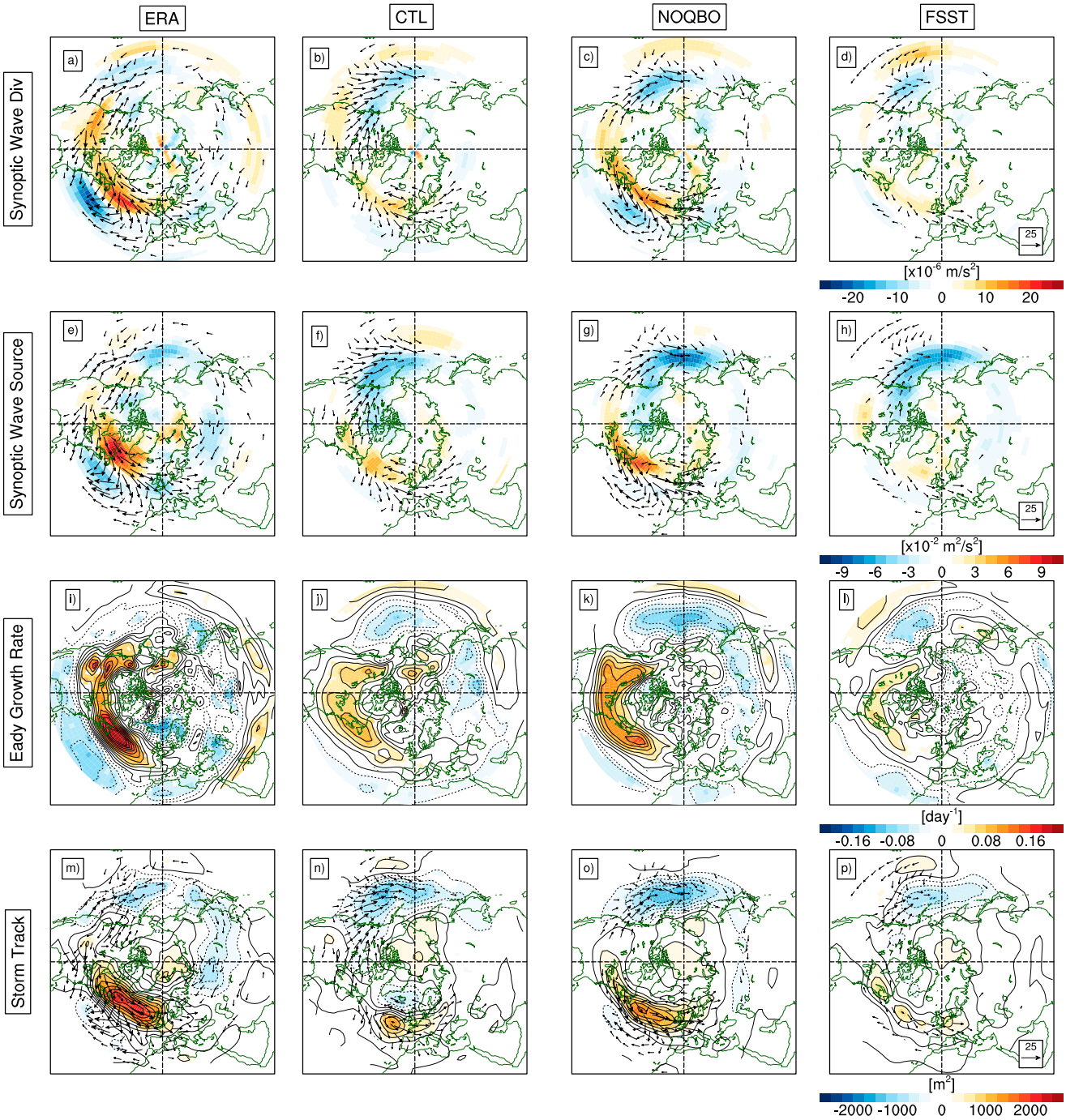

FIG. 11. The composites of (a)–(d) 250-hPa synoptic wave divergence (colored shading, $\times 10^{-6}\,\mathrm{m\,s^{-2}}$), (e)–(h) 700-hPa synoptic wave source (colored shading, $\times 10^{-2}\,\mathrm{m^2\,s^{-2}}$), (i)–(l) 700-hPa Eady's maximum growth rate (colored shading, $\mathrm{day^{-1}}$), and (m)–(p) 250-hPa storm-track anomalies (colored shading, $\mathrm{m^2}$) during the period of maximum DWC impact on the troposphere in JFM. The vectors in (a)–(h) and (m)–(p) are the **E** vectors ($\mathrm{m\,s^{-1}}$ with horizontal components E_x and E_y). The vertical component of the **E** vectors in (e)–(h) is calculated by $-f\overline{v'\theta'}(\partial\theta/\partial p)^{-1}$, representing the synoptic wave source where the positive (negative) values indicate upward (downward) synoptic wave fluxes. The Eady growth rate anomaly in (i)–(l) is calculated by $0.31|f||\partial u/\partial z|/N$. The color shading in (m)–(p) indicates the high-pass (<6-day period) filtered height covariance ($\overline{Z'^2}$). The shadings are only drawn for anomalies that are statistically significant at the 95% confidence level using a Monte Carlo approach.

studies have shown that cold (warm) ENSO drives a strengthening (weakening) of the polar vortex, leading to surface anomalies projecting on a positive (negative) NAO-like pattern (Manzini et al. 2006; Ineson and Scaife 2009). This suggests that the differences in the tropical Pacific SSTs among the model experiments may also contribute to the differences in the strength of the NAO-like response. Nevertheless, it should be noted that

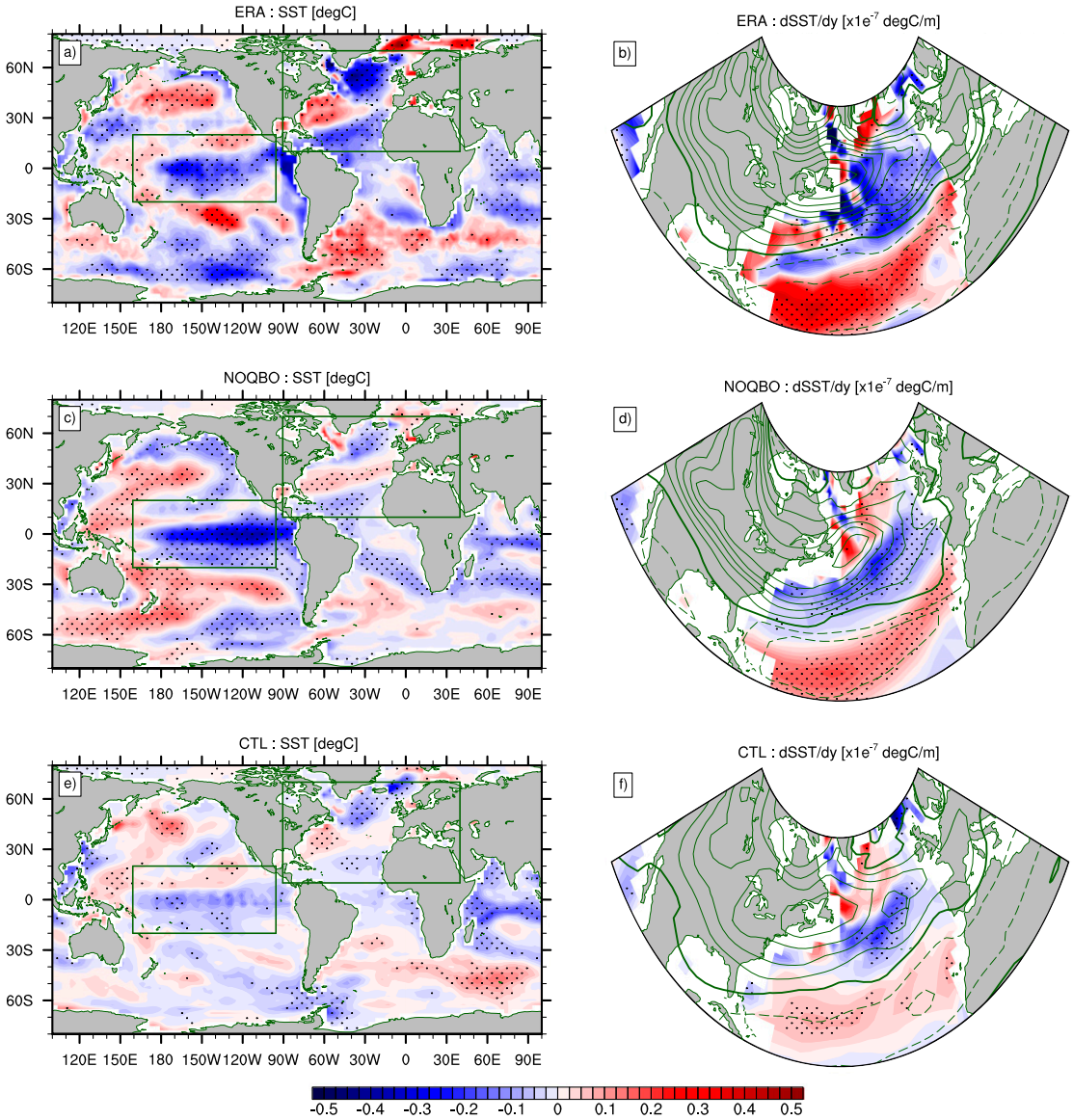

FIG. 12. The composites of (a),(c),(e) global SST anomalies (°C) and (b),(d),(f) meridional SST gradient anomalies (°C m^{-1}) during the period of maximum DWC impact on the troposphere (i.e., 5-day average around the central date) in JFM for (top to bottom) ERA, NOQBO, and CTL. Green contours indicate the Eady growth rate anomalies (day^{-1}) at 700 hPa. The dots indicate where the anomalies are significant at the 95% confidence level using a Monte Carlo approach.

the remote effect of tropical SST forcing on the NAO typically invokes downward propagation of zonal-mean stratospheric wind anomalies; thus, the connection between downward zonal-mean coupling induced by tropical Pacific SST forcing and the tropospheric impact of DWC needs to be further investigated. Furthermore, the cause for strong differences between the tropical Pacific SSTs in the CTL and NOQBO experiments might at least partly be due to a damping effect of the nudging of lower stratospheric winds on the tropical tropospheric circulation in the CTL experiment, but more detailed studies are needed to understand this effect.

To summarize, the composite analysis indicates that differences in the strength of the following synoptic-scale eddy–mean flow feedbacks can explain the differences in tropospheric response to DWC in the North Atlantic region between the NOQBO and FSST experiments: a strengthening and poleward shift of the tropospheric jet (Figs. 9e–h) is enhanced by the divergence of the anomalous synoptic-scale waves (Figs. 11b–d). This zonal-mean wind strengthening and shifting is accompanied by a strengthening and shifting of the Eady growth rate (Figs. 11j–l) and the synoptic wave sources (Figs. 11f–h), which in turn are consistent with the strengthening and

poleward shifting of the synoptic-scale wave activity (Figs. 11b–d). In addition, the positive–negative dipole of the anomalous Eady growth rate field is consistent with a similar dipole of the anomalous meridional SST gradient in the North Atlantic during a DWC event. These results suggest that the synoptic-scale eddy–mean flow feedbacks and the possible contribution of the SST anomalies during a DWC event play a central role in setting the strength of the tropospheric responses to DWC. The latter might be due to strengthened storm tracks due to stronger SST gradients, reduced thermal damping at the ocean surface, and positive atmosphere–ocean feedbacks, but more detailed studies are needed to examine this and, in particular, to distinguish the effects of interannual SST variability, which is also missing from the fixed SST experiment.

6. Conclusions

In this study, the influence of the QBO and SST variability on downward wave coupling (DWC) and its subsequent impacts on the troposphere–surface system were investigated in CESM1(WACCM) experiments in comparison to ERA data. We performed a set of sensitivity simulations with NCAR's fully coupled CESM1 (WACCM) model, by systematically switching on and off the QBO and interactive SSTs and sea ice in the model. We address the attribution of these forcing factors on DWC by examining the differences in background wind, wave source, wave–mean flow interaction, and the time-lagged vertical wave-1 coupling as well as the evolution of wave geometry. Afterward, the tropospheric impact of DWC is investigated based on the stratospheric heat flux extremes as proposed by Shaw et al. (2014). Our results can be summarized as follows:

1) The CESM1(WACCM) is able to capture the main features of DWC during NH winter (1958–2005). Consistent with the ERA dataset, DWC in the model maximizes during midwinter when the stratospheric basic state exhibits a bounded wave geometry associated with a high-latitude meridional waveguide in the lower stratosphere and a vertical reflecting surface in the upper stratosphere. The model, however, exhibits a bias in its seasonal cycle of DWC (Figs. 3a,b), which is associated with common model biases of the background zonal-mean winds that feed back on the wave dynamics. The results highlight that an accurate representation of the stratospheric basic-state wave geometry is necessary for a proper representation of the seasonal evolution of DWC in CESM1(WACCM).
2) Without the QBO nudging, the occurrence of DWC between the stratosphere and the troposphere is significantly suppressed. This is associated with a less persistent configuration of bounded wave geometries, which allows more wave dispersion in the meridional direction (Figs. 7c,d) and a stronger wave absorption (convergent EP flux) on the equatorward flank of the polar vortex (Figs. S1a–d). In particular, when the QBO nudging is switched off and equatorial winds are permanent easterly, planetary wave propagation from the troposphere into the stratosphere is enhanced, leading to a stronger wave absorption in the upper stratosphere, and thus a weaker DWC activity toward the troposphere (Fig. 5 and Figs. S1a–d). The enhanced wave convergence results in a weakening of the polar night jet (Fig. 5) and a strengthening of the stratospheric residual mean circulation at high latitudes (Figs. S2a–d).
3) Without SST variability, in contrast, the occurrence of DWC between the stratosphere and the troposphere is significantly enhanced. The DWC starts earlier and ends later in the seasonal cycle (November–April). This is associated with a longer and more persistent configuration of bounded wave geometries (Figs. 7e,f), which focuses planetary wave reflection in the vertical direction toward the troposphere. An increased DWC activity is consistent with anomalous downward wave flux activity, which leads to stronger wave divergence and thus to stronger DWC activity (Figs. S1e–h). A stronger DWC activity throughout the season is consistent through wave–mean flow interaction with an acceleration of the polar night jet (Figs. 5e–h and Figs. S1e–h) and anomalous weakening of the residual mean circulation (Figs. S2e–h).
4) Even though the downward wave-1 coupling is much larger in the FSST experiment and much smaller in the NOQBO experiment, compared to the CTL (Figs. 6, 8), the associated tropospheric changes in the North Atlantic region are weaker for the FSST and stronger for the NOQBO relative to the CTL experiment (Fig. 9). This apparently counterintuitive result might be explained by differences in the strength of the synoptic-scale eddy–mean flow feedbacks and the possible contribution of the ocean and associated SST anomalies between the FSST, the NOQBO, and the CTL experiments.

A recent study by Hansen et al. (2014) using the same model experiments showed that the frequency of major SSWs in winter is significantly reduced (increased) when the SST variability (QBO) is removed in the simulations. It was also reported that the tropospheric impact of major SSWs seems to be less significant and confined to a smaller area when the SST variability is excluded,

while removing the QBO seems to shift the period of significant tropospheric influence by about 10 days. The significant increase (decrease) of SSW frequency in the experiment without QBO (SST variability) is consistent with stronger (weaker) wave absorption in the polar vortex region found in our study, which results in significant decreased (increased) DWC activity between the stratosphere and the troposphere. This suggests a clear dynamical link between the wave absorption in the stratosphere and the probability of the occurrence of SSW and DWC events.

Several other recent studies have documented the importance of the QBO and SST variability as well as its coupling to the ocean on the behavior of SSWs in climate models (e.g., Calvo et al. 2009; Richter et al. 2011; Hansen et al. 2014). Our results show that these two factors are also important for DWC in the model and for establishing a correct representation of stratosphere–troposphere coupling. In particular, these two factors can influence the tropospheric response to DWC both through a modification of wave propagation and interaction with the mean flow in the stratosphere, and through a modification of the internal tropospheric feedbacks, which strongly affect the response to a given DWC event. While the current work represents an advance in our understanding of DWC in response to natural forcing factors, clearly more work is needed to understand the role of the ocean and of other important factors, such as the 11-yr solar cycle, volcanic eruptions, and anthropogenic climate change.

Most of the chemistry–climate models (CCMs) used for the scientific assessment of ozone are not coupled to an interactive ocean (WMO 2011). Our study suggests that the SST variability and thus two-way ocean–atmosphere interaction are important in order to represent stratosphere–troposphere coupling and thus correct responses to recent and future ozone changes.

Acknowledgments. We acknowledge support received from the German–Israeli Foundation for Scientific Research and Development under Grant GIF1151-83.8/2011. This work has also been partially performed within the Helmholtz-University Young Investigators Group NATHAN funded by the Helmholtz Association through the President's Initiative and Networking Fund and the GEOMAR Helmholtz Centre for Ocean Research Kiel. NH is also partly supported by a Rossby Visiting Fellowship from the International Meteorological Institute (IMI), Stockholm, Sweden. The authors also would like to thank Alan Plumb for discussions on the tropospheric impact of DWC. We are also grateful to Christof Petrick, Felicitas Hansen, and Wuke Wang for setting up the fully coupled model experiments used in this study. The model simulations were performed at the German Climate Computing Centre [Deutsches Klimarechenzentrum (DKRZ)], Hamburg. Finally, we also acknowledge COST ACTION ES1005 TOSCA for financing the participation of SWL at the first training school on "Solar Variability and Climate Response," Thessaloniki, Greece, 2013.

APPENDIX

Planetary Wave Forcing of the Mean Flow

To quantify the drag exerted by planetary-scale waves on the zonal-mean flow, the EP flux ($\mathbf{F} = \{F_\phi, F_z\}$) and its divergence $(\rho_0 a\cos\phi)^{-1}\nabla\cdot\mathbf{F}$ are computed in a spherical log–pressure coordinate based on Andrews et al. (1987), where the components are given as follows:

$$F_\phi \equiv \rho_0 a\cos\phi\left(\overline{u}_z\frac{\overline{v'\theta'}}{\overline{\theta}_z} - \overline{v'u'}\right) \quad \text{and} \tag{A1}$$

$$F_z \equiv \rho_0 a\cos\phi\left\{[f-(a\cos\phi)^{-1}(\overline{u}\cos\phi)_\phi]\frac{\overline{v'\theta'}}{\overline{\theta}_z} - \overline{w'u'}\right\}, \tag{A2}$$

where u, v, and w are, respectively, the zonal, meridional, and vertical components of the velocity, a is Earth's radius, f is the Coriolis parameter, ϕ is latitude, z is height (in log-pressure coordinates), ρ_0 is air density, which varies with height as $\exp(-z/H)$, H is the density scale height taken as 7000 m, and θ is potential temperature. The subscript means the derivative with respect to the corresponding coordinate. The primes denote deviations from the zonal means, and overbars indicate zonal means.

In addition, the 3D wave activity flux (Plumb 1985) to diagnose the potential regional sources (sinks) and propagation characteristics of planetary-scale wave activity is computed as follows:

$$\mathbf{F}_s \equiv \frac{p\cos\phi}{p_o}\times\left\{\begin{array}{c} v'^2 - \dfrac{1}{2\Omega a\sin 2\phi}\dfrac{\partial(v'\Phi')}{\partial\lambda} \\ -v'u' + \dfrac{1}{2\Omega a\sin 2\phi}\dfrac{\partial(u'\Phi')}{\partial\lambda} \\ \dfrac{2\Omega\sin\phi}{S}\left[v'T' - \dfrac{1}{2\Omega a\sin 2\phi}\dfrac{\partial(T'\Phi')}{\partial\lambda}\right] \end{array}\right\}, \tag{A3}$$

where $S = \partial\hat{T}/\partial z + \kappa\hat{T}/H$ is the static stability (the caret indicating the areal average over the region north of

20°N), Φ is the geopotential, $\kappa = R/c_p \approx 0.286$, λ is longitude, and p_o is 1000 hPa.

REFERENCES

Andrews, D. G., J. R. Holton, and C. B. Leovoy, 1987: *Middle Atmosphere Dynamics*. International Geophysics Series, Vol. 40, Academic Press, 489 pp.

Baldwin, M. P., and T. J. Dunkerton, 2001: Stratospheric harbingers of anomalous weather regimes. *Science*, **294**, 581–584, doi:10.1126/science.1063315.

Barsugli, J. J., and D. S. Battisti, 1998: The basic effects of atmosphere–ocean thermal coupling on midlatitude variability. *J. Atmos. Sci.*, **55**, 477–493, doi:10.1175/1520-0469(1998)055<0477:TBEOAO>2.0.CO;2.

Brayshaw, D. J., B. Hoskins, and M. Blackburn, 2008: The storm-track response to idealized SST perturbations in an aqua-planet GCM. *J. Atmos. Sci.*, **65**, 2842–2860, doi:10.1175/2008JAS2657.1.

Bretherton, C. S., C. Smith, and J. M. Wallace, 1992: An intercomparison of methods for finding coupled patterns in climate data. *J. Climate*, **5**, 541–560, doi:10.1175/1520-0442(1992)005<0541:AIOMFF>2.0.CO;2.

Calvo, N., M. A. Giorgetta, R. Garcia-Herrera, and E. Manzini, 2009: Nonlinearity of the combined warm ENSO and QBO effects on the Northern Hemisphere polar vortex in MAECHAM5 simulations. *J. Geophys. Res.*, **114**, D13109, doi:10.1029/2008JD011445.

Charney, J. G., and P. G. Drazin, 1961: Propagation of planetary-scale disturbances from the lower into the upper atmosphere. *J. Geophys. Res.*, **66**, 83–109, doi:10.1029/JZ066i001p00083.

Chen, H., and E. K. Schneider, 2014: Comparison of the SST-forced responses between coupled and uncoupled climate simulations. *J. Climate*, **27**, 740–756, doi:10.1175/JCLI-D-13-00092.1.

——, ——, B. P. Kirtman, and I. Colfescu, 2013: Evaluation of weather noise and its role in climate model simulations. *J. Climate*, **26**, 3766–3784, doi:10.1175/JCLI-D-12-00292.1.

Czaja, A., and C. Frankignoul, 2002: Observed impact of Atlantic SST anomalies on the North Atlantic Oscillation. *J. Climate*, **15**, 606–623, doi:10.1175/1520-0442(2002)015<0606:OIOASA>2.0.CO;2.

Dee, D. P., and Coauthors, 2011: The ERA-Interim reanalysis: Configuration and performance of the data assimilation system. *Quart. J. Roy. Meteor. Soc.*, **137**, 553–597, doi:10.1002/qj.828.

Deser, C., R. A. Tomas, and S. Peng, 2007: The transient atmospheric circulation response to North Atlantic SST and sea ice anomalies. *J. Climate*, **20**, 4751–4767, doi:10.1175/JCLI4278.1.

Dunn-Sigouin, E., and T. A. Shaw, 2015: Comparing and contrasting extreme stratospheric events, including their coupling to the tropospheric circulation. *J. Geophys. Res. Atmos.*, **120**, 1374–1390, doi:10.1002/2014JD022116.

Eliassen, A., and E. Palm, 1961: *On the Transfer of Energy in Stationary Mountain Waves*. I Kommisjon hos Aschehoug, 23 pp.

Garfinkel, C. I., T. A. Shaw, D. L. Hartmann, and D. W. Waugh, 2012: Does the Holton–Tan mechanism explain how the quasi-biennial oscillation modulates the Arctic polar vortex? *J. Atmos. Sci.*, **69**, 1713–1733, doi:10.1175/JAS-D-11-0209.1.

——, D. W. Waugh, and E. P. Gerber, 2013: The effect of tropospheric jet latitude on coupling between the stratospheric polar vortex and the troposphere. *J. Climate*, **26**, 2077–2095, doi:10.1175/JCLI-D-12-00301.1.

Gent, P. R., and Coauthors, 2011: The Community Climate System Model version 4. *J. Climate*, **24**, 4973–4991, doi:10.1175/2011JCLI4083.1.

Gray, L. J., and Coauthors, 2010: Solar influences on climate. *Rev. Geophys.*, **48**, RG4001, doi:10.1029/2009RG000282.

Hamilton, K., 1993: An examination of observed Southern Oscillation effects in the Northern Hemisphere stratosphere. *J. Atmos. Sci.*, **50**, 3468–3474, doi:10.1175/1520-0469(1993)050<3468:AEOOSO>2.0.CO;2.

Hansen, F., K. Matthes, and L. J. Gray, 2013: Sensitivity of stratospheric dynamics and chemistry to QBO nudging width in the chemistry–climate model WACCM. *J. Geophys. Res. Atmos.*, **118**, 10 464–10 474, doi:10.1002/jgrd.50812.

——, ——, C. Petrick, and W. Wang, 2014: The influence of natural and anthropogenic factors on major stratospheric sudden warmings. *J. Geophys. Res. Atmos.*, **119**, 8117–8136, doi:10.1002/2013JD021397.

Harnik, N., 2009: Observed stratospheric downward reflection and its relation to upward pulses of wave activity. *J. Geophys. Res.*, **114**, D08120, doi:10.1029/2008JD010493.

——, and R. S. Lindzen, 2001: The effect of reflecting surfaces on the vertical structure and variability of stratospheric planetary waves. *J. Atmos. Sci.*, **58**, 2872–2894, doi:10.1175/1520-0469(2001)058<2872:TEORSO>2.0.CO;2.

Holton, J. R., and H.-C. Tan, 1980: The influence of the equatorial quasi-biennial oscillation on the global circulation at 50 mb. *J. Atmos. Sci.*, **37**, 2200–2208, doi:10.1175/1520-0469(1980)037<2200:TIOTEQ>2.0.CO;2.

Hoskins, B. J., I. N. James, and G. H. White, 1983: The shape, propagation and mean-flow interaction of large-scale weather systems. *J. Atmos. Sci.*, **40**, 1595–1612, doi:10.1175/1520-0469(1983)040<1595:TSPAMF>2.0.CO;2.

Hurrell, J. W., Y. Kushnir, G. Ottersen, and M. Visbeck, 2013: An overview of the North Atlantic Oscillation. *The North Atlantic Oscillation: Climatic Significance and Environmental Impact*, J. W. Hurrell et al., Eds., Amer. Geophys. Union, 1–35, doi:10.1029/134GM01.

Hurwitz, M. M., P. A. Newman, and C. I. Garfinkel, 2012: On the influence of North Pacific sea surface temperature on the Arctic winter climate. *J. Geophys. Res*, **117**, D19110, doi:10.1029/2012JD017819.

Ineson, S., and A. Scaife, 2009: The role of the stratosphere in the European climate response to El Niño. *Nat. Geosci.*, **2**, 32–36, doi:10.1038/ngeo381.

Jaiser, R., K. Dethloff, and D. Handorf, 2013: Stratospheric response to Arctic sea ice retreat and associated planetary wave propagation changes. *Tellus*, **65A**, 19375, doi:10.3402/tellusa.v65i0.19375.

Keenlyside, N., and N.-E. Omrani, 2014: Has a warm North Atlantic contributed to recent European cold winters? *Environ. Res. Lett.*, **9**, 061001, doi:10.1088/1748-9326/9/6/061001.

Kinnison, D. E., and Coauthors, 2007: Sensitivity of chemical tracers to meteorological parameters in the MOZART-3 chemical transport model. *J. Geophys. Res.*, **112**, D20302, doi:10.1029/2006JD007879.

Kunz, T., and R. J. Greatbatch, 2013: On the northern annular mode surface signal associated with stratospheric variability. *J. Atmos. Sci.*, **70**, 2103–2118, doi:10.1175/JAS-D-12-0158.1.

Kushnir, Y., W. Robinson, I. Blad, N. Hall, S. Peng, and R. Sutton, 2002: Atmospheric GCM response to extratropical SST anomalies: Synthesis and evaluation. *J. Climate*, **15**, 2233–2256, doi:10.1175/1520-0442(2002)015<2233:AGRTES>2.0.CO;2.

Labitzke, K., 1982: On the interannual variability of the middle stratosphere during the northern winters. *J. Meteor. Soc. Japan*, **60**, 124–139.

Li, Y., and N.-C. Lau, 2013: Influences of ENSO on stratospheric variability, and the descent of stratospheric perturbations into the lower troposphere. *J. Climate*, **26**, 4725–4748, doi:10.1175/JCLI-D-12-00581.1.

Limpasuvan, V., and D. L. Hartmann, 2000: Wave-maintained annular modes of climate variability. *J. Climate*, **13**, 4414–4429, doi:10.1175/1520-0442(2000)013<4414:WMAMOC>2.0.CO;2.

Lorenz, D. J., and D. L. Hartmann, 2003: Eddy–zonal flow feedback in the Northern Hemisphere winter. *J. Climate*, **16**, 1212–1227, doi:10.1175/1520-0442(2003)16<1212:EFFITN>2.0.CO;2.

Lu, H., T. J. Bracegirdle, T. Phillips, A. Bushell, and L. Gray, 2014: Mechanisms for the Holton–Tan relationship and its decadal variation. *J. Geophys. Res. Atmos.*, **119**, 2811–2830, doi:10.1002/2013JD021352.

Manzini, E., M. A. Giorgetta, M. Esch, L. Kornblueh, and E. Roeckner, 2006: The influence of sea surface temperatures on the northern winter stratosphere: Ensemble simulations with the MAECHAM5 model. *J. Climate*, **19**, 3863–3881, doi:10.1175/JCLI3826.1.

Marsh, D. R., R. R. Garcia, D. E. Kinnison, B. A. Boville, F. Sassi, S. C. Solomon, and K. Matthes, 2007: Modeling the whole atmosphere response to solar cycle changes in radiative and geomagnetic forcing. *J. Geophys. Res.*, **112**, D23306, doi:10.1029/2006JD008306.

——, M. J. Mills, D. E. Kinnison, J.-F. Lamarque, N. Calvo, and L. M. Polvani, 2013: Climate change from 1850 to 2005 simulated in CESM1(WACCM). *J. Climate*, **26**, 7372–7391, doi:10.1175/JCLI-D-12-00558.1.

Matsuno, T., 1970: Vertical propagation of stationary planetary waves in the winter Northern Hemisphere. *J. Atmos. Sci.*, **27**, 871–883, doi:10.1175/1520-0469(1970)027<0871:VPOSPW>2.0.CO;2.

Matthes, K., D. R. Marsh, R. R. Garcia, D. E. Kinnison, F. Sassi, and S. Walters, 2010: Role of the QBO in modulating the influence of the 11 year solar cycle on the atmosphere using constant forcings. *J. Geophys. Res.*, **115**, D18110, doi:10.1029/2009JD013020.

McIntyre, M. E., and T. N. Palmer, 1983: Breaking planetary waves in the stratosphere. *Nature*, **305**, 593–600, doi:10.1038/305593a0.

Nakamura, H., T. Sampe, A. Goto, W. Ohfuchi, and S.-P. Xie, 2008: On the importance of midlatitude oceanic frontal zones for the mean state and dominant variability in the tropospheric circulation. *Geophys. Res. Lett.*, **35**, L15709, doi:10.1029/2008GL034010.

Omrani, N.-E., N. Keenlyside, J. Bader, and E. Manzini, 2014: Stratosphere key for wintertime atmospheric response to warm Atlantic decadal conditions. *Climate Dyn.*, **42**, 649–663, doi:10.1007/s00382-013-1860-3.

——, J. Bader, N. Keenlyside, and E. Manzini, 2016: Troposphere–stratosphere response to large-scale North Atlantic Ocean variability in an atmosphere/ocean coupled model. *Climate Dyn.*, **46**, 1397–1415, doi:10.1007/s00382-015-2654-6, in press.

Peng, S., W. A. Robinson, and S. Li, 2003: Mechanisms for the NAO responses to the North Atlantic SST tripole. *J. Climate*, **16**, 1987–2004, doi:10.1175/1520-0442(2003)016<1987:MFTNRT>2.0.CO;2.

Perlwitz, J., and N. Harnik, 2003: Observational evidence of a stratospheric influence on the troposphere by planetary wave reflection. *J. Climate*, **16**, 3011–3026, doi:10.1175/1520-0442(2003)016<3011:OEOASI>2.0.CO;2.

Plumb, R., 1985: On the three-dimensional propagation of stationary waves. *J. Atmos. Sci.*, **42**, 217–229, doi:10.1175/1520-0469(1985)042<0217:OTTDPO>2.0.CO;2.

Richter, J. H., K. Matthes, N. Calvo, and L. J. Gray, 2011: Influence of the quasi-biennial oscillation and El Niño–Southern Oscillation on the frequency of sudden stratospheric warmings. *J. Geophys. Res.*, **116**, D20111, doi:10.1029/2011JD015757.

Robock, A., 2000: Volcanic eruptions and climate. *Rev. Geophys.*, **38**, 191–219, doi:10.1029/1998RG000054.

Sampe, T., H. Nakamura, and A. Goto, 2013: Potential influence of a midlatitude oceanic frontal zone on the annular variability in the extratropical atmosphere as revealed by aqua-planet experiments. *J. Meteor. Soc. Japan*, **91A**, 243–267, doi:10.2151/jmsj.2013-A09.

Schimanke, S., T. Spangehl, H. Huebener, and U. Cubasch, 2013: Variability and trends of major stratospheric warmings in simulations under constant and increasing GHG concentrations. *Climate Dyn.*, **40**, 1733–1747, doi:10.1007/s00382-012-1530-x.

Schreck, C. J., L. Shi, J. P. Kossin, and J. J. Bates, 2013: Identifying the MJO, equatorial waves, and their impacts using 32 years of HIRS upper-tropospheric water vapor. *J. Climate*, **26**, 1418–1431, doi:10.1175/JCLI-D-12-00034.1.

Shaw, T. A., and J. Perlwitz, 2013: The life cycle of Northern Hemisphere downward wave coupling between the stratosphere and troposphere. *J. Climate*, **26**, 1745–1763, doi:10.1175/JCLI-D-12-00251.1.

——, ——, and N. Harnik, 2010: Downward wave coupling between the stratosphere and troposphere: The importance of meridional wave guiding and comparison with zonal-mean coupling. *J. Climate*, **23**, 6365–6381, doi:10.1175/2010JCLI3804.1.

——, ——, and O. Weiner, 2014: Troposphere–stratosphere coupling: Links to North Atlantic weather and climate, including their representation in CMIP5 models. *J. Geophys. Res. Atmos.*, **119**, 5864–5880, doi:10.1002/2013JD021191.

Song, Y., and W. A. Robinson, 2004: Dynamical mechanisms for stratospheric influences on the troposphere. *J. Atmos. Sci.*, **61**, 1711–1725, doi:10.1175/1520-0469(2004)061<1711:DMFSIO>2.0.CO;2.

SPARC CCMVal, 2010: SPARC report on the evaluation of chemistry-climate models. Stratosphere–Troposphere Processes and Their Role in Climate Tech. Rep. 5, WCRP-132, WMO/TD-1526, 426 pp. [Available online at http://www.sparc-climate.org/publications/sparc-reports/sparc-report-no5/.]

Uppala, S. M., and Coauthors, 2005: The ERA-40 Re-Analysis. *Quart. J. Roy. Meteor. Soc.*, **131**, 2961–3012, doi:10.1256/qj.04.176.

van Loon, H., and K. Labitzke, 1987: The Southern Oscillation. Part V: The anomalies in the lower stratosphere of the Northern Hemisphere in winter and a comparison with the quasi-biennial oscillation. *Mon. Wea. Rev.*, **115**, 357–369, doi:10.1175/1520-0493(1987)115<0357:TSOPVT>2.0.CO;2.

WMO, 2011: Scientific assessment of ozone depletion: 2010. Global Ozone Research and Monitoring Project Rep. 52, 516 pp.

Chapter 3

How Does Downward Planetary Wave Coupling Affect Polar Stratospheric Ozone in the Arctic Winter Stratosphere?

This chapter will be submitted as an article to Atmospheric Chemistry and Physics (ACP).

Lubis, S. W., V. Silverman, K. Matthes, N. Harnik, N. Omrani, and S. Wahl, 2016: How Does Downward Planetary Wave Coupling Affect Polar Stratospheric Ozone in the Arctic Winter Stratosphere? (to be submitted).

The authors' contributions to this publication are as follows:

- S. Lubis initiated the study, performed all the analyses, produced all figures and wrote the manuscript.
- V. Silverman contributed with ideas and discussion on the analysis, helped with analysis for the last section of the paper.
- K. Matthes, N. Harnik and N-E. Omrani contributed with ideas and discussions on the analysis and with comments on the manuscript.
- S. Wahl performed a model simulation used in this study.

Abstract

It is well established that variable wintertime planetary wave forcing in the stratosphere controls the variability of Arctic stratospheric ozone via changes in the strength of the polar vortex and the residual circulation. While previous studies focused on the variations in upward wave flux entering the lower stratosphere, here the impact of downward planetary wave coupling (DWC) on ozone is investigated for the first time. Utilizing the MERRA reanalysis and a coupled chemistry-climate simulation with NCAR's Community Earth System Model (CESM1[WACCM]), we find two DWC effects on ozone: (1) the direct effect via residual circulation changes that prevent the typical increase of ozone due to upward planetary wave events, and (2) the indirect effect through

the polar temperature, which affects the amount of springtime ozone destruction. Both effects together lead to lower ozone concentration at the end of winter and in spring.

Winter seasons dominated by DWC events (reflective winters) are characterized by lower Arctic column ozone, while seasons dominated by increased upward wave events (absorptive winters) are characterized by relatively higher column ozone in spring. These findings are consistent with the cumulative effects of downward and upward planetary wave events on ozone through the residual circulation and the polar vortex. The results establish a new perspective on dynamical processes controlling Arctic ozone variability.

3.1 Introduction

The dynamical linkage between the stratosphere and troposphere is dominated by planetary waves, which are generated in the troposphere by orographic and/or nonorographic forcing (Kuroda and Kodera 1999; Kodera and Kuroda 2000; Baldwin and Dunkerton 2001; Christiansen 2001; Plumb and Semeniuk 2003; Polvani and Waugh 2004). These waves propagate upward into the stratosphere where they either dissipate (often manifested as a sudden stratospheric warming, SSW) and initiate downward zonal-mean coupling (e.g., Baldwin and Dunkerton 2001; Limpasuvan et al. 2004); or are reflected downward toward the troposphere, which results in downward wave coupling (DWC) (Perlwitz and Harnik 2003; Shaw et al. 2010; Lubis et al. 2016b). The DWC occurs when upward pulses of wave activity decelerate the flow in the upper stratosphere, forming a downward-reflecting surface that redirects waves back to the troposphere (see Harnik and Lindzen 2001, for theoretical considerations). The occurrence of DWC is tied to the so-called bounded wave geometry of the stratospheric basic state, which is characterized by a well-defined high-latitude meridional waveguide in the lower stratosphere and a vertical reflecting surface in the upper stratosphere (e.g., Shaw et al. 2010; Lubis et al. 2016b).

The vertical coupling of planetary-scale waves between the stratosphere and troposphere can be directly examined via the meridional eddy heat flux value, as it represents the vertical group velocity of the planetary waves (e.g., Shaw and Perlwitz 2013; Lubis et al. 2016b). Using extreme total (climatology plus anomaly) negative wave-1 heat flux values, the life cycle of DWC and its subsequent impact on the circulation in the NH have been studied (e.g., Shaw and Perlwitz 2013; Shaw and Perlwitz 2014; Lubis et al. 2016b). Shaw and Perlwitz (2014) showed that DWC events are associated with a transient reversal of the residual circulation and cooling of the Arctic lower stratosphere. This result is consistent with Eliassen-Palm (EP) flux divergence during the event, which is induced by transient downward wave propagation (Dunn-Sigouin and Shaw, 2015; Lubis et al., 2016b). Since the variations in the stratospheric EP flux divergence force commensurate changes in the residual circulation (Plumb, 2002), it is therefore expected that DWC may influence the dynamical ozone transport to the pole.

It is well established that planetary waves play an important role in shaping the ozone hole through their impact on the polar vortex and on the residual circulation (e.g., Solomon 1999; Fusco

and Salby 1999; Randel et al. 2002). Randel et al. (2002) showed that variations in planetary wave forcing in the lower stratosphere during winter-spring exhibit a strong correlation with column ozone. The mechanism for this correlation is that increases (decreased) wave dissipation in the stratosphere leads to strengthening (weakening) of residual circulation, which in turn increased (decreases) transport of ozone-rich air to the polar lower stratosphere. On the other hand, strong (weak) midwinter planetary wave forcing causes a warmer (cooler) Arctic lower stratosphere in early spring (Newman et al., 2001), resulting in smaller (larger) chemical ozone losses in spring. The study by Manney et al. (2011) revealed that the unprecedented large Arctic ozone loss in 2011 is highly correlated with extremely cold lower-stratospheric temperatures in early spring. These extremely low temperatures are attributed to the unusually weak midwinter planetary wave forcing in the stratosphere (Hurwitz et al., 2011), as expected from a close relationship between polar spring temperatures and eddy heat flux in mid to late winter (Newman et al., 2001). In the Arctic, both dynamical ozone supply and chemical ozone losses are equally important for the interannual variability of the column ozone (Tegtmeier et al., 2008).

Weaker planetary wave driving in the stratosphere, which affects ozone through both dynamical and chemical processes, could arise from an enhanced number of extreme negative wave-1 heat flux events (i.e., DWC events), or from anomalously low positive heat flux values. Many studies have shown that an increased number of major SSW events that are associated with enhanced upward wave propagation into the stratosphere have led to significant increases of total column ozone and polar temperature in the winter, and subsequently less springtime ozone destruction (e.g., Rose and Brasseur 1985; Randel 1993; Liu et al. 2011; Hocke et al. 2015). However, so far the impact of DWC events on the stratospheric ozone in the Arctic has never been explored. Establishing the connection between DWC, stratospheric residual circulation, and polar temperatures will help to improve our understanding of the link between stratospheric dynamics and ozone variability.

The goal of this study is to investigate the impact of downward planetary wave reflection in the stratosphere on polar stratospheric ozone in the NH using both Modern Era Retrospective-analysis for Research and Applications (MERRA) and the NCAR's Community Earth System Model (CESM1 [WACCM]) model simulation. CESM1(WACCM) is able to capture the main features of DWC during NH winter (Lubis et al., 2016b), so it can be used to study the impact of DWC on ozone. Here, we focus on two DWC effects on ozone: (1) the direct effect, which is analyzed over the whole life cycle of the individual DWC event, and (2) indirect effect, which is analyzed through the impact of DWC on polar temperatures.

3.2 Data and Methods

3.2.1 MERRA Ozone

MERRA daily ozone product from 1979 to 2013 (Rienecker et al., 2011) was used to investigate the impact of DWC on polar stratospheric ozone. Ozone in MERRA is a fully prognostic model variable with tendencies calculated from advection and chemistry, as well as from the data analysis. The ozone product is derived from the Solar Backscattered Ultra Violet (SBUV2 v.8) retrievals from October 1978 to present and are assimilated with the Goddard Earth Observing System Model, Version 5 (GEOS-5) by using odd-oxygen mixing ratio (O_x) as its prognostic variable (Rienecker et al., 2011). This includes an odd-oxygen family transport model providing the ozone concentration necessary for solar absorption. The vertically integrated ozone tendency is given by (Lucchesi, 2012):

$$\frac{\partial \overline{O_x}}{\partial t} = \left[-\nabla \bullet (\overline{\vec{v}\, O_x})\right]_{DYN} + \left[\frac{\partial \overline{O_x}}{\partial t}\right]_{PHY} + \left[\frac{\partial \overline{O_x}}{\partial t}\right]_{ANA} \tag{3.1}$$

The dynamical contribution to the total ozone tendency is the convergence of odd-oxygen mixing ratio products (the first right-hand side term of Eq. 3.1). The total physics product (second term) includes the parameterized production and loss terms, and the analysis product (third term) is the corrected ozone tendency from data analysis (Lucchesi, 2012). In MERRA, the total ozone tendency from physics is decomposed into contributions from the chemistry, turbulence, and moist physics. Given a simplified chemical scheme used in MERRA model (Rienecker et al., 2011), the total ozone tendency from chemistry (CHM) is analyzed together with the correcting tendency term (i.e., CHM+ANA). The contributions of the turbulence and moist physics are negligible in the stratosphere (not shown) and therefore, are not considered in this analysis. We confirm that there are no major differences between the MERRA and Aura Microwave Limb Sounder (MLS) ozone concentrations in the polar lower-to-mid stratosphere (not shown). In addition, daily three-dimensional geopotential height, wind, and temperature fields from MERRA were also employed to understand the connection between DWC, residual mean transport and Arctic temperature.

3.2.2 Model and Simulation

In this study one 100-yr simulation (1955-2054) performed with CESM1(WACCM) was run with fixed surface emissions of GHGs and ODSs at 1960s levels. Fixing the GHG and ODS at 1960 levels allows us to study the ozone variability unmasked from any anthropogenic influence. The simulation is run with interactive ocean and sea ice components. To represent a more realistic interaction between the tropics and extra-tropical dynamics, the QBO is nudged by relaxing tropical stratospheric zonal-mean winds towards observations following Matthes et al. (2010). The solar cycle is prescribed as spectrally resolved daily variations following Lean et al. (2005). Observed volcanic eruptions of the twentieth century are included. An overview of this simulation and details of the model can be found in Chapter 2.

3.2.3 Dynamical Diagnostics

The influence of eddies on tracer transport (e.g., ozone) is quantified from the transform Eulerian mean (TEM) continuity equation for zonal mean tracer concentration (Andrews et al. 1987). For linear, steady, conservative waves, the TEM tracer transport equation can be written in the form:

$$\overline{\chi}_t = -\overline{v}^*\overline{\chi}_y - \overline{w}^*\overline{\chi}_z + e^{z/H}(\nabla \cdot \mathbf{M}) + \overline{S} \tag{3.2}$$

The Eq. 3.2 separates the local change in tracer concentration $\overline{\chi}_t$ as a result of transport processes that occur due to advection by the residual circulation $(\overline{v}^*, \overline{w}^*)$, the eddy effects $(\rho_0^{-1}\nabla \cdot \mathbf{M})$, and the chemical production minus loss rate $(\overline{S})$ (Andrews et al., 1987). The eddy effects are defined as the divergence of the eddy transport vector $(\mathbf{M})$, having the components as:

$$\mathbf{M}^{(y)} = -e^{-z/H}(\overline{v'\chi'} - \overline{v'\theta'}\,\overline{\chi}_z/\overline{\theta}_z) \tag{3.3}$$

$$\mathbf{M}^{(z)} = -e^{-z/H}(\overline{w'\chi'} + \overline{v'\theta'}\,\overline{\chi}_y/\overline{\theta}_z) \tag{3.4}$$

The $\overline{v}^*$ and $\overline{w}^*$ in Eq. 3.2 denote the TEM residual meridional and vertical winds defined as $\overline{v}^* = \overline{v} - \rho_0^{-1}(\rho_0\overline{v'\theta'}/\overline{\theta}_z)_z$ and $\overline{w}^* = \overline{w} + (a\cos\phi)^{-1}(\cos\phi\,\overline{v'\theta'}/\overline{\theta}_z)_\phi$, respectively. In addition, the residual mean circulation calculated from the streamfunction (Ψ_m) and the wave geometry diagnostic (Harnik and Lindzen, 2001) are also used in this study. The residual mass streamfunction $\Psi_m($ units in kg/s) is calculated as:

$$\Psi_m = (2\pi a)\,\rho_o \cos\phi \int_z^\infty \overline{v}^* e^{-z/H}\partial z. \tag{3.5}$$

The overbars indicate zonal means, primes are deviations from it and subscripts denote partial derivatives. The potential temperature and scale height are represented by θ and H, respectively. The Coriolis parameter and Earth's radius are, respectively, denoted by f and a.

3.2.4 Identification of DWC Event

We used a similar definition of DWC event as in Lubis et al. (2016b) based on daily total negative wave-1 meridional heat flux $(\overline{v'T'}_{k=1})$ at 50 hPa averaged between 60° and 90°N, which represents the 5th percentile of the daily $\overline{v'T'}_{k=1}$ distribution. The analysis focused on January, February and March (JFM), which is the period of maximum wave coupling between the troposphere and stratosphere. For time-lagged composites, the central date is the day on which $\overline{v'T'}_{k=1}$ has a minimum. The central dates of DWC event must be separated by at least 15 days. The time separation threshold is motivated by the time scale of planetary wave coupling Perlwitz and Harnik (2003). Applying our identification algorithm leads a total number of 20 DWC events in MERRA and 58 events in WACCM.

3.3 Observed Effects of DWC on Ozone

In this section, the direct effects of the DWC on polar stratospheric ozone is examined by first discussing the connection between transient wave forcing, residual circulation, and Arctic temperatures during the composite life cycle. Then, the connection between DWC and ozone is examined.

3.3.1 Connection between DWC, Stratospheric Residual Circulation, and Arctic Temperatures

Figure 3.1 shows the evolution of the high-latitude wave-1 heat flux anomaly (a), wave-1 EP flux divergence anomaly (b), residual circulation anomaly (c), and total potential temperature tendency (d), following the life cycle of DWC event. DWC is preceded by upward propagation of planetary-scale waves, indicated by a positive heat flux anomaly that migrates from the troposphere into the stratosphere from days -15 to -5 (Fig. 3.1a). This behavior is consistent with anomalous EP flux convergence in the stratosphere (Fig. 3.1b), which is dominated by the vertical divergence of the vertical EP flux (not shown). The heat flux evolution coincides with a positive (poleward) residual circulation anomaly (Fig. 3.1c) and the corresponding positive potential temperature tendency in the stratosphere. This tendency is consistent with air being advected downward over the pole, producing adiabatic warming (Fig. 3.1d).

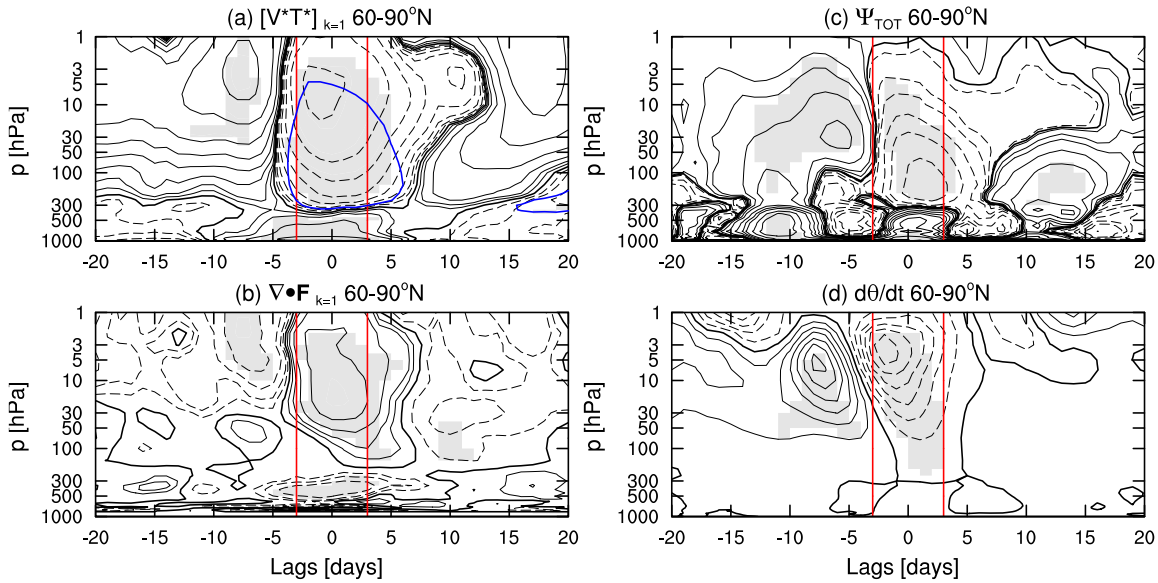

FIGURE 3.1: Evolution of the downward planetary wave events as a function of time from days -20 to +20 and pressure in MERRA: (a) wave-1 meridional heat flux anomaly (black contours) and zero contour of the total wave-1 meridional heat flux (blue contour), (b) wave-1 EP flux divergence anomaly, (c) residual mass-streamfunction anomaly, and (d) potential temperature tendency averaged from 60 to 90°N. The black contour intervals are: [1, 2, 4, 8, 16, 32, 64,..] Kms^{-1} for Fig. 3.1a, $\pm$ 0.5 m s^{-1}day^{-1} for Fig. 3.1b, $\pm$ 1 x 10^9 [0.5, 1, 2, 4, 8, 16, 32, 64,..] kg s^{-1} for Fig. 3.1c and $\pm$ 0.5 K day^{-1} for Fig. 3.1d. The gray shading indicates statistical significance at the 95%. All the significances are evaluated using a Monte Carlo approach.

From days -5 to +5, the stratospheric heat flux anomaly subsequently changes sign and reaches its minimum value. This negative heat flux value indicates that waves are reflected downward to the troposphere, resulting in DWC. Notably, the upward propagating waves encounter the reflecting surface and are forced to reflect and propagate downward into the troposphere due to a narrow meridional waveguide (not shown). The transient downward wave propagation leads to an EP flux divergence anomaly in the stratosphere (Fig. 3.1b), which in turn drives a negative (equatorward) residual circulation anomaly (Fig. 3.1c), and the subsequent negative potential temperature tendency in the stratosphere (Fig. 3.1d).

The evolution of the heat flux anomalies for downward planetary wave events is in agreement with the results of Dunn-Sigouin and Shaw (2015). Our results further indicate that the life cycle of DWC involves a transient reversal of anomalous poleward to equatorward residual circulation, and subsequent changes in potential temperature tendency (from positive to negative value). We note that the time-integrated potential temperature tendency over the life cycles is negative, indicating a net cooling of the polar vortex, while the time-integrated residual circulation is zero, showing that the impacts is reversible.

3.3.2 Observed Ozone Changes Induced by DWC

The former analysis suggests that DWC has a significant impact on the strength and structure of residual circulation. In this section, we analyze the implication of transient changes in residual circulation induced by DWC on polar stratospheric ozone. Figure 3.2 shows the corresponding transient evolution of the zonal-mean ozone tendencies averaged between 60 to 90^{o}N during upward downward planetary wave events. During downward wave events, the total ozone tendency transitions from a large positive value in the upper stratosphere to a large negative value in the lower stratosphere around day -4 (Fig. 3.2a). The evolution of the total ozone tendency is consistent with the evolution of high-latitude residual circulation anomalies (Fig. 3.1c). The large positive (poleward) residual circulation anomalies in the stratosphere from days -15 to -5 lead to more ozone transport to the polar vortex, and the subsequent negative (equatorward) residual circulation anomalies between days -4 to +5 leads to less ozone transport to the polar vortex.

To quantify the source of the transient changes in polar stratospheric ozone during DWC events, the decomposition of total ozone tendency into dynamics and chemistry-plus-analysis terms were analyzed. It is shown that the evolution of the total ozone tendency in the mid-lower stratosphere is dominated by the dynamical term (Fig. 3.2b). The ozone tendency due to dynamic in the mid-lower stratosphere is mainly attributed to the ozone transport via vertical (advection) residual circulation (Fig. 3.2e), while the tendency in the mid-upper stratosphere is mainly attributed to effects of eddy transport (Fig. 3.2f). Therefore, the dominance of the dynamical term on the total ozone tendency in the mid-lower stratosphere during the composite life cycle is consistent with the transient changes in residual circulation (Fig. 3.1c). On the other hand, the contribution of the chemistry to the total ozone tendency (Fig. 3.2c) is evident in the upper stratosphere. While

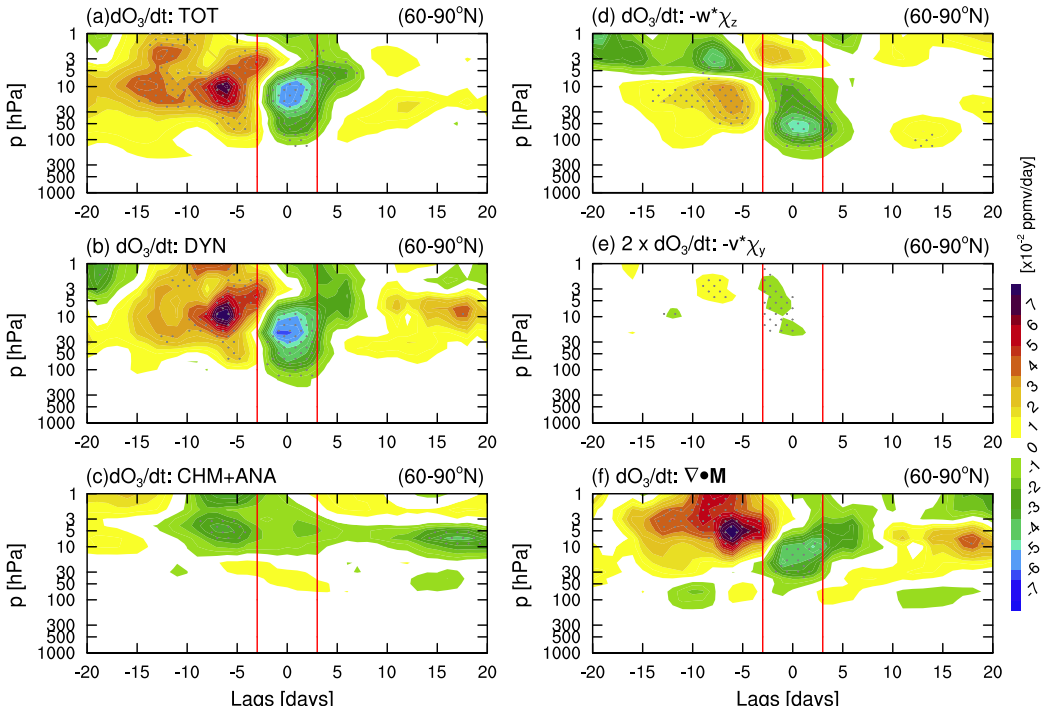

FIGURE 3.2: Evolution of the ozone tendencies for the composite DWC event as a function of time and pressure, averaged from 60 to 90°N in MERRA: (a) total ozone tendency, (b) ozone tendency anomaly due to dynamics and (c) due to parameterized chemistry. Tendency from the dynamics is decomposed into (d) vertical advection, (e) meridional advection, and (e) eddy transport effects. Stippling indicates statistical significance at the 95% level using a Monte Carlo approach.

small significant regions of negative ozone tendency from chemistry are seen prior to the maturation phase of DWC (above 10 hPa days -10 to -5, Fig. 3.2c), the magnitudes over the whole life cycle are relatively small compared to those caused by dynamics. These results suggest that transient changes in the polar mid-lower stratospheric ozone during the DWC life cycle are primarily due to changes in dynamical ozone transport.

The same conclusion can be drawn by assessing the instantaneous correlation between the two extreme stratospheric wave-1 heat flux events. Figure 3.3a shows a two dimensional histogram of total ozone tendency versus residual vertical wind anomaly (w*) averaged over 60-90°N at 50 hPa. The black contour lines indicate the distribution of all daily JFM samples from 1979 - 2013 (90 days yr^{-1} x 35 yr = 3150 days). The red and blue dots indicate the days with positive and negative extremes in total wave-1 heat flux, respectively (the top and bottom 5%). Negative extremes are associated with DWC events. The overall circular pattern of contours is evidence of a strong negative correlation between polar cap-averaged ozone tendency and w*. This is consistent with a direct calculation of time series correlation, which is statistically significant (R=-0.80). In addition, the days with positive and negative extremes (red and blue dots, respectively) are systematically skewed compared to the background distribution, suggesting that enhanced extreme negative heat flux (i.e., stronger DWC event) corresponds to a weaker residual circulation and a higher negative ozone tendency, and vice versa for positive extremes. In addition, Fig. 3.3b

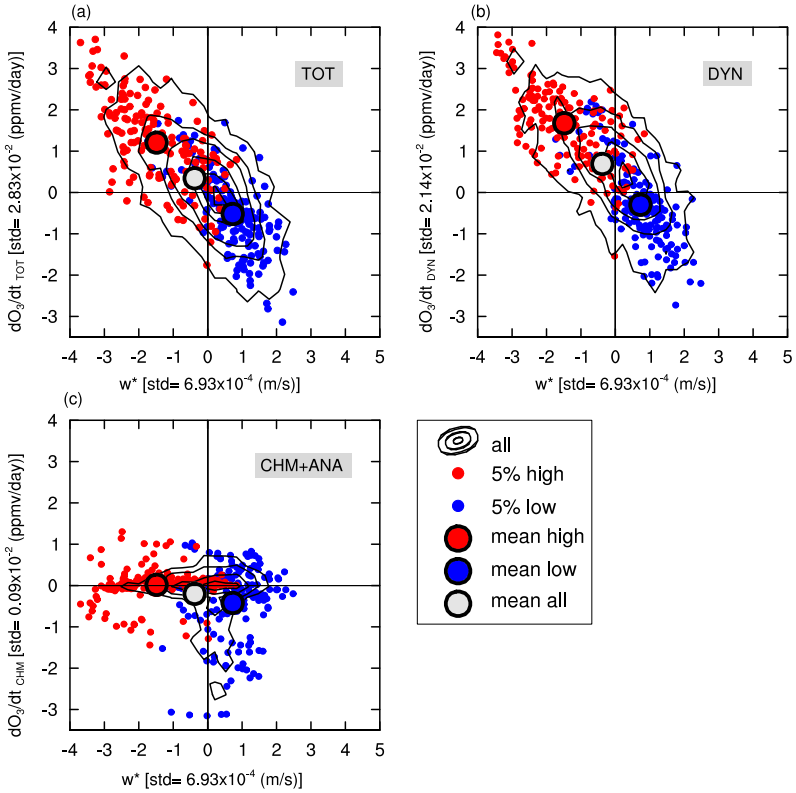

FIGURE 3.3: Two-dimensional joint probability density distribution of (a) total ozone tendency vs residual vertical wind velocity (averaged over 60 to 90°N at 50 hPa) in JFM, (b-c) as in Fig. 3.3a, but for total ozone tendency due to dynamics and to parameterized chemistry, respectively. The axes are normalized to standard deviations in each quantity. Black contours show the probability distribution of all JFM days during 1979-2013 (contour shown are 1, 2, 3, 4, 5,.. % of total). Red and blue dots show days with 5% extreme maximum and minimum total wave-1 meridional heat flux. Larger circles indicate the mean of the distribution of all points (white), high extremes (red), and low extremes (blue).

shows a similar diagnostic for the dynamical ozone tendency versus w*. Again, the overall two dimensional distribution suggests a strong negative correlation between dynamical ozone tendency and the vertical component of the residual circulation, with a temporal correlation coefficient of -0.83. This reflects the fact that the dynamical ozone tendency is strongly correlated with changes in residual circulation. We found no instantaneous relationship between chemical ozone tendency and w* (R=-0.04). Although analyses in Fig. 3.3 are based on the 5% negative extreme events, the described relationships do not depend on the fraction of extreme events considered (not shown), and thus these results are representative of the general behavior. The same conclusions are also obtained, and are even more robust, when using total column ozone tendency (TCO) instead of an ozone-mixing ratio at 50 hPa (not shown).

Finally, the direct cumulative effects of DWC events over the whole composite life cycle are analyzed. We previously showed that DWC events are transient and involve a positive to negative total ozone tendency evolution. Therefore, it is possible that the effects on ozone could integrate to zero over their life cycles, meaning the impacts would be reversible. To check this, we

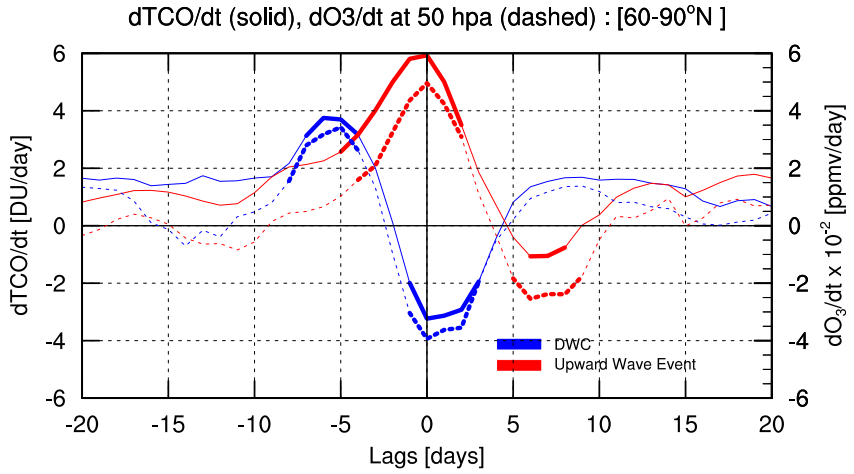

FIGURE 3.4: Evolution of the total column ozone tendency (solid lines) and mixing ratio ozone tendency (dashed lines) tendency at 50 hPa, averaged between 60-90°N for DWC event (blue) and upward wave event (red). Statistical significance at the 95% level is denoted with thick lines using a Monte Carlo approach.

calculated the evolution of total column ozone (TCO) tendency and ozone tendency at 50 hPa averaged between 60 to 90°N for both DWC events (blue lines) and upward wave events[1] (red lines) (Fig. 3.4).

The time integration of the significant TCO and ozone tendencies over the DWC life cycles is zero, indicating a reversible impact on ozone (Fig. 3.4). This is consistent with the reversible impact of DWC on residual circulation (Fig. 3.1c). On the other hand, the time integration of the significant TCO and ozone tendencies during upward wave events is positive, indicating a net-increased ozone (Fig. 3.4). This is again consistent with an irreversible poleward residual circulation during upward planetary wave events (not shown). These results suggest that the direct cumulative effect of DWC is to prevent the typical increase of ozone due to upward planetary wave events.

3.4 Modeled Effects of DWC on Ozone

Determining the connection between DWC, stratospheric residual circulation, and Arctic temperature is one of the keys to improving our understanding of the link between stratospheric dynamics and ozone variability both in the real atmosphere and in the stratosphere-resolving chemistry-climate models. In this section, we attempt to test if the linkages between DWC and transient changes in polar stratospheric ozone can be confirmed in a current chemistry-climate model, CESM1(WACCM).

[1] An upward planetary wave event is identified when the time series $\overline{v'T'}_{k=1}$ first crosses the 95th percentile of the JFM distribution.

3.4.1 Connection between DWC, Residual Circulation, and Arctic Temperatures in CESM1(WACCM)

Figure 3.5 shows the evolution of the high-latitude wave-1 heat flux anomaly, wave-1 EP flux divergence anomaly, residual circulation anomaly, and potential temperature tendency during downward planetary wave events in CESM1(WACCM). In general, the life cycle of downward wave events in simulation reveals similar connections between high-latitude wave-1 heat flux anomalies, wave-1 EP flux divergence anomalies, residual circulation anomalies, and potential temperature tendency, as shown in MERRA reanalysis. In particular, the upward propagating waves begin from days -20 to -6, indicated by a migration of a positive high-latitude stratospheric heat flux anomaly from the troposphere to the stratosphere (Fig. 3.5a). The high-latitude positive heat flux anomaly coincides with a positive residual circulation anomaly (Fig. 3.5c), and the corresponding positive potential temperature tendency in the Arctic stratosphere (Fig. 3.5d). The enhanced downwelling is consistent with enhanced EP flux convergence in the stratosphere (Fig. 3.5b).

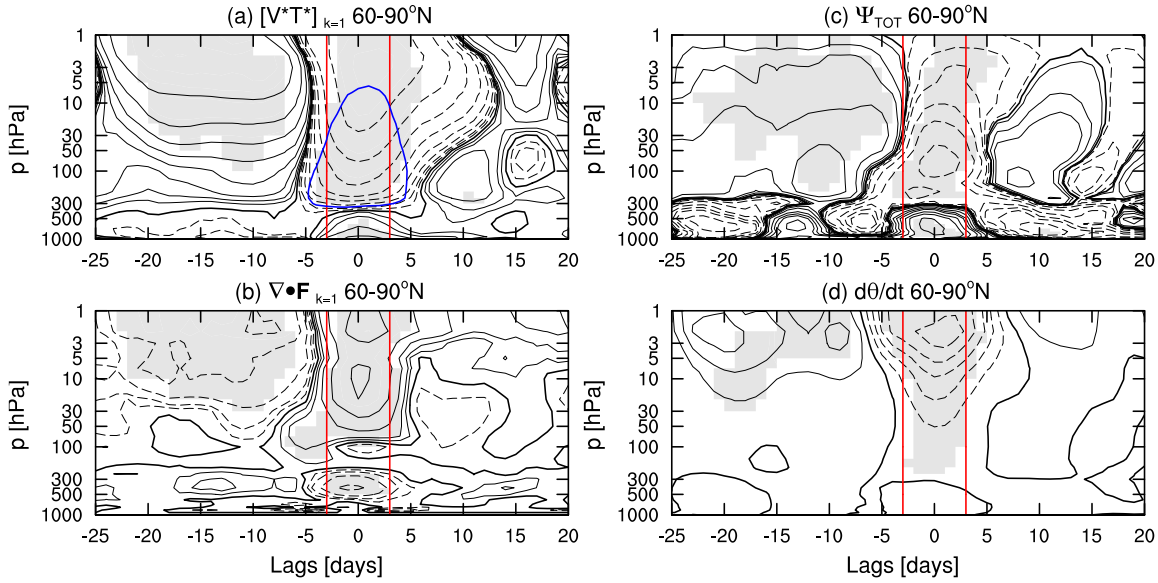

FIGURE 3.5: As in Fig. 3.1, but for a 100-yr CESM1(WACCM) simulation.

Furthermore, the stratospheric heat flux anomaly subsequently changes sign and reaches its minimum value from days -5 to +5 (Fig. 3.5a). The transition from positive to negative heat flux is suggestive of upward wave propagation from the tropospheric source followed by downward wave propagation from the stratosphere. The negative heat flux anomaly coincides with anomalous equatorward residual circulation and the corresponding positive potential temperature tendency in the polar stratosphere. Overall, the results from the model simulation support our observational-based analysis, showing that the life cycle of DWC events involve a transient reversal of residual circulation anomalies and potential temperature tendencies. In addition, the

impacts on residual circulation (potential temperature tendency) are reversible (irreversible) over the lifecycle.

3.4.2 Simulated Ozone Changes Induced by DWC

To investigate the direct effect of DWC on ozone in the model simulation, the ozone tendency budget analysis similar to Fig. 3.2 is repeated here. Figure 3.6 shows the time evolution of total ozone tendencies during the composite life cycle. Consistent with MERRA, the negative ozone tendency in the model occurs during the time of maximum DWC events (days -3 to +3), between 100 and 5 hPa (Fig. 3.6a). This negative ozone tendency is preceded by a positive ozone tendency (days -20 to 5). The transition of positive to negative ozone tendency in the lower-to-mid stratosphere is consistent with poleward to equatorward residual circulation anomalies (Fig. 3.5c). Interestingly, there is a strong positive ozone tendency in the upper stratosphere (above 5 hPa) during the time of maximum DWC events, which is not captured by MERRA.

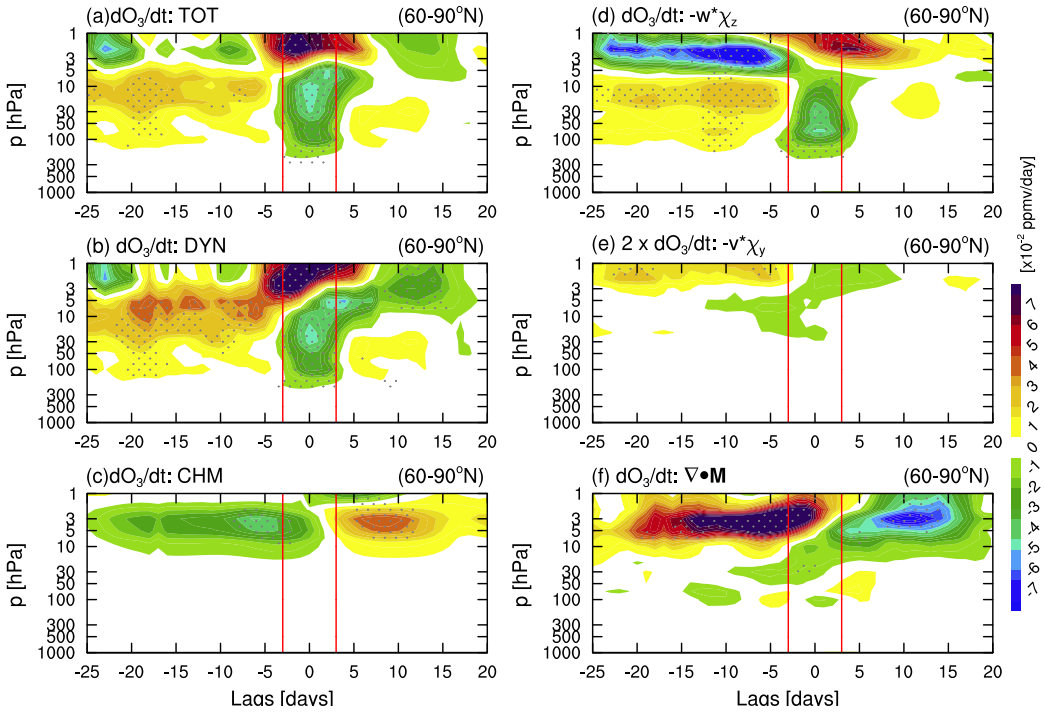

FIGURE 3.6: As in Fig. 3.1, but for a 100-yr CESM1(WACCM) simulation.

By decomposing the total ozone tendency into dynamical and chemical terms, it can be seen that transient changes in ozone dynamics dominate the total ozone tendency during the composite life cycle (Fig. 3.6b-c). In the mid-lower stratosphere, this tendency is mainly attributed to the vertical advection process (Fig. 7d), while in the upper stratosphere the eddy transport effect becomes dominant (Fig. 3.6f). In addition, the strong positive total ozone tendency in the upper stratosphere during the time of maximum DWC events is attributed to the dynamical ozone tendency due to eddy transport effect and vertical advection through the residual circulation (Fig.

3.6f). The magnitude of these two quantities in the upper stratosphere is relatively higher in the model compared to MERRA; thus leading to the discrepancy of the total ozone tendency over this region. Furthermore, the ozone tendency due to chemistry in the upper stratosphere is relatively weaker and in the opposite sign of the ozone tendency due to dynamics (Fig. 3.6c). The overall results supports our observational-based analysis that the transient changes in polar stratospheric ozone during a DWC event are mainly due to changes in the dynamical ozone transport.

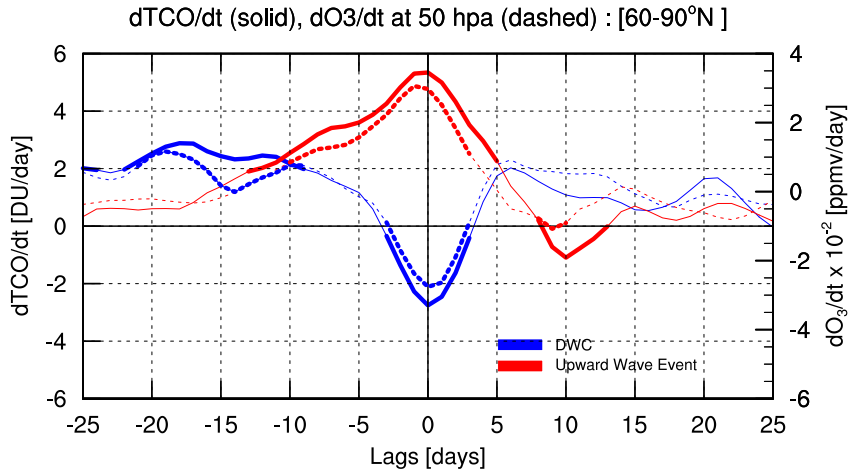

FIGURE 3.7: As in Fig. 3.4, but for a 100-yr CESM1(WACCM) simulation.

As a last step, the direct cumulative effects of DWC events were examined in the same way as the reanalysis. The previous results showed that DWC events are transient and involves a positive to negative total ozone tendency evolution. The time evolution of total column ozone (TCO) tendency and ozone tendency at 50 hPa averaged between 60 to 90°N for the composite of DWC event (blue lines) and upward wave event (red lines) is shown in Fig. 3.7. Consistent with MERRA, the time integration of significant TCO and ozone tendencies during the DWC events is zero, indicating a reversible impact on the ozone (Fig. 3.7). On the other hand, the time integration of the significant TCO and ozone tendencies during upward wave event are positive, indicating a net increased ozone (Fig. 3.7). This confirms our previous finding suggesting that the direct effect of the full wave reflection life cycle is to prevent the typical increase of ozone due to upward planetary wave events.

3.5 Seasonal Impact of DWC on Ozone

The former analysis shows that an individual DWC event has a statistically significant impact on the polar stratospheric ozone. While an individual event's impact occurs on a short time scale, several events in an individual JFM season may produce an impact on a longer time scale. In this section, we briefly examine the cumulative impacts on Arctic total column ozone during seasons that are dominated by DWC events.

3.5.1 Reflective versus Absorptive Winters

In order to analyze the seasonal impact of DWC on column ozone, we classify winter stratospheric basic states into reflective and absorptive states. The classifications are based on the vertical wave numbers (m) (averaged between 1-5 hPa and 65-75°N) and zonal mean wind (U) at 30 hPa (averaged between 60-85°N), similar to Perlwitz and Harnik (2003).

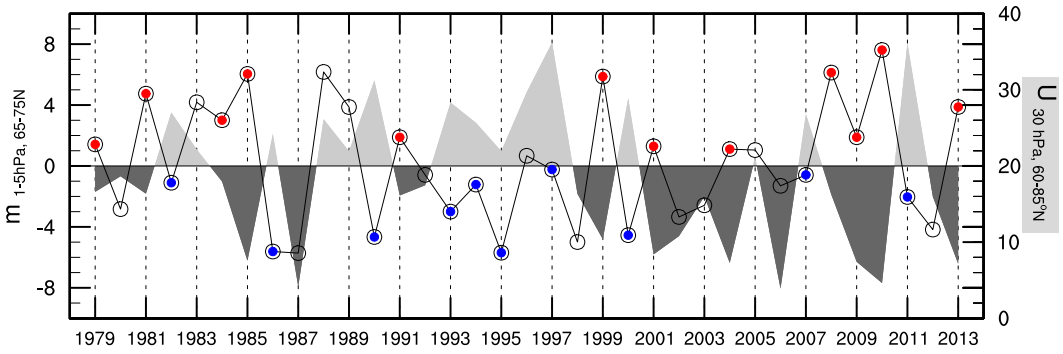

FIGURE 3.8: Time series of seasonal (JFM) mean m and $U(30)$ from MERRA. The blue (red) circles indicate the most reflective (absorptive) winters (further discussed in the text).

Reflective winters (favourable for DWC events) are defined when $m < 0$ and $U(30) > 2.5\sigma$, while absorptive winters (with dominant upward events) are defined when $m > 0$ and $U(30) < 2.5\sigma$. We exclude the years with (without) SSW events from the potential reflective (absorptive) winters. The time series of selected reflective and absorptive winters are shown in Fig. 3.8. Using this definition, we found the most reflective (absorptive) winters, 8 (11) in MERRA and 19 (21) in CESM1(WACCM). We also note that the composites of total vertical components of wave-1 EP flux during reflective (absorptive) winters are negative (positive) in the lower-to-mid stratosphere, which is consistent with downward (upward) wave events (not shown).

Figure 3.9 shows composites of the zonal-mean wind, wave-1 geopotential height, and temperature difference in JFM for the composite of reflective and absorptive winters in MERRA. During reflective winters, the maximum zonal-mean zonal wind resides in the mid-stratosphere, and consequently the region of vertical reflecting surface extends down to 3 hPa (Fig. 3.9a). This vortex configuration is favorable for DWC events, which is indicated by eastward phase tilt with heights of the wave-1 structure from the mid-troposphere to the mid-stratosphere (Fig. 3.9b). In addition, the Arctic mid-lower stratosphere is significantly colder; the polar cap temperature at 50 hPa is 7 K lower than the climatological mean (Fig. 3.9c). This cooling is consistent with a strong and stable polar vortex, which is associated with less wave absorption in the stratosphere due to enhanced DWC events.

In contrast, during absorptive winters, the vertical reflecting surface shifts upward into the upper stratosphere and the meridional waveguide becomes wider in the mid-stratosphere (Fig. 3.9d). This configuration is favorable for upward wave events, indicated by the westward phase tilt with height of the wave-1 structure (Fig. 3.9e). The Arctic mid-lower stratosphere is significantly

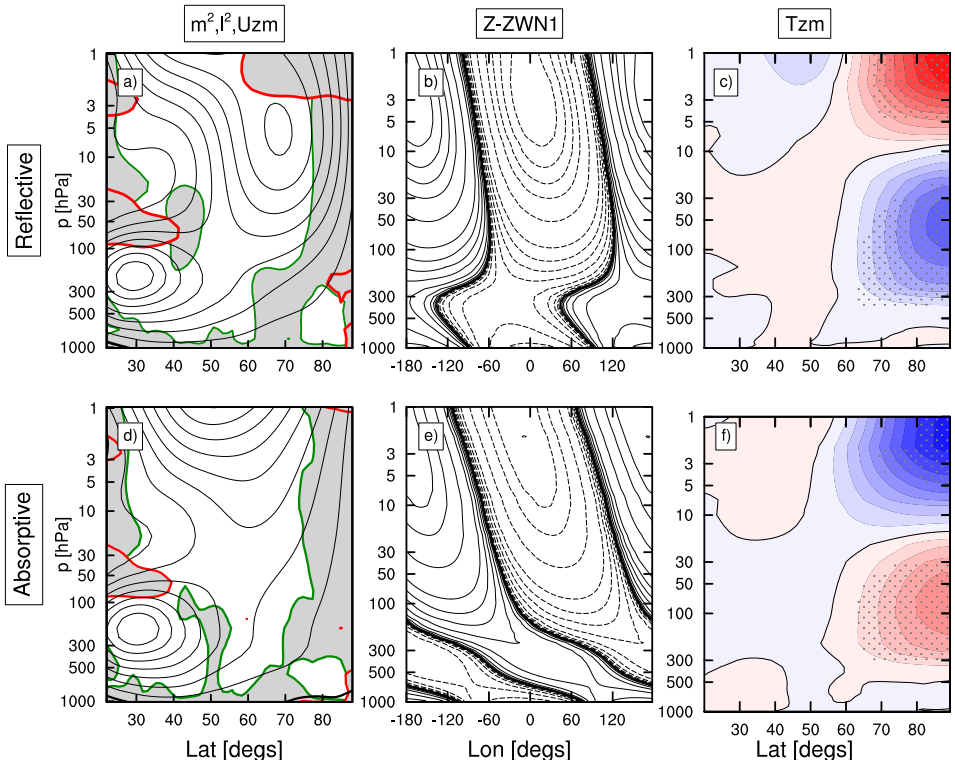

FIGURE 3.9: (a, d) Composites of the zonal wind and wave geometry for (top) reflective and (bottom) absorptive winters in JFM from MERRA. The grey shading indicates regions of wave evanescence and the red (green) contour lines indicates the vertical reflecting surface $m^2 = 0$ (meridional wave guide $l^2 = 0$); contour interval for the zonal wind is 5 m/s. (b-e) As in (a, d), but for composites of the wave-1geopotential heights averaged between 60 to 70°N; contour interval is logarithmic powers of 2: $\pm$ [0.5, 1, 2, 4, 8, 16, 32, 64, 128, 256,..]m. (c, f) temperature differences: (c) reflective years from the 1979-2013 climatological mean (i.e., blue contours indicate regions where temperature is cooler than the climatology); (f) absorptive years from the climatological mean. The contour interval is 1 K and stipplings denote differences significant at the 95% confidence level.

warmer, by approximately 6 K higher than the climatological mean at 50 hPa (Fig. 3.9f). The warmer and more disturbed polar vortex during absorptive winters is consistent with enhanced upward propagating waves into the stratosphere. The structures of the vortex, wave geometry, vertical wave-1 pattern, and polar temperature anomalies during reflective and absorptive winters are confirmed by the model simulation (not shown).

3.5.2 Seasonal Impact on Arctic Column Ozone

In order to estimate the seasonal impacts of DWC events on Arctic column ozone, the evolution of high-latitude averaged daily column ozone during reflective and absorptive winters was determined by calculating the daily seasonal cycle averaged over each sub group of winters both in MERRA and CESM1(WACCM) simulation (Fig. 3.10). On average, relatively lower (higher) total column ozone is observed during the reflective (absorptive) years, particularly in late winter and early spring. We note that a less severe springtime ozone destruction in CESM1(WACCM) during

reflective years (in March and April) compared to MERRA, is due to the fact that the simulation is run with fixed GHG and ODS forcings.

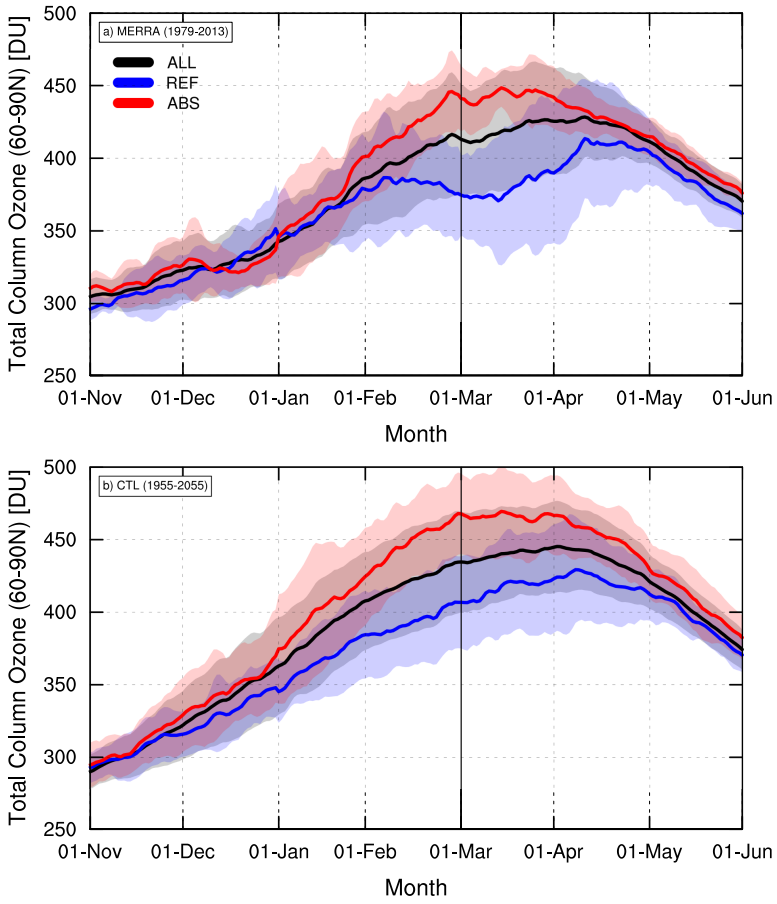

FIGURE 3.10: Evolution of daily column ozone (DU) averaged from 60 to 90°N for the composite of reflective (blue) and of absorptive (red) years in (a) MERRA and (b) CESM1(WACCM). The shading indicates the region of ± one standard deviation for reflective years (reddish), absorptive years (bluish), and all years (light gray).

During reflective years, the column ozone in late winter and early spring (Fig. 3.10) is relatively lower compared to the all-year and absorptive mean. This is consistent with a strong and cold polar vortex due to increased DWC events (Fig. 3.9), which leads to high amount of ozone destruction in spring via heterogeneous processes. This process is termed as an indirect effect of DWC. In addition, a relatively low column ozone during reflective winters is also attributed to the direct effect of DWC, preventing the typical increase of ozone due to upward planetary wave events (Figs. 3.4 and 3.7). These two effects altogether result in lower column ozone in late winter and in spring.

Conversely, during absorptive years (with SSW events), a relatively higher column ozone compared to the climatological mean (Fig. 3.10) is consistent with a weak and warm polar vortex (Fig. 3.9), resulting in less springtime ozone destruction, and with increased dynamical ozone supply

induced by enhanced upward wave events (Figs. 3.4 and 3.7). This result is consistent with previous studies, showing that SSWs lead to significantly increased polar ozone concentrations in the lower stratosphere (e.g., Liu et al. 2011; Hocke et al. 2015).

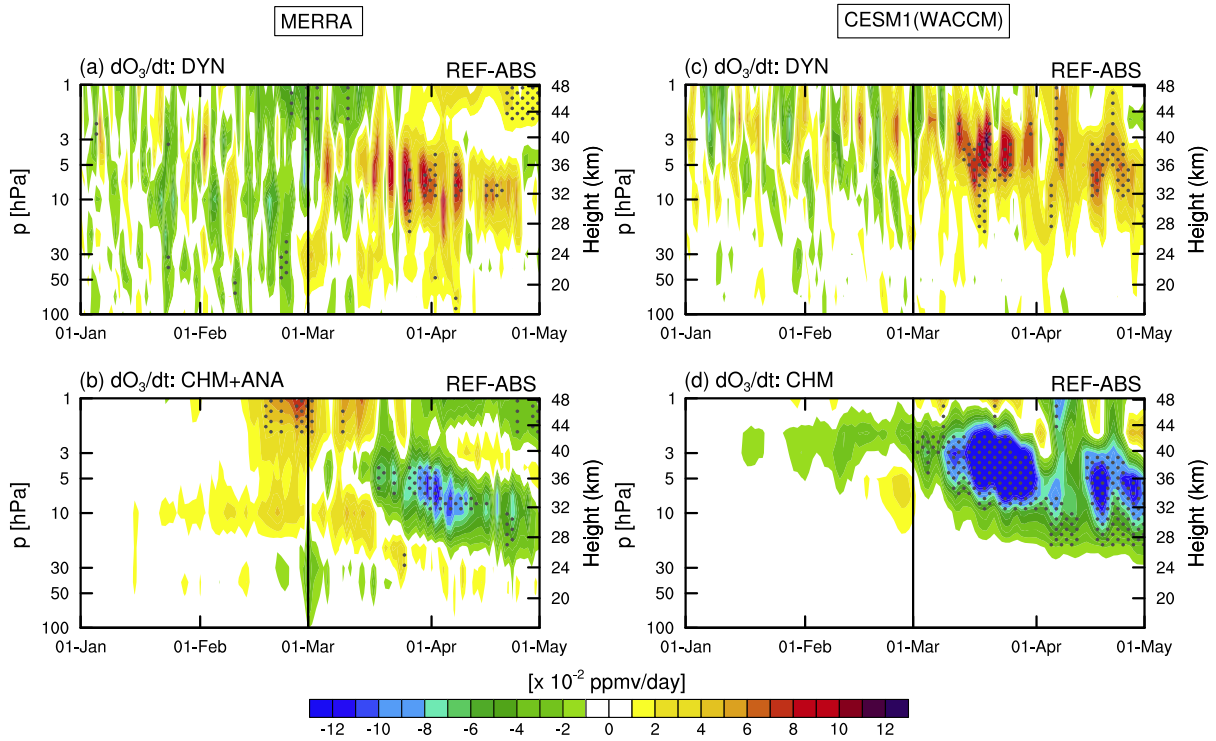

FIGURE 3.11: Differences in the daily-mean ozone tendency (averaged from 60-90°N) between REF and ABS in MERRA (left) and CESM1(WACCM) (right) as a function of time and pressure, due to (a,c) dynamics, and (b,d) chemistry. Stipplings denote differences significant at the 95% confidence level.

The aforementioned indirect effect of DWC should only affect ozone concentration in spring when the polar stratosphere becomes sunlit. To show this, we calculated the differences in total ozone tendency due to dynamics and chemistry between reflective and absorptive years (Fig. 3.11). Both MERRA and the model simulation show that, a significant reduction in ozone chemistry tendency in early spring is stronger in reflective years compared to absorptive years (Figs. 3.11a,d). This result is consistent with relatively low springtime column ozone during reflective years, which is attributed to a cold polar temperature that leads to large chemical ozone destruction in spring via heterogeneous processes. On the other hand, an increased tendency from dynamics in spring during reflective years is likely to the sharpened meridional and vertical gradients of ozone after the spring time ozone loss occurs.

3.6 Conclusions and Discussion

The goal of this study was to investigate the impact of DWC on polar stratospheric ozone in order to fully understand the mechanisms controlling the variability of Arctic stratospheric ozone. The

key results of this study are as follows:

1. The life cycle of DWC events involves a transient reversal of poleward to equatorward residual circulation anomalies, and subsequent changes in potential temperature tendency.

2. The time-integrated potential temperature tendency over the composite life cycles is negative, indicating a net cooling of the polar vortex induced by DWC, while the time-integrated residual circulation is zero, showing that the impacts is reversible.

3. The transient changes in polar stratospheric ozone during the life cycle of DWC events are primarily attributed to changes in the dynamical ozone transport.

4. The direct effect of DWC events on ozone is to prevent the typical increase of ozone due to upward planetary wave events, which is consistent with the reversible impact of DWC on the residual circulation.

5. The indirect effect of DWC leads to increase springtime ozone loss due to cold polar temperature. This effect is consistent with the irreversible cooling induced by DWC during the composite life cycles.

6. Winter seasons dominated by DWC events (reflective winters) lead to lower Arctic column ozone, while seasons dominated by increased wave absorption (absorptive winters) lead to relatively higher Arctic column ozone. This is consistent with the cumulative impacts of downward and upward planetary wave events on ozone via changes in the strength of the polar vortex and the residual circulation.

The results of this study establish a new perspective on dynamical processes controlling the Arctic ozone variability. Previous studies have shown that weaker midwinter planetary wave forcing due to less wave activity entering the lower stratosphere, leads to cooler spring Arctic temperatures, and thus to more ozone destruction (e.g., Randel et al. 2002; Newman et al. 2001; Weber et al. 2003; Tegtmeier et al. 2008). Our results suggest that weaker midwinter planetary wave forcing in the stratosphere can also be attributed to enhanced DWC events in the presence of the vertical reflecting surface (instead of weaker tropospheric wave source). The results establish that dynamical processes via DWC events can contribute to a large springtime ozone destruction through their impact on the polar temperatures.

Recent studies have shown that large chemical ozone loss in the spring of 2011 is one of the major reasons for the unprecedented low Arctic column ozone (e.g., Manney et al. 2011; Isaksen et al. 2012; Hommel et al. 2014). This is attributed to extremely low mid-winter temperatures in the lower stratosphere resulting from weaker midwinter planetary wave forcing (Hurwitz et al., 2011). Since winter of 2011 is classified as a reflective winter based on our definition (with a strong polar vortex and downward wave reflection), the unprecedented low Arctic column ozone of 2011 could be also attributed to the cumulative effects of DWC events.

Our results also reveal that the amount of wave absorption directly influences polar Arctic temperatures, and therefore the amount of ozone destruction in spring. Since wave absorption is minimal during reflective winters, the winters tend to be cold with more ozone destruction. The process of wave reflection and absorption is highly variable, and the amount and location depend on the tropospheric source of the waves, on the structure of the vortex (on which the waves propagate), and on non-conservative effects (McIntyre and Palmer, 1983; Harnik and Heifetz, 2007; Harnik, 2009). A better understanding of the tropospheric conditions that lead to such events is needed to improve the understanding of the link between stratospheric dynamics and ozone variability.

A recent multi-model inter-comparison of chemistry climate models (CCMs) concludes that the models do not produce a consistent prediction of the evolution of Arctic temperatures and ozone loss in the twenty-first century, mainly because of discrepancies in the model's dynamics (SPARC CCMVal 2010, Chapter 4). Understanding the impact of DWC events on polar stratospheric ozone and temperatures could provide a useful diagnostic to validate the influence of stratospheric dynamics on springtime column ozone in coupled CCMs.

Chapter 4

Climate Change Effects on the Variability of Downward Wave Coupling in the Northern Hemisphere

This chapter will be submitted as an article to Geophysical Research Letters (GRL).

Lubis, S. W., K. Matthes, N. Harnik, N. Omrani, and S. Wahl, 2016: Climate Change Effects on the Variability of Downward Wave Coupling in the Northern Hemisphere (to be submitted).

The authors' contributions to this publication are as follows:

- S. Lubis contributed with ideas, performed timeslice experiments and all analyses, produced all figures and wrote the manuscript.
- K. Matthes initiated the study and model experiments, contributed to ideas and discussions on the analysis and paper writing.
- N-E. Omrani and N. Harnik contributed with ideas and discussion on the analysis and with comments on the manuscript.
- S. Wahl contributed with comments on the manuscript and helped to setup some timeslice simulations.

Abstract

The occurrences of downward wave coupling (DWC) between the stratosphere and troposphere in the NH have been recently shown to be strongly influenced by the QBO and the SST variability. However, the effects of the anthropogenic factors on DWC in the NH have not been investigated so far. Here we examine the effects of anthropogenic forcing on DWC in the NH using a set of transient and timeslice simulations performed with CESM1(WACCM) chemistry-climate model. The analysis shows that a significant reduction of DWC events is detected in the future, with a shift of their timing toward midwinter. This is attributed to a change in the timing of the reflecting surface formation and increased wave absorption in early winter. The tropospheric response to DWC in the future is less reminiscent of the positive phase of the NAO. This is associated

with a weaker DWC event, which leads to weaker baroclinic eddy feedbacks in the troposphere. The results indicate for the first time how a future change in stratospheric dynamics via DWC, as simulated under the extreme climate change conditions, may affect the troposphere-surface system.

4.1 Introduction

Planetary waves play important roles in many aspects of the climate system, including their roles on regional climate (e.g., Petoukhov et al. 2013; Screen and Simmonds 2014), on stratospheric ozone (e..g, Randel et al. 2002), and on downward dynamical links between the stratosphere and troposphere (e.g., Kuroda and Kodera 1999; Baldwin and Dunkerton 1999; Song and Robinson 2004). Recent climate model studies have found that planetary wave activity will intensify with the increase of GHGs, due to an increased meridional temperature gradient in the lower stratosphere (e.g., Sigmond et al. 2004; Eichelberger and Hartmann 2005) or to changes in the location of critical layers within the subtropical lower stratosphere (Shepherd and McLandress, 2011). On the other hand, cooling of the polar lower stratosphere induced by ozone depletion, can also increase the meridional temperature gradient in the lower stratosphere and hence could enhance extratropical wave activity in the same fashion as GHG increases (e.g., Neff et al. 2008; Hu and Fu 2009; Lubis et al. 2016a). Therefore, understanding the effects of both the GHG increase and ozone changes will help to better understand the evolution of planetary wave activity in the future. Most previous studies on the impact of future changes in GHG and ozone on planetary wave activity in the NH focus on the upward propagating wave activity from the troposphere to the stratosphere, while the impact of climate change on downward wave activity between the stratosphere and troposphere (called downward wave coupling [DWC]) is not understood. Here the impact of anthropogenic forcing factors on DWC in the NH is examined for the first time.

DWC can impact the tropospheric wave patterns (both stationary and transient) and surface weather via a well-defined bounded wave geometry[1] (e.g., Perlwitz and Harnik 2003; Shaw et al. 2010; Lubis et al. 2016b). DWC occurs during midwinter in the NH when the upward propagating planetary waves decelerate the flow in the upper stratosphere, causing the potential vorticity gradient to become negative (Harnik, 2009; Lubis et al., 2016b). Recent studies have shown that the tropospheric impact of DWC resembles the positive phase of the North-Atlantic Oscillation (NAO), including a poleward jet shift over the North Atlantic sector (Shaw and Perlwitz, 2013; Dunn-Sigouin and Shaw, 2015; Lubis et al., 2016b). More recently, Lubis et al. (2016b) found that the strength of the tropospheric response to DWC is controlled by synoptic-scale eddy feedback and atmosphere-ocean interaction. Thus, a better knowledge of DWC event and the involved mechanisms will help to improve the representation of tropospheric circulation under climate change in climate models.

[1] a configuration where the vertical reflecting surface sits above the meridional waveguide

A recent set of sensitivity experiments with the CESM1(WACCM) chemistry-climate model, consisting of a number of single natural forcing experiments (QBO and SSTs), showed that variability related with SSTs and the QBO are equally important in establishing a correct representation of DWC in the CCM (Lubis et al., 2016b). Excluding SST (QBO) forcing, the DWC frequency dropped (increased) significantly. In addition, these two natural forcing factors also influence the tropospheric response to DWC, both through a modification of wave propagation and interaction with the mean flow in the stratosphere, and through a modification of the internal tropospheric feedbacks (Lubis et al., 2016b). However, the mechanisms by which anthropogenic forcing factors affect the DWC in the NH remains unclear.

The goal of this study is to examine how DWC variability in the NH, particularly their seasonality, will change in the future, and what the relative contribution of GHGs and ODSs to this change is. To this end, we use different transient and timeslice CESM1(WACCM) simulations that represent present and future climate conditions.

4.2 Data and Methods

4.2.1 Model Simulations

All simulations used were performed with the National Center for Atmospheric Research (NCAR) Community Earth System Model (CESM) version 1.0.2, a fully coupled global Earth system model, which contains an interactive ocean, land, sea ice, and atmosphere components (see Chapter 2 for details).

We used two transient (TR) simulations covering the period from 1955 to 2099 (145 years), TR-NAT and TR-RCP8.5, similar as in Lubis et al. (2016b). The TR-NAT simulation uses fixed GHG and ODSs at 1960s levels, while the TR-RCP8.5 uses transient anthropogenic forcing following observations until 2005 and the RCP Scenario 8.5 (Meinshausen et al., 2011) thereafter. Future changes in DWC characteristics are assessed by comparing the last 40 winters of the simulation (2060 to 2099, "future") with the first 40 ones (1960 to 1999, "past"). In addition, results from the TR-NAT simulation are compared with the extreme climate change scenario of the TR-RCP8.5 run in order to understand the role of future changes in GHG and ODS forcing.

We also employ different timeslice (TS) simulations of about 40 years with the same model which include changes in concentrations in GHGs and ODS for present and projected future climate. The TS-GHG experiment uses seasonally varying surface emissions of ODSs at 1960s levels, in combination with surface emissions of GHGs at 2080s levels. For the TS-ODS experiment, ODSs at 2080 levels in combination with surface emissions of GHGs at 1960s levels are used. All timeslice experiments are initialized using restart files from the year 2080 of the TR-RCP8.5 run, and are coupled with interactive ocean and sea ice. The sensitivity simulations allow us to isolate the influence of each anthropogenic forcing (GHG and ODS) on DWC. See Table 4.1 for a detailed description of each TR and TS simulations.

TABLE 4.1: Description of CESM1(WACCM) transient and timeslice experiments. TR = transient run and TS = timeslice run. All experiments are run with interactive SSTs-sea ice.

Experiment	Period	GHGs	ODSs
TR-NAT	1955-2099 (145 yr)	1960s level	1960s level
TR-RCP8.5	1955-2099 (145 yr)	OBS+RCP8.5	OBS+RCP8.5
TS-ODS	40 yr	1960s level	2080s level
TS-GHG	40 yr	2080s level	1960s level

4.2.2 Statistical-Dynamic Approach

Upward and downward propagating planetary wave signals are isolated using a time-lagged singular value decomposition (SVD), similar as in Perlwitz and Harnik (2003) and Lubis et al. (2016b). This diagnostic considers two geopotential heights of zonal wavenumber k both at different altitudes. The maximal relationship between the two wave fields is determined by the correlation of the daily temporal expansion coefficients (A an B) of the leading coupled mode $\left[A^k(t), B^k(t+\tau)\right]$ for each time lag τ. The tropospheric field is held fixed at 500 hPa, and the respective stratospheric levels are shifted so that a negative (positive) time lag indicates that the stratospheric (tropospheric) wave fields are leading.

In addition, a diagnostic of the basic-state wave propagation characteristics of Harnik and Lindzen (2001) is used to determine the existence and location of turning surfaces for meridional and vertical propagation. This diagnostic is a more accurate indicator of wave propagation regions than the index of refraction, since it diagnoses meridional and vertical propagation separately (Harnik and Lindzen, 2001; Lubis et al., 2016b).

4.3 Seasonality of DWC Events

We first focus on the analysis of the seasonal variation of DWC events. Figure 4.1 shows three-month overlapping periods of lagged SVD correlations (rSVD) between Z-ZWN1 at 500 and 10 hPa. DWC events occur if the correlation peaks at a negative time lag (when the stratospheric field is leading), and is statistically significant at the 99% level. DWC events in the recent past occur throughout the winter; indicated by significant correlation at negative time lags from November to April (Fig. 4.1a). In the future, however, DWC events occur over a shorter time period from January to April, with no statistically significant signals found in early winter (Fig. 4.1b). The overall correlations of DWC signals in the future are lower compared to the recent past, indicating a significant reduction of downward wave activity from the stratosphere to the troposphere.

The timeslice simulations suggest that weaker DWC signals in the future are mainly due to increases in GHG forcing (Figs. 4.1c-d). In particular, in the experiment with future ODS changes (TS-ODS), DWC signals were notably more persistent over a longer period (from November through April, Fig. 4.1c), with a pattern resembling the seasonal variation of DWC in the recent past. In contrast, a weak and less persistent DWC signal is observed in the experiment with increased GHGs

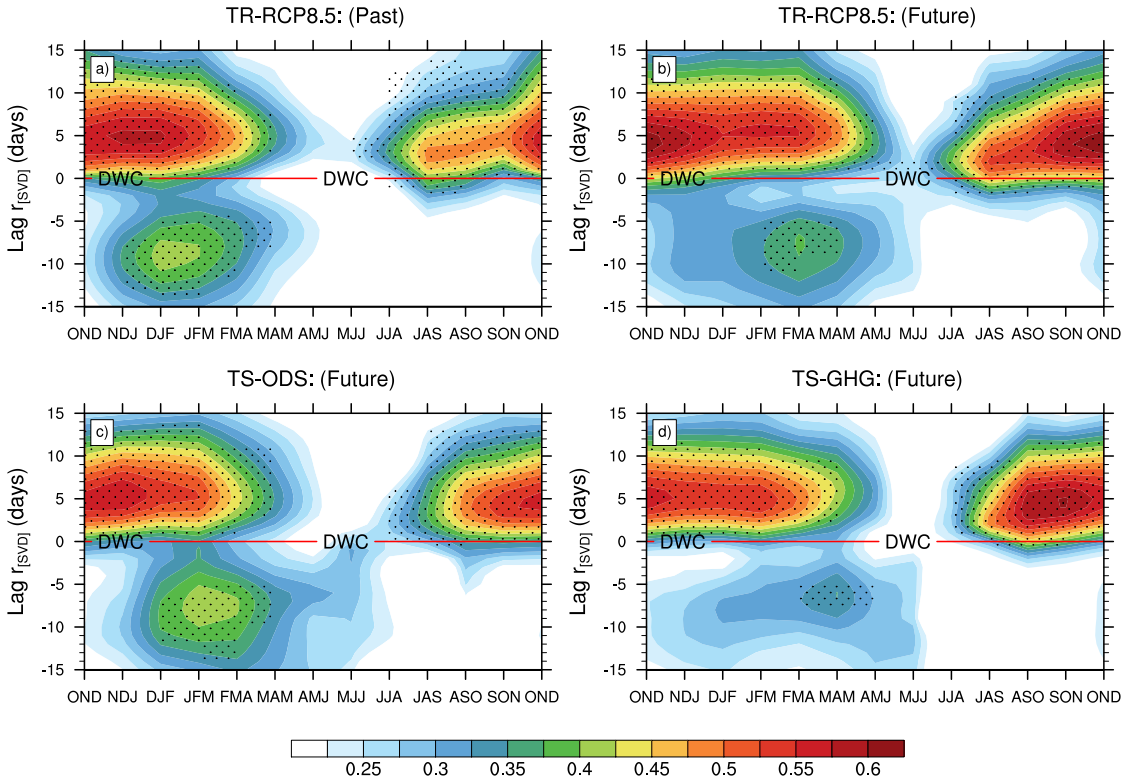

FIGURE 4.1: Three-month overlapping periods of lagged SVD correlations between wave-1 geopotential height (Z-ZWN1) at 500 hPa and 10 hPa for (a) TR-RCP8.5 past, (b) TR-RCP8.5 future, and two timeslice experiments with (c) future ODSs forcing and (d) future GHG forcing. Solid dots represent values significant at the 99% level. A negative (positive) time lag indicates that the stratospheric (tropospheric) wave field is leading.

(Fig. 4.1d). We also note that there is no significant difference in DWC seasonality between the future and past in the experiment with fixed GHG and ODS at 1960s levels (Fig. S1), suggesting that future changes in DWC activity are mainly induced by anthropogenic GHGs.

Furthermore, decreased DWC activity in the future can be also examined from the associated amplitudes of DWC in midwinter. Figure 4.2 shows the regression wave patterns when the time series of the stratospheric field leads that of the tropospheric field by 9 days in JFM. For this figure, we regressed the wave fields of both pressure levels to the standardized temporal expansion coefficients of the stratospheric SVD pattern. It can be seen that future DWC amplitudes at the 500-hPa and 10-hPa levels from the TR-RCP8.5 simulation are significantly weaker compared to the past (Figs. 4.2a-b). Based on the timeslice simulations (Figs. 4.2c-d), a significant decrease in DWC amplitude is observed in TS-GHG (Fig. 4.2d), while a qualitatively similar wave pattern and amplitude is observed in TS-ODS in comparison to the past (Fig. 4.2c). These results are in agreement with the wave coupling correlation analysis, suggesting that a future decrease in the occurrence of DWC in the NH is mainly attributed to increase in GHG forcing.

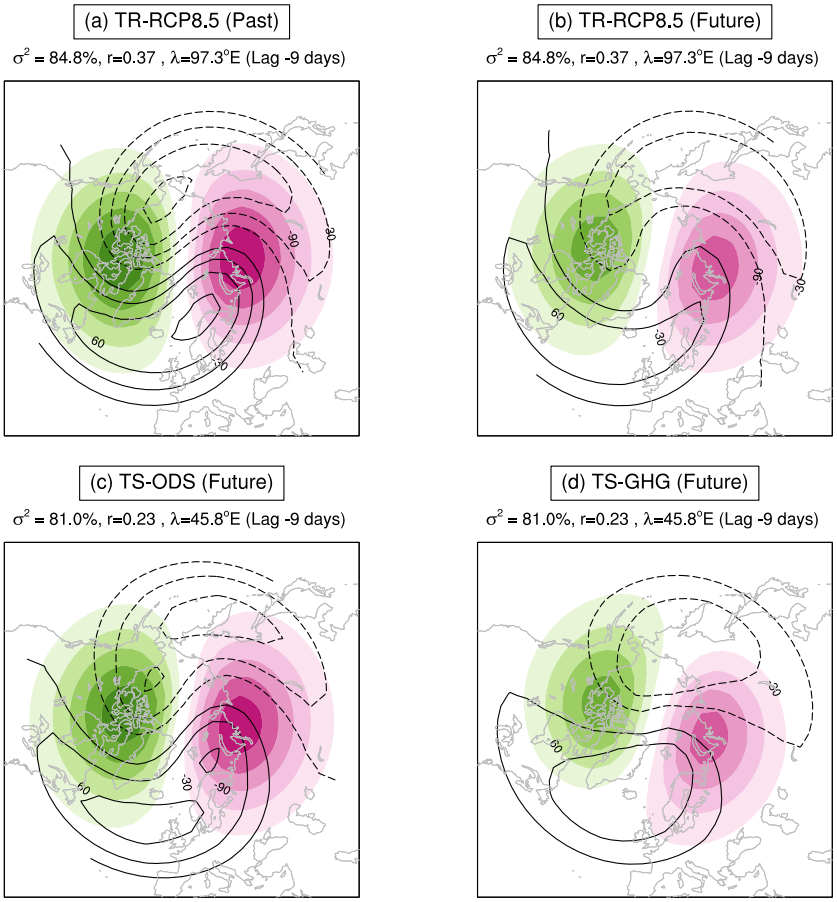

FIGURE 4.2: Heterogeneous regression patterns at 10 hPa (colour shaded) and 500 hPa (contour lines) associated with DWC in JFM (i.e., Z-ZWN1$_{10}$ leads Z-ZWN1$_{500}$ by 9 days) for (a) TR-RCP8.5 past, (b) TR-RCP8.5 future, and two timeslice experiments with (c) future ODSs forcing and (d) future GHG forcing. Contour interval is 30 m (shaded) for Z-ZWN1 at 10 hPa, and 5 m (black) for Z-ZWN1 at 500 hPa. The zero contour is omitted.

4.4 Mechanisms for Changes in Seasonality of DWC Events

The former analysis showed that there is a significant reduction of DWC events in the future, with a shift of their timing toward midwinter (i.e., no significant DWC signals occur in early winter). To elucidate the mechanisms responsible for decreased DWC activity in the future, we analyzed the seasonal evolution of the wave geometry. Figure 4.3 shows the climatological seasonal evolution of the vertical wavenumber (m^2) averaged from 60 to 80^{0}N for the transient (TR) and timeslice (TS) simulations. In the past, the stratospheric reflecting surface persists from early to late winter (October to April, Fig. 4.3a). This vertical reflecting surface is bounded by the extended meridional waveguide from November to April (Fig. S2a), and therefore is consistent with the significant DWC signals in Fig. 4.1a.

In the future, vertical reflecting surfaces occur only from December to April (Fig. 4.3b), while

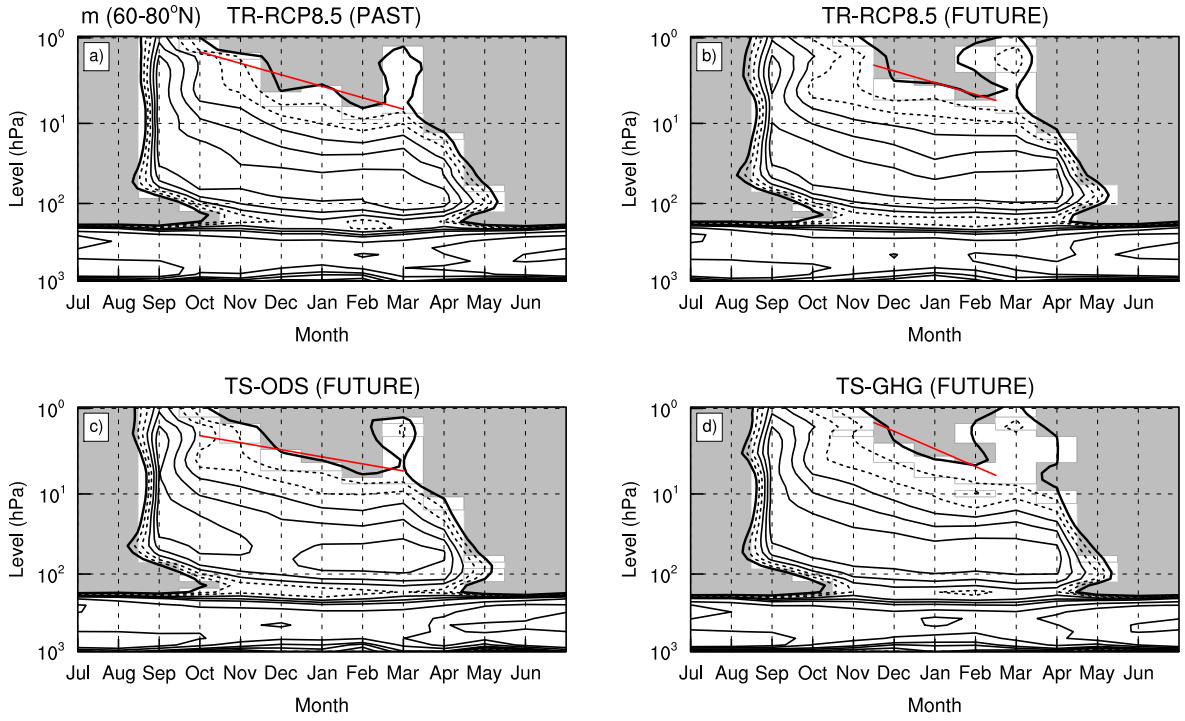

FIGURE 4.3: The climatological seasonal cycle of the vertical wavenumbers averaged between 60-80^{o}N for (a) TR-RCP8.5 past, (b) TR-RCP8.5 future, and two timeslice experiments with (c) future ODSs forcing and (d) future GHG forcing. The vertical wavenumbers (units 10^{-5} m^{-1}) are contoured with 0.01 (thick line); 2, 4 (dashed line); 6-30 in jumps of 3 (thin lines). Finally, the shading indicates the regions of wave evanescence in vertical directions ($m < 0$).

the meridional waveguide exhibits the same seasonal evolution as in the past (Fig. S2b). By combining the seasonal cycles of meridional and vertical wavenumbers, the high-latitude meridional waveguide is completely bounded above by a vertical reflecting surface from December to April. This configuration is consistent with significant seasonal DWC signals in Fig. 4.1b, occurring from January to April. The insignificant DWC signal in November (Fig. 4.1b), in particular, is consistent with an absence of vertical reflecting surfaces (Fig. 4.3b), which allows waves to propagate to the upper stratosphere and dissipate there (Shaw et al., 2010; Lubis et al., 2016b). We note that the insignificant DWC signals in December cannot be explained by the bounded wave geometry. Furthermore, by using the timeslice simulations we showed that future changes in the reflecting surface are mainly attributed to GHG forcing (Fig. 4.3d), dominating the opposing influence of ozone recovery.

Although changes in the bounded wave geometry (Fig. 4.3) can explain the seasonal evolution of DWC in the future (Fig. 4.1), this diagnostic is not able to explain the future seasonal shift of DWC, as well as the insignificant DWC signals in December. A recent study by Lubis et al. (2016b) showed that a significant reduction of DWC can be also attributed to increased wave absorption in the stratosphere. To check this, we calculated the response of the stratospheric zonal-mean wind from October to April in TR-RCP8.5 (future minus past), and the two timeslice experiments. A significant weakening of the future polar vortex in TR-RCP8.5 starts from November to January

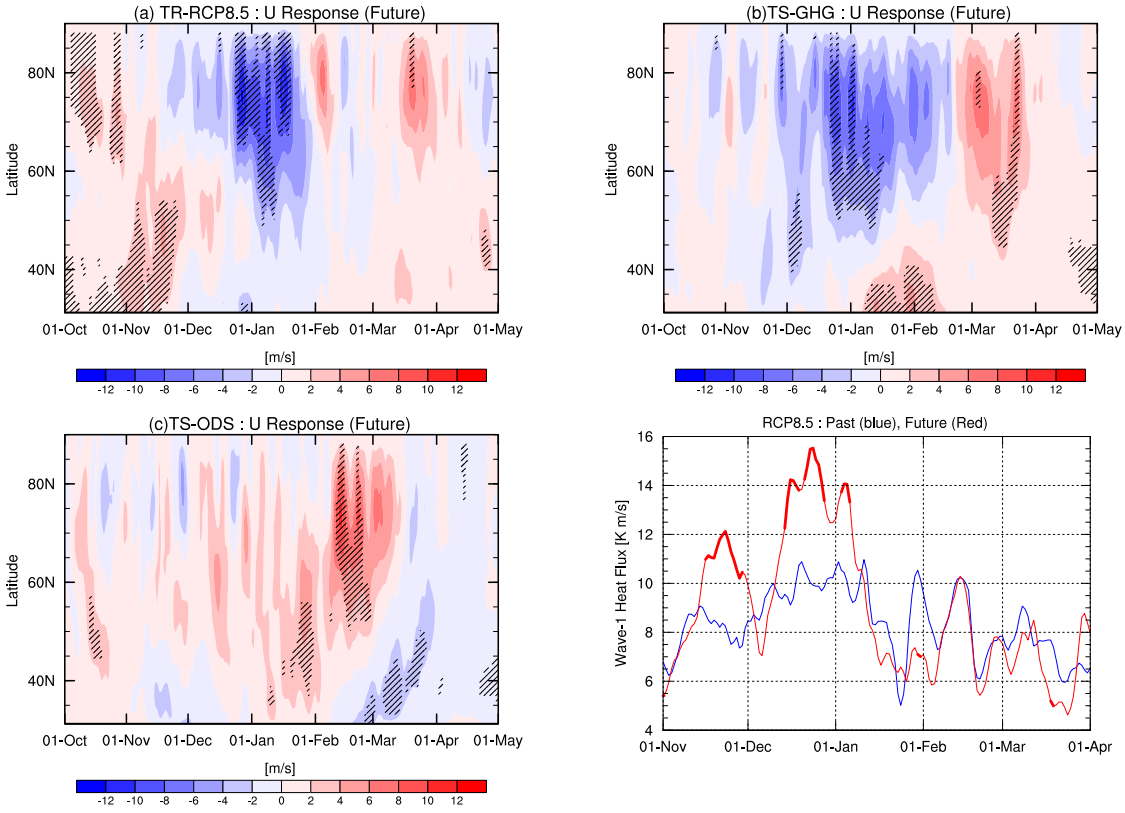

FIGURE 4.4: (a) Differences of daily climatology of 10 hPa zonal-mean zonal wind from November to April between future and past in TR-RCP8.5 simulation. (b-c) Changes of the same variable from different forcings: (b) GHG only and (c) ODS only. Contour interval is 2 m/s, and stipplings indicate statistically significant values at a 95% confidence level (two-tailed Student's t-test). (d) Differences of daily climatology of 100 hPa eddy heat flux averaged over 45-75^{0}N for RCP8.5 (future minus past). Thick lines correspond to statistically significant differences of heat flux from those of the past period (95% confidence level).

(Fig. 4.1a). This weakening is mainly driven by GHG forcing (Fig. 4.4b), which dominates the influence of ODS emission (Fig. 4.4c). This result is in agreement with the weak amplitude of future polar stratospheric wind in the Arctic stratosphere under increased GHGs (e.g., Ayarzaguena et al. 2013; Manzini et al. 2014). The weakening of the future polar vortex in early winter is attributed to enhanced wave absorption (convergent EP flux) in the upper stratosphere (Fig. S3), which is driven mainly by enhanced upward propagating planetary-scale waves in early winter (Fig. 4.4d and Fig. S4). Therefore, the future decrease of DWC events in early winter and a shift of their timing toward midwinter can be attributed to stronger wave absorption in the stratosphere, leading to less downward wave reflection to the troposphere.

4.5 Tropospheric Impact of DWC in the Future

As a last step, we briefly analyzed the impact of DWC on tropospheric circulation. We use a similar definition of DWC events as Lubis et al. (2016b), based on daily total negative wave-1 meridional heat flux ($\overline{v'T'}_{k=1}$) at 50 hPa averaged between 60^0 and 90^{0}N, which represents the 5th percentile

of the daily $\overline{v'T'}_{k=1}$ distribution. We focused on the most active winter season JFM, as it is a favourable period for DWC in the NH.

Figure 4.5 shows the composites of 500-hPa geopotential height (a,d), 700-hPa zonal-mean wind (b,e), and mean sea level pressure (c,f) anomalies north of 20^0N during the time when DWC impact on the troposphere maximizes (days -3 to 3). In the past, the tropospheric response to DWC events clearly resembles the patterns projecting onto the positive phase of the NAO. Notably, the geopotential height anomalies exhibit a seesaw shape between mid- and high latitudes (Fig. 4.5a), and tropospheric zonal wind anomalies reflect the strengthening and poleward shift of the tropospheric jet over the North Atlantic basin (Fig. 4.5b). The sea level pressure anomalies show a similar pattern as the 500-hPa geopotential height anomalies, indicating a quasi-barotropic, tropospheric, NAO-like structure in association with downward wave activity (Fig. 4.5c). This result is consistent with the impact of DWC in reanalyses shown in previous studies (e.g., Shaw and Perlwitz 2013; Lubis et al. 2016b).

However, in the future the surface influence of DWC in the North Atlantic basin is less reminiscent of the positive phase of the NAO. In particular, the poleward shift of the tropospheric zonal-mean wind is located more eastward of the North Atlantic basin (Fig. 4.5e), which is consistent with the eastward shift of geopotential height at 500 hPa (Fig. 4.5f). In addition, the sea level pressure anomalies do not resemble the Annular Mode-like pattern, as has been observed in the past. In addition, the overall impact of future DWC on the tropospheric circulation in midwinter prevails only over limited regions. The differences in the magnitude and pattern of the tropospheric responses to DWC between the future and past, may be related to the strength of DWC events, which affect the baroclinic eddy feedback (through vertical wind shear) on the anomalous positive NAO (Fig. S4). The results suggest that decreased DWC events in the future can affect the future tropospheric weather during Northern winter trough changes in the baroclinicity of the troposphere.

4.6 Concluding Remarks

In this study, the impact of anthropogenic forcing factors, namely GHGs and ODSs, on DWC variability in the NH was examined in both transient and timeslice simulations of the past and future, performed with the CESM1 (WACCM) chemistry climate model. The key results of this study are:

1. Under extreme climate change conditions, a significant reduction in DWC events is detected in the future, with a shift of their timing toward midwinter. This variation is related to a change in the timing of the bounded wave geometry configuration and increased wave absorption.

2. Future increase in GHG emissions is largely responsible for the decrease in the number of DWC events in early winter.

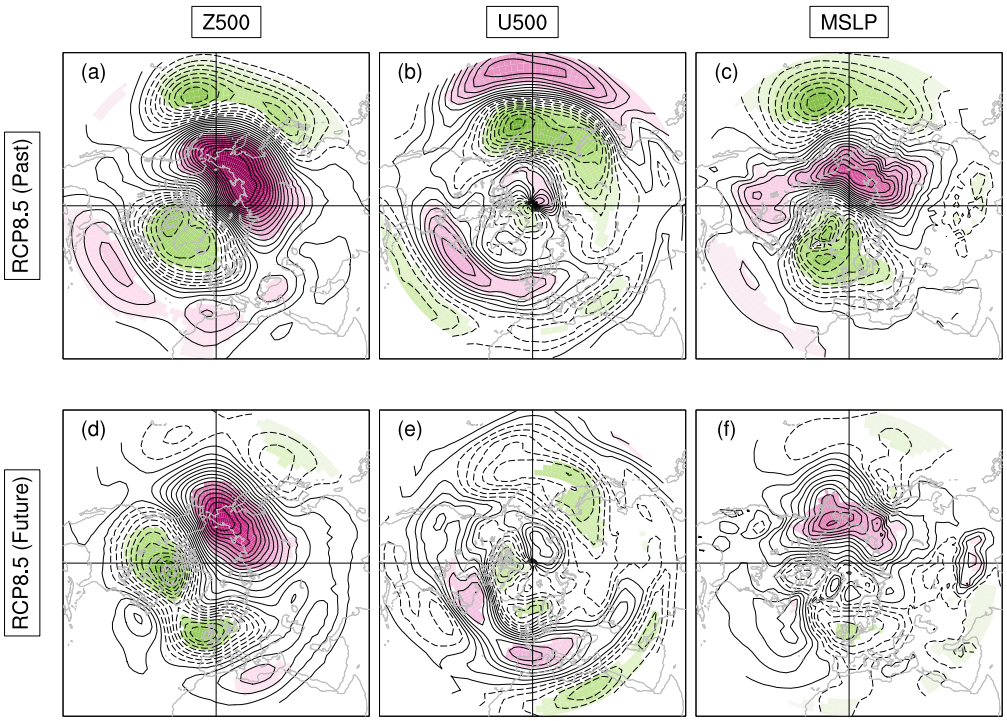

FIGURE 4.5: The composites of (a,d) 500-hPa geopotential height (Z500), (b,e) 500-hPa zonal wind (U500), and (c,f) mean sea level pressure (MSLP) anomalies during the period of maximum DWC impact on the troposphere (days -3 to 3) in JFM for (top) TR-RCP8.5 past and (bottom) TR-RCP8.5 future. Contour interval is 10 m for Z500, 1 m/s for U500, and 1 hPa for MSLP. The zero contour is omitted. The color shadings are only drawn for anomalies that are statistically significant at the 95% confidence level using a Monte Carlo approach.

3. The tropospheric response to DWC in the future is less reminiscent of the positive phase of the NAO. This is associated with a weaker DWC event, which leads to weaker baroclinic eddy feedbacks in the troposphere, particularly over the North Atlantic sector.

To our knowledge, this is the first sensitivity analysis carried out to explain the origin of future changes in the timing of DWC events. Most of the previous studies on the impact of increased future GHGs on tropospheric circulation have focused on changes in the in zonal-mean downward coupling between the stratosphere and troposphere (Butchart et al., 2000; Bell et al., 2010b). Our results show that future GHG changes also cause changes in DWC between the stratosphere and troposphere, and thus its impact on the tropospheric circulation.

We expanded the work by Lubis et al. (2016b) on investigation of the factors controlling the variability of DWC in the NH. Here we have stressed that changes in the anthropogenic forcing factors also lead to changes in DWC in the NH winter. We also applied similar analysis for the SH, and found that a significant change in DWC in the SH is mainly caused by ozone changes (not shown), which is in agreement with the results of Shaw et al. (2011). The results of the present study indicates for the first time how a future change in stratospheric dynamics via DWC in the NH, under the extreme climate change conditions, may affect the future troposphere-surface

system. These results are interesting and await confirmation with other CCMs to determine which aspects of the modelled tropospheric responses to the DWC are robust between models.

4.7 Appendix : Supplementary Figures

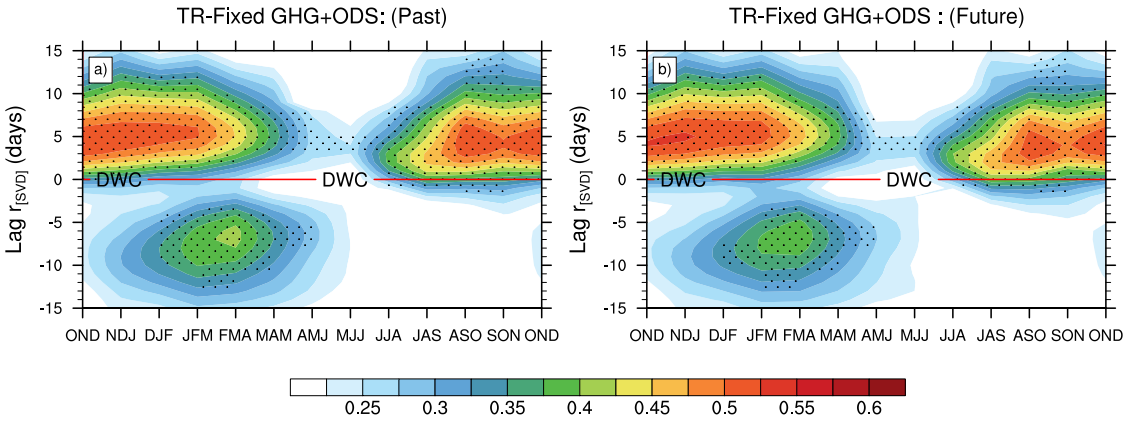

FIGURE 4.6: (**S1**). As in Fig. 4.1 but for the TR-NAT simulation.

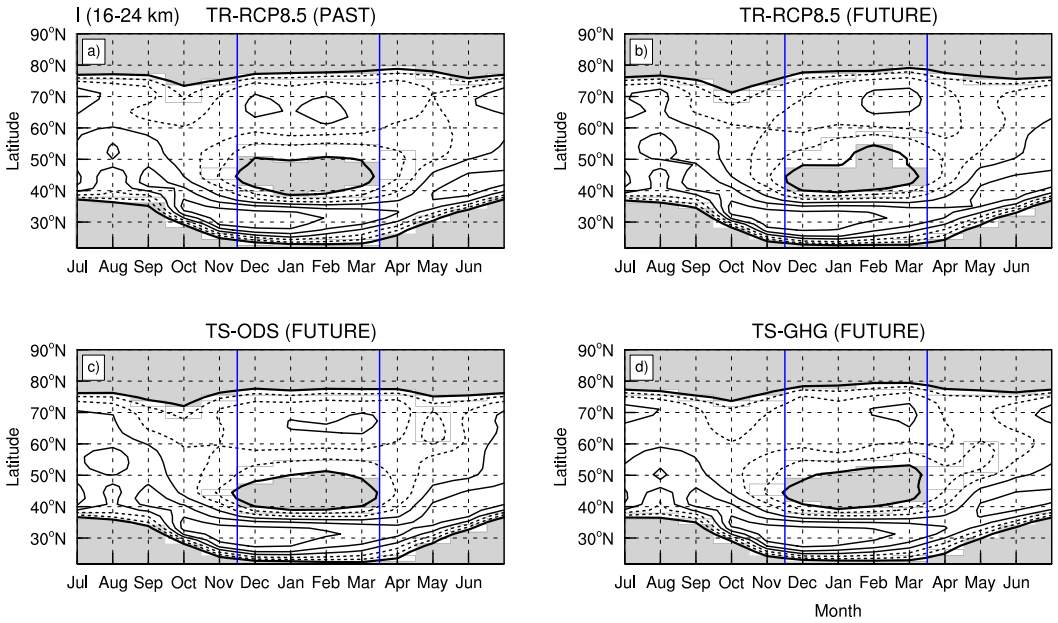

FIGURE 4.7: (**S2**). The climatological seasonal cycle of the meridional wavenumbers averaged between 16-24 km for (a) TR-RCP8.5 past, (b) TR-RCP8.5 future, and two timeslice experiments with (c) future ODSs forcing and (d) future GHG forcing. The meridional wavenumbers are contoured with 1 (solid) and 0.01 rad^{-1} (thick solid line). Finally, the shading indicates the regions of wave evanescence in meridional directions ($l < 0$).

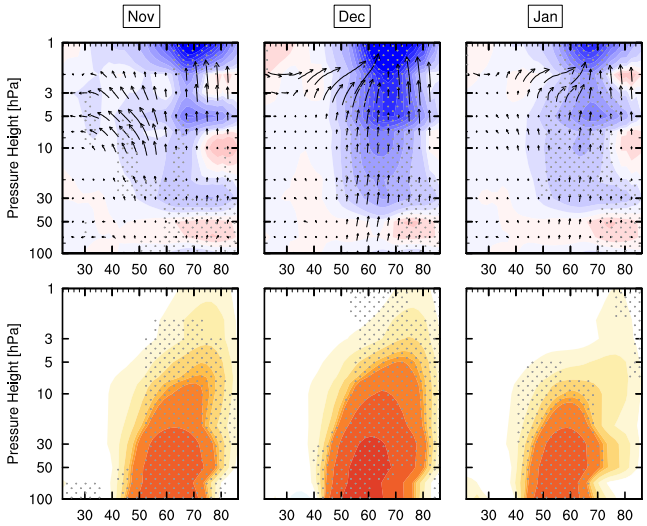

FIGURE 4.8: (**S3**). (top) Wave-1 EP flux divergence differences between future and past in TR-RCP8.5 simulation from November to January, superimposed with EP-flux vectors. (bottom) Vertical component of the EP-flux differences between future and past in TR-RCP8.5 simulation. Stippling indicates regions where the change exceeds the 95% significance level.

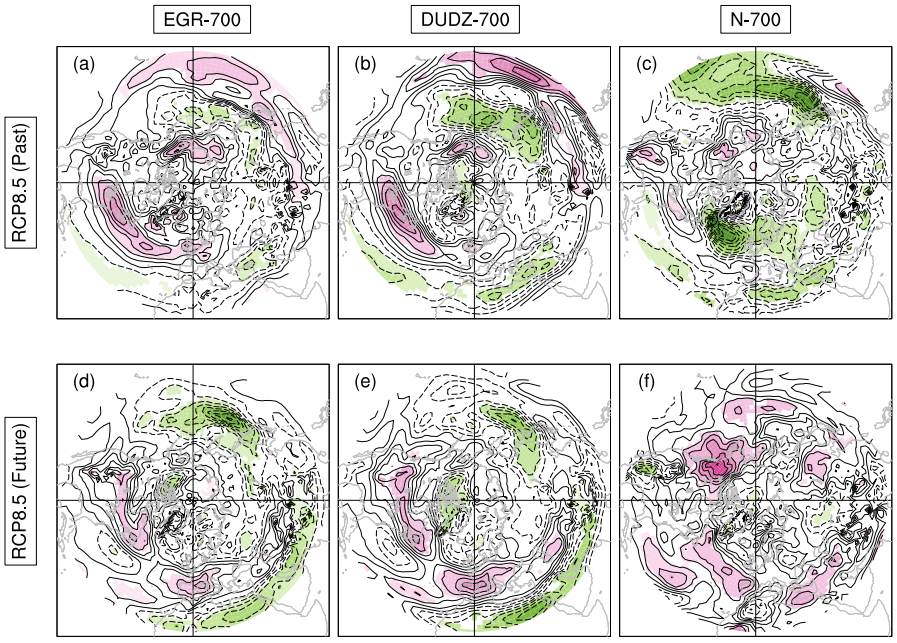

FIGURE 4.9: (**S4**). The composites of (a,d) 700-hPa Eady's growth rate (EGR-700), (b,e) 700-hPa vertical zonal wind shear (DUDZ-700), and (c,f) 700-hPa Brunt-Vaisala frequency (N-700) anomalies during the period of maximum DWC impact on the troposphere (days -3 to 3) in JFM for (top) TR-RCP8.5 past and (bottom) TR-RCP8.5 future. Contour interval is 1×10^{-2} day^{-1} for EGR-700, and 1×10^{-4} s^{-1} for DUDZ-700 and N-700. The zero contour is omitted. The color shadings are only drawn for anomalies that are statistically significant at the 95% confidence level using a Monte Carlo approach.

Chapter 5

Impact of the Antarctic Ozone Hole on the Vertical Coupling of the Stratosphere-Mesosphere-Lower Thermosphere System

While previous chapters elucidated the mechanism controlling NH polar stratosphere variability and its coupling to the troposphere via DWC, in this chapter, mechanisms controlling the SH polar stratosphere variability and its coupling to the mesosphere and lower thermosphere (MLT) during the Antarctic ozone hole period were investigated. This analysis provides a first detailed investigation of the vertical coupling between the stratosphere and MLT regions, in which both dynamical (resolved and non-resolved wave driving) and radiative effects are examined in detail. For this study, two transient simulations with fixed and varying GHG and ODS forcings as introduced in Chapter 4, are analyzed. In addition, three timeslice simulations with a combination of GHG and ODS forcings are also examined to quantify of the effects of the corresponding factor separately.

This chapter is a reprint of **Lubis, S., N. Omrani, K. Matthes, and S. Wahl, 2016: Impact of the Antarctic Ozone Hole on the Vertical Coupling of the Stratosphere-Mesosphere-Lower Thermosphere System. J. Atmos. Sci. 73, 2509-2528, doi: 10.1175/JAS-D- 15-0072.1, in press.**

The authors' contributions to this publication are as follows:

- S. Lubis contributed with ideas, performed all analyses, setup some timeslice experiments, produced all figures, and wrote the manuscript.
- N-E. Omrani initiated the study and contributed with ideas and discussion on the analysis.
- K. Matthes contributed with ideas and discussions on the analysis.
- S. Wahl performed some timeslice simulations used in this study.

Impact of the Antarctic Ozone Hole on the Vertical Coupling of the Stratosphere–Mesosphere–Lower Thermosphere System

SANDRO W. LUBIS

GEOMAR Helmholtz Centre for Ocean Research Kiel, Kiel, Germany

NOUR-EDDINE OMRANI

Geophysical Institute, University of Bergen, and Bjerknes Centre for Climate Research, Bergen, Norway, and GEOMAR Helmholtz Centre for Ocean Research Kiel, Kiel, Germany

KATJA MATTHES

GEOMAR Helmholtz Centre for Ocean Research Kiel, and Christian-Albrechts Universität zu Kiel, Kiel, Germany

SEBASTIAN WAHL

GEOMAR Helmholtz Centre for Ocean Research Kiel, Kiel, Germany

(Manuscript received 9 July 2015, in final form 9 March 2016)

ABSTRACT

There is evidence that the strengthened stratospheric westerlies arising from the Antarctic ozone hole–induced cooling cause a polar mesospheric warming and a subsequent cooling in the lower thermosphere. While previous studies focus on the role of nonresolved (gravity) wave drag filtering, here the role of resolved (planetary) wave drag and radiative forcing on the Antarctic mesosphere and lower thermosphere (MLT) is explored in detail. Using simulations with NCAR's Community Earth System Model, version 1 (Whole Atmosphere Community Climate Model) [CESM1(WACCM)], it is found that in late spring and early summer the anomalous polar mesospheric warming induced by easterly nonresolved wave drag is dampened by anomalous dynamical cooling induced by westerly resolved wave drag. This resolved wave drag is attributed to planetary-scale wave (k = 1–3) activity, which is generated in situ as a result of increased instability of the summer mesospheric easterly jet induced by the ozone hole. On the other hand, the anomalous cooling in the polar lower thermosphere induced by westerly nonresolved wave drag is enhanced by anomalous dynamical cooling due to westerly resolved wave drag. In addition, radiative effects from increased greenhouse gases during the ozone hole period contribute partially to the cooling in the polar lower thermosphere.

The polar MLT temperature response to the Antarctic ozone hole is, through thermal wind balance, accompanied by the downward migration of anomalous zonal-mean wind from the lower thermosphere to the stratopause. The results highlight that a proper accounting of both dynamical and radiative effects is required in order to correctly attribute the causes of the polar MLT response to the Antarctic ozone hole.

1. Introduction

Ever since the first observation of the Antarctic ozone hole in the mid-1980s, the cause of springtime ozone loss and its impacts on the atmospheric circulation and surface climate has been investigated in great detail (e.g., Thompson and Solomon 2002; Gillett and Thompson 2003; Pawson et al. 2008; Son et al. 2010; Eyring et al. 2010, chapters 4–8; Polvani et al. 2011; Orr et al. 2012,

Supplemental information related to this paper is available at the Journals Online website: http://dx.doi.org/10.1175/JAS-D-15-0189.s1.

Corresponding author address: Sandro W. Lubis, GEOMAR Helmholtz Centre for Ocean Research Kiel, Düsternbrooker Weg. 20, 24105 Kiel, Germany.
E-mail: slubis@geomar.de

DOI: 10.1175/JAS-D-15-0189.1

2013; WMO 2014). This springtime ozone loss is mainly caused by increased anthropogenic emissions of chlorofluorocarbons (CFC) and other halogenated species containing bromine and chlorine (Solomon et al. 1986; Molina and Molina 1987; WMO 2014). In particular, when there is not enough sunlight in the polar winter stratosphere to initiate photochemistry, the conversion of reservoir chlorine molecules into chlorine gas takes place on the surface of polar stratospheric clouds (PSCs) (e.g., Solomon et al. 1986). In the spring, when the polar stratosphere becomes sunlit, solar ultraviolet (UV) radiation splits the chlorine gas molecules into radical chlorine atoms and makes them much more effective at destroying ozone through catalytic cycles (e.g., Molina and Molina 1987).

One striking effect of the stratospheric ozone loss is the radiative cooling associated with a reduction of absorbed solar UV radiation. This effect is evident in observations as indicated by negative trends of polar lower-stratospheric temperatures during spring and early summer (e.g., Thompson and Solomon 2002; Randel et al. 2009). Through thermal wind balance, the resulting increased meridional temperature gradient must be accompanied by increased vertical shear of the geostrophic wind, leading to a strengthening of the polar vortex (e.g., Waugh et al. 1999; Thompson and Solomon 2002; Orr et al. 2012). In the troposphere, this anomalous circulation change resembles the patterns projecting onto the positive phase of the southern annular mode (SAM) [see Son et al. (2010) for an overview of possible mechanisms], which is often described as the poleward shift in the tropospheric jet and extratropical storm track (e.g., Simmonds and Keay 2000; Wang et al. 2013). Changes in SAM trends during the ozone hole period have had a significant impact on the Southern Hemisphere (SH) regional surface climate (e.g., Thompson and Solomon 2002; Ummenhofer et al. 2009).

Changes in the SH stratosphere due to the ozone hole can also affect the mesosphere and lower thermosphere (MLT). The primary mechanism is changes in the propagation of gravity waves (GWs) due to the change in background stratospheric winds (Smith et al. 2010; Smith 2012). Smith et al. (2010), using simulations with the Whole Atmosphere Community Climate Model (WACCM), show that ozone-loss-induced changes in the stratospheric wind lead to a warming of the polar summer mesopause. This is attributed to a weakening of the westerly gravity wave drag (GWD) in the mesosphere during late spring and early summer (November–December). In particular, strengthened westerly winds in the stratosphere enhance filtering of westerly GWD as they approach critical levels (i.e., the phase speed of GWs becomes equal to the background wind speed). This results in increased easterly GWD in the mesosphere, leading to a weakening of the polar summer upwelling and the associated adiabatic warming in this region. However, the role of resolved planetary wave drag on the MLT temperature and circulation responses to the Antarctic ozone hole remains unclear.

More recently, Lossow et al. (2012), using simulations with the Canadian Middle Atmosphere Model (CMAM), show that SH mesospheric responses to the stratospheric ozone loss differ significantly between late spring and early summer. In late spring, the strengthened lower-stratospheric westerlies increase filtering of the westerly GWD, resulting in more anomalous easterly GWD in the mesosphere. This leads to anomalous polar downwelling and associated anomalous warming in the polar summer mesosphere, similar to Smith et al. (2010). In early summer, however, the strengthened mesospheric easterlies due to increased easterly GWD, induce a westerly resolved planetary wave drag anomaly through baroclinic instability. The resulting polar mesospheric cooling induced by this process dominates the upper-mesospheric temperature responses to the ozone hole in early summer. The latter result is in contrast to the Smith et al. (2010) findings, which do not show a significant difference in the mesospheric temperature responses between late spring and early summer. These differing results could be associated with a delayed breakdown of the SH vortex in WACCM, which is approximately a few weeks later than it occurs in CMAM (Lossow et al. 2012). Consequently, the mesospheric warming induced by the ozone hole in WACCM persists longer into early summer. Nevertheless, the structures of the changes that occur in dynamical variables are very similar between WACCM and CMAM. Despite these results, it is still not clear how large the radiative effects from increased ozone-depleting substances (ODSs) and greenhouse gases (GHGs) are and how they influence the MLT temperature and circulation responses during the Antarctic ozone hole period. We attempt to address this question with this study.

It is well established that planetary waves contribute to the circulation and the large dynamical variability in the MLT (Becker 2012; Smith 2012). Although most of these waves are generated in the troposphere, they can be also forced in situ in the mesosphere via instability of the zonal-mean state (Garcia et al. 2005; Becker 2012; Smith 2012). Two examples are in situ generation of the quasi-2-day wave (QTDW) and 5-day planetary wave ($k = 1$) via baroclinic instability of the easterly jet in the summer mesosphere (Plumb 1983; Pfister 1985; Norton and Thuburn 1999; Garcia et al. 2005). The strengthening of the mesospheric easterlies induced by the ozone hole could affect the susceptibility of the mesosphere to

be more baroclinically or barotropically unstable and hence increase the probability of in situ planetary wave generation. Lossow et al. (2012) finds that there is a pronounced increase of the resolved wave drag in the summer upper mesosphere due to the Antarctic ozone hole. However, their calculations show that such changes are mainly attributed to synoptic-scale waves rather than planetary-scale waves like QTDW ($k = 3$) or 5-day waves ($k = 1$). As discussed in Lossow et al. (2012), there are at least two potential issues that might affect the resolved wave drag response in their simulations: 1) the use of the Scinocca (2003) nonorographic GWD parameterization in CMAM tends to dampen the amplitude of the QTDW (McLandress and Scinocca 2005) and 2) the response of the resolved planetary wave drag in the upper mesosphere was possibly affected by the location of the model lid (~95 km), as indicated by the large negative PV gradient maximizing close to this location ~90 km [see Lossow et al. (2012) for a detailed explanation]. Therefore, further investigations with a higher-lid model are needed to address this possibility.

A prominent feature of mesospheric dynamics is the interhemispheric circulation from summer to winter pole (Murgatroyd and Singleton 1961; Plumb 2002; Butchart 2014). This circulation is driven primarily by upward-propagating GWs, with their effect on the mesospheric mean flow depending on their phase velocities and the background wind patterns (Holton 1983; Plumb 2002). In the summer (winter) hemisphere, an equatorward (a poleward) residual circulation in the mesosphere is induced by westerly (easterly) GWD, resulting from filtering of easterly (westerly) GWD by stratospheric background winds. In contrast to the mesosphere, the winter stratosphere is dominated by a poleward residual circulation from the tropics to the pole (Plumb 2002; Butchart 2014). This circulation arises primarily from the dissipation of upward-propagating planetary-scale Rossby waves in the stratosphere. In the upper troposphere and lower stratosphere, the poleward flow of the residual circulation is driven mainly by synoptic-scale wave activity, which persists throughout the year (Plumb 2002).

The radiatively or wave-induced strengthening of the polar vortex can suppress the upward wave propagation from the troposphere into the stratosphere (Charney and Drazin 1961), which results in further strengthening of the polar vortex. This positive feedback can be strengthened by the buoyancy frequency and the westerly winds near the tropopause (Chen and Robinson 1992), which lead to additional reduction of the upward-propagating wave and, thus, inducing downward propagation of the wind anomalies toward the tropopause (e.g., Kuroda and Kodera 1998). Orr et al. (2012) show that this positive feedback mechanism explains the downward migration of zonal-mean wind anomalies toward the tropopause during the Antarctic ozone hole period. For the ozone-induced tropospheric changes, there is recent evidence that the internal tropospheric eddy-driven dynamics play crucial role for shaping and maintaining the tropospheric response to the ozone hole (Ogawa et al. 2015). Given the fact that stratosphere–troposphere coupling associated with the ozone hole has been widely investigated, our study will focus on the mechanisms maintaining the vertical coupling in the middle atmosphere from the stratosphere toward the mesosphere and lower thermosphere.

In this paper, we perform experiments with the NCAR's Community Earth System Model, version 1 (Whole Atmosphere Community Climate Model) [CESM1(WACCM)], a state-of-the-art fully coupled chemistry–climate model, to further investigate the impact of the Antarctic ozone hole on the vertical coupling of the stratosphere–MLT system. While previous studies focused on the impact of nonresolved (gravity) wave drag filtering, this study investigates in detail the role of both resolved (planetary) wave drag and radiative forcing (short- and longwave radiation) during the Antarctic ozone hole period in the model. We address the following questions:

1) What are the roles of resolved wave drag and radiative forcing on the MLT temperature responses to the Antarctic ozone hole?
2) What are the dynamical mechanisms responsible for maintaining the downward propagation of zonal wind anomalies in the MLT?
3) What is the dynamical origin of the pronounced change in the resolved wave drag responses in the MLT?

Section 2 describes the data and methods. The results are presented in sections 3–5. Finally, the paper finishes with a summary and discussion in section 6.

2. Model, simulations, and analysis

a. *Model description*

We use version 1.0.2 of the NCAR's Community Earth System Model (CESM), a fully coupled general circulation model developed based on the Community Climate System Model version 4 (CCSM-4; Gent et al. 2011), which includes an interactive ocean, land, sea ice, and atmosphere (Marsh et al. 2013). For the simulations analyzed here, we use WACCM version 4 as the atmosphere component of CESM, which is the successor of WACCM version 3.5 used by Smith et al. (2010). WACCM uses the finite-volume dynamical core with a horizontal resolution of 1.9° latitude by 2.5° longitude

TABLE 1. Description of CESM1(WACCM) transient and timeslice experiments. TR = transient run and TS = timeslice run. All experiments are run with interactive SSTs and sea ice.

Experiment	Period	GHGs	ODSs
CTL-TR	1955–2099 (145 yr)	1960s level	1960s level
GHGODS-TR	1955–2099 (145 yr)	OBS+RCP8.5[a]	OBS+RCP8.5[a]
ODS2010-TS	40 yr	1960s level	2010s level
GHG2010-TS	40 yr	2010s level	1960s level
REF-TS	40 yr	2010s level	2010s level

[a] GHG/ODS follows observations until 2005 and the RCP8.5 scenario thereafter.

and 66 vertical levels from the surface to the lower thermosphere at an altitude of ~140 km (~5.9×10^{-6} hPa). Chemical processes in WACCM are represented by the 3D chemical transport Model of Ozone and Related Chemical Tracers, version 3 (MOZART-3; Kinnison et al. 2007). This includes the O_x, NO_x, HO_x, ClO_x, and BrO_x chemical families, along with CH_4 species within the chemical and physical processes in the troposphere through the lower thermosphere (i.e., fully interactive and fully coupled chemistry and physics). WACCM is not able to resolve small-scale GWs with horizontal wavelengths of tens up to several hundred kilometers, and hence they need to be parameterized (Richter et al. 2010). Therefore, WACCM employs an updated parameterization of nonorographic GWs generated by frontal systems and convection and surface stress due to unresolved topography (Richter et al. 2010). Other processes important for the mesosphere and lower thermosphere such as ion chemistry, auroral processes, and extreme ultraviolet and nonlocal thermodynamic equilibrium radiation are also implemented [see Marsh et al. (2013) for specific details].

b. *Model simulations*

We perform five model experiments (summarized in Table 1) to study the impact of the Antarctic ozone hole on the vertical coupling of the stratosphere–MLT system. The first two transient (TR) experiments are CTL-TR and GHGODS-TR, covering 145 yr from 1955 to 2099. Both experiments use a nudged quasi-biennial oscillation (QBO) signal in zonal-mean winds between 22°S and 22°N following the approach by Matthes et al. (2010). The QBO is projected into the future by developing Fourier coefficients for the QBO time series based on climatological values of Giorgetta[1] from the past records (1954–2004). The QBO nudging allows us to study the dynamical impact of the tropics on the extratropics and the high latitudes. The effects of QBO nudging in CESM1(WACCM) on extratropical and high latitude dynamics agrees well with observations (Hansen et al. 2013). The solar cycle was prescribed using spectrally resolved daily variations of solar incoming radiation at the top of the atmosphere following Lean et al. (2005) and was projected into the future by repeating cycles 20–23 from the years 1965 to 2008. The CTL-TR experiment uses a perpetual annual cycle of all anthropogenic forcing including airplane emissions at pre–ozone hole conditions averaged from 1955 to 1965, which we refer to as 1960s conditions, and therefore no ozone hole develops in this simulation.

The GHGODS-TR experiment uses transient anthropogenic forcing following observations until 2005 and phase 5 of the Coupled Model Intercomparison Project (CMIP5) representative concentration pathways (RCP) scenario 8.5 (Taylor et al. 2012; Meinshausen et al. 2011) thereafter, and consequently an ozone hole develops, peaking in 2010. The RCP8.5 scenario includes future projections of surface emissions of both GHGs and ODSs as described in Meinshausen et al. (2011). Both model simulations are initialized using initial files for January 1955 from a CESM-piControl experiment[2] from the CESM contribution to CMIP5, which runs for several hundred years to reach an equilibrium state in the ocean. Therefore, the differences between GHGODS-TR and CTL-TR experiments can be used to study the relative effects of ODSs and GHGs during the period of the ozone hole or future ozone recovery (depending on the time periods used for the analysis).

To examine whether the responses obtained from the transient simulation during the Antarctic ozone hole period are attributed mainly to ozone depletion or due to the effects of GHGs, three 40-yr timeslice (TS) experiments with different combinations in prescribed surface emissions of the ODSs and GHGs are performed. The reference timeslice experiment (REF-TS) uses a perpetual annual cycle of surface emissions of

[1] http://www.pa.op.dlr.de/CCMVal/Forcings/qbo_data_ccmval/u_profile_195301-200412.html.

[2] http://www.cgd.ucar.edu/ccr/strandwg/CMIP5_experiment_list.html.

both ODSs and GHGs averaged from 2005 to 2015, which represent emissions during the deep ozone hole condition (refer to as 2010 conditions). The GHG2010-TS experiment uses seasonally varying surface emissions of ODSs at 1960s levels in combination with surface emissions of GHGs at 2010 levels. For the ODS2010-TS experiment, ODSs at 2010 levels in combination with surface emissions of GHGs at 1960s levels are used. All timeslice experiments are initialized using restart files from year 2010 of the GHGODS-TR run and are coupled with interactive ocean and sea ice. All other external forcings are kept constant at the 2010 levels. Therefore, the differences between the GHG2010-TS (ODS2010-TS) and REF-TS experiments reveal the effects of polar stratospheric ozone depletion (climate change due to increased GHGs).

c. *Analysis framework*

The transformed Eulerian mean (TEM) zonal momentum and thermodynamic budget analysis are used to study the vertical coupling associated with the ozone hole (Andrews et al. 1987; Orr et al. 2012, 2013; Keeble et al. 2014), as follows:

$$[u]_t + \zeta_a[v]^\dagger + [w]^\dagger[u]_z - [X] = \frac{1}{\rho_0 a\cos\phi}\nabla\cdot\mathbf{F} \quad \text{and} \tag{1}$$

$$[\theta]_t + \frac{1}{a}[v]^\dagger[\theta]_\phi + [w]^\dagger[\theta]_z - [Q_{\rm dia}] = -\frac{1}{\rho_0}\left\{\rho_0\left(\frac{[v^*\theta^*][\theta_\phi]}{a[\theta]_z} + [w^*\theta^*]\right)\right\}_z, \tag{2}$$

where $\zeta_a = (a\cos\phi)^{-1}([u]\cos\phi)_\phi - f$; $[Q_{\rm dia}]$ is a total diabatic source; u, v, and w are, respectively, the zonal, meridional, and vertical components of the velocity; a is Earth's radius; f is the Coriolis parameter; ϕ is latitude; z is height (in log-pressure coordinates); ρ_0 is air density, which varies with height as $\exp(-z/H)$; H is the density-scale height taken as 7000 m; and θ is potential temperature. The subscripts mean the derivative with respect to the corresponding coordinate. The asterisks are used for the total waves (deviation from the zonal mean in all frequencies) and square brackets for the zonal mean. The $[v]^\dagger$ and $[w]^\dagger$ in Eq. (1) denote the TEM residual meridional and vertical winds, which are defined as $[v]^\dagger = [v] - \rho_0^{-1}(\rho_0[v^*\theta^*]/[\theta]_z)_z$ and $[w]^\dagger = [w] + (a\cos\phi)^{-1}(\cos\phi[v^*\theta^*]/[\theta]_z)_\phi$. The term $[X]$ represents the unresolved forcing that includes the nonresolved GWs, smaller-scale turbulent diffusion, friction, etc.

We use the term "resolved wave drag" as a synonym for the divergence of the Eliassen–Palm (EP) flux $(\rho_0 a\cos\phi)^{-1}\nabla\cdot\mathbf{F}(F_y, F_z)$, associated with resolved planetary wave activity, where the components are given by

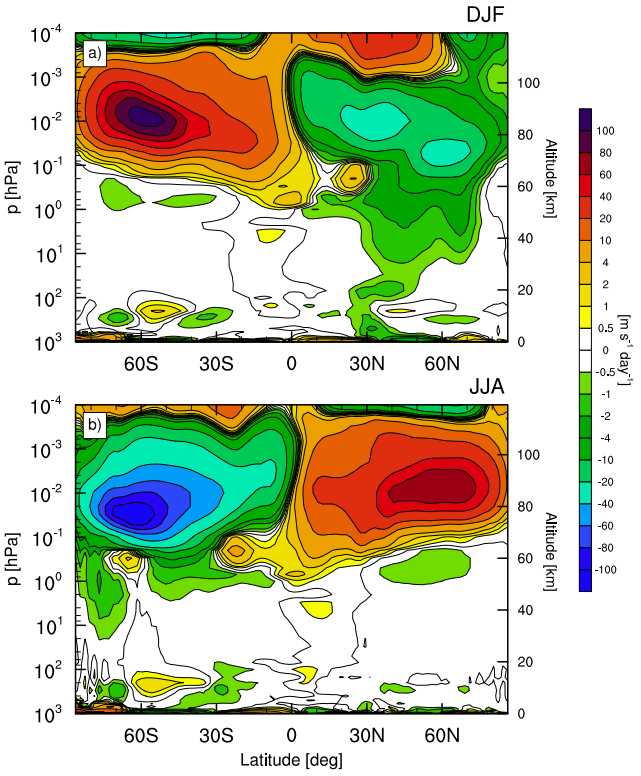

FIG. 1. Climatology of total nonresolved wave drag computed as the residual of the TEM zonal momentum equation $[X]$ for the 145-yr CTL-TR simulation averaged over (a) DJF and (b) JJA. Color contour intervals are ± (0.5, 1, 2, 4, 10, 20, 40, 60, 80, and 100) m s^{-1} day^{-1}.

$$F_y = \rho_0 a\cos\phi\left(-[u^*v^*] + \frac{[u]_z[v^*\theta^*]}{[\theta_z]}\right),$$

$$F_z = \rho_0 a\cos\phi\left(\frac{-\zeta_a[v^*\theta^*]}{[\theta_z]} - [u^*w^*]\right), \quad \text{and} \tag{3}$$

$$\nabla\cdot\mathbf{F} = \frac{1}{a\cos\phi}\frac{\partial(F_y\cos\phi)}{\partial\phi} + \frac{\partial F_z}{\partial z}. \tag{4}$$

Given that not all parameterized wave drags were saved in the simulations, the "nonresolved wave drag" is defined as the residual of the TEM zonal momentum equation $[X]$. Figures 1a and 1b show the climatology of nonresolved wave drag $[X]$ from the CTL-TR experiment averaged over December–February (DJF) and June–August (JJA). Compared to the previous analysis of parameterized GWD in WACCM [Richter et al. (2010), see their Fig. 6d], it can be seen that the total nonresolved wave drag calculated from Eq. (1) (Fig. 1a) is comparable to the total parameterized GWD, which includes both orographic and nonorographic GWD. In addition, the westerly (easterly) nonresolved wave drag dominates the summer (winter) mesosphere, which is consistent

with filtering of the easterly (westerly) GWD by stratospheric easterlies (westerlies) in the summer (winter) (Figs. 1a,b). This result indicates that the nonresolved wave drag is mainly attributed to parameterized GWD.

According to the TEM zonal momentum budget [Eq. (1)], the easterly (westerly) wave drag exerted on the mean flow leads, through the Coriolis force, to a poleward and downward (upward and equatorward) residual circulation in high latitudes, resulting in adiabatic warming (cooling) over this region. To diagnose the residual circulation induced by the resolved wave drag, we computed the mass streamfunction using the downward control principle (Haynes et al. 1991) as

$$\Psi_{\mathrm{rw}}(\phi,p)=\frac{\cos\phi}{g}\int_p^0\left\{\frac{(\rho_0 a\cos\phi)^{-1}\nabla\cdot\mathbf{F}}{f-(a\cos\phi)^{-1}([u]\cos\phi)}\right\}dp, \tag{5}$$

where g is the acceleration due to gravity. The mass streamfunction for the nonresolved wave drag (Ψ_{nrw}) is deduced by the difference between the total mass streamfunction $\Psi(\phi,p)=-\cos\phi/g\int_p^0[v]^{\dagger}\,dp'$, and the downward control streamfunction Ψ_{rw} [Eq. (5)], similar as in (Karpechko and Manzini 2012), as follows:

$$\Psi_{\mathrm{nrw}}(\phi,p)=\frac{\cos\phi}{g}\left\langle\int_p^0[v]^{\dagger}\,dp'-\int_p^0\left\{\frac{(\rho_0 a\cos\phi)^{-1}\nabla\cdot\mathbf{F}}{f-(a\cos\phi)^{-1}([u]\cos\phi)}\right\}dp\right\rangle. \tag{6}$$

In addition, the total dynamical heating rates (i.e., temperature tendency $[\theta]_t$ due to dynamical processes) are computed by rearranging the TEM thermodynamic balance [Eq. (2)], similar as in (e.g., Dunkerton et al. 1981; Orr et al. 2013), as follows:

$$[Q_{\mathrm{dyn}}]^{\theta}=-\frac{1}{\rho_0}\left\{\rho_0\left(\frac{[v^*\theta^*][\theta_\phi]}{a[\theta]_z}+[w^*\theta^*]\right)\right\}_z-\frac{1}{a}[v]^{\dagger}[\theta]_\phi-[w]^{\dagger}[\theta]_z. \tag{7}$$

The first term on the right-hand side of (7) is a contribution to dynamical heating from nonquasi-geostrophic motions (i.e., eddy-heat flux term). This term is generally much smaller than the other two terms on the right-hand side of this equation. Hence, changes in total dynamical heating rates $[Q_{\mathrm{dyn}}]^{\theta}$ mainly result from the advective terms $(-a^{-1}[v]^{\dagger}[\theta]_\phi-[w]^{\dagger}[\theta]_z)$. The shortwave and longwave radiative heating rates are the primary components of the total diabatic heating source $[Q_{\mathrm{dia}}]$ in the middle atmosphere. These radiative heating rates were diagnosed directly from the model. To compare the dynamical heating with radiative heating from the model, the result of $[Q_{\mathrm{dyn}}]^{\theta}$ is converted to absolute temperature as $[Q_{\mathrm{dyn}}]=[Q_{\mathrm{dyn}}]^{\theta}(p/p_0)^{R/C_p}$, where R is the gas constant of air and C_p is the specific heat capacity. Furthermore, the dynamical heating rates attributed to resolved and nonresolved wave forcing are computed by first calculating the vertical residual velocity for different type of waves as $[w]^{\dagger}_{(\mathrm{rw,nrw})}=(gH/pa\cos\phi)\Psi_{(\mathrm{rw,nrw})\phi}$, and then these values are used to calculate the dynamical heating rates from the vertical advection terms in Eq. (7).

To investigate in situ wave generation in the MLT via instability of the mean states, the meridional gradient of quasigeostrophic potential vorticity (PV), $[q]_y$, in spherical coordinates (Matsuno 1970) is calculated as

$$[q]_y=\frac{1}{a}[q]_\phi=\beta-\frac{1}{a^2}\left\{\frac{1}{\cos\phi}([u]\cos\phi)_\phi\right\}_\phi-\frac{f^2}{\rho_0}\left(\frac{\rho}{N^2}[u]_z\right)_z, \tag{8}$$

where β is the meridional gradient of Coriolis parameter and N is the Brunt–Väisälä frequency. To estimate the effects of different wind structures on the source of instability, the relative contributions of meridional (barotropic) terms $-a^{-2}\{\cos\phi^{-1}([u]\cos\phi)_\phi\}_\phi$ and vertical (baroclinic) terms $-f^2\rho_0^{-1}(\rho N^{-2}[u]_z)_z$ of $[q]_y$ are also examined separately.

3. Ozone response to anthropogenic forcing

Before analyzing the stratosphere and MLT responses to the Antarctic ozone hole, we first examine the global changes in stratospheric ozone in response to natural and anthropogenic forcing factors under the RCP8.5 scenario and then quantify the total southern polar-cap ozone changes during the Antarctic ozone hole period in the model.

a. Global ozone responses

The evolution of ozone in response to natural forcing factors (CTL-TR, green solid curves) and anthropogenic forcing factor under the RCP8.5 scenario (GHGODS-TR, solid red curves) from 1955 to 2099 is illustrated in

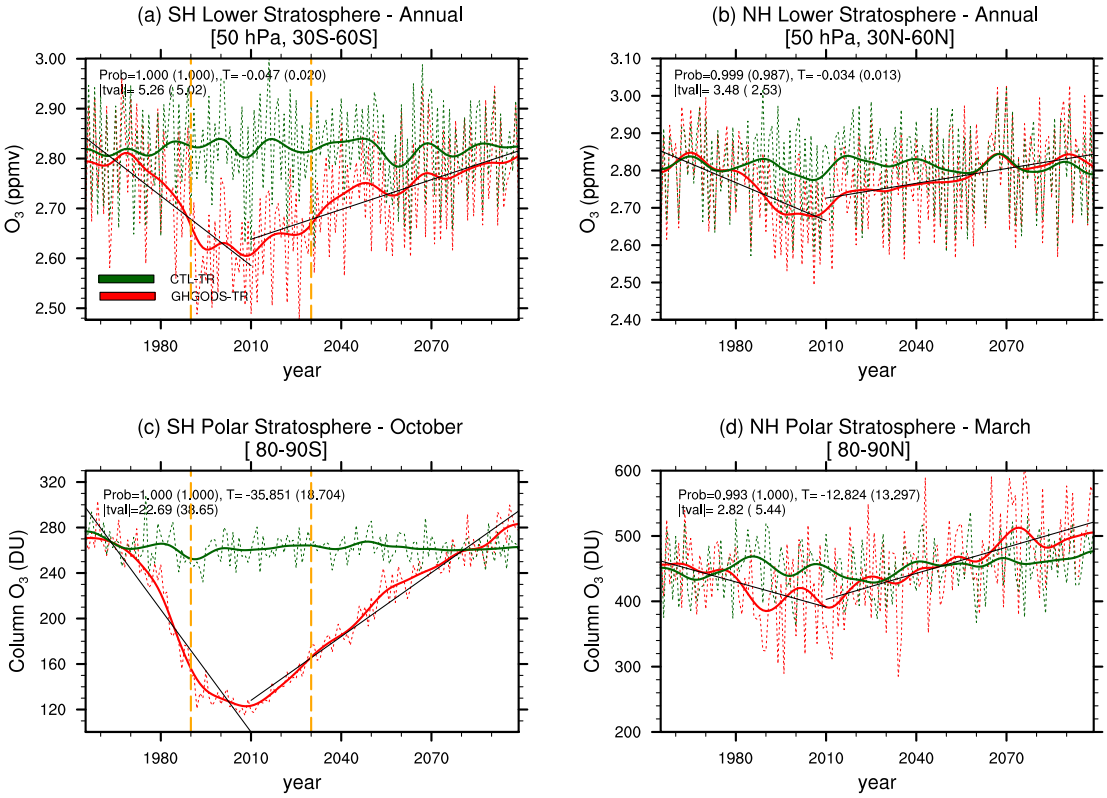

FIG. 2. Evolution of zonal-mean ozone from the CTL-TR (green) and GHGODS-TR (red) simulations for (a) 50 hPa, 30°–60°S; (b) 50 hPa, 30°–60°N; (c) column ozone, 80°–90°S; and (d) column ozone, 80°–90°N. (a),(b) Annual means, (c) the October mean, and (d) the March mean. Thick curves are smoothed versions of the thin curves, calculated by applying a 1–2–1 filter iteratively 30 times (see Waugh et al. 2009). Solid lines for the trend lines represent trends found to be more than 95% statistically significant. The probability (prob), slope per decade (T), and t-statistic values of the trends from 1955 to 2010 (2011–99) are shown with (without) the parentheses. Vertical orange dashed lines indicate the time frame of maximum Antarctic ozone loss.

Figs. 2a–d. In general, the ozone decrease in the GHGODS-TR simulation occurred steadily from 1955 to 2010 and increase throughout the twenty-first century, consistent with previous chemistry–climate model (CCM) studies (e.g., Eyring et al. 2013). The annual-mean evolution of ozone in the midlatitude lower stratosphere differs between hemispheres (Figs. 2a,b). The anthropogenic-induced changes in the southern midlatitude ozone by 2010 are much more skewed, and stronger, compared to the northern midlatitude ozone. In 2010, anthropogenic-induced ozone in the southern midlatitude average was significantly lower (~8%) than 1980s values.

Figures 2c and 2d show the time evolution of spring column ozone in both hemispheres. In response to anthropogenic forcing, the total spring column ozone in both hemispheres decreases from 1950s values to minimum values in 2010 and then increase to approximately 1980s values by 2060 in the SH or by 2040 in the NH (Figs. 2c,d). The rate of decline of the springtime polar column ozone from 1955 to 2010 is much more rapid and larger in the SH than in the NH [−35.88 and −12.82 DU $(10\,\text{yr})^{-1}$, respectively], consistent with the earliest findings of CCM studies (e.g., Austin and Wilson 2006; Waugh et al. 2009; Eyring et al. 2013). The deep Antarctic ozone hole in the anthropogenic forcing simulation occurs from 1990 to 2030, with column ozone concentration reduced down to ~130 DU.

b. *Antarctic ozone hole*

Guided by the evolution of spring column ozone in the SH (Fig. 2c), we focus our analysis in the period from 1990 to 2030, during which the deep Antarctic ozone hole is present in the model simulation. Hereafter, all transient simulation responses shown in the rest of the manuscript are in reference to the averaged period of 1990–2030. The differences in global, monthly mean, and zonal-mean total column ozone between GHGODS-TR and CTL-TR are shown in Fig. 3a. The largest ozone decrease is found in the SH polar region during austral spring and peaks in October–November, with a decrease of ~130 DU. However, during the summer, the total

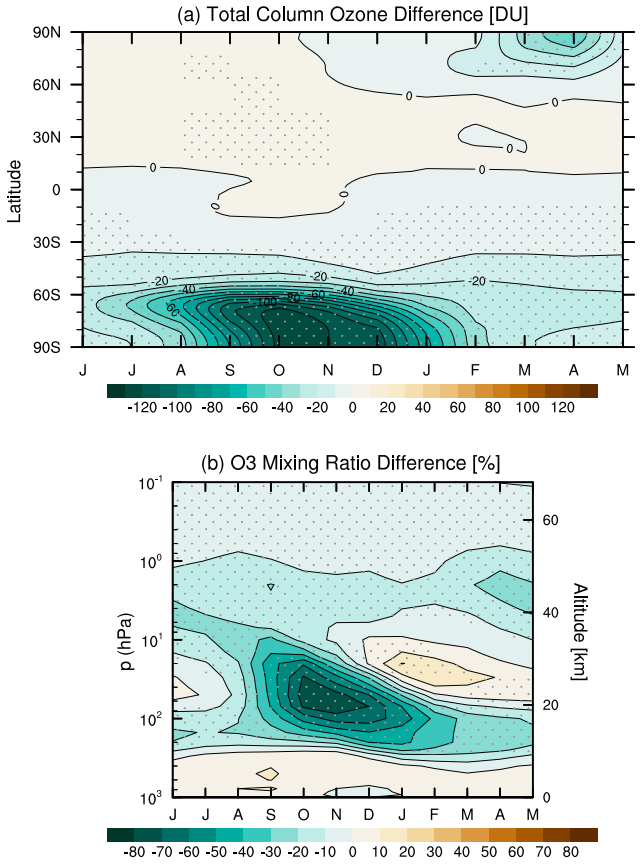

FIG. 3. (a) Zonal-mean, monthly mean total column ozone differences between GHGODS-TR and CTL-TR averaged over the years 1990–2030 as a function of month. The contour interval is 10 DU and colors range from 0 to ±120 DU. (b) Differences in the polar-cap average (90°–70°S) ozone concentration as a function of month and pressure. The contour interval is 10% and colors range from 0% to ±80%. Stippling indicates regions where the change exceeds the 95% significance level based on a two-tailed Student's *t* test.

column ozone decrease is limited up to 10–30 DU. In the SH midlatitudes (30°–60°S), the column ozone decreases by up to 20 DU throughout the seasons. This seasonal variation of the Antarctic ozone loss is in good agreement with previous CCM studies (e.g., Manzini et al. 2003; Marsh et al. 2013; Keeble et al. 2014).

Figure 3b shows the percentage change of the zonal-mean ozone mixing ratio averaged over the polar cap (70°–90°S). The strong ozone loss begins in September at 20 hPa and descends in altitude over time. The largest ozone loss occurs during October–November with a maximum of 77.4% ozone destroyed at 50 hPa. The ozone hole is followed by a distinct increase in ozone mixing ratios in the mid stratosphere during summer through autumn, peaking in February at 20 hPa. The temporal extent of this positive ozone response from late summer to autumn in the midstratosphere is to a large degree associated with increased downwelling induced by resolved planetary wave drag (see section 4 for detailed analysis).

4. Middle-atmosphere temperature coupling

In this section, the impact of the Antarctic ozone hole on the stratosphere and MLT temperatures is examined by discussing the seasonal structure of the temperature responses, the contribution of radiative and dynamical heating components, and the effects of different types of wave drag to the dynamical heating responses.

a. Temperature responses

Figure 4a shows the zonal-mean, monthly mean temperature differences between GHGODS-TR and CTL-TR, averaged over the polar cap (90°–70°S) as a function of pressure and month. Consistent with previous observations and model studies (e.g., Thompson and Solomon 2002; Manzini et al. 2003; Marsh et al. 2013; Keeble et al. 2014), the polar stratospheric ozone loss leads to a strong seasonal temperature response in the lower stratosphere. Consistent with the negative ozone response shown in Fig. 3b, the strong cooling of the lower polar stratosphere begins in September when sunlight activates the catalytic cycles to rapidly deplete ozone and continues until April. The maximum cooling occurs from November to December, when the polar-cap average temperature response at 70 hPa is up to 16 K. In addition, there is also a statistically significant positive temperature response in the middle to upper stratosphere beginning in November and persisting through February and March, which is associated with enhanced downwelling and dynamically induced ozone increase near 10 hPa over the polar cap (Fig. 3b and see section 3b for further details). The maximum warming over this region occurs in December, during which temperatures at 7 hPa increase by 4 K.

In contrast to the stratosphere, the mesosphere begins to warm from October to December (Fig. 4a). The maximum warming occurs in November, with temperature increases of ~8 K at 0.01 hPa around the mesopause. On the other hand, the lower thermosphere cools by up to 14 K above 0.001 hPa throughout the seasons. In addition, Fig. 4 also includes the zonal-mean temperature responses from the timeslice experiments by isolating the effects of the ozone depletion (Fig. 4b) and increased GHGs (Fig. 4c). The differences between these temperature responses confirm that the polar stratospheric ozone loss is largely responsible for spring to summer temperature changes in the stratosphere and MLT regions (Fig. 4b). It is also worth noting that the significant cooling of the lower thermosphere (10^{-3} and 10^{-4} hPa) between October and December is partly caused by the increased GHG concentration (Fig. 4c).

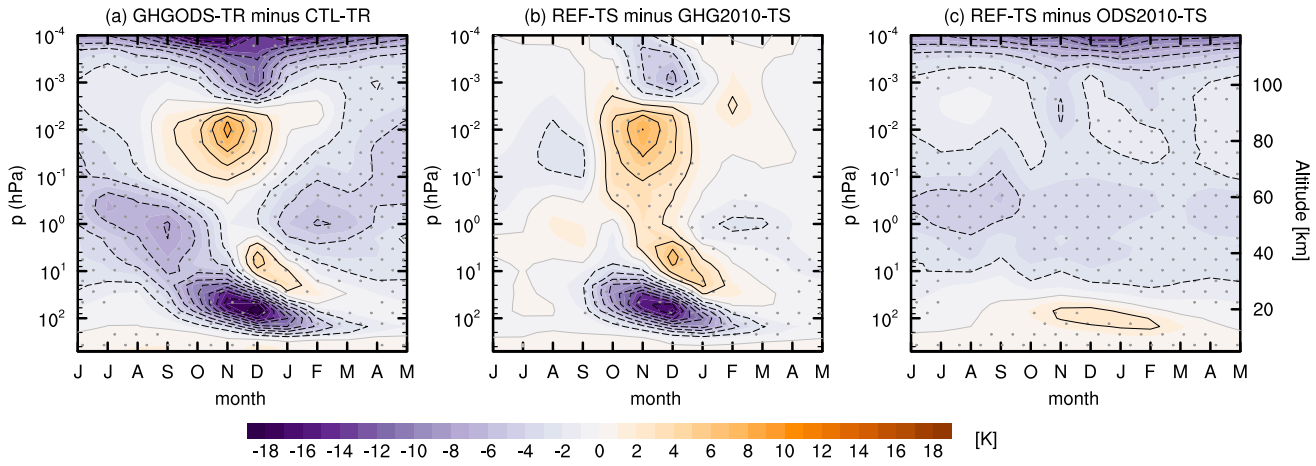

FIG. 4. (a) Polar-cap-average (90°–70°S) temperature differences between GHGODS-TR and CTL-TR averaged over the 1990–2030 period as a function of month and pressure. (b),(c) As in (a), but for the timeslice experiments: (b) REF-TS minus GHG2010-TS (impact of ozone only) and (c) REF-TS minus ODS2010-TS (impact of GHGs only). The contour interval is 2 K, solid (dashed) contours represent positive (negative) changes, and colors range from 0 to ±18 K. The zero contour is shown with solid gray lines. Stippling indicates regions where the change exceeds the 95% significance level based on a two-tailed Student's *t* test.

b. *Dynamical and radiative contributions to temperature coupling*

To examine the contribution of dynamics and radiation to the temperature responses, we computed the dynamical, shortwave, and longwave heating-rate responses from both the transient (Figs. 5a–d) and timeslice simulations (Fig. S1 in the supplemental material). Here we focus our analysis on December, since the stratospheric temperature changes resulting from the Antarctic ozone hole are at their maximum in this period. Qualitatively similar results are also found in November (not shown).

Figure 5 shows a meridional cross section of the zonal-mean temperature differences between GHGODS-TR and CTL-TR as well as the dynamical and radiative (short- and longwave) heating-rate differences. In the lower to midstratosphere (between 250 and 10 hPa), temperature decreases significantly by ~16 K (Fig. 5a). This cooling is caused by a reduction of shortwave heating rates (up to 0.6 K day^{-1}) as a result of ozone destruction via catalytic chemical reactions (Fig. 5c). This result is comparable to a coupled CCM study by Keeble et al. (2014), showing a maximum reduction of shortwave heating rates by ~0.6 K day^{-1} in December. In addition, the cooling in the lower to midstratosphere is enhanced by anomalous dynamical cooling (up to −0.25 K day^{-1}) induced by anomalous upwelling between ~300 and ~100 hPa (see solid contour lines in Fig. 5b). This is in agreement with previous findings by Orr et al. (2013), which show that the radiative cooling in the lower stratosphere is enhanced by a reduction in dynamical heating rates. This overall lower-stratospheric temperature response is due mainly to the effects of the stratospheric ozone depletion (Figs. S1a–d).

An increase of the mid- to upper-stratospheric polar temperatures (between 10 and 1 hPa) by up to ~5 K is due to anomalous dynamical heating induced by anomalous polar downwelling (Fig. 5b) and to a smaller degree by anomalous shortwave heating due to increased ozone concentrations (Fig. 3b). The warming above the lower-stratospheric cooling is consistent with the previous CCM studies, which is attributed to the Antarctic ozone hole (e.g., Manzini et al. 2003; Lossow et al. 2012; Marsh et al. 2013; Keeble et al. 2014). In addition, the dynamical warming between 0.7 and 0.1 hPa is dampened by radiative cooling, resulting in insignificant anomalous cooling over this region. Further analysis by separating the effects of stratospheric ozone depletion and increased GHGs show that this radiative cooling is mainly attributed to increased GHGs (Figs. S1e,f).

In the mid- to upper mesosphere (0.7 to 0.002 hPa), a significant temperature increase by ~10 K is associated with the dynamical warming induced by anomalous polar downwelling (Fig. 5b). On the other hand, the anomalous cooling in the lower thermosphere (0.001–0.0001 hPa) is caused by a combination of anomalous dynamical cooling (up to 5 K day^{-1}) induced by anomalous polar upwelling (Fig. 5b) and anomalous radiative cooling due to increased GHGs (Fig. 5d and Figs. S1e,h). The effects of increased GHG concentrations also explain the significant temperature decreases in the MLT regions from late summer to late winter.

To quantify the effects of resolved and nonresolved wave drag on the dynamical heating rates, we performed a downward control analysis [Eqs. (5) and (6)] to calculate

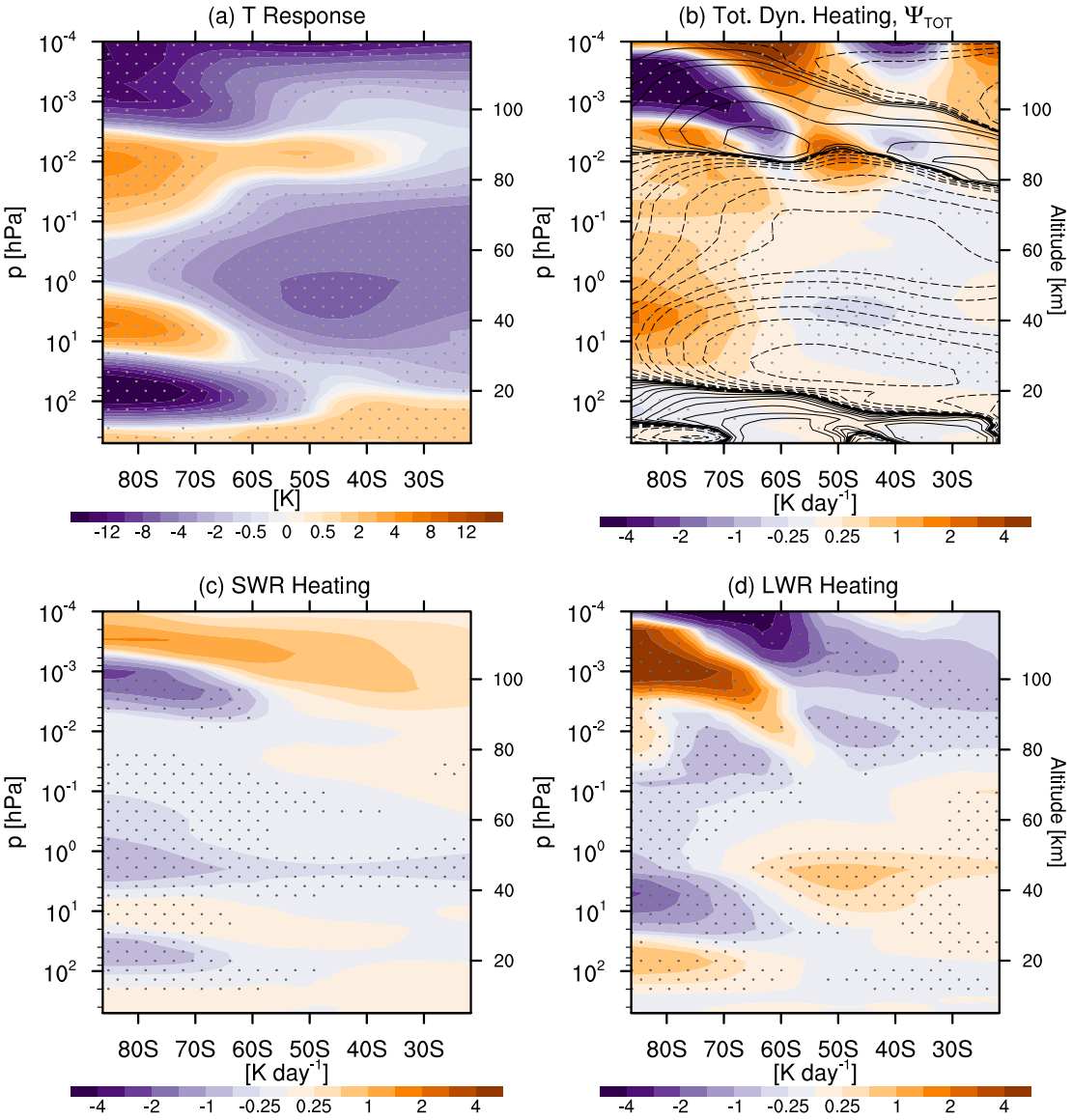

FIG. 5. December zonally averaged temperature and heating-rate differences between GHGODS-TR and CTL-TR averaged over the 1990–2030 period as a function of latitude and pressure. (a) Temperature (K), (b) total dynamical heating rate {[Q_{dyn}] see Eq. (8), K day^{-1}}, (c) shortwave heating rate (K day^{-1}), and (d) longwave heating rate (K day^{-1}). Contours in (b) denote the residual mass streamfunction (Ψ) at intervals of $\pm\{1 \times 10^5 \times$ [0.01, 0.05, 0.1, 0.5, 1, 2, 4, 8, 16, 32,. . .]} kg s^{-1} with solid (dashed) contours indicating upwelling (downwelling) of air parcels in a counterclockwise (clockwise) direction. Stippling indicates regions where the change exceeds the 95% significance level. For clarity, a nonlinear color scale is used for temperature and heating-rate differences [interval of 0.25 K (0.25 K day^{-1}) for absolute values $<$ 1 K (1 K day^{-1}) and interval of 1 K (1 K day^{-1}) for absolute values $>$ 1 K (1 K day^{-1})].

the separate contributions to residual circulation and dynamical heating from different types of wave drag. Figure 6 shows the meridional cross section of dynamical heating rates and residual circulation from total (Fig. 6a), resolved (Fig. 6b), and nonresolved (Fig. 6c) wave contributions. The anomalous dynamical cooling from the upper troposphere to lower stratosphere (~250–100 hPa, Fig. 5b) is associated with anomalous upwelling induced by resolved waves [Fig. 6b, consistent with Orr et al. (2013)]. Furthermore, the anomalous dynamical heating in the mid- to upper stratosphere (50–1 hPa, Fig. 5b) can be explained by anomalous dynamical heating induced by both resolved waves (0.5–2 K day^{-1} between 50 and 1 hPa) and nonresolved waves (0.5–1.5 K day^{-1} between 5 and 1 hPa). This indicates that both the resolved and nonresolved wave drag play crucial roles in determining the anomalous dynamical heating in the mid- to upper

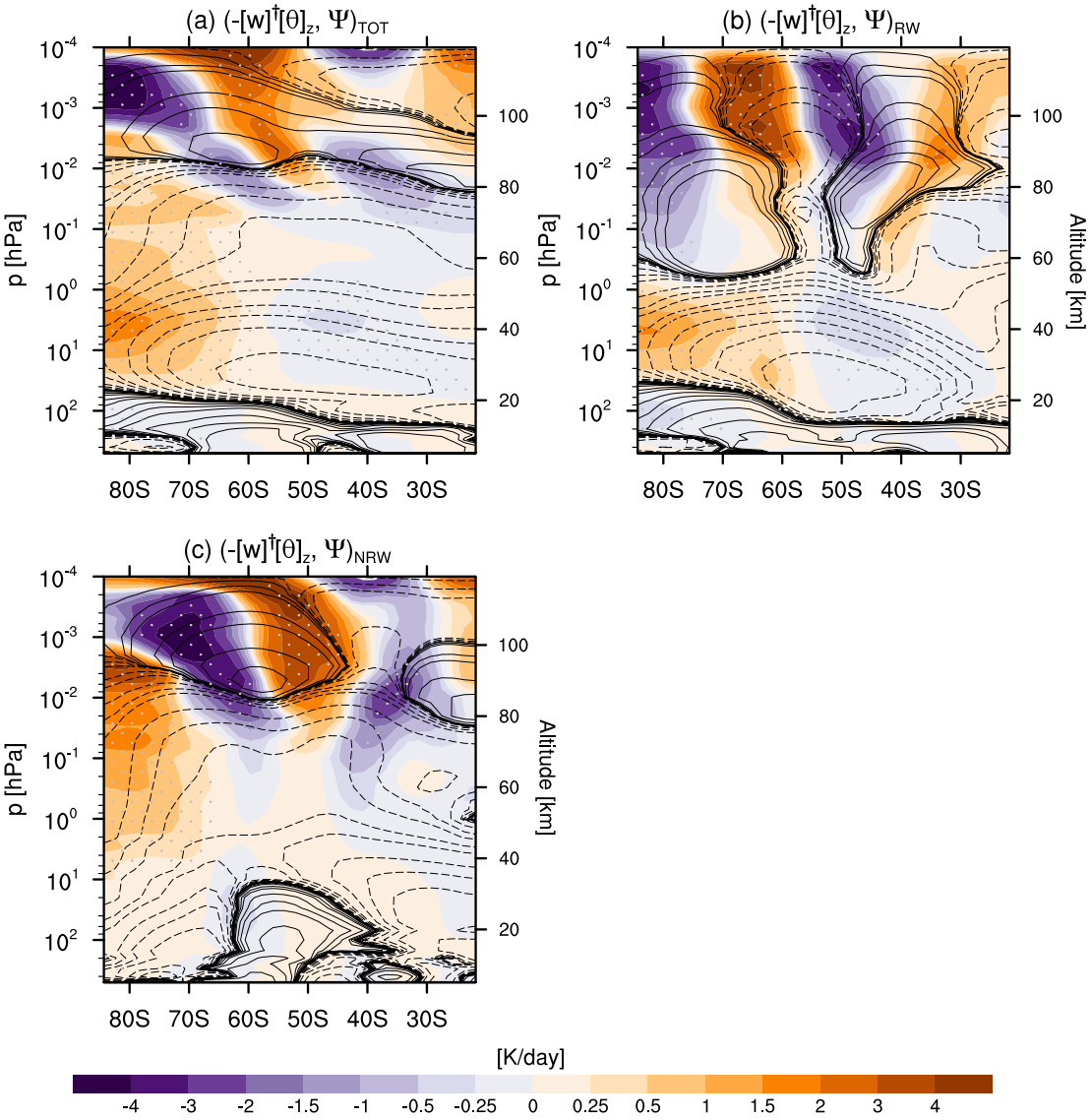

FIG. 6. December zonally averaged dynamical heating-rate and residual circulation differences between GHGODS-TR and CTL-TR averaged for the 1990–2030 period as a function of latitude and pressure. (a) Total $[w]^{\dagger}$ advection, (b) $[w]^{\dagger}$ advection from resolved waves, and (c) $[w]^{\dagger}$ advection from nonresolved waves. Contour intervals are as in Fig. 5b for the heating-rate responses and $\pm\{1\times10^{5}\times[0.01, 0.05, 0.1, 0.5, 1, 2, 4, 8, 16, 32,...]\}$ kg s^{-1} for residual (mass) streamfunction responses. Solid (dashed) contours of Ψ indicate clockwise (counterclockwise) circulation with upwelling (downwelling) in the Antarctic regions. Stippling indicates regions where the change exceeds the 95% significance level.

stratosphere in response to the ozone hole, which was not shown in previous studies.

Furthermore, the adiabatic warming in the mesosphere (0.1–0.003 hPa, Fig. 5b) is caused by anomalous downwelling induced by nonresolved waves (Fig. 6c). Our analysis for the first time shows that this anomalous downwelling is dampened by ~50%–60% by the effects of the anomalous upwelling induced by resolved wave drag (Fig. 6b). The net of the two effects yields a weakening of the summer upwelling in the mesosphere, which is consistent with positive trends in SH summer mesospheric temperatures shown by Smith et al. (2010). In the lower thermosphere (0.001–0.0001 hPa), the anomalous cooling is not only attributed to anomalous nonresolved wave-driven upwelling [as shown by Smith et al. (2010)] but also to the effects of anomalous upwelling induced by resolved wave drag (Figs. 6b,c). This combined effect leads to a weakening of the SH summer downwelling above 0.001 hPa and, thus, is consistent with decreased SH summer temperatures in the lower thermosphere (Fig. 5a).

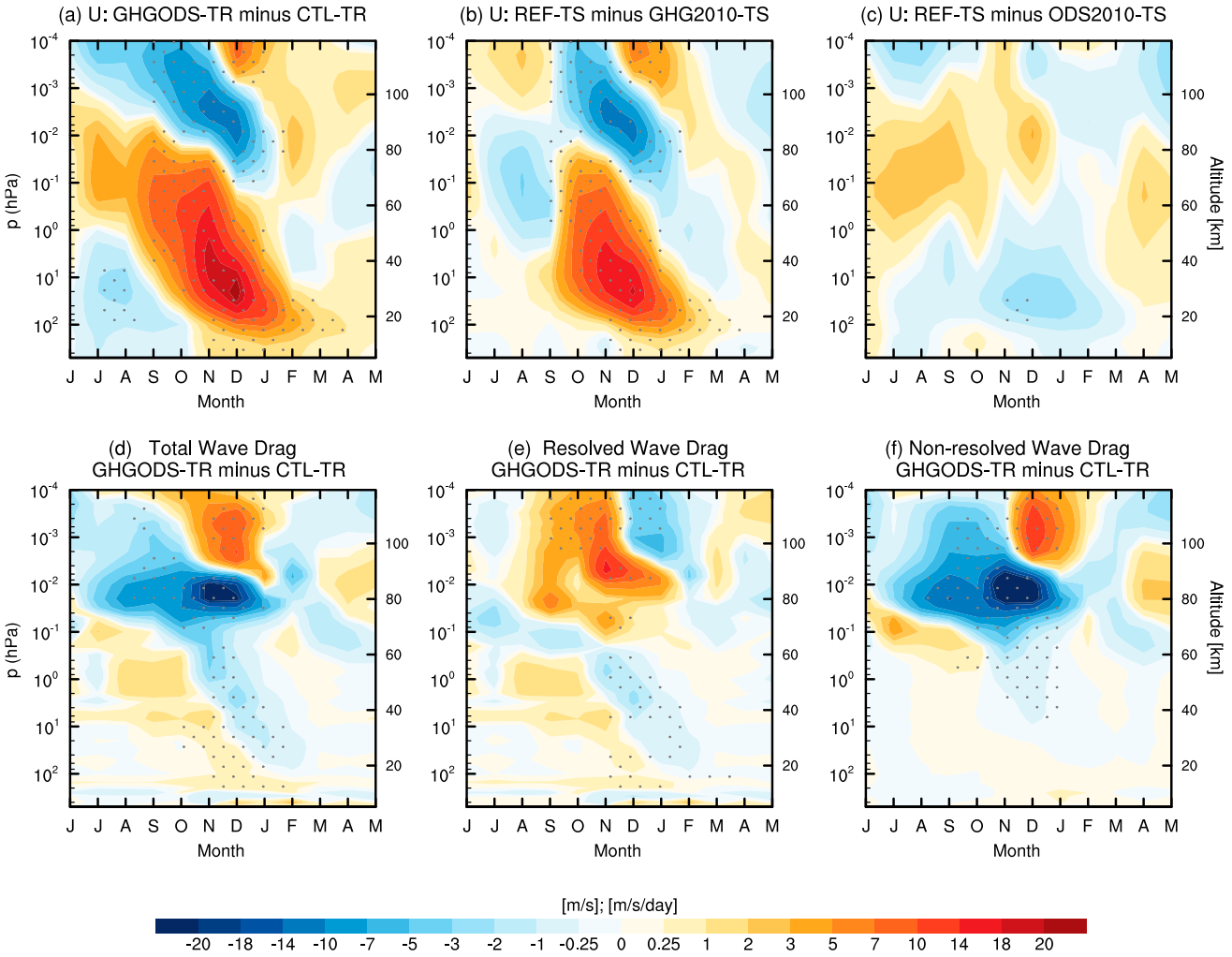

FIG. 7. (a) Zonal-mean, monthly mean zonal wind differences between GHGODS-TR and CTL-TR averaged from 75° to 55°S, and averaged for the 1990–2030 period, as a function of month and pressure. (b),(c) As in (a), but for the timeslice experiments: (b) REF-TS minus GHG2010-TS (impact of ozone only) and (c) REF-TS minus ODS2010-TS (impact of GHGs only). (d)–(f) Wave drag ($m\,s^{-1}\,day^{-1}$) differences between GHGODS-TR and CTL-TR divided into contributions from (d) total waves, (e) resolved waves, and (f) nonresolved waves. Stippling indicates regions where the change exceeds the 95% significance level.

5. Middle atmosphere zonal wind coupling

This section focuses on the mechanisms responsible for maintaining downward propagation of the zonal-mean wind anomalies in the MLT due to the Antarctic ozone hole. We begin by discussing the vertical coupling of the zonal-mean wind anomalies, the roles of resolved and nonresolved wave drag in maintaining downward propagation of zonal wind responses and the dynamical origin of the positive resolved wave responses in the MLT.

a. Downward propagation of the zonal wind anomalies

Figure 7a shows the zonal-mean, monthly mean zonal wind response averaged over 75°–55°S between GHGODS-TR and CTL-TR. Consistent with the increased meridional temperature gradient (Fig. 5a), the stratospheric westerlies are significantly strengthened from midspring to late summer, with maximum changes of nearly $20\,m\,s^{-1}$ near 20 hPa in December. This is indicated by the downward propagation of the westerly wind anomalies from the lower mesosphere to the surface (Fig. 7a). The strengthening of the westerlies has been shown to cause a delay in the final vortex breakdown by about several weeks (e.g., Karpechko et al. 2010; Lossow et al. 2012; Keeble et al. 2014).

In conjunction with stratospheric zonal wind changes occurs a strengthening of the prevailing easterlies in the mesosphere from late spring to early summer. This is indicated by a downward propagation of the easterly wind anomalies from the lower thermosphere to lower mesosphere, with maximum changes of nearly $15\,m\,s^{-1}$

near 0.005 hPa in December. Stronger summer easterlies in the mesosphere are consistent with the simulated negative trends of the summer mesospheric winds in the SH found by Smith et al. (2010) and the observed persistence of the winter mesospheric wind condition into summer during the ozone hole period (Venkateswara Rao et al. 2015). In addition, there is a strengthening of prevailing westerlies in the lower thermosphere (between 0.001 and 0.0001 hPa) during the period of the strongest Antarctic ozone hole in the model. This is associated with a significant downward propagation of the westerly wind anomalies from the lower thermosphere to the upper mesosphere from November to February. The strengthening of the prevailing westerlies in the lower thermosphere during the strongest Antarctic ozone hole in the model is interesting, but needs to be verified by further observational studies. In addition, Fig. 7 includes the zonal-mean wind response from the timeslice experiments by separating the effects of ozone depletion (Fig. 7b) and global warming (Fig. 7c). The differences between the two timeslice simulations confirm that it is indeed the Antarctic ozone hole that is responsible for the downward coupling of the zonal-mean wind anomalies in the stratosphere and MLT regions (Figs. 7b,c).

b. *Wave-maintained vertical zonal wind coupling*

To understand the mechanisms responsible for maintaining downward propagation of the zonal wind anomalies in the stratosphere and MLT, the total, resolved, and nonresolved wave drag differences between GHGODS-TR and CTL-TR are examined (Figs. 7d–f).

In the period of initial (radiative) strengthening of lower-stratospheric winds (from October to late November, Fig. 7a) there is decreased resolved (planetary) wave breaking in the stratosphere indicated by positive westerly wave drag anomalies in the lower through the middle stratosphere (Figs. 7d,e). In particular, the increasing westerly wind above the critical value dampens upward planetary wave activity into the stratosphere, as indicated by anomalous negative vertical EP flux during this period (not shown). This condition can initiate a positive feedback mechanism, in which the strengthened westerlies associated with weaker wave driving can cause further vortex strengthening and induce downward migration of the wind anomalies toward the tropopause [consistent with the mechanism proposed by Orr et al. (2012)]. Conversely, in the summer (from December to late February) the delayed breakdown of the polar vortex allows planetary waves to propagate higher into the stratosphere. This results in increased resolved wave breaking, as diagnosed by anomalous negative EP-flux divergence between ~100 and 1 hPa (Figs. 7d,e). The strong increase in wave breaking in response to the ozone hole during the austral summer is consistent with Keeble et al. (2014).

The downward propagation of easterly wind anomalies from the lower thermosphere to lower mesosphere is maintained by total easterly wave drag anomalies (Fig. 7d). These total wave drag anomalies are formed by resolved and nonresolved wave drag that have almost similar structures but are opposite in sign (Figs. 7e,f). However, since the contribution from easterly nonresolved wave drag anomalies exceeds that of westerly resolved wave drag anomalies, the sum of the two yields the net easterly wave drag anomalies that preserve the downward propagation of the easterly wind anomalies in the MLT from spring to early summer. The increased easterly nonresolved wave drag during this period is consistent with an increased filtering of the westerly nonresolved wave drag by stratospheric westerly winds (Fig. 7a).

In addition, the downward propagation of westerly wind anomalies in the lower thermosphere from November to February is maintained by the total westerly wave drag anomalies (Fig. 7d). These total westerly wave drag anomalies consist of both nonresolved wave drag (dominant component) and resolved wave drag (Figs. 7e,f). The increased westerly nonresolved waved drag in the lower thermosphere is a result of increased filtering of the easterly nonresolved wave drag by mesospheric easterly winds (Fig. 7a), while the increased westerly resolved wave drag in the lower thermosphere is associated with in situ wave generation in the upper mesosphere via zonal-mean state instabilities (see section 5c for details). These results for the first time show that both resolved and nonresolved wave drag are important in maintaining the downward propagation of the zonal wind anomalies in the MLT during the ozone hole period.

c. *Dynamical origin of the resolved wave drag responses in the MLT*

The emergence of pronounced changes in resolved wave drag in the MLT from late spring to early summer (from November to December) is interesting and requires further investigation. One possible mechanism is associated with changes in in situ wave excitation via instability of the background zonal-mean state (Lossow et al. 2012). To examine this process, we analyze the latitude–height cross sections of the meridional gradient of PV response in December along with total resolved wave drag and zonal-mean wind responses (Fig. 8). We focus our analysis on the transient simulation response, since most changes in the zonal-mean wind during a period of strong Antarctic ozone hole in the model are

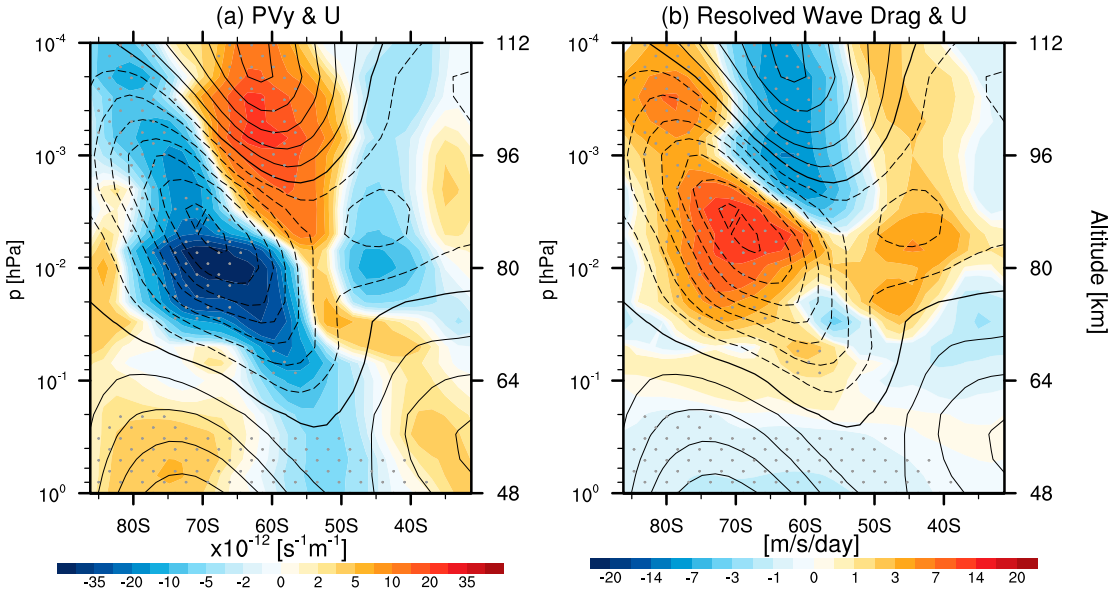

FIG. 8. (a) Meridional PV gradient $[q]_y$ (shading, $\times 10^{-12}\,\mathrm{s^{-1}\,m^{-1}}$) and (b) resolved wave drag (shading, $\mathrm{m\,s^{-1}\,day^{-1}}$) differences between GHGODS-TR and CTL-TR averaged for the 1990–2030 period as a function of latitude and pressure in December. The contour lines denote the zonal-mean wind (U) differences between the two simulations (intervals are $2\,\mathrm{m\,s^{-1}}$). Stippling indicates regions where the change exceeds the 95% significance level.

largely due to the stratospheric ozone depletion. The qualitatively similar results are also found in November (not shown).

The negative PV gradient response in December (Fig. 8a) is visible over a wide range of high latitudes, with a maximum response occurring near 0.01 hPa. This response strengthens the climatological negative PV gradients in the upper mesosphere and lower thermosphere during early summer. According to Pedlosky (1979), regions where the PV gradient is negative are potentially baroclinically or barotropically unstable and, thus, represent potential sources of in situ wave generation. The stronger easterlies, which have larger and deeper regions of the negative PV gradients, coincide with a region of positive EP-flux divergence anomalies (Fig. 8b). This condition indicates that the westerly resolved wave drag anomalies in the upper mesosphere are locally generated via instability of the zonal-mean state [consistent with Lossow et al. (2012)]. The types of instability responsible for this in situ wave excitation in the upper mesosphere could be a mix of barotropic and baroclinic processes (e.g., Plumb 1983; Garcia et al. 2005; Riggin et al. 2006). To examine this, we decomposed the PV gradient responses into contributions of barotropic (i.e., meridional curvature) and baroclinic (i.e., vertical shear and curvature) terms of the meridional PV gradient equation (Fig. S2 in supplemental material). It should be noted that the barotropic instability is associated with PV gradient changes of sign between different latitudes, due to meridional wind curvature ($[u]_{\phi\phi}$), while baroclinic instability is associated with PV gradient changes of sign between the lower and upper levels, due to vertical wind structure ($\rho N^{-2}[u]_z$) (Pedlosky 1979). Our results show quantitatively that both changes in vertical shear and meridional curvature of the zonal-mean wind appear to be largely responsible for the negative PV gradient response in this region (Fig. S2). This indicates that in situ wave generation in the upper mesosphere during the strongest Antarctic ozone hole in the model is not solely associated with baroclinic instability [as suggested by Lossow et al. (2012)], but also with barotropic instability.

To investigate which type of waves is responsible for the resolved wave drag response in the upper mesosphere, we decompose the resolved wave drag response into different zonal wavenumber (k) contributions. Figure 9 shows latitude–height cross sections of the resolved wave drag differences divided into contributions from planetary-scale waves $k = 1$, planetary-scale waves $k = 2$–3, and synoptic-scale waves ($k > 3$), with the associated EP-flux vectors superimposed. Comparing resolved wave drag responses from total wavenumbers (Fig. 8b) and to planetary-scale wavenumber $k = 1$–3 (Figs. 9a,b), it is obvious that positive resolved wave drag responses between 0.01 and 0.0001 hPa are mostly dominated by planetary-scale waves ($k = 1$–3). In particular, planetary waves ($k = 1$) dominate total westerly resolved wave drag anomalies between 80° and 65°S and 0.01 and 0.0001 hPa, while the planetary waves ($k = 2$–3) contribute to the total westerly resolved wave drag anomalies

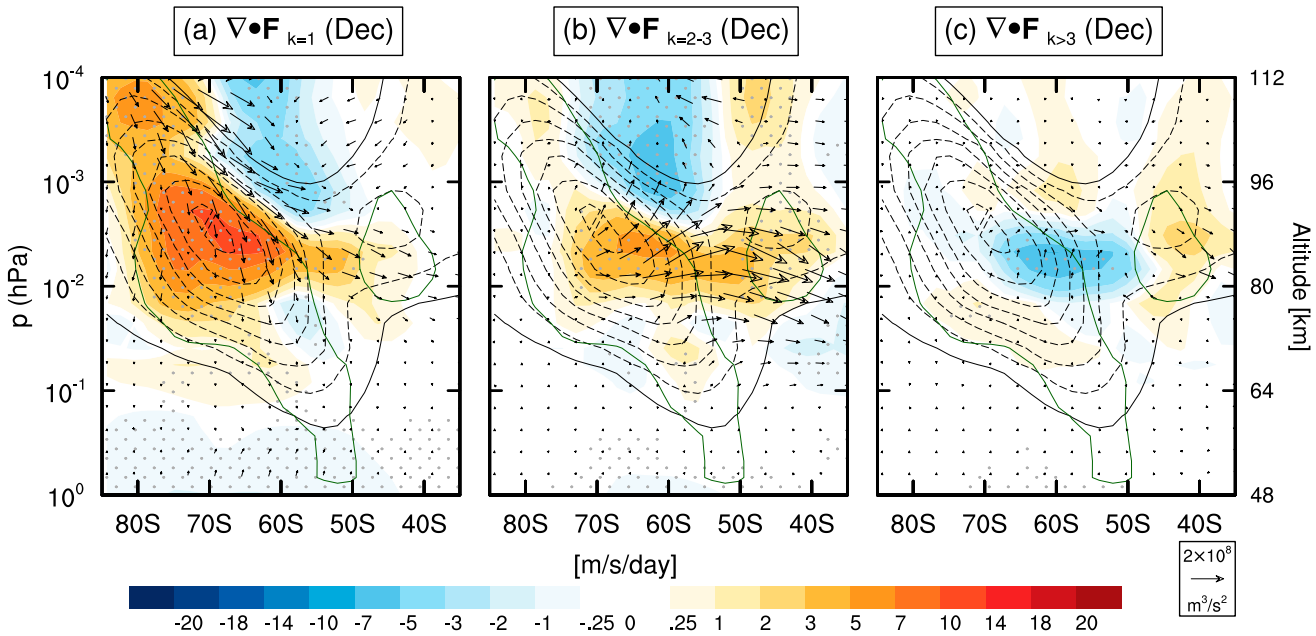

FIG. 9. Resolved wave drag differences between GHGODS-TR and CTL-TR in December averaged for the 1990–2030 period and separated into different zonal wavenumbers: (a) planetary-scale waves $k = 1$, (b) planetary-scale waves $k = 2$–3, and (c) synoptic-scale waves $k > 3$ ($m\,s^{-1}\,day^{-1}$), superimposed with EP-flux vectors. The dark green contours enclose regions where $[q]_y < 0$, which is the necessary condition for baroclinic or barotropic instability. The dashed gray contours indicate negative zonal-mean winds (intervals are $2\,m\,s^{-1}$). The zero contours are denoted by solid gray contours. Stippling indicates regions where the change exceeds the 95% significance level.

in mid- to high latitudes between 70° and 45°S and 0.01 and 0.001 hPa. In contrast to planetary-scale waves (k = 1–3), the response of the synoptic wave ($k > 3$) EP-flux divergence gives the anomalous easterly forcing in the region of larger negative PV gradients (Fig. 9c). This indicates that the resolved synoptic-scale wave ($k > 3$) drag cannot explain the westerly resolved wave drag anomaly in the upper mesosphere, which is in contrast to the results of Lossow et al. (2012) showing the opposite response.

Further understanding of the in situ wave generation can be obtained by decomposing the resolved wave drag responses from the dominant zonal wavenumbers k = 1–3 (Fig. 9) into the most prominent periods of traveling planetary waves in the SH summer: 16-day waves k = 1, 10-day waves k = 1, quasi-5-day waves k = 1, and QTDW k = 3 (Forbes et al. 1995; Lieberman et al. 2003; Day and Mitchell 2010; Garcia et al. 2005). We should note, since the aliasing in space–time filter appears as folding about the Nyquist frequency (per 2 days here), the QTDW is approximated as shorter period (<4 days) waves with k = 3. Figure 10 shows the most dominant traveling resolved wave drag responses: for (Fig. 10a) the 16-day planetary wave (k = 1), (Fig. 10b) the 5-day planetary waves (k = 1), and (Fig. 10c) shorter period (<4 days) waves (k = 3), with the associated EP-flux vectors superimposed. Our results show that both the 16- and the 5-day waves (Figs. 10a,b) dominate the positive planetary wave drag (k = 1) responses (Fig. 9a) in the region with strong negative PV gradients, with the 5-day wave contributing to changes up to ~50%. On the other hand, shorter period (<4 days) waves k = 3 (Fig. 10c) dominate the positive response in EP-flux divergence for planetary waves k = 2–3 in December (Fig. 9b).

6. Summary and discussion

We have presented results from a fully coupled chemistry–climate model CESM1(WACCM) to study the impact of the Antarctic ozone hole on the vertical coupling of the stratosphere–MLT system. Two fully coupled simulations from 1955 to 2099 are performed: one with time-varying anthropogenic ODSs and GHGs following the RCP8.5 scenario and the other with fixed ODS and GHG concentrations at 1960 values. This resulted in two simulated responses, one of which simulates the severe ozone depletion (and recovery) and GHG increases, and one of which does not. Specifically, we analyzed the averaged responses between 1990 and 2030, which represents the period of the strongest Antarctic ozone hole in the model simulations. Using a set of timeslice simulations, we further examine whether the responses from the transient simulation during the period of the strongest Antarctic ozone hole in the model are the result of ozone depletion alone or also affected by increased GHGs. This work can be viewed as a complementary study to that of Smith et al. (2010) and Lossow

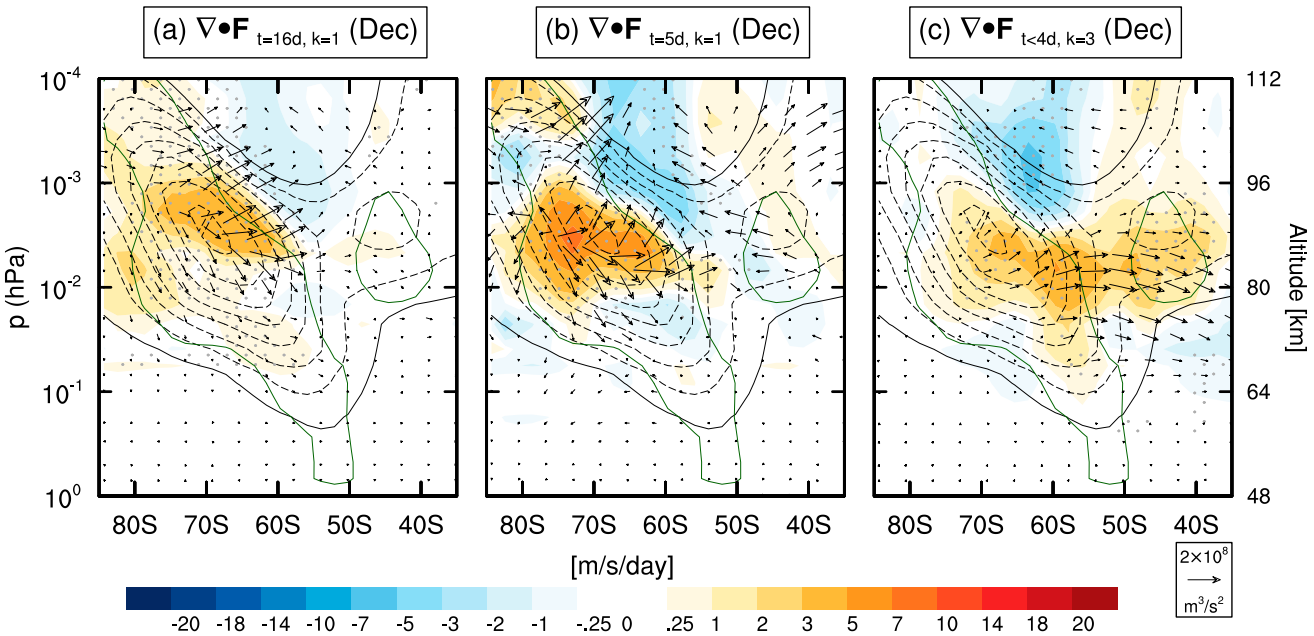

FIG. 10. As in Fig. 9, but divided into different wave periods and zonal wavenumbers: (a) 16-day waves ($k = 1$), (b) quasi-5-day waves ($k = 1$), and (c) short-period (<4 days) waves ($k = 3$) ($m\,s^{-1}\,day^{-1}$), superimposed with EP flux vectors. Stippling indicates regions where the change exceeds the 95% significance level.

et al. (2012), who particularly examined the impact of the ozone hole on the Antarctic summer mesopause region. However, we extend the analysis by quantifying the radiative and dynamical components of the stratosphere–MLT temperature coupling responses. We furthermore explain the mechanism responsible for maintaining the downward propagation of zonal wind anomalies in the MLT and clarify the dynamical origin of the resolved wave drag responses in the upper mesosphere. The key processes responsible for the vertical coupling of the stratosphere and MLT due to the Antarctic ozone loss in late spring and early summer are summarized schematically in Fig. 11.

In the lower to midstratosphere (250–10 hPa), the significant temperature decrease during late spring and early summer is due mainly to anomalous shortwave cooling induced by stratospheric ozone depletion, which is consistent with previous CCM studies (e.g., Manzini et al. 2003; Smith et al. 2010; Orr et al. 2013; Keeble et al. 2014). This anomalous radiative cooling is enhanced by anomalous dynamical cooling between 250 and 100 hPa (Fig. 6a and Fig. 11) but is somewhat mitigated by anomalous dynamical heating above ~70 hPa. Our analysis further clarified that the anomalous dynamical cooling induced by the resolved wave drag in the lower stratosphere (~250–100 hPa, Fig. 6b) is dampened by the effects of anomalous downwelling induced by nonresolved wave drag (Figs. 6b and 6c). This suggests that the easterly nonresolved wave drag anomalies in the lower stratosphere act to weaken the anomalous adiabatic cooling induced by the resolved wave drag.

The significant increase in upper-stratosphere temperature (10–1 hPa) from late spring to early summer is a result of both anomalous dynamical heating induced by anomalous polar downwelling (the dominant component) and anomalous shortwave heating due to ozone increases (Figs. 6b,c and 11). Unlike previous studies (e.g., Manzini et al. 2003; Keeble et al. 2014), our results for the first time show that both resolved and nonresolved wave drag play a crucial role in driving the anomalous polar downwelling in this region, with resolved waves contributing ~0.5–2 K day^{-1} between 10 and 5 hPa and nonresolved waves contributing ~0.5–1.5 K day^{-1} between 5 and 1 hPa. This suggests that anomalous downwelling in the upper stratosphere (10–1 hPa) induced by the ozone hole is not only due to increased dissipation of resolved planetary waves but also to the effects of anomalous easterly nonresolved wave drag in the upper stratosphere resulting from filtering of westerly GWD.

Our analysis also clarifies the cause of the lack of significance of polar temperature cooling trends in the lower mesosphere (~0.7–0.1 hPa) in response to the ozone hole, as reported by Smith et al. (2010, see their Fig. 1a). We find that in late spring to early summer, the anomalous adiabatic warming due to a weakening of the mesospheric upwelling is canceled by the effects of radiative cooling due to increased GHGs in the middle atmosphere (Figs. 5c,d and S1e). This results in an insignificant cooling response in this region.

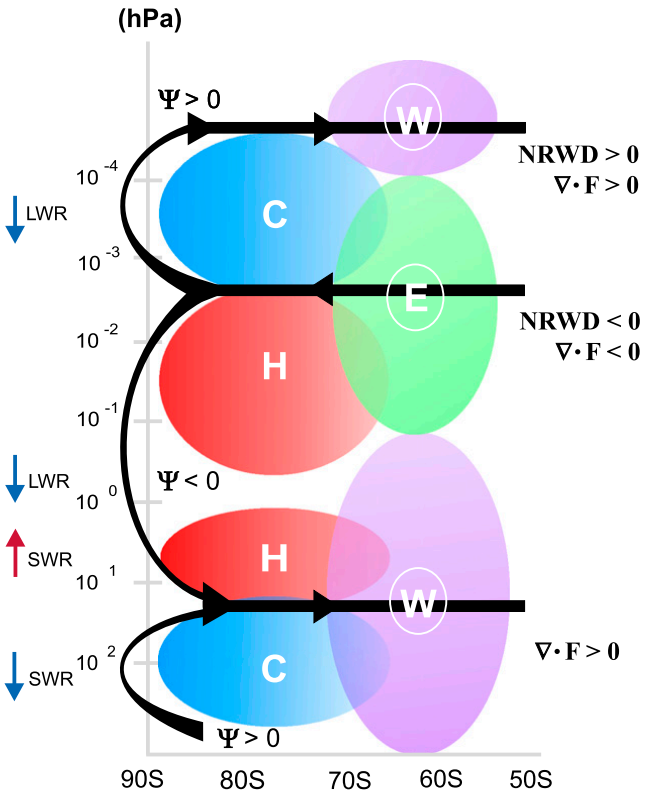

FIG. 11. Schematic diagram of the Antarctic ozone hole modulated anomalies of the temperature [cold (C) and hot (H)], zonal-mean wind [westerly (W) and easterly (E)], residual circulation (Ψ), resolved and nonresolved wave drag ($\nabla \cdot \mathbf{F}$ and NRWD, respectively), and radiative heating–cooling during late spring and early summer. The anomalous positive (negative) wave drag leads, through the Coriolis force, to an upward and equatorward (poleward and downward) residual circulation in high latitudes.

Our results further reveal that the warming in the mid- to upper mesosphere (0.07–0.002 hPa) driven by the anomalous nonresolved wave-driven downwelling is dampened by ~50%–60% through the effects of anomalous upwelling induced by resolved wave drag (Figs. 6b,c). This suggests that the westerly resolved wave drag anomalies in this region dampen the anomalous adiabatic heating induced by nonresolved wave drag. In addition, the Antarctic ozone hole also causes a significant cooling in the lower thermosphere (above 0.001 hPa). Our analysis quantitatively shows that this anomalous cooling is not only driven by anomalous nonresolved wave-driven upwelling [as shown by Smith et al. (2010)] but also to the effects of anomalous upwelling induced by resolved wave drag (see Fig. 6). This combined effect causes a weakening of SH summer downwelling above 0.001 hPa and, thus, is consistent with the temperature decreases in this region (Fig. 5a). Above 0.0002 hPa (uppermost levels), this cooling is also partly attributed to anomalous radiative cooling due to increased GHG concentrations (Figs. S1e and 11).

The results also explain for the first time the role of resolved and nonresolved wave driving in maintaining the downward propagation of zonal wind anomalies in the MLT region during the Antarctic ozone hole period. From spring to early summer, the downward propagation of easterly wind anomalies in the MLT is maintained by total easterly wave drag anomalies, which result from a net balance between easterly nonresolved wave drag (the dominant component) and westerly resolved drag (Figs. 7e,f). Notably, the anomalously easterly nonresolved wave drag is a result of enhanced filtering of westerly GWD by stratospheric westerly winds, while anomalously westerly resolved wave drag is associated with in situ wave generation via baroclinic–barotropic instability. In addition, the downward propagation of westerly wind anomalies in the lower thermosphere from late spring to summer is maintained by both westerly resolved and nonresolved wave drag anomalies (due to enhanced filtering of easterly GWD by mesospheric easterly winds).

The regions of positive resolved wave drag responses in the upper mesosphere during late spring and early summer are consistent with the wave excitation via instability in the upper mesosphere (Fig. 8). Our results show quantitatively that the types of instability for the in situ wave generation are not only associated with baroclinic processes [as suggested by Lossow et al. (2012)] but also with barotropic processes (Fig. S2). It is shown that the in situ wave generation produces a spectrum of zonal wavenumbers, which peaks in the planetary-scale waves (k = 1–3). Further analysis shows that these planetary-scale waves are dominated by the 5-day wave (k = 1) and shorter-period (<4 days) waves (k = 3). Previous studies have shown that the 5-day waves observed in the summer mesosphere can be excited in situ via baroclinic instability in the upper mesosphere (e.g., Garcia et al. 2005; Riggin et al. 2006). Our simulation suggests that increased instability of the easterly summer jet during the Antarctic ozone hole period can possibly increase the 5-day wave activity in the upper mesosphere. Furthermore, the shorter period wave drag (k = 3) can be associated with enhanced in situ QTDW (k = 3) generation as a result of the baroclinic–barotropic instability of summertime mesospheric easterlies in the SH (Plumb 1983; Garcia et al. 2005). Nevertheless, a future study using higher-temporal-resolution output (i.e., higher than daily resolution) is required to verify this response. It should be noted, however, that the resolved wave drag responses in our analysis are in contrast to the results of Lossow et al. (2012), which show a dominant synoptic-scale wave drag (k > 3) response in the upper mesosphere. These differences could be due to the model lid height

effects in their simulations (95 km in CMAM vs 140 km in our model) that possibly alters the resolved wave drag responses (indicated by the large negative PV gradient maximizing close to the model lid ~90 km; see Lossow et al. 2012) and also to the use of Scinocca (2003) nonorographic GWD parameterization in CMAM that largely dampens the amplitude of the QTDW (McLandress and Scinocca 2005).

As in most CCMs, WACCM also exhibits biases in simulating stratospheric westerly jets in the SH (Marsh et al. 2013). This bias is associated with the model cold-pole problem, which is a common bias in chemistry–climate middle-atmosphere models (Austin et al. 2003; Eyring et al. 2010, chapters 4–8). The bias in the SH polar temperature and the westerly jet leads to a delay in the vortex breakdown by a few weeks relative to the observed timing (Butchart et al. 2011). Therefore, the observed early summer mesospheric warming and lower-thermospheric cooling may in reality occur somewhat earlier. The magnitude of the simulated temperature response may be also exaggerated because of a possible delay in ozone recovery in the model relative to the observed timing, although we do not have sufficient observations to verify this. Nevertheless, the temperature and circulation responses confirm the findings of earlier CCM studies (e.g., Smith et al. 2010; Lossow et al. 2012), suggesting that the middle-atmosphere responses to the ozone hole are robust among models.

CCMs predict that after the recovery to pre-1980 levels in 2050, the ozone layer will continue to grow until the end of 2100 (e.g., Eyring et al. 2007; Waugh et al. 2009; WMO 2014). Therefore, the changes discussed here will most likely reverse or cease. Clearly, further model studies are required to understand how competing effects between future ozone recovery and global warming determine the strength of the southern polar vortex and, thus, the characteristics of its vertical coupling.

Acknowledgments. We acknowledge support received from the German-Israeli Foundation for Scientific Research and Development under Grant GIF1151-83.8/2011. This work has also been partially performed within the Helmholtz University Young Investigators Group NATHAN funded by the Helmholtz Association through the Presidents Initiative and Networking Fund and the GEOMAR Helmholtz Centre for Ocean Research Kiel. We are grateful to Christof Petrick and Wuke Wang for setting up some of the fully coupled model experiments used in this study. The authors thank Nili Harnik for useful discussions on the theory of baroclinic instability and traveling wave activity in the middle atmosphere. The authors are also grateful to two anonymous reviewers and Dr. Anne Smith, whose comments helped improve the manuscript. The model simulations were performed at the German Climate Computing Centre (Deutsches Klimarechenzentrum, DKRZ) Hamburg.

REFERENCES

Andrews, D. G., J. R. Holton, and C. B. Leovoy, 1987: *Middle Atmosphere Dynamics*. International Geophysics Series, Vol. 40, Academic Press, 489 pp.

Austin, J., and R. J. Wilson, 2006: Ensemble simulations of the decline and recovery of stratospheric ozone. *J. Geophys. Res.*, **111**, D16314, doi:10.1029/2005JD006907.

——, and Coauthors, 2003: Uncertainties and assessments of chemistry-climate models of the stratosphere. *Atmos. Chem. Phys.*, **3**, 1–27, doi:10.5194/acp-3-1-2003.

Becker, E., 2012: Dynamical control of the middle atmosphere. *Space Sci. Rev.*, **168**, 283–314, doi:10.1007/s11214-011-9841-5.

Butchart, N., 2014: The Brewer-Dobson circulation. *Rev. Geophys.*, **52**, 157–184, doi:10.1002/2013RG000448.

——, and Coauthors, 2011: Multimodel climate and variability of the stratosphere. *J. Geophys. Res.*, **116**, D05102, doi:10.1029/2010JD014995.

Charney, J. G., and P. G. Drazin, 1961: Propagation of planetary-scale disturbances from the lower into the upper atmosphere. *J. Geophys. Res.*, **66**, 83–109, doi:10.1029/JZ066i001p00083.

Chen, P., and W. A. Robinson, 1992: Propagation of planetary waves between the troposphere and stratosphere. *J. Atmos. Sci.*, **49**, 2533–2545, doi:10.1175/1520-0469(1992)049<2533:POPWBT>2.0.CO;2.

Day, K. A., and N. J. Mitchell, 2010: The 5-day wave in the Arctic and Antarctic mesosphere and lower thermosphere. *J. Geophys. Res.*, **115**, D01109, doi:10.1029/2009JD012545.

Dunkerton, T., C. Hsu, and M. McIntyre, 1981: Some Eulerian and Lagrangian diagnostics for a model stratospheric warming. *J. Atmos. Sci.*, **38**, 819–844, doi:10.1175/1520-0469(1981)038<0819:SEALDF>2.0.CO;2.

Eyring, V., and Coauthors, 2007: Multimodel projections of stratospheric ozone in the 21st century. *J. Geophys. Res.*, **112**, D16303, doi:10.1029/2006JD008332.

——, T. G. Shepherd, and D. W. Waugh, Eds., 2010: SPARC report on the evaluation of chemistry-climate models. SPARC Rep. 5, WCRP-132, WMO/TD-1526, 426 pp.

——, and Coauthors, 2013: Long-term ozone changes and associated climate impacts in CMIP5 simulations. *J. Geophys. Res. Atmos.*, **118**, 5029–5060, doi:10.1002/jgrd.50316.

Forbes, J. M., M. E. Hagan, S. Miyahara, F. Vial, A. H. Manson, C. E. Meek, and Y. I. Portnyagin, 1995: Quasi 16-day oscillation in the mesosphere and lower thermosphere. *J. Geophys. Res.*, **100**, 9149–9163, doi:10.1029/94JD02157.

Garcia, R. R., R. Lieberman, J. M. Russell, and M. G. Mlynczak, 2005: Large-scale waves in the mesosphere and lower thermosphere observed by SABER. *J. Atmos. Sci.*, **62**, 4384–4399, doi:10.1175/JAS3612.1.

Gent, P. R., and Coauthors, 2011: The Community Climate System Model version 4. *J. Climate*, **24**, 4973–4991, doi:10.1175/2011JCLI4083.1.

Gillett, N. P., and D. W. J. Thompson, 2003: Simulation of recent Southern Hemisphere climate change. *Science*, **302**, 273–275, doi:10.1126/science.1087440.

Hansen, F., K. Matthes, and L. J. Gray, 2013: Sensitivity of stratospheric dynamics and chemistry to QBO nudging width

in the chemistry–climate model WACCM. *J. Geophys. Res. Atmos.*, **118**, 10 464–10 474, doi:10.1002/jgrd.50812.

Haynes, P. H., M. E. McIntyre, T. G. Shepherd, C. J. Marks, and K. P. Shine, 1991: On the ''downward control'' of extratropical diabatic circulations by eddy-induced mean zonal forces. *J. Atmos. Sci.*, **48**, 651–678, doi:10.1175/1520-0469(1991)048<0651:OTCOED>2.0.CO;2.

Holton, J. R., 1983: The influence of gravity wave breaking on the general circulation of the middle atmosphere. *J. Atmos. Sci.*, **40**, 2497–2507, doi:10.1175/1520-0469(1983)040<2497:TIOGWB>2.0.CO;2.

Karpechko, A. Y., and E. Manzini, 2012: Stratospheric influence on tropospheric climate change in the Northern Hemisphere. *J. Geophys. Res.*, **117**, D05133, doi:10.1029/2011JD017036.

——, N. P. Gillett, L. J. Gray, and M. Dall'Amico, 2010: Influence of ozone recovery and greenhouse gas increases on Southern Hemisphere circulation. *J. Geophys. Res.*, **115**, D22117, doi:10.1029/2010JD014423.

Keeble, J., P. Braesicke, N. L. Abraham, H. K. Roscoe, and J. A. Pyle, 2014: The impact of polar stratospheric ozone loss on Southern Hemisphere stratospheric circulation and climate. *Atmos. Chem. Phys.*, **14**, 13 705–13 717, doi:10.5194/acp-14-13705-2014.

Kinnison, D. E., and Coauthors, 2007: Sensitivity of chemical tracers to meteorological parameters in the MOZART-3 chemical transport model. *J. Geophys. Res.*, **112**, D20302, doi:10.1029/2006JD007879.

Kuroda, Y., and K. Kodera, 1998: Interannual variability in the troposphere and stratosphere of the southern hemisphere winter. *J. Geophys. Res.*, **103**, 13 787–13 799, doi:10.1029/98JD01042.

Lean, J., G. Rottman, J. Harder, and G. Kopp, 2005: SORCE contributions to new understanding of global change and solar variability. *The Solar Radiation and Climate Experiment (SORCE)*, G. Rottman, T. Woods, and V. George, Eds., Springer, 27–53, doi:10.1007/0-387-37625-9_3.

Lieberman, R. S., and Coauthors, 2003: The 6.5-day wave in the mesosphere and lower thermosphere: Evidence for baroclinic/barotropic instability. *J. Geophys. Res.*, **108**, 4640, doi:10.1029/2002JD003349.

Lossow, S., C. McLandress, A. I. Jonsson, and T. G. Shepherd, 2012: Influence of the Antarctic ozone hole on the polar mesopause region as simulated by the Canadian Middle Atmosphere Model. *J. Atmos. Sol.-Terr. Phys.*, **74**, 111–123, doi:10.1016/j.jastp.2011.10.010.

Manzini, E., B. Steil, C. Brhl, M. A. Giorgetta, and K. Krger, 2003: A new interactive chemistry-climate model: 2. Sensitivity of the middle atmosphere to ozone depletion and increase in greenhouse gases and implications for recent stratospheric cooling. *J. Geophys. Res.*, **108**, 4429, doi:10.1029/2002JD002977.

Marsh, D. R., M. J. Mills, D. E. Kinnison, J.-F. Lamarque, N. Calvo, and L. M. Polvani, 2013: Climate change from 1850 to 2005 simulated in CESM1 (WACCM). *J. Climate*, **26**, 7372–7391, doi:10.1175/JCLI-D-12-00558.1.

Matsuno, T., 1970: Vertical propagation of stationary planetary waves in the winter Northern Hemisphere. *J. Atmos. Sci.*, **27**, 871–883, doi:10.1175/1520-0469(1970)027<0871:VPOSPW>2.0.CO;2.

Matthes, K., D. R. Marsh, R. R. Garcia, D. E. Kinnison, F. Sassi, and S. Walters, 2010: Role of the QBO in modulating the influence of the 11 year solar cycle on the atmosphere using constant forcings. *J. Geophys. Res.*, **115**, D18110, doi:10.1029/2009JD013020.

McLandress, C., and J. F. Scinocca, 2005: The GCM response to current parameterizations of nonorographic gravity wave drag. *J. Atmos. Sci.*, **62**, 2394–2413, doi:10.1175/JAS3483.1.

Meinshausen, M., and Coauthors, 2011: The RCP greenhouse gas concentrations and their extensions from 1765 to 2300. *Climatic Change*, **109**, 213–241, doi:10.1007/s10584-011-0156-z.

Molina, L. T., and M. J. Molina, 1987: Production of chlorine oxide (Cl2O2) from the self-reaction of the chlorine oxide (ClO) radical. *J. Phys. Chem.*, **91**, 433–436, doi:10.1021/j100286a035.

Murgatroyd, R. J., and F. Singleton, 1961: Possible meridional circulations in the stratosphere and mesosphere. *Quart. J. Roy. Meteor. Soc.*, **87**, 125–135, doi:10.1002/qj.49708737202.

Norton, W. A., and J. Thuburn, 1999: Sensitivity of mesospheric mean flow, planetary waves, and tides to strength of gravity wave drag. *J. Geophys. Res.*, **104**, 30 897–30 911, doi:10.1029/1999JD900961.

Ogawa, F., N.-E. Omrani, K. Nishii, H. Nakamura, and N. Keenlyside, 2015: Ozone-induced climate change propped up by the Southern Hemisphere oceanic front. *Geophys. Res. Lett.*, **42**, 10 056–10 063, doi:10.1002/2015GL066538.

Orr, A., T. J. Bracegirdle, J. Hosking, T. Jung, J. D. Haigh, T. Phillips, and W. Feng, 2012: Possible dynamical mechanisms for Southern Hemisphere climate change due to the ozone hole. *J. Atmos. Sci.*, **69**, 2917–2932, doi:10.1175/JAS-D-11-0210.1.

——, ——, ——, W. Feng, H. K. Roscoe, and J. D. Haigh, 2013: Strong dynamical modulation of the cooling of the polar stratosphere associated with the Antarctic ozone hole. *J. Climate*, **26**, 662–668, doi:10.1175/JCLI-D-12-00480.1.

Pawson, S., R. S. Stolarski, A. R. Douglass, P. A. Newman, J. E. Nielsen, S. M. Frith, and M. L. Gupta, 2008: Goddard Earth Observing System chemistry-climate model simulations of stratospheric ozone-temperature coupling between 1950 and 2005. *J. Geophys. Res.*, **113**, D12103, doi:10.1029/2007JD009511.

Pedlosky, J., 1979: *Geophysical Fluid Dynamics.* Springer-Verlag, 626 pp., doi:10.1007/978-1-4684-0071-7.

Pfister, L., 1985: Baroclinic instability of easterly jets with applications to the summer mesosphere. *J. Atmos. Sci.*, **42**, 313–330, doi:10.1175/1520-0469(1985)042<0313:BIOEJW>2.0.CO;2.

Plumb, R. A., 1983: Baroclinic instability of the summer mesosphere: A mechanism for the quasi-two-day wave? *J. Atmos. Sci.*, **40**, 262–270, doi:10.1175/1520-0469(1983)040<0262:BIOTSM>2.0.CO;2.

——, 2002: Stratospheric transport. *J. Meteor. Soc. Japan.*, **80**, 793–809, doi:10.2151/jmsj.80.793.

Polvani, L. M., D. W. Waugh, G. J. Correa, and S. Son, 2011: Stratospheric ozone depletion: The main driver of twentieth-century atmospheric circulation changes in the Southern Hemisphere. *J. Climate*, **24**, 795–812, doi:10.1175/2010JCLI3772.1.

Randel, W. J., and Coauthors, 2009: An update of observed stratospheric temperature trends. *J. Geophys. Res.*, **114**, D02107, doi:10.1029/2008JD010421.

Richter, J. H., F. Sassi, and R. R. Garcia, 2010: Toward a physically based gravity wave source parameterization in a general circulation model. *J. Atmos. Sci.*, **67**, 136–156, doi:10.1175/2009JAS3112.1.

Riggin, D. M., and Coauthors, 2006: Observations of the 5-day wave in the mesosphere and lower thermosphere. *J. Atmos. Sol.-Terr. Phys.*, **68**, 323–339, doi:10.1016/j.jastp.2005.05.010.

Scinocca, J. F., 2003: An accurate spectral nonorographic gravity wave drag parameterization for general circulation models. *J. Atmos. Sci.*, **60**, 667–682, doi:10.1175/1520-0469(2003)060<0667:AASNGW>2.0.CO;2.

Simmonds, I., and K. Keay, 2000: Variability of Southern Hemisphere extratropical cyclone behavior, 1958–97. *J. Climate*, **13**, 550–561, doi:10.1175/1520-0442(2000)013<0550:VOSHEC>2.0.CO;2.

Smith, A. K., 2012: Interactions between the lower, middle and upper atmosphere. *Space Sci. Rev.*, **168**, 1–21, doi:10.1007/s11214-011-9791-y.

——, R. R. Garcia, D. R. Marsh, D. E. Kinnison, and J. H. Richter, 2010: Simulations of the response of mesospheric circulation and temperature to the Antarctic ozone hole. *Geophys. Res. Lett.*, **37**, L22803, doi:10.1029/2010GL045255.

Solomon, S., R. R. Garcia, F. Rowland, and D. J. Wuebbles, 1986: On the depletion of Antarctic ozone. *Nature*, **321**, 755–758, doi:10.1038/321755a0.

Son, S.-W., and Coauthors, 2010: Impact of stratospheric ozone on southern hemisphere circulation change: A multimodel assessment. *J. Geophys. Res.*, **115**, D00M07, doi:10.1029/2010JD014271.

Taylor, K. E., R. J. Stouffer, and G. A. Meehl, 2012: An overview of CMIP5 and the experiment design. *Bull. Amer. Meteor. Soc.*, **93**, 485–498, doi:10.1175/BAMS-D-11-00094.1.

Thompson, D. W. J., and S. Solomon, 2002: Interpretation of recent Southern Hemisphere climate change. *Science*, **296**, 895–899, doi:10.1126/science.1069270.

Ummenhofer, C. C., A. Sen Gupta, and M. H. England, 2009: Causes of late twentieth-century trends in New Zealand precipitation. *J. Climate*, **22**, 3–19, doi:10.1175/2008JCLI2323.1.

Venkateswara Rao, N., P. J. Espy, R. E. Hibbins, D. C. Fritts, and A. J. Kavanagh, 2015: Observational evidence of the influence of Antarctic stratospheric ozone variability on middle atmosphere dynamics. *Geophys. Res. Lett.*, **42**, 7853–7859, doi:10.1002/2015GL065432.

Wang, X. L., Y. Feng, G. P. Compo, V. R. Swail, F. W. Zwiers, R. J. Allan, and P. D. Sardeshmukh, 2013: Trends and low frequency variability of extra-tropical cyclone activity in the ensemble of twentieth century reanalysis. *Climate Dyn.*, **40**, 2775–2800, doi:10.1007/s00382-012-1450-9.

Waugh, D. W., W. J. Randel, S. Pawson, P. A. Newman, and E. R. Nash, 1999: Persistence of the lower stratospheric polar vortices. *J. Geophys. Res.*, **104**, 27 191–27 201, doi:10.1029/1999JD900795.

——, L. Oman, S. R. Kawa, R. S. Stolarski, S. Pawson, A. R. Douglass, P. A. Newman, and J. E. Nielsen, 2009: Impacts of climate change on stratospheric ozone recovery. *Geophys. Res. Lett.*, **36**, L03805, doi:10.1029/2008GL036223.

WMO, 2014: Scientific assessment of ozone depletion: 2014. World Meteorological Organization Global Ozone Research and Monitoring Project Rep. 55, 416 pp. [Available online at http://www.wmo.int/pages/prog/arep/gaw/ozone_2014/documents/Full_report_2014_Ozone_Assessment.pdf.]

Chapter 6

Conclusions and Outlook

In this thesis, processes controlling the variability of the stratospheric polar vortex and the effect of this variability on ozone and circulations in the troposphere and mesosphere were investigated. In the first part, new dynamical aspects of the stratosphere-troposphere coupling mechanism via DWC was examined in both observation and model simulations. This included investigation of the effects of different natural and anthropogenic factors on the variability of DWC, the impact of DWC on polar stratospheric ozone, and the underlying mechanism responsible for the tropospheric responses to DWC. In the last part, the mechanisms of vertical coupling between stratosphere and MLT during the Antarctic ozone hole period were studied.

Analyses were conducted on the basis of the model simulations with NCAR's CESM1(WACCM) model, a coupled model system which includes an interactive ocean, an interactive chemistry, and a well-resolved stratosphere and mesosphere. A set of sensitivity experiments was designed to investigate the contributions from both natural and anthropogenic factors (including the QBO, SSTs, GHGs and ODSs) by systematically switching the respective factor, on and off. Several time-slice experiments with perpetual GHG and ODS forcings were also performed to study the relative contribution of GHG versus ODS during ozone hole or ozone recovery period. In addition, different reanalysis datasets (ERA and MERRA), which are considered to provide a good approximation of the real world on the global scale for a large range of altitudes, were used to validate the results derived from the model simulations.

6.1 Conclusions

A detailed summary of the results and conclusions obtained from the different chapters of this thesis, is given in the following.

- *How do various natural forcing factors, like the QBO and SST variability, contribute to the variability of DWC between the stratosphere and troposphere? How these factors affect the downward influence of DWC in the troposphere? What is a dominant feedback responsible for the poleward shift of the tropospheric jet during DWC events in the NH?*

- Without the QBO, the occurrence of DWC is significantly suppressed. In contrast, stronger and more persistent DWC occurs when SST variability is excluded. Decreased DWC activity

in the absence of the QBO is consistent with a less persistent configuration of bounded wave geometries, which allows more wave dispersion in the meridional direction and stronger wave absorption on the equatorward flank of the polar vortex. While increased DWC activity in the absence of SST variability is associated with a more persistent configuration of bounded wave geometries, which focuses planetary wave reflection in the vertical direction toward the troposphere.

- Although DWC is suppressed in the absence of the QBO variability, the tropospheric signal to DWC is enhanced, and vice versa when the SST variability is excluded. This apparently counterintuitive result is explained by differences in the strength of the synoptic-scale eddy-mean flow feedbacks and the possible contribution of SST anomalies during DWC events. In particular, a weaker eddy-mean flow feedback in the absence of SST variability is consistent with modest Eady growth rate and synoptic wave source anomalies, which results in decreased synoptic-scale wave divergence. In addition, the sense of SST anomalies during DWC event is consistent with positive feedbacks onto the synoptic-scale eddy and large-scale flow anomalies. In particular, a weaker tropospheric response to DWC is observed when the positive NAO-related SST-tripole pattern during DWC event is absent. The results demonstrate the importance of changes in synoptic-scale eddy fluxes and SST anomalies in driving the tropospheric response to DWC.

- We suggest that a key mechanism for downward influence of DWC on the surface weather may be related to enhanced baroclinic instability in the troposphere. Following the wave reflection, a wave-1 anomaly-like pattern emerges in the high latitude troposphere. This anomaly gives rise to increased winds in the high-latitude North Atlantic sector, as indicated by a poleward shift of the tropospheric jet, and an anomalous positive North Atlantic Oscillation (NAO). The positive NAO is further strengthened by baroclinic eddy feedback, leading to further strengthening of the tropospheric jet and enhanced vertical wind shear in the upper troposphere in mid-winter.

- *What is the impact of DWC on the residual circulation and stratospheric temperatures in the Arctic? How is this related to ozone levels?*

- DWC is instantaneously linked to a deceleration of the residual circulation and a cooling of the Arctic lower stratosphere. This behavior is consistent with a wave-1 EP flux divergence in the stratosphere, which is attributed to transient downward wave propagation from the stratosphere to the troposphere.

- The direct effect of DWC events on ozone is to prevent the typical increase of ozone due to upward planetary wave events, which is consistent with the reversible impact of DWC on the residual circulation.

- The indirect effect of DWC leads to increased springtime ozone loss due to cold polar temperature. This effect is consistent with the irreversible cooling induced by DWC during the composite life cycles.

- Winter seasons dominated by DWC events are characterized by lower Arctic column ozone. This is attributed to accumulation of ODS on PSCs due to cold temperatures leading to increased springtime ozone loss (the indirect effect of DWC), and the reduction in poleward advection by the residual mean circulation leading to less ozone transport to the pole (the direct effect of DWC). In contrast, stratospheric winter dynamics dominated by increased wave absorption (with major SSWs), in contrast, are characterized by a warm polar vortex, and thereby less springtime ozone loss. The results establish a new perspective of dynamical processes controlling the Arctic ozone variability.

- *What is the effect of climate change on the variability of DWC in the future? Do future changes in DWC influence the troposphere-surface system?*

- Under extreme climate change conditions, a significant reduction in DWC events is detected in the future, with a shift of their timing toward midwinter. This variation is related to a change in the timing of the bounded wave geometry configuration and increased wave absorption.

- Future increase in GHG emissions is largely responsible for the decrease in the number of DWC events, dominating the opposing influence of future ozone recovery.

- The tropospheric response to DWC in the future is less reminiscent of the positive phase of the NAO. This is consistent with a weaker DWC event, which leads to weaker baroclinic eddy feedbacks onto the large-scale flow anomalies in the North Atlantic sector.

- *What are the responses of the polar mesosphere and lower thermosphere (MLT) coupled system to the Antarctic ozone hole? What are the roles of resolved and non-resolved wave drag, as well as radiative forcing on the MLT temperature responses? What are the dynamical mechanisms responsible for maintaining the downward propagation of zonal wind anomalies in the MLT?*

- The strengthened stratospheric westerlies arising from the Antarctic ozone hole-induced cooling cause a polar mesospheric warming, and a subsequent cooling in the lower thermosphere during late spring and early summer.

- The anomalous polar mesospheric warming is attributed to adiabatic heating induced by easterly non-resolved (gravity) wave drag. However, this effect is dampened by anomalous

adiabatic cooling induced by westerly resolved (planetary) waves, which are generated in-situ due to increased instability of the mesospheric easterly jet induced by the ozone hole. On the other hand, the anomalous cooling in the polar lower thermosphere induced by westerly gravity wave drag is enhanced by dynamical cooling induced by westerly planetary wave drag.

- Radiative cooling induced by increased GHGs dampens (enhances) the polar mesospheric warming (lower thermospheric cooling) induced by the ozone hole.

- Through thermal wind balance, the polar MLT temperature changes induced by the ozone hole are accompanied by a downward migration of anomalous zonal-mean wind from the lower thermosphere to the stratopause. This vertical coupling is maintained by the combined forcings of both planetary and gravity waves.

6.2 Outlook

This thesis provides an advanced understanding of the mechanisms responsible for the coupling between the troposphere, stratosphere, and higher layers in both the upward and downward directions. In particular, the importance of natural and anthropogenic forcing factors for the stratosphere-troposphere coupling mechanism via DWC, the underlying mechanisms for tropospheric impact of DWC, and the implication for ozone levels have been investigated in this study for the first time. Nevertheless, there are still several questions and new ideas that are worth exploring and investigating in future research.

In terms of the behavior of stratosphere-troposphere dynamical coupling via DWC, the results of this thesis suggest that a weaker tropospheric response to DWC occurs when the SST variability is excluded from the simulation (as shown in Chapter 2). However, the underlying mechanisms by which the SST forcing affects the tropospheric response to DWC are not fully understood. One possible strategy is to analyze the links between surface ocean heat flux and the baroclinic eddy feedbacks during composite life cycles. In addition, we also note that the differences between the CTL and FSST experiments in Chapter 2 are rather an expression of the lack of SST variability than an expression of the coupling between atmosphere and ocean. Therefore, the role of atmosphere-ocean coupling on the variability of DWC still remains unclear. In order to address whether atmosphere-ocean coupling plays a role, it is needed to carry out the atmospheric model experiments with the same SST/sea ice evolution. In our case the simulated SST/sea ice evolutions from the CTL experiment should be prescribed in the FSST experiment. This experiment would therefore isolate the effects of atmosphere-ocean coupling on the interactions between the stratosphere and troposphere via DWC.

The results of this study also highlight the importance of DWC events on the residual circulation, Arctic stratospheric temperatures, and ozone (as shown in Chapter 3), but do not

address the conditions that lead to such events. Harnik (2009) suggested that short-time-scale positive heat flux pulses from the troposphere are more likely to lead to wave reflection. A better understanding of the tropospheric conditions that produce heat flux pulses is needed to improve the understanding of the link between stratospheric dynamics and ozone variability. This can be a subject for future research, e.g., using an idealized GCM dynamical core with explicit topographic forcing or zonally asymmetric/symmetric diabatic heating, in order to understand which tropospheric conditions affecting the ability of upward heat flux pulses to be reflected downward.

Future changes in stratospheric dynamics, as simulated in CESM1 (WACCM) model under the RCP8.5 scenario, cause a reduction in DWC activity in the NH winter, and may eventually lead to changes in tropospheric circulation in a future climate (as shown in Chapter 4). However, resolving the entire cause-and-effect relationship involved in the transmission of dynamical disturbances induced by DWC between the stratosphere and the troposphere, would require additional sensitivity simulations in CESM1(WACCM). For example, by performing a set of experiments with a combination of anthropogenic and natural forcings (e.g., GHG+tropical SST forcing, GHG+extra tropical SST forcing, future tropical SST forcing only, etc), the origin of the future changes in the timing of DWC and the associated surface impact can be understood better. In addition, since the current results are only based on simulations with one model, further model studies are required in order to determine which aspects of the modeled tropospheric responses to the DWC in the future are robust between models.

CESM1(WACCM) simulations suggest that the Antarctic ozone hole leads to cooling in the polar lower thermosphere. Moreover, it has also been shown that increased instability of the mesospheric easterly jet increases in-situ wave generation of traveling planetary wave activity (Rossby 5-day wave and QTDW) in the mesosphere (Chapter 5). These particular results are interesting and have never been verified in observations, possibly due to limited observational datasets (e.g., Smith et al. 2010) or few observational studies on the vertical coupling of MLT during the Antarctic ozone hole period (e.g., Venkateswara Rao et al. 2015), and therefore warrant further investigation. In addition, since the detailed mechanisms of vertical coupling between the stratosphere and MLT during the Antarctic ozone hole revealed in this work are only based on one model, further model studies are indeed required to determine which aspects of the modeled MLT responses to the ozone hole are robust.

Acknowledgements

The completion of this degree would not have occurred without the support of many people, whom I acknowledge below.

First and foremost, I'd like to thank my advisor, Katja Matthes, for taking me on as a graduate student and providing invaluable guidance and support over the years. I remember the first time I met Katja; she was an invited speaker for training school on Solar Variability and Climate Response in Thessaloniki, Greece, 2013. After awkwardly hovering around, I worked up the courage to introduce myself to her. I told her I was looking for a doctoral position and was very interested in working with her. Katja, of course, was as gracious as ever, and a few weeks later I received my acceptance letter. Katja is a wonderful research advisor, very calm, kind, and perceptive. I'm very grateful for the many times that she's suggested a way forward conceptually, and for reading and helping me improve manuscript drafts multiple times. It has been a pleasure working with Katja.

I'd especially like to thank Nour-Eddine Omrani, for all his support, for many useful discussions, and for trying to teach me some numerical techniques. I'd also like to thank Nili Harnik for her time and assistance, and for sharing many useful thoughts and suggestions regarding my research. Her enthusiasm for research is infectious. I'd also like to thank my thesis committee, Richard Greatbatch, Daniela Domeisen, and Wolf-Christian Dullo, for their time and assistance, and for sharing many useful thoughts and suggestions regarding my research. Sincere thanks to the current and former members of the physics of the atmosphere working group, in particular Sabine, Sebastian, Felicitas, Wuke, Robin, Tim, Remi, Lisa and Ming for enlightening discussions and advices. I do appreciate the great support from all colleagues at GEOMAR - Helmholtz Centre for Ocean Research Kiel.

On a last personal note, I am deeply grateful to my family (particularly my sisters and uncles) and my loving girl friend (Rani Marselia), for their tremendous and constant support for everything I ever wanted to accomplish. They have been there for me through thick and thin and I truly would not be where I am today without their love and support. They have shared in my successes and believed in me even when I didn't believe in myself. I dedicate this thesis to them and to my parents in heaven (mom, dad, I did this!).

This work was supported by the German-Israeli Foundation for Scientific Research and Development under Grant GIF1151-83.8/2011. This work has also been partially funded by the Helmholtz University Young Investigators Group NATHAN and the GEOMAR Helmholtz Centre for Ocean Research Kiel. I'd also like to acknowledge high-performance computing support from German Climate Computing Centre [Deutsches Klimarechenzentrum (DKRZ)], Hamburg, and the NEC-HPC Linux Cluster at Kiel University, Kiel.

Bibliography

Ambaum, M. H. P. and B. J. Hoskins (2002). "The NAO Troposphere–Stratosphere Connection". In: *Journal of Climate* 15.14, pp. 1969–1978. DOI: 10.1175/1520-0442(2002)015<1969:TNTSC>2.0.CO;2.

Andrews, D. G., J. R. Holton, and C. B. Leovoy (1987). *Middle Atmosphere Dynamics*. Vol. 40. International Geophysics Series. Academic Press, p. 128.

Arblaster, J. M. and G. A. Meehl (2006). "Contributions of External Forcings to Southern Annular Mode Trends". In: *Journal of Climate* 19.12, pp. 2896–2905. DOI: 10.1175/JCLI3774.1.

Austin, J. and N. Butchart (2003). "Coupled chemistry–climate model simulations for the period 1980 to 2020: Ozone depletion and the start of ozone recovery". In: *Quarterly Journal of the Royal Meteorological Society* 129.595, pp. 3225–3249. ISSN: 1477-870X. DOI: 10.1256/qj.02.203.

Ayarzaguena, B. et al. (2013). "The role of climate change and ozone recovery for the future timing of major stratospheric warmings". In: *Geophysical Research Letters* 40.10, pp. 2460–2465. ISSN: 1944-8007. DOI: 10.1002/grl.50477.

Baldwin, M. P. et al. (2001). "The quasi-biennial oscillation". In: *Reviews of Geophysics* 39.2, pp. 179–229. ISSN: 1944-9208. DOI: 10.1029/1999RG000073.

Baldwin, M. P. and T. J. Dunkerton (1999). "Propagation of the Arctic Oscillation from the stratosphere to the troposphere". In: *Journal of Geophysical Research: Atmospheres* 104.D24, pp. 30937–30946. ISSN: 2156-2202. DOI: 10.1029/1999JD900445.

— (2001). "Stratospheric Harbingers of Anomalous Weather Regimes". In: *Science* 294.5542, pp. 581–584. DOI: 10.1126/science.1063315.

Baldwin, M. P. et al. (2003). "Stratospheric Memory and Skill of Extended-Range Weather Forecasts". In: *Science* 301.5633, pp. 636–640. ISSN: 0036-8075. DOI: 10.1126/science.1087143.

Bates, J. R. (1981). "A dynamical mechanism through which variations in solar ultraviolet radiation can influence tropospheric climate". In: *Solar Physics* 74.2, pp. 399–415. ISSN: 1573-093X. DOI: 10.1007/BF00154526.

Becker, E. (2012). "Dynamical Control of the Middle Atmosphere". English. In: *Space Science Reviews* 168.1-4, pp. 283–314. ISSN: 0038-6308. DOI: 10.1007/s11214-011-9841-5.

Bell, C. J., L. J. Gray, and J. Kettleborough (2010a). "Changes in Northern Hemisphere stratospheric variability under increased CO2 concentrations". In: *Quarterly Journal of the Royal Meteorological Society* 136.650, pp. 1181–1190. ISSN: 1477-870X. DOI: 10.1002/qj.633.

— (2010b). "Changes in Northern Hemisphere stratospheric variability under increased CO2 concentrations". In: *Quarterly Journal of the Royal Meteorological Society* 136.650, pp. 1181–1190. ISSN: 1477-870X. DOI: 10.1002/qj.633.

Black, R. X. (2002). "Stratospheric Forcing of Surface Climate in the Arctic Oscillation". In: *Journal of Climate* 15.3, pp. 268–277. DOI: 10.1175/1520-0442(2002)015<0268:SFOSCI>2.0.CO;2.

Boville, B. A. (1984). "The Influence of the Polar Night Jet on the Tropospheric Circulation in a GCM". In: *Journal of the Atmospheric Sciences* 41.

Butchart, N. and A. A. Scaife (2001). "Removal of chlorofluorocarbons by increased mass exchange between the stratosphere and troposphere in a changing climate". In: *Nature* 410.6830, pp. 799–802. ISSN: 0028-0836. DOI: 10.1038/35071047.

Butchart, N. et al. (2000). "The Response of the Stratospheric Climate to Projected Changes in the Concentrations of Well-Mixed Greenhouse Gases from 1992 to 2051". In: *Journal of Climate* 13.13, pp. 2142–2159. DOI: 10.1175/1520-0442(2000)013<2142:TROTSC>2.0.CO;2.

Butler, A. H., D. W. J. Thompson, and R. Heikes (2010). "The Steady-State Atmospheric Circulation Response to Climate Change–like Thermal Forcings in a Simple General Circulation Model". In: *Journal of Climate* 23.13, pp. 3474–3496. DOI: 10.1175/2010JCLI3228.1.

Calvo, N. et al. (2009). "Nonlinearity of the combined warm ENSO and QBO effects on the Northern Hemisphere polar vortex in MAECHAM5 simulations". In: *Journal of Geophysical Research: Atmospheres* 114.D13, n/a–n/a. ISSN: 2156-2202. DOI: 10.1029/2008JD011445.

Charlton-Perez, A. J. et al. (2008). "The frequency and dynamics of stratospheric sudden warmings in the 21st century". In: *Journal of Geophysical Research: Atmospheres* 113.D16. D16116, n/a–n/a. ISSN: 2156-2202. DOI: 10.1029/2007JD009571.

Charlton-Perez, A. J. et al. (2013). "On the lack of stratospheric dynamical variability in low-top versions of the CMIP5 models". In: *Journal of Geophysical Research: Atmospheres* 118.6, pp. 2494–2505. ISSN: 2169-8996. DOI: 10.1002/jgrd.50125.

Charney, J. G. and P. G. Drazin (1961). "Propagation of planetary-scale disturbances from the lower into the upper atmosphere". In: *Journal of Geophysical Research* 66.1, pp. 83–109. ISSN: 2156-2202. DOI: 10.1029/JZ066i001p00083.

Chen, G. and I. M. Held (2007). "Phase speed spectra and the recent poleward shift of Southern Hemisphere surface westerlies". In: *Geophysical Research Letters* 34.21. L21805, n/a–n/a. ISSN: 1944-8007. DOI: 10.1029/2007GL031200.

Cho, Y.-M. et al. (2004). "MLT cooling during stratospheric warming events". In: *Geophysical Research Letters* 31.10. L10104, n/a–n/a. ISSN: 1944-8007. DOI: 10.1029/2004GL019552.

Christiansen, B. (2001). "Downward propagation of zonal mean zonal wind anomalies from the stratosphere to the troposphere: Model and reanalysis". In: *Journal of Geophysical Research: Atmospheres* 106.D21, pp. 27307–27322. ISSN: 2156-2202. DOI: 10.1029/2000JD000214. URL: http://dx.doi.org/10.1029/2000JD000214.

Coughlin, K. and K. K. Tung (2005). "Tropospheric wave response to decelerated stratosphere seen as downward propagation in northern annular mode". In: *Journal of Geophysical Research: Atmospheres* 110.D1, n/a–n/a. DOI: 10.1029/2004JD004661.

Coughlin, K. and K.-K. Tung (2001). "QBO signal found at the extratropical surface through northern annular modes". In: *Geophysical Research Letters* 28.24, pp. 4563–4566. DOI: 10.1029/2001GL013565.

Domeisen, D. I. V., L. Sun, and G. Chen (2013). "The role of synoptic eddies in the tropospheric response to stratospheric variability". In: *Geophysical Research Letters* 40.18, pp. 4933–4937. ISSN: 1944-8007. DOI: 10.1002/grl.50943.

Domeisen, D. I. V. et al. (2015). "Seasonal Predictability over Europe Arising from El Niño and Stratospheric Variability in the MPI-ESM Seasonal Prediction System". In: *Journal of Climate* 28.1, pp. 256–271. DOI: 10.1175/JCLI-D-14-00207.1.

Dowdy, A. J. et al. (2004). "The large-scale dynamics of the mesosphere–lower thermosphere during the Southern Hemisphere stratospheric warming of 2002". In: *Geophysical Research Letters* 31.14. L14102, n/a–n/a. ISSN: 1944-8007. DOI: 10.1029/2004GL020282.

Dunn-Sigouin, E. and T. A. Shaw (2015). "Comparing and contrasting extreme stratospheric events, including their coupling to the tropospheric circulation". In: *Journal of Geophysical Research: Atmospheres* 120.4. 2014JD022116, pp. 1374–1390. ISSN: 2169-8996. DOI: 10.1002/2014JD022116.

Eichelberger, S. J. and D. L. Hartmann (2005). "Changes in the strength of the Brewer-Dobson circulation in a simple AGCM". In: *Geophysical Research Letters* 32.15. L15807, n/a–n/a. ISSN: 1944-8007. DOI: 10.1029/2005GL022924.

Esler, J. G. and R. K. Scott (2005). "Excitation of Transient Rossby Waves on the Stratospheric Polar Vortex and the Barotropic Sudden Warming". In: *Journal of the Atmospheric Sciences* 62.10, pp. 3661–3682. DOI: 10.1175/JAS3557.1.

Eyring, V. et al. (2006). "Assessment of temperature, trace species, and ozone in chemistry-climate model simulations of the recent past". In: *Journal of Geophysical Research: Atmospheres* 111.D22, n/a–n/a. ISSN: 2156-2202. DOI: 10.1029/2006JD007327.

Eyring, V. et al. (2007). "Multimodel projections of stratospheric ozone in the 21st century". In: *Journal of Geophysical Research: Atmospheres* 112.D16, n/a–n/a. ISSN: 2156-2202. DOI: 10.1029/2006JD008332.

Fischer, E. M. et al. (2007). "European climate response to tropical volcanic eruptions over the last half millennium". In: *Geophysical Research Letters* 34.5. L05707, n/a–n/a. ISSN: 1944-8007. DOI: 10.1029/2006GL027992.

Fritts, D. C. and S. L. Vadas (2008). "Gravity wave penetration into the thermosphere: sensitivity to solar cycle variations and mean winds". In: *Annales Geophysicae* 26.12, pp. 3841–3861. DOI: 10.5194/angeo-26-3841-2008.

Fusco, A. C. and M. L. Salby (1999). "Interannual Variations of Total Ozone and Their Relationship to Variations of Planetary Wave Activity". In: *J. Climate* 12.6, pp. 1619–1629. DOI: 10.1175/1520. URL: http://dx.doi.org/10.1175/1520.

Garcia, R. R. and W. J. Randel (2008). "Acceleration of the Brewer–Dobson Circulation due to Increases in Greenhouse Gases". In: *Journal of the Atmospheric Sciences* 65.8, pp. 2731–2739. DOI: 10.1175/2008JAS2712.1.

Garfinkel, C. I. et al. (2012). "Does the Holton–Tan Mechanism Explain How the Quasi-Biennial Oscillation Modulates the Arctic Polar Vortex?" In: *Journal of the Atmospheric Sciences* 69.5, pp. 1713–1733. ISSN: 0022-4928. DOI: 10.1175/JAS-D-11-0209.1.

Geller, M. A. and J. C. Alpert (1980). "Planetary Wave Coupling between the Troposphere and the Middle Atmosphere as a Possible Sun-Weather Mechanism". In: *Journal of the Atmospheric Sciences* 37.6, pp. 1197–1215. DOI: 10.1175/1520-0469(1980)037<1197:PWCBTT>2.0.CO;2.

Gillett, N. P. and D. W. J. Thompson (2003). "Simulation of Recent Southern Hemisphere Climate Change". In: *Science* 302.5643, pp. 273–275. ISSN: 0036-8075. DOI: 10.1126/science.1087440.

Gray, W. M., J. D. Sheaffer, and J. A. Knaff (1992). "Hypothesized mechanism for stratospheric QBO influence on ENSO variability". In: *Geophysical Research Letters* 19.2, pp. 107–110. ISSN: 1944-8007. DOI: 10.1029/91GL02950.

Hamilton, K. (1993). "An Examination of Observed Southern Oscillation Effects in the Northern Hemisphere Stratosphere". In: *Journal of the Atmospheric Sciences* 50.20, pp. 3468–3474. ISSN: 0022-4928. DOI: 10.1175/1520-0469(1993)050<3468:AEOOSO>2.0.CO;2.

Hansen, F. et al. (2014). "The influence of natural and anthropogenic factors on Major Stratospheric Sudden Warmings". In: *Journal of Geophysical Research: Atmospheres*, 2013JD021397. ISSN: 2169-8996. DOI: 10.1002/2013JD021397.

Harnik, N. (2009). "Observed stratospheric downward reflection and its relation to upward pulses of wave activity". In: *Journal of Geophysical Research: Atmospheres* 114.D8, p. D08120. ISSN: 2156-2202. DOI: 10.1029/2008JD010493.

Harnik, N. and E. Heifetz (2007). "Relating Overreflection and Wave Geometry to the Counter-propagating Rossby Wave Perspective: Toward a Deeper Mechanistic Understanding of Shear Instability". In: *Journal of the Atmospheric Sciences* 64.7, pp. 2238–2261. ISSN: 0022-4928. DOI: 10.1175/JAS3944.1.

Harnik, N. and R. S. Lindzen (2001). "The Effect of Reflecting Surfaces on the Vertical Structure and Variability of Stratospheric Planetary Waves". In: *Journal of the Atmospheric Sciences* 58.19, pp. 2872–2894. ISSN: 0022-4928. DOI: 10.1175/1520-0469(2001)058<2872:TEORSO>2.0.CO;2.

Hartley, D. E. et al. (1998). "A new perspective on the dynamical link between the stratosphere and troposphere". In: *Nature* 391.6666, pp. 471–474. ISSN: 0028-0836. DOI: 10.1038/35112. URL: http://dx.doi.org/10.1038/35112.

Hartmann, D. L. et al. (2000). "Can ozone depletion and global warming interact to produce rapid climate change?" In: *Proceedings of the National Academy of Sciences* 97.4, pp. 1412–1417. DOI: 10.1073/pnas.97.4.1412.

Haynes, P. H. et al. (1991). "On the "Downward Control" of Extratropical Diabatic Circulations by Eddy-Induced Mean Zonal Forces". In: *Journal of the Atmospheric Sciences* 48.4, pp. 651–678. ISSN: 0022-4928. DOI: 10.1175/1520-0469(1991)048<0651:OTCOED>2.0.CO;2.

Hernandez, G. (2003). "Climatology of the upper mesosphere temperature above South Pole (90S): Mesospheric cooling during 2002". In: *Geophysical Research Letters* 30.10. 1535, n/a–n/a. ISSN: 1944-8007. DOI: 10.1029/2003GL016887. URL: http://dx.doi.org/10.1029/2003GL016887.

Hines, C. O. (1974). "A Possible Mechanism for the Production of Sun-Weather Correlations". In: *Journal of the Atmospheric Sciences* 31.2, pp. 589–591. DOI: 10.1175/1520-0469(1974)031<0589:APMFTP>2.0.CO;2.

Ho, C.-H. et al. (2009). "Influence of stratospheric quasi-biennial oscillation on tropical cyclone tracks in the western North Pacific". In: *Geophysical Research Letters* 36.6. L06702, n/a–n/a. ISSN: 1944-8007. DOI: 10.1029/2009GL037163.

Hocke, K., M. Lainer, and A. Schanz (2015). "Composite analysis of a major sudden stratospheric warming". In: *Annales Geophysicae* 33.6, pp. 783–788. DOI: 10.5194/angeo-33-783-2015. URL: http://www.ann-geophys.net/33/783/2015/.

Holton, J. R. (1983). "The Influence of Gravity Wave Breaking on the General Circulation of the Middle Atmosphere". In: *J. Atmos. Sci.* 40.10, pp. 2497–2507. DOI: 10.1175/1520.

Holton, J. R. and H.-C. Tan (1980). "The Influence of the Equatorial Quasi-Biennial Oscillation on the Global Circulation at 50 mb". In: *Journal of the Atmospheric Sciences* 37.10, pp. 2200–2208. ISSN: 0022-4928. DOI: 10.1175/1520-0469(1980)037<2200:TIOTEQ>2.0.CO;2.

— (1982). "The Quasi-Biennial Oscillation in the Northern Hemisphere Lower Stratosphere". In: *Journal of the Meteorological Society of Japan. Ser. II* 60.1, pp. 140–148.

Holton, J. R. et al. (1995). "Stratosphere-troposphere exchange". In: *Reviews of Geophysics* 33.4, pp. 403–439. ISSN: 1944-9208. DOI: 10.1029/95RG02097. URL: http://dx.doi.org/10.1029/95RG02097.

Hommel, R. et al. (2014). "Chemical ozone loss and ozone mini-hole event during the Arctic winter 2010/2011 as observed by SCIAMACHY and GOME-2". In: *Atmospheric Chemistry and Physics* 14.7, pp. 3247–3276. DOI: 10.5194/acp-14-3247-2014. URL: http://www.atmos-chem-phys.net/14/3247/2014/.

Horel, J. D. and J. M. Wallace (1981). "Planetary-Scale Atmospheric Phenomena Associated with the Southern Oscillation". In: *Monthly Weather Review* 109.4, pp. 813–829. DOI: 10.1175/1520-0493(1981)109<0813:PSAPAW>2.0.CO;2.

Hu, Y. and Q. Fu (2009). "Stratospheric warming in Southern Hemisphere high latitudes since 1979". In: *Atmospheric Chemistry and Physics* 9.13, pp. 4329–4340. DOI: 10.5194/acp-9-4329-2009. URL: http://www.atmos-chem-phys.net/9/4329/2009/.

Hurwitz, M. M., P. A. Newman, and C. I. Garfinkel (2011). "The Arctic vortex in March 2011: a dynamical perspective". In: *Atmospheric Chemistry and Physics* 11.22, pp. 11447–11453. DOI: 10.5194/acp-11-11447-2011. URL: http://www.atmos-chem-phys.net/11/11447/2011/.

Hurwitz, M. M., P. A. Newman, and C. I. Garfinkel (2012). "On the influence of North Pacific sea surface temperature on the Arctic winter climate". In: *Journal of Geophysical Research: Atmospheres* 117.D19, n/a–n/a. ISSN: 2156-2202. DOI: 10.1029/2012JD017819.

Ialongo, I. et al. (2012). "Ozone zonal asymmetry and planetary wave characterization during Antarctic spring". In: *Atmospheric Chemistry and Physics* 12.5, pp. 2603–2614. DOI: 10.5194/acp-12-2603-2012.

IPCC (2013). *Climate Change 2013: The Physical Science Basis, Contribution of Working Group I to the Fifth Assessment Report of the Intergovernmental Panel on Climate Change*. Tech. rep. 1535 pp.

Isaksen, I. S. A. et al. (2012). "Attribution of the Arctic ozone column deficit in March 2011". In: *Geophysical Research Letters* 39.24. L24810, n/a–n/a. ISSN: 1944-8007. DOI: 10.1029/2012GL053876. URL: http://dx.doi.org/10.1029/2012GL053876.

Jaiser, R., K. Dethloff, and D. Handorf (2013). "Stratospheric response to Arctic sea ice retreat and associated planetary wave propagation changes". In: *Tellus A* 65.0. ISSN: 1600-0870.

Karpechko, A. Y. et al. (2008). "Stratospheric influence on circulation changes in the Southern Hemisphere troposphere in coupled climate models". In: *Geophysical Research Letters* 35.20. L20806, n/a–n/a. ISSN: 1944-8007. DOI: 10.1029/2008GL035354.

Keenlyside, N. and N.-E. Omrani (2014). "Has a warm North Atlantic contributed to recent European cold winters?" In: *Environmental Research Letters* 9.6, p. 061001.

Kidston, J. et al. (2010). "A robust increase in the eddy length scale in the simulation of future climates". In: *Geophysical Research Letters* 37.3, n/a–n/a. ISSN: 1944-8007. DOI: 10.1029/2009GL041615.

Kidston, J. et al. (2015). "Stratospheric influence on tropospheric jet streams, storm tracks and surface weather". In: *Nature Geosci* 8.6. Review, pp. 433–440. ISSN: 1752-0894.

Kodera, K. and Y. Kuroda (2000). "A mechanistic model study of slowly propagating coupled stratosphere-troposphere variability". In: *Journal of Geophysical Research: Atmospheres* 105.D10, pp. 12361–12370. ISSN: 2156-2202. DOI: 10.1029/2000JD900094. URL: http://dx.doi.org/10.1029/2000JD900094.

— (2002). "Dynamical response to the solar cycle". In: *Journal of Geophysical Research: Atmospheres* 107.D24. 4749, ACL 5–1–ACL 5–12. ISSN: 2156-2202. DOI: 10.1029/2002JD002224.

Kodera, K. et al. (1990). "Downward propagation of upper stratospheric mean zonal wind perturbation to the troposphere". In: *Geophysical Research Letters* 17.9, pp. 1263–1266. ISSN: 1944-8007. DOI: 10.1029/GL017i009p01263.

Kodera, K. et al. (1991). "A Possible Influence of the Polar Night Stratospheric Jet on the Subtropical Tropospheric Jet". In: *Journal of the Meteorological Society of Japan. Ser. II* 69.6, pp. 715–721.

Kunz, T. and R. J. Greatbatch (2013). "On the Northern Annular Mode Surface Signal Associated with Stratospheric Variability". In: *J. Atmos. Sci.* 70.7, pp. 2103–2118. DOI: 10.1175/JAS.

Kuroda, Y. (2008). "Role of the stratosphere on the predictability of medium-range weather forecast: A case study of winter 2003–2004". In: *Geophysical Research Letters* 35.19. L19701, n/a–n/a. ISSN: 1944-8007. DOI: 10.1029/2008GL034902.

Kuroda, Y. and K. Kodera (1999). "Role of planetary waves in the stratosphere-troposphere coupled variability in the northern hemisphere winter". In: *Geophysical Research Letters* 26.15, pp. 2375–2378. ISSN: 1944-8007. DOI: 10.1029/1999GL900507. URL: http://dx.doi.org/10.1029/1999GL900507.

Labitzke, K. and H. van Loon (1996). In: vol. 42. NATO ASI Series. Springer Berlin Heidelberg. Chap. The Effect on the Stratosphere of Three Tropical Volcanic Eruptions, pp. 113–125. ISBN: 978-3-642-64731-4. DOI: 10.1007/978-3-642-61173-5_11.

Labitzke, K. (1982). "On the Interannual Variability of the Middle Stratosphere during the Northern Winters". In: *Journal of the Meteorological Society of Japan. Ser. II* 60.1, pp. 124–139.

Lean, J. et al. (2005). In: Springer New York. Chap. SORCE Contributions to New Understanding of Global Change and Solar Variability, pp. 27–53. ISBN: 978-0-387-30242-3. DOI: 10.1007/0-387-37625-9_3.

Li, Y. and N.-C. Lau (2013). "Influences of ENSO on Stratospheric Variability, and the Descent of Stratospheric Perturbations into the Lower Troposphere". In: *Journal of Climate* 26.13, pp. 4725–4748. ISSN: 0894-8755. DOI: 10.1175/JCLI-D-12-00581.1.

Limpasuvan, V. and D. L. Hartmann (2000). "Wave-Maintained Annular Modes of Climate Variability*". In: *Journal of Climate* 13.24, pp. 4414–4429. ISSN: 0894-8755. DOI: 10.1175/1520-0442(2000)013<4414:WMAMOC>2.0.CO;2.

Limpasuvan, V., D. W. Thompson, and D. L. Hartmann (2004). "The Life Cycle of the Northern Hemisphere Sudden Stratospheric Warmings". In: *J. Climate* 17.13, pp. 2584–2596. DOI: 10.1175/1520.

Limpasuvan, V. et al. (2012). "The roles of planetary and gravity waves during a major stratospheric sudden warming as characterized in {WACCM}". In: *Journal of Atmospheric and Solar-Terrestrial Physics* 78–79. Structure and Dynamics of Mesosphere and Lower Thermosphere, pp. 84 –98. ISSN: 1364-6826. DOI: http://dx.doi.org/10.1016/j.jastp.2011.03.004.

Lindzen, R. S. and J. R. Holton (1968). "A Theory of the Quasi-Biennial Oscillation". In: *Journal of the Atmospheric Sciences* 25.6, pp. 1095–1107. DOI: 10.1175/1520-0469(1968)025<1095:ATOTQB>2.0.CO;2.

Liu, H.-L. and R. G. Roble (2002). "A study of a self-generated stratospheric sudden warming and its mesospheric–lower thermospheric impacts using the coupled TIME-GCM/CCM3". In: *Journal of Geophysical Research: Atmospheres* 107.D23. 4695, ACL 15–1–ACL 15–18. ISSN: 2156-2202. DOI: 10.1029/2001JD001533.

Liu, Y. et al. (2011). "Middle stratospheric polar vortex ozone budget during the warming Arctic winter, 2002–2003". In: *Advances in Atmospheric Sciences* 28.5, pp. 985–996. ISSN: 1861-9533. DOI: 10.1007/s00376-010-0045-9.

Loon, H. van and K. Labitzke (1987). "The Southern Oscillation. Part V: The Anomalies in the Lower Stratosphere of the Northern Hemisphere in Winter and a Comparison with the Quasi-Biennial Oscillation". In: *Monthly Weather Review* 115.2, pp. 357–369. ISSN: 0027-0644. DOI: 10.1175/1520-0493(1987)115<0357:TSOPVT>2.0.CO;2.

Lossow, S. et al. (2012). "Influence of the Antarctic ozone hole on the polar mesopause region as simulated by the Canadian Middle Atmosphere Model". In: *Journal of Atmospheric and Solar-Terrestrial Physics* 74.0, pp. 111 –123. ISSN: 1364-6826. DOI: http://dx.doi.org/10.1016/j.jastp.2011.10.010.

Lu, H. et al. (2014). "Mechanisms for the Holton-Tan relationship and its decadal variation". In: *Journal of Geophysical Research: Atmospheres* 119.6, pp. 2811–2830. ISSN: 2169-8996. DOI: 10.1002/2013JD021352.

Lubis, S. W. et al. (2016a). "Impact of the Antarctic Ozone Hole on the Vertical Coupling of the Stratosphere-Mesosphere-Lower Thermosphere System". In: *Journal of the Atmospheric Sciences*. DOI: 10.1175/JAS-D-15-0189.1.

Lubis, S. W. et al. (2016b). "Influence of the Quasi-Biennial Oscillation and Sea Surface Temperature Variability on Downward Wave Coupling in the Northern Hemisphere". In: *Journal of the Atmospheric Sciences* 73.5, pp. 1943–1965. DOI: 10.1175/JAS-D-15-0072.1.

Lucchesi, R. (2012). "File Specification for MERRA Products". In: *GMAO Office Note No. 1(Version 2.3)*, p. 82. DOI: 10.5067/8D4LU4390C4S.

Manney, G. L. et al. (2011). "Unprecedented Arctic ozone loss in 2011". In: *Nature* 478.7370, pp. 469–475. DOI: 10.1038/nature10556.

Manzini, E. et al. (2003). "A new interactive chemistry-climate model: 2. Sensitivity of the middle atmosphere to ozone depletion and increase in greenhouse gases and implications for recent stratospheric cooling". In: *Journal of Geophysical Research: Atmospheres* 108.D14, n/a–n/a. ISSN: 2156-2202. DOI: 10.1029/2002JD002977.

Manzini, E. et al. (2006). "The Influence of Sea Surface Temperatures on the Northern Winter Stratosphere: Ensemble Simulations with the MAECHAM5 Model". In: *Journal of Climate* 19.16, pp. 3863–3881. ISSN: 0894-8755. DOI: 10.1175/JCLI3826.1.

Manzini, E. et al. (2014). "Northern winter climate change: Assessment of uncertainty in CMIP5 projections related to stratosphere-troposphere coupling". In: *Journal of Geophysical Research: Atmospheres* 119.13, pp. 7979–7998. ISSN: 2169-8996. DOI: 10.1002/2013JD021403.

Marsh, D. R. et al. (2013). "Climate Change from 1850 to 2005 Simulated in CESM1 (WACCM)". In: *Journal of Climate* 26.19, pp. 7372–7391. ISSN: 0894-8755. DOI: 10.1175/JCLI-D-12-00558.1.

Marshall, A. G. and A. A. Scaife (2009). "Impact of the QBO on surface winter climate". In: *Journal of Geophysical Research: Atmospheres* 114.D18. D18110, n/a–n/a. ISSN: 2156-2202. DOI: 10.1029/2009JD011737.

Matsuno, T. (1970). "Vertical Propagation of Stationary Planetary Waves in the Winter Northern Hemisphere". In: *Journal of the Atmospheric Sciences* 27.6, pp. 871–883. ISSN: 0022-4928. DOI: 10.1175/1520-0469(1970)027<0871:VPOSPW>2.0.CO;2.

Matthes, K. et al. (2006). "Transfer of the solar signal from the stratosphere to the troposphere: Northern winter". In: *Journal of Geophysical Research: Atmospheres* 111.D6. D06108, n/a–n/a. ISSN: 2156-2202. DOI: 10.1029/2005JD006283.

Matthes, K. et al. (2010). "Role of the QBO in modulating the influence of the 11 year solar cycle on the atmosphere using constant forcings". In: *Journal of Geophysical Research: Atmospheres* 115.D18, p. D18110. ISSN: 2156-2202. DOI: 10.1029/2009JD013020.

McIntyre, M. E. and T. N. Palmer (1983). "Breaking planetary waves in the stratosphere". In: *Nature* 305.5935, pp. 593–600. DOI: 10.1038/305593a0. URL: http://dx.doi.org/10.1038/305593a0.

McLandress, C. and T. G. Shepherd (2009). "Simulated Anthropogenic Changes in the Brewer-Dobson Circulation, Including Its Extension to High Latitudes". In: *J. Climate* 22.6, pp. 1516–1540. DOI: 10.1175/2008JCLI2679.1.

McLandress, C. et al. (2010). "Separating the Dynamical Effects of Climate Change and Ozone Depletion. Part II: Southern Hemisphere Troposphere". In: *J. Climate* 24.6, pp. 1850–1868. DOI: 10.1175/2010JCLI3958.1.

Meinshausen, M. et al. (2011). "The RCP greenhouse gas concentrations and their extensions from 1765 to 2300". In: *Climatic Change* 109.1, pp. 213–241. ISSN: 1573-1480. DOI: 10.1007/s10584-011-0156-z.

Mitchell, D. M. et al. (2012). "The Effect of Climate Change on the Variability of the Northern Hemisphere Stratospheric Polar Vortex". In: *Journal of the Atmospheric Sciences* 69.8, pp. 2608–2618. DOI: 10.1175/JAS-D-12-021.1.

Nakamura, H. et al. (2008). "On the importance of midlatitude oceanic frontal zones for the mean state and dominant variability in the tropospheric circulation". In: *Geophysical Research Letters* 35.15. L15709, n/a–n/a. ISSN: 1944-8007. DOI: 10.1029/2008GL034010.

Naoe, H. and K. Shibata (2010). "Equatorial quasi-biennial oscillation influence on northern winter extratropical circulation". In: *Journal of Geophysical Research: Atmospheres* 115.D19. D19102, n/a–n/a. ISSN: 2156-2202. DOI: 10.1029/2009JD012952.

Naujokat, B. et al. (2002). "The early major warming in December 2001 - exceptional?" In: *Geophysical Research Letters* 29.21. 2023, pp. 191–194. DOI: 10.1029/2002GL015316.

Neff, W., J. Perlwitz, and M. Hoerling (2008). "Observational evidence for asymmetric changes in tropospheric heights over Antarctica on decadal time scales". In: *Geophysical Research Letters* 35.18. L18703, n/a–n/a. ISSN: 1944-8007. DOI: 10.1029/2008GL035074.

Newman, P. A., E. R. Nash, and J. E. Rosenfield (2001). "What controls the temperature of the Arctic stratosphere during the spring?" In: *Journal of Geophysical Research: Atmospheres* 106.D17, pp. 19999–20010. ISSN: 2156-2202. DOI: 10.1029/2000JD000061. URL: http://dx.doi.org/10.1029/2000JD000061.

Ogawa, F. et al. (2015). "Ozone-induced climate change propped up by the Southern Hemisphere oceanic front". In: *Geophysical Research Letters* 42.22. 2015GL066538, pp. 10,056–10,063. ISSN: 1944-8007. DOI: 10.1002/2015GL066538.

Oman, L. et al. (2009). "On the influence of anthropogenic forcings on changes in the stratospheric mean age". In: *Journal of Geophysical Research: Atmospheres* 114.D3. D03105, n/a–n/a. ISSN: 2156-2202. DOI: 10.1029/2008JD010378.

Omrani, N.-E. et al. (2014). "Stratosphere key for wintertime atmospheric response to warm Atlantic decadal conditions". In: *Climate Dynamics* 42.3-4, pp. 649–663. ISSN: 0930-7575. DOI: 10.1007/s00382-013-1860-3.

Omrani, N.-E. et al. (2015). "Troposphere–stratosphere response to large-scale North Atlantic Ocean variability in an atmosphere/ocean coupled model". In: *Climate Dynamics*, pp. 1–19. ISSN: 0930-7575. DOI: 10.1007/s00382-015-2654-6.

Perlwitz, J. and N. Harnik (2003). "Observational Evidence of a Stratospheric Influence on the Troposphere by Planetary Wave Reflection". In: *Journal of Climate* 16.18, pp. 3011–3026. ISSN: 0894-8755. DOI: 10.1175/1520-0442(2003)016<3011:OEOASI>2.0.CO;2.

Petoukhov, V. et al. (2013). "Quasiresonant amplification of planetary waves and recent Northern Hemisphere weather extremes". In: *Proceedings of the National Academy of Sciences* 110.14, pp. 5336–5341. DOI: 10.1073/pnas.1222000110.

Plumb, R. A. (2002). "Stratospheric Transport". In: *Journal of the Meteorological Society of Japan. Ser. II* 80.4B, pp. 793–809. DOI: 10.2151/jmsj.80.793.

Plumb, R. A. and K. Semeniuk (2003). "Downward migration of extratropical zonal wind anomalies". In: *Journal of Geophysical Research: Atmospheres* 108.D7. 4223, n/a–n/a. ISSN: 2156-2202. DOI: 10.1029/2002JD002773. URL: http://dx.doi.org/10.1029/2002JD002773.

Polvani, L. M. and D. W. Waugh (2004). "Upward Wave Activity Flux as a Precursor to Extreme Stratospheric Events and Subsequent Anomalous Surface Weather Regimes". In: *J. Climate* 17.18, pp. 3548–3554. DOI: 10.1175/1520. URL: http://dx.doi.org/10.1175/1520.

Polvani, L. M. et al. (2011). "Stratospheric Ozone Depletion: The Main Driver of Twentieth-Century Atmospheric Circulation Changes in the Southern Hemisphere". In: *J. Climate* 24.3, pp. 795–812. DOI: 10.1175/2010JCLI3772.1.

Quiroz, R. S. (1977). "The tropospheric-stratospheric polar vortex breakdown of January 1977". In: *Geophysical Research Letters* 4.4, pp. 151–154. DOI: 10.1029/GL004i004p00151.

— (1986). "The association of stratospheric warmings with tropospheric blocking". In: *Journal of Geophysical Research: Atmospheres* 91.D4, pp. 5277–5285. ISSN: 2156-2202. DOI: 10.1029/JD091iD04p05277.

Ramaswamy, V. et al. (2001). "Stratospheric temperature trends: Observations and model simulations". In: *Reviews of Geophysics* 39.1, pp. 71–122. DOI: 10.1029/1999RG000065.

Randel, W. J. (1993). "Global Variations of Zonal Mean Ozone during Stratospheric Warming Events". In: *Journal of the Atmospheric Sciences* 50.19, pp. 3308–3321. ISSN: 0022-4928. DOI: 10.1175/1520-0469(1993)050<3308:GVOZMO>2.0.CO;2. URL: http://dx.doi.org/10.1175/1520-0469(1993)050<3308:GVOZMO>2.0.CO;2.

Randel, W. J., F. WU, and R. Stolarski (2002). "Changes in Column Ozone Correlated with the Stratospheric EP Flux ". In: *Journal of the Meteorological Society of Japan. Ser. II* 80.4B, pp. 849–862. DOI: 10.2151/jmsj.80.849.

Reichler, T. and J. Kim (2008). "How Well Do Coupled Models Simulate Today's Climate?" In: *Bulletin of the American Meteorological Society* 89.3, pp. 303–311. DOI: 10.1175/BAMS-89-3-303.

Reichler, T. et al. (2012). "A stratospheric connection to Atlantic climate variability". In: *Nature Geosci* 5.11, pp. 783–787. ISSN: 1752-0894. DOI: 10.1038/ngeo1586.

Richter, J. H. et al. (2008). "Dynamics of the middle atmosphere as simulated by the Whole Atmosphere Community Climate Model, version 3 (WACCM3)". In: *Journal of Geophysical Research: Atmospheres* 113.D8, n/a–n/a. ISSN: 2156-2202. DOI: 10.1029/2007JD009269.

Richter, J. H. et al. (2011). "Influence of the quasi-biennial oscillation and El Niño–Southern Oscillation on the frequency of sudden stratospheric warmings". In: *Journal of Geophysical Research: Atmospheres* 116.D20, n/a–n/a. ISSN: 2156-2202. DOI: 10.1029/2011JD015757.

Rienecker, M. M. et al. (2011). "MERRA: NASA's Modern-Era Retrospective Analysis for Research and Applications". In: *J. Climate* 24.14, pp. 3624–3648. DOI: 10.1175/JCLI.

Robock, A. and J. Mao (1992). "Winter warming from large volcanic eruptions". In: *Geophysical Research Letters* 19.24, pp. 2405–2408. ISSN: 1944-8007. DOI: 10.1029/92GL02627.

Rose, K. and G. Brasseur (1985). "Atmospheric Ozone: Proceedings of the Quadrennial Ozone Symposium held in Halkidiki, Greece 3–7 September 1984". In: ed. by C. S. Zerefos and A. Ghazi. Dordrecht: Springer Netherlands. Chap. Ozone During Sudden Stratospheric Warming : A Three-Dimensional Simulation, pp. 28–32. ISBN: 978-94-009-5313-0. DOI: 10.1007/978-94-009-5313-0_6.

Sampe, T., H. Nakamura, and A. Goto (2013). "Potential Influence of a Midlatitude Oceanic Frontal Zone on the Annular Variability in the Extratropical Atmosphere as Revealed by Aqua-Planet Experiments". In: *Journal of the Meteorological Society of Japan. Ser. II* 91A, pp. 243–267. DOI: 10.2151/jmsj.2013-A09.

Scaife, A. A. et al. (2013). "A mechanism for lagged North Atlantic climate response to solar variability". In: *Geophysical Research Letters* 40.2, pp. 434–439. ISSN: 1944-8007. DOI: 10.1002/grl.50099.

Schmitz, G. and N. Grieger (1980). "Model calculations on the structure of planetary waves in the upper troposphere and lower stratosphere as a function of the wind field in the upper stratosphere". In: *Tellus* 32.3, pp. 207–214. ISSN: 2153-3490. DOI: 10.1111/j.2153-3490.1980.tb00948.x. URL: http://dx.doi.org/10.1111/j.2153-3490.1980.tb00948.x.

Screen, J. A. and I. Simmonds (2014). "Amplified mid-latitude planetary waves favour particular regional weather extremes". In: *Nature Clim. Change* 4.8. Letter, pp. 704–709. ISSN: 1758-678X.

Shaw, T. A. and J. Perlwitz (2013). "The Life Cycle of Northern Hemisphere Downward Wave Coupling between the Stratosphere and Troposphere". In: *Journal of Climate* 26.5, pp. 1745–1763. ISSN: 0894-8755. DOI: 10.1175/JCLI-D-12-00251.1.

— (2014). "On the Control of the Residual Circulation and Stratospheric Temperatures in the Arctic by Planetary Wave Coupling". In: *J. Atmos. Sci.* 71.1, pp. 195–206. DOI: 10.1175/JAS.

Shaw, T. A., J. Perlwitz, and N. Harnik (2010). "Downward Wave Coupling between the Stratosphere and Troposphere: The Importance of Meridional Wave Guiding and Comparison with Zonal-Mean Coupling". In: *Journal of Climate* 23.23, pp. 6365–6381. ISSN: 0894-8755. DOI: 10.1175/2010JCLI3804.1.

Shaw, T. A. et al. (2011). "The Impact of Stratospheric Ozone Changes on Downward Wave Coupling in the Southern Hemisphere". In: *Journal of Climate* 24.16, pp. 4210–4229. ISSN: 0894-8755. DOI: 10.1175/2011JCLI4170.1.

Shaw, T. A., J. Perlwitz, and O. Weiner (2014). "Troposphere-stratosphere coupling: Links to North Atlantic weather and climate, including their representation in CMIP5 models". In: *Journal of Geophysical Research: Atmospheres* 119.10, pp. 5864–5880. ISSN: 2169-8996. DOI: 10.1002/2013JD021191.

Shepherd, T. G. and C. McLandress (2011). "A Robust Mechanism for Strengthening of the Brewer–Dobson Circulation in Response to Climate Change: Critical-Layer Control of Subtropical Wave Breaking". In: *Journal of the Atmospheric Sciences* 68.4, pp. 784–797. DOI: 10.1175/2010JAS3608.1.

Shindell, D. T., D. Rind, and P. Lonergan (1998). "Increased polar stratospheric ozone losses and delayed eventual recovery owing to increasing greenhouse-gas concentrations". In: *Nature* 392.6676, pp. 589–592. ISSN: 0028-0836. DOI: 10.1038/33385.

Sigmond, M. et al. (2004). "A Simulation of the Separate Climate Effects of Middle-Atmospheric and Tropospheric CO2 Doubling". In: *Journal of Climate* 17.12, pp. 2352–2367. DOI: 10.1175/1520-0442(2004)017<2352:ASOTSC>2.0.CO;2.

Simpson, I. R., M. Blackburn, and J. D. Haigh (2009). "The Role of Eddies in Driving the Tropospheric Response to Stratospheric Heating Perturbations". In: *Journal of the Atmospheric Sciences* 66.5, pp. 1347–1365. DOI: 10.1175/2008JAS2758.1.

Sjoberg, J. P. and T. Birner (2012). "Transient Tropospheric Forcing of Sudden Stratospheric Warmings". In: *Journal of the Atmospheric Sciences* 69.11, pp. 3420–3432. DOI: 10.1175/JAS-D-11-0195.1.

Smith, A. K. et al. (2010). "Simulations of the response of mesospheric circulation and temperature to the Antarctic ozone hole". In: *Geophysical Research Letters* 37.22, n/a–n/a. ISSN: 1944-8007. DOI: 10.1029/2010GL045255.

Solomon, S. (1999). "Stratospheric ozone depletion: A review of concepts and history". In: *Reviews of Geophysics* 37.3, pp. 275–316. ISSN: 1944-9208. DOI: 10.1029/1999RG900008. URL: http://dx.doi.org/10.1029/1999RG900008.

Song, Y. and W. A. Robinson (2004). "Dynamical Mechanisms for Stratospheric Influences on the Troposphere". In: *J. Atmos. Sci.* 61.14, pp. 1711–1725. DOI: 10.1175/1520.

SPARC CCMVal (2010). "SPARC report on the evaluation of chemistry-climate models". In: *SPARC-Report No.5, WCRP-132, WMO/TD-No. 1526*.

Sun, L. and W. A. Robinson (2009). "Downward influence of stratospheric final warming events in an idealized model". In: *Geophysical Research Letters* 36.3. L03819, n/a–n/a. ISSN: 1944-8007. DOI: 10.1029/2008GL036624.

Taylor, K. E., R. J. Stouffer, and G. A. Meehl (2011). "An Overview of CMIP5 and the Experiment Design". In: *Bull. Amer. Meteor. Soc.* 93.4, pp. 485–498. DOI: 10.1175/BAMS.

Tegtmeier, S. et al. (2008). "Relative importance of dynamical and chemical contributions to Arctic wintertime ozone". In: *Geophysical Research Letters* 35.17. L17801, n/a–n/a. ISSN: 1944-8007. DOI: 10.1029/2008GL034250. URL: http://dx.doi.org/10.1029/2008GL034250.

Thieblemont, R. et al. (2015). "Solar forcing synchronizes decadal North Atlantic climate variability". In: *Nat Commun* 6. Article.

Thompson, D. W. J. and T. Birner (2012). "On the Linkages between the Tropospheric Isentropic Slope and Eddy Fluxes of Heat during Northern Hemisphere Winter". In: *Journal of the Atmospheric Sciences* 69.6, pp. 1811–1823.

Thompson, D. W. J. and S. Solomon (2002). "Interpretation of Recent Southern Hemisphere Climate Change". In: *Science* 296.5569, pp. 895–899. DOI: 10.1126/science.1069270.

Thompson, D. W. and J. M. Wallace (2000). "Annular Modes in the Extratropical Circulation. Part I: Month-to-Month Variability*". In: *J. Climate* 13.5, pp. 1000–1016. DOI: 10.1175/1520.

Thompson, D. W. et al. (2011). "Signatures of the Antarctic ozone hole in Southern Hemisphere surface climate change". In: *Nature Geosci* 4.11, pp. 741–749. DOI: 10.1038/ngeo1296.

Tung, K. K. and R. S. Lindzen (1979). "A Theory of Stationary Long Waves. Part I: A Simple Theory of Blocking". In: *Monthly Weather Review* 107.6, pp. 714–734. DOI: 10.1175/1520-0493(1979)107<0714:ATOSLW>2.0.CO;2.

Venkateswara Rao, N. et al. (2015). "Observational evidence of the influence of Antarctic stratospheric ozone variability on middle atmosphere dynamics". In: *Geophysical Research Letters* 42.19. 2015GL065432, pp. 7853–7859. ISSN: 1944-8007. DOI: 10.1002/2015GL065432.

Walterscheid, R. L., G. G. Sivjee, and R. G. Roble (2000). "Mesospheric and lower thermospheric manifestations of a stratospheric warming event over Eureka, Canada (80N)". In: *Geophysical Research Letters* 27.18, pp. 2897–2900. ISSN: 1944-8007. DOI: 10.1029/2000GL003768.

Wang, L. and P. J. Kushner (2011). "Diagnosing the stratosphere-troposphere stationary wave response to climate change in a general circulation model". In: *Journal of Geophysical Research: Atmospheres* 116.D16, n/a–n/a. DOI: 10.1029/2010JD015473.

Weber, M. et al. (2003). "Dynamical control of NH and SH winter/spring total ozone from GOME observations in 1995–2002". In: *Geophysical Research Letters* 30.11. 1583, n/a–n/a. ISSN: 1944-8007. DOI: 10.1029/2002GL016799. URL: http://dx.doi.org/10.1029/2002GL016799.

Wittman, M. A. H., A. J. Charlton, and L. M. Polvani (2007). "The Effect of Lower Stratospheric Shear on Baroclinic Instability". In: *Journal of the Atmospheric Sciences* 64.2, pp. 479–496. DOI: 10.1175/JAS3828.1.

WMO (2014). *Scientific Assessment of Ozone Depletion: 2014*. Vol. 55. World Meteorol. Organ., Geneva, Switzerland., p. 416.

Woollings, T. et al. (2010). "Associations between stratospheric variability and tropospheric blocking". In: *Journal of Geophysical Research: Atmospheres* 115.D6. D06108, n/a–n/a. ISSN: 2156-2202. DOI: 10.1029/2009JD012742. URL: http://dx.doi.org/10.1029/2009JD012742.

Yamashita, C., H.-L. Liu, and X. Chu (2010). "Responses of mesosphere and lower thermosphere temperatures to gravity wave forcing during stratospheric sudden warming". In: *Geophysical Research Letters* 37.9, n/a–n/a. ISSN: 1944-8007. DOI: 10.1029/2009GL042351.

Yoo, C. and S.-W. Son (2016). "Modulation of the boreal wintertime Madden-Julian oscillation by the stratospheric quasi-biennial oscillation". In: *Geophysical Research Letters* 43.3. 2016GL067762, pp. 1392–1398. ISSN: 1944-8007. DOI: 10.1002/2016GL067762.

Own Publications

Part of this thesis:

- **Lubis, S. W.**, Omrani, N.-E., Matthes, K., and Wahl, S., 2016: "Impact of the Antarctic Ozone Hole on the Vertical Coupling of the Stratosphere-Mesosphere-Lower Thermosphere System". In: *Journal of the Atmospheric Sciences*. DOI: 10.1175/JAS-D-15-0189.1.

- **Lubis, S. W.**, Matthes, K., Omrani, N.-E., Harnik, N., and Wahl, S., 2016: "Influence of the Quasi-Biennial Oscillation and Sea Surface Temperature Variability on Downward Wave Coupling in the Northern Hemisphere". In: *Journal of the Atmospheric Sciences*, 73.5, pp. 1943-1965. DOI: 10.1175/JAS-D-15-0072.1.

- **Lubis, S. W.**, Silverman, V., Matthes, K., Harnik, N., Omrani, N.-E., and Wahl, S., 2016: "How Does Downward Planetary Wave Coupling Affect Polar Stratospheric Ozone in the Arctic Winter Stratosphere?". (submitted to *Atmospheric Chemistry and Physics*).

- **Lubis, S. W.**, Matthes, K., Harnik, N., Omrani, N.-E., and Wahl, S., 2016: "Effect of Climate Change on the Variability of the Downward Wave Coupling in the Northern Hemisphere". (to be submitted to *Geophysical Research Letters*).

Other:

- Omrani, N.-E., Keenlyside, N. S., **Lubis, S. W.**, Matthes, K., and Ogawa, F., 2016: "Competing Stratospheric and Tropospheric Dynamical Bridges in the Northern Hemisphere Anthropogenic Climate Change". (submitted to *Journal of the Atmospheric Sciences*).

- Silverman, V., N. Harnik, K. Matthes, **Lubis, S. W.**, and S. Wahl., 2016: Radiative effects of ozone waves on polar vortex seasonal cycle and extratropical QBO signals. (to be submitted to *Journal of the Atmospheric Sciences*).

Abbreviations

BDC	Brewer-Dobson circulation
CCM	Chemistry Climate Model
CCMVal	Chemistry-Climate Model Validation Activity
CESM	Community Earth System Model
DWC	Downward Wave Coupling
ECMWF	European Center for Medium-Range Weather Forecasting
ENSO	El Niño-Southern Oscillation
E-P flux	Eliassen-Palm flux
ERA	ECMWF re-analysis
GHG	Green House Gas
MERRA	Modern Era Retrospective-Analysis for Research and Application
MLT	Mesosphere-Lower Thermosphere
NAM	Northern Annular Mode
NAO	North-Atlantic Oscillation
NCAR	National Center for Atmospheric Research
ODS	Ozone Depleting Substances
QBO	Quasi-Biennial Oscillation
QTDW	Quasi-Two-Day Wave
SPARC	Stratospheric Processes and their Role in Climate
SST	Sea Surface Temperature
SSW	Sudden Stratospheric Warming
TEM	Transformed Eulerian Mean
WACCM	Whole Atmosphere Community Climate Model
WMO	World Meteorological Organizational

Declaration of Authorship

I, Sandro W. Lubis, hereby declare that this thesis titled, "Processes Controlling Stratospheric Dynamic Variability, the Implications for Ozone Levels, and the Coupling to the Troposphere and Mesosphere", is my own work apart from my supervisors' guidance and acknowledged assistance. This thesis has not been submitted for the award of doctoral degree in any other examining body and was prepared according to the Rules of Good Scientific Practice of the German Research Foundation.

Sandro W. Lubis

Kiel, 17. 05. 2016